

OF MOSQUITOES AND MEN: TARGETING INWARD RECTIFIER POTASSIUM (KIR)
CHANNELS FOR THE DEVELOPMENT OF NEW THERAPEUTICS AND INSECTICIDES

By

Rene Raphemot

Dissertation

Submitted to the Faculty of the
Graduate School of Vanderbilt University
in partial fulfillment of the requirements

for the degree of

DOCTOR OF PHILOSOPHY

in

Pharmacology

August, 2014

Nashville, Tennessee

Approved:

Professor Jerod S. Denton

Professor Charles C. Hong

Professor C. David Weaver

Professor Corey R. Hopkins

Professor Julián F. Hillyer

To my family and my amazing wife, Cenean, for the continuous support over these years

ACKNOWLEDGEMENTS

My doctoral research experience has been fulfilling both professionally and personally. This journey would not have been possible without the encouragements of many people who have crossed my path. First, I would like to thank my thesis advisor and mentor Dr. Jerod S. Denton. I really appreciate how you believed in me and supported me during the past four years in your laboratory. You have been a great mentor, providing me with continuous encouragement and advice to become a better scientist. You have always challenged me to think critically about my work and given me the flexibility to explore various scientific questions. Importantly, you were always available when I needed some help or guidance with my research. While this journey was not without difficulties, you have always been patient and constantly made sure that I remained focused to be as successful as I could be during my training. I am deeply indebted to you for all the technical expertise and personal guidance you have given me over the years.

I would like to thank all the former and current members of the Denton laboratory who have made my days at work enjoyable and provided me with continuous support throughout my research. I want to especially thank Sreedatta “Riya” Banerjee who trained me in various molecular biology techniques when I first joined the lab and provided me with much assistance during the early years of my training.

I am thankful to all the staff at the high-throughput screening facility. You have been an important part of my work by providing me with invaluable technical assistance and resources. In particular, I would like to extend my thanks to Emily Days for all the help in running several high-throughput screens. In addition, I would like to thank the Departments of Pharmacology and Anesthesiology, the Interdisciplinary Graduate Program, and the BRET office that ensured

the good fulfillment of my graduate education and career development here at Vanderbilt University.

I am honored to have been surrounded by such exceptional scientists as part of my dissertation committee. Drs. Charles C. Hong, C. David Weaver, Corey R. Hopkins and Julián F. Hillyer have been incredibly supportive of my work. They provided me with insightful suggestions and great expertise in their respective fields, which has greatly contributed to the success of my dissertation research project. The discussions that we had help shaped my critical thinking and positively influenced my work as a scientist. I would like to thank you all also for the words of wisdom that you have shared with me, as they have and will continue to influence my career development. I would like to especially thank Dr. Julián F. Hillyer for welcoming me in his laboratory and providing me with the resources to advance and contribute to the success of my research. I am grateful for Tania Y. Estévez-Lao in the Hillyer laboratory for the training, technical assistance and continuous encouragement, and his lab members for supporting my efforts. I am thankful for all the collaborators with whom I had the opportunity to work, and particularly for a fruitful collaboration with the laboratory of Peter M. Piermarini.

I would like to thank my family for their unconditional support throughout the years. They have always believed in me and despite being apart for numerous years, continuously cheered me up during trying times. I am also thankful for the friends that I made during my graduate career. Lastly, I am grateful for my wife, Cenean, for being there for me every step of the way. Thank you so much for endless encouragements during the pursuit of this degree.

TABLE OF CONTENTS

ACKNOWLEDGEMENTS	iii
LIST OF TABLES	x
LIST OF FIGURES	xii
LIST OF ABBREVIATIONS	xvi

Chapter

I. INTRODUCTION	1
Overview of Kir channels in humans	1
Molecular structure and functions of Kir channels.....	1
Pharmacology of Kir channels	9
Overview of Kir channels in mosquitoes	15
Molecular structure and functions of Kir channels.....	16
Pharmacology of Kir channels	18
Objective.....	18
Notes on figures and tables.....	19
II. HIGH-THROUGHPUT SCREENING FOR SMALL-MOLECULE MODULATORS OF INWARD RECTIFIER POTASSIUM CHANNELS.....	20
Abstract	20
Video link	21
Experimental Protocol	22
Generation of stable polyclonal cell lines.....	22
Generation of stable monoclonal cell lines.....	23
General TI^+ flux assay procedure.....	25
Determination of optimal TI^+ concentration.....	27
Determination of assay sensitivity to DMSO.....	28
Determination of assay sensitivity to known pharmacological modulators.....	29
Checkerboard Analysis.....	31
Pilot Screen	32
Representative Results	34
Discussion	41
III. DISCOVERY, CHARACTERIZATION AND STRUCTURE-ACTIVITY RELATIONSHIPS OF AN INHIBITOR OF INWARD RECTIFIER POTASSIUM (KIR) CHANNELS WITH PREFERENCE FOR KIR2.3, KIR3.X AND KIR7.1	44

Abstract	44
Introduction	45
Materials and Methods	47
Expression vectors.....	47
Cell lines	48
Two-electrode voltage clamp analysis	48
Whole-cell patch clamp electrophysiology.....	49
Test compound and stimulus plate preparation.....	50
Kinetic imaging, data analysis, and statistics	51
Chemical synthesis.....	52
Results	54
VU573: A weak Kir1.1 inhibitor with preference for GIRK	54
VU573 shows preference for Kir2.3, GIRK and Kir7.1 over Kir1.1 and Kir2.1	57
Patch clamp analysis of VU573 potency in mammalian cells	60
Development of TI ⁺ flux assays for Kir2.3 and Kir7.1-M125R	62
Synthesis and structure-activity relationships of VU573 analogs	69
Discussion	72
IV. DEVELOPMENT AND VALIDATION OF FLUORESCENCE- AND AUTOMATED PATCH CLAMP-BASED FUNCTIONAL ASSAYS FOR THE INWARD RECTIFIER POTASSIUM CHANNELS KIR4.1	76
Abstract	76
Introduction	77
Materials and Methods	80
Molecular biology and stable cell line generation	80
Manual patch clamp electrophysiology.....	80
Western blot analysis	81
TI ⁺ flux assay development and library screening.....	82
Concentration-response curves.....	83
Automated patch clamp electrophysiology.....	84
Animals.....	85
Astrocyte cultures.....	85
Astrocyte electrophysiology	86
Results	87
Cell line characterization.....	87
TI ⁺ flux assay	90
Discovery of a novel Kir4.1 inhibitor.....	93
Development of an automated patch clamp assay for Kir4.1 using the IonFlux HT	95
Characterization of small-molecule Kir4.1 antagonists with the IonFlux HT	99
VU717 inhibits native Kir4.1 channels in astrocytes	101
Discussion	103
V. DIRECT ACTIVATION OF β-CELL KATP CHANNELS WITH A NOVEL XANTHINE DERIVATIVE	107
Abstract	107

Introduction	108
Materials and Methods	109
Expression vectors.....	109
Cell lines and transfections	109
Western blot analysis	110
TI ⁺ flux assays.....	110
Patch clamp electrophysiology.....	112
Calcium imaging	113
Measurement of complex II activity.....	114
Chemicals	114
Results	114
Serendipitous discovery of the Kir6.2/SUR1 activator VU0071063	114
Effects of VU0071063 on pancreatic Kir6.2/SUR1 K _{ATP} channels.....	118
VU0071063 is selective SUR1-containing K _{ATP} channels	123
VU0071063 inhibits glucose-stimulated β-cell Ca ²⁺ influx	126
Kir6.2/SUR1 activation by VU0071063 is not mediated by a PDE inhibitory pathway	128
Ancillary Pharmacology.....	130
Discussion	133
VI. ELICITING RENAL FAILURE IN MOSQUITOES WITH A SMALL-MOLECULE INHIBITOR OF INWARD-RECTIFYING POTASSIUM CHANNELS	139
Abstract	139
Introduction	140
Materials and Methods	141
Expression vectors and sub-cloning	141
Stable cell line generation	142
Whole-cell patch clamp electrophysiology.....	142
Test compound and stimulus plate preparation.....	143
Thallium flux assays	143
Chemical synthesis.....	144
Mosquito colonies	144
Mosquito toxicology experiments.....	145
Isolated Malpighian tubule experiments	145
Mosquito excretion experiments	146
Statistical analyses.....	147
Results and Discussion	148
VII. MOLECULAR AND FUNCTIONAL CHARACTERIZATION OF ANOPHELES GAMBIAE INWARD RECTIFIER POTASSIUM (KIR1) CHANNELS: A NOVEL ROLE IN EGG PRODUCTION	167
Abstract	167
Introduction	168
Materials and Methods	169
Mosquito rearing	169
Sequencing of <i>Anopheles gambiae</i> Kir1 from Malpighian tubule cDNA.....	169

Heterologous expression and electrophysiology in <i>Xenopus</i> oocytes.....	174
RNA isolation, cDNA synthesis, and quantitative real-time PCR	175
RNA interference (RNAi)-based gene silencing	176
Antibody production	178
Western blotting	178
Survival assays.....	179
Fecundity assays.....	179
Results	180
<i>Anopheles gambiae Kir1</i> gene structure.....	180
Phylogenetic analysis of AgKir channels	184
Functional characterization of AgKir1 channels in <i>Xenopus</i> oocytes	189
Developmental and tissue distribution of <i>Kir1</i> in <i>Anopheles gambiae</i>	191
<i>AgKir1</i> knockdown does not affect survival	195
<i>AgKir1</i> knockdown decreases fecundity	199
Discussion	201
VIII. DISCOVER AND CHARACTERIZATION OF A POTENT AND SELECTIVE INHIBITOR OF AEADES AEGYPTI INWARD RECTIFIER POTASSIUM CHANNELS	205
Abstract	205
Introduction	206
Materials and Methods	208
Tl ⁺ flux assays.....	208
Compound synthesis	210
Patch clamp electrophysiology.....	212
Heterologous expression of <i>AeKir1</i> and <i>AeKir2B</i> in <i>Xenopus</i> oocytes	212
Electrophysiology of <i>Xenopus</i> oocytes	213
Mosquito colony	214
Mosquito toxicology experiments.....	215
Mosquito excretion experiments	215
Statistical analyses.....	216
Results	217
Discovery of novel <i>AeKir1</i> inhibitors via high-throughput screening	217
VU625 is a potent and preferential inhibitor of <i>AeKir1</i>	219
Chemical lead optimization and structure-activity relationships.....	225
VU625-induced toxicity is increased by probenecid.....	235
VU625-induced reduction of urine excretion is enhanced by probenecid	238
Discussion	242
Perspective.....	245
IX. SUMMARY AND FUTURE DIRECTIONS.....	246
Summary	246
Future Directions.....	247

Appendix

**A. PHARMACOLOGICAL VALIDATION OF AN INWARD-RECTIFIER
POTASSIUM (KIR) CHANNELS AS AN INSECTICIDE TARGET IN THE
YELLOW FEVER MOSQUITO Aedes Aegypti..... 252**

B. LIST OF PUBLICATIONS..... 256

REFERENCES..... 257

LIST OF TABLES

Chapter I

Table	Page
1 Kir channel modulators.....	10
2 Summary of qualitative assessment of <i>Aedes aegypti</i> Kir channel functions and tissue distributions	17

Chapter III

Table	Page
1 Structure-activity relationships and lead optimization summary.....	67

Chapter V

Table	Page
1 Percent inhibition of Complex II activity in response to VU0071063 and diazoxide	138

Chapter VI

Table	Page
1 Structure-activity relationships for VU573 and its analogs.....	154
2 Effects of VU573 (10 μ M) and barium (5 mM) on the basolateral membrane voltage (V_{bl}) and input resistance (R_{pc}) of principal cells in isolated Malpighian tubules	161

Chapter VII

Table	Page
1 Primers used for cloning and sequencing <i>Anopheles gambiae</i> Kir1 (<i>AgKir1</i>).....	172
2 Positions and lengths of <i>Anopheles gambiae</i> Kir1 exons and introns in the <i>Anopheles</i> genome	172
3 Accession numbers of <i>A. aegypti</i> , <i>A. gambiae</i> , <i>C. quinquefasciatus</i> , <i>D. melanogaster</i> and <i>M. vaginatus</i> Kir channel sequences	174
4 Primer sequences used for amplification of Kir channel genes for expression analyses and RNA interference	178

Chapter VIII

Table	Page
1 Compositions (in mM) of solutions used in <i>Xenopus</i> oocyte electrophysiology.....	214
2 Selectivity of VU625 against human Kir channels assessed in Tl ⁺ flux assays	222
3 Summary of results obtained from the activity of the VU625 compound in radioligand binding assays	223
4 Structure-activity relationships and lead optimization summary of VU0077625 scaffold...	229
5 SAR around the left-hand sulfonamide.....	231

LIST OF FIGURES

Chapter I

Figure	Page
1 Overall Kir channel structure and characteristic currents.....	7
2 Tissue distribution of Kir channel subunits	8

Chapter II

Figure	Page
1 Cell plating maps used for Tl ⁺ flux assay development	37
2 Determination of optimal assay Tl ⁺ concentration	38
3 Assay tolerance to DMSO	39
4 Assay sensitivity to known pharmacologically active compounds.....	40
5 Determination of assay suitability for HTS.	41

Chapter III

Figure	Page
1 VU573 inhibits mGluR8-activated Kir3.1/3.2 channel activity in thallium flux assays	57
2 Effect of VU573 on Kir channels expressed in oocytes	60
3 VU573-dependent inhibition of Kir3.1/3.2, Kir2.3 and Kir7.1 channel activity expressed in HEK-293 cells.....	62
4 Development of a thallium flux assay for Kir2.3	65
5 Development of a thallium flux assay for Kir7.1 (M125R).....	66
6 Lack of effect of R70 on wild type Kir7.1 activity.....	72

Chapter IV

Figure	Page
1 Tetracycline-inducible Kir4.1 expression in stably transfected T-REx-HEK293 cells.....	90
2 Thallium flux reporter assay of Kir4.1 channel function.....	93
3 Discovery of a novel Kir4.1 channel inhibitor in a TI^+ flux-based pilot screen.....	95
4 Automated patch clamp electrophysiology assay for Kir4.1.....	98
5 The IonFlux HT assay is reproducible.....	99
6 Characterization of small-molecule Kir4.1 inhibitors using the IonFlux HT.....	101
7 VU717 inhibition of native Kir4.1 activity channels in astrocytes.....	103

Chapter V

Figure	Page
1 T-REx-HEK293-Kir6.2/SUR1 cell line characterization.....	117
2 Discovery of VU0071063 in a TI^+ flux assay of Kir6.2/SUR1.....	118
3 Characterization of VU0071063 activity against Kir6.2/SUR1 in TI^+ flux assays.....	121
4 Characterization of VU0071063 activity against Kir6.2/SUR1 with patch clamp electrophysiology.....	122
5 VU0071063 activates Kir6.2/SUR1 in excised inside-out patches.....	123
6 VU0071063 is selective for SUR1-containing K_{ATP} channels.....	125
7 Lack of effect of VU0071063 on Kir6.2/SUR2A channels.....	126
8 VU0071063 inhibits glucose-stimulated β -cell calcium entry.....	128
9 Lack of effect of theophylline on Kir6.2/SUR1-dependent TI^+ flux.....	130
10 Selectivity of VU0071063 among members of the Kir channel family.....	132
11 Effects of VU0071063 on heterologously expressed Kv2.1.....	133

Chapter VI

Figure	Page
1 Small-molecule probes of <i>AeKir1</i> expressed in T-REx-HEK-293 cells.....	151
2 Functional expression of <i>AeKir1</i> in T-REx-HEK293 cells and its inhibition by barium (Ba^{2+})	152
3 Effects of VU573 and VU342 on adult female mosquitoes (<i>Aedes aegypti</i>)	164
4 Incapacitating effects of VU573 in three species of mosquitoes	166

Chapter VII

Figure	Page
1 Gene structure of <i>Anopheles gambiae AgKir1</i>	183
2 Hydrophobicity plot of AgKir1	184
3 Amino acid sequence alignment of <i>Anopheles gambiae</i> Kir channels.....	187
4 ClustalW protein sequence alignment of the K^+ -selectivity filter (TXGY[F]G) from <i>Aedes aegypti</i> , <i>Anopheles gambiae</i> , <i>Culex quinquefasciatus</i> , <i>Drosophila melanogaster</i> , <i>Homo sapiens</i> and <i>Microcoleus vaginatus</i> Kir channels.....	188
5 Phylogenetic analysis of the <i>Anopheles gambiae</i> , <i>Aedes aegypti</i> , <i>Culex quinquefasciatus</i> , and <i>Drosophila melanogaster</i> Kir channel families.....	189
6 Current-voltage (I-V) relationships of AgKir1 channels in <i>Xenopus</i> oocytes.....	191
7 Quantitative RT-PCR analysis of the expression of <i>A. gambiae AgKir1</i> in different developmental stages	193
8 Quantitative RT-PCR analysis of the expression of <i>A. gambiae AgKir1</i> in different body segments and tissues	194

9	Quantitative RT-PCR analysis of the expression of <i>A. gambiae Kir</i> genes in different body segments and tissues	195
10	Quantitative RT-PCR and western blot analyses showing <i>AgKir1</i> RNAi-based knockdown efficiencies	198
11	<i>AgKir1</i> knockdown does not affect mosquito survival after a blood meal.....	199
12	<i>AgKir1</i> knockdown decreases mosquito fecundity.....	201

Chapter VIII

Figure	Page	
1	Tl ⁺ flux assay of <i>AeKir1</i> channel activity for high-throughput screening.....	220
2	VU625 is a potent inhibitor of <i>AeKir1</i> in Tl ⁺ flux assays.....	221
3	VU625 is preferential inhibitor of <i>AeKir1</i> over <i>AeKir2B</i> in whole-cell electrophysiology .	226
4	Design and chemical lead optimization strategy for VU625	228
5	Summary of structure-activity relationship (SAR).....	236
6	Effects of probenecid and VU625 on survival of adult female mosquitoes (<i>A. aegypti</i>)	239
7	VU625 and probenecid share a sulfonamide moiety	240
8	The dose-response curve of the toxic effects of VU625 on adult mosquitoes (<i>A. aegypti</i>) is biphasic	241
9	Effects of probenecid and VU625 on the in vivo excretory capacity of adult female mosquitoes (<i>A. aegypti</i>)	243

LIST OF ABBREVIATIONS

°C:	Degree Celsius
AA:	Amino acid
AB:	Assay buffer
ABC transporter:	ATP-binding cassette transporter
ACSF:	Artificial cerebral spinal fluid
BH-medium:	Blasticidin/Hygromycin-medium
<i>bla</i> (<i>Ap</i> ^R):	β-lactamase mediating ampicilin resistance gene
B-medium:	Blasticidin medium
BMP:	Bone morphogenetic protein
[Ca ²⁺] _i :	Intracellular calcium concentration
CRC:	Concentration-response curve
DCT:	Distal convoluted tubule
DMEM:	Dulbecco's Modified Eagle Medium
DMSO:	Dimethyl sulfoxide
dsRNA:	Double-stranded RNA
EC ₂₀ :	20% effective concentration
EC ₅₀ :	50% effective concentration
EC ₈₀ :	80% effective concentration
ED ₅₀ :	50% effective dose
E _K :	Nernst electrochemical equilibrium potential for potassium
EMEM:	Eagle's Minimum Essential Medium
FBS:	Fetal bovine serum
FCS:	Fetal calf serum
FDSS:	Functional drug screening system
GIRK:	G protein-coupled inward rectifying potassium channel

HBS:	HEPES-buffered saline
HBSS:	Hank's Balanced Salt Solution
HPLC:	High-performance liquid chromatography
HRP:	Horseradish peroxidase
HTS:	High-throughput screening
IC ₅₀ :	50% inhibitory concentration
I _m :	Membrane potential
I _{K1} :	Cardiac inward rectifying current
K _{ATP} :	ATP-sensitive potassium channel
KCO:	Potassium channel opener
K _{ir} :	Inward rectifier potassium channel
K _v :	Voltage-gated potassium channel
LC/MS:	Liquid chromatography mass spectrometry
mGluR8:	Metabotropic glutamate receptor 8
NCC:	Sodium-chloride co-transporter
NCI:	National Cancer Institute
NMR:	Nuclear magnetic resonance
OAT:	Organic anion transporter
ORF:	Open reading frame
PBS:	Phosphate-buffered saline
PDE:	Phosphodiesterase
pH _i :	Intracellular pH
qRT-PCR:	quantitative Reverse Transcriptase-Polymerase Chain Reaction
RACE:	Rapid amplification of cDNA ends
RNAi:	RNA interference
Rpc:	Input resistance
<i>rps7</i> :	Ribosomal protein S7 gene

SAR:	Structure-activity relationship
SBS:	Society for Biomolecular Screening
SF:	Selectivity filter
SUR:	Sulfonylurea receptor
Tl ⁺ :	Thallium
TM:	Transmembrane-spanning domain
T-Rex-HEK293:	Tetracycline inducible human embryonic kidney
UTR:	Untranslated region
UV:	Ultra-violet
V _{bl} :	Basolateral membrane voltage
VDCC:	L-type voltage-dependent calcium channels
VICB:	Vanderbilt Institute of Chemical Biology
V _m :	Membrane potential

INTRODUCTION

Overview of Kir channels in humans

Potassium channels represent an important and evolutionary conserved family of ion channels expressed in all living cells. Inward rectifier potassium (Kir) channels are a class of potassium channels expressed in a variety of excitable and non-excitable cells. They play essential roles in the regulation of various physiological processes ranging from maintaining the resting membrane potential, cardiac and neuronal excitability, epithelial transport, metabolic homeostasis, muscle contraction, and cellular signaling [1-4]. Given the important physiological roles of Kir channels and genetic evidences that disease-causing mutations affecting these channels cause numerous diseases [3,5], Kir channel have emerged as important therapeutic targets. Here, we will briefly describe some features of human Kir channel subtypes focusing on their molecular characteristics, functions and pharmacology.

Molecular structure and functions of Kir channels

The inward rectifier family of potassium (Kir) channels encoded by the *KCNJx* genes is comprised of at least sixteen members, which play essential physiological roles in modulating the functions of most organ systems [1,3,4]. This gene family is further subdivided in seven groups (Kir1.x to Kir7.x) based on amino acid sequence homology. High-resolution X-ray crystal structures reveal that Kir channels exhibit a simple structural topology characterized by N- and C-terminus cytoplasmic domains, two transmembrane-spanning domains (TM1 and TM2), and a pore-forming loop containing the conserved K⁺ selectivity filter (SF) sequence—GYG [1,6,7] (**Fig. 1A**). With the exception of ATP-sensitive Kir (K_{ATP}) channels, which form

octomeric complexes of Kir6.x and sulfonylurea receptors (SURx) [8], Kir channels generally assemble as tetrameric complexes constituted of identical (homomers) or different (heteromers) Kir subunits. This tetrameric assembly of Kir channels creates a water-filled pore permitting the movement of K^+ ions down their electrochemical gradient and across the cell membrane (**Fig. 1A, B**). In other terms, under physiological conditions, Kir channels conduct K^+ ions from the inside to the outside of cell as result of the difference between intracellular and extracellular concentration of K^+ ions.

Unlike voltage-gated potassium (Kv) channels, Kir channels do not possess a voltage-sensing domain, but exhibit a voltage-dependent decrease in currents. By convention, the movement of K^+ ions inside a cell generates an inward current, whereas K^+ ions efflux generates an outward current. The voltage-dependent decrease in outward current is called “rectification” and results from a physical block of Kir channels by intracellular divalent cations such as magnesium and polyamines (e.g. putrescine, spermine and spermidine) [9]; thus, the term “inward rectification” (**Fig. 1C**). Because of the physical property of inward rectification, Kir channels exhibit typically larger inward currents at hyperpolarized potentials (more negative than the Nerst potential for potassium, E_K) as compared to outward currents. Furthermore, Kir channels display various degrees of inward rectification between family members, which are broadly classified as “strong” or “weak” rectification. This unique rectification property of Kir channels contributes to potassium homeostasis in different tissues and organ systems (**Fig. 1C**). In general, strong inward rectifiers are expressed in excitable cells such as neurons and muscle cells, whereas weak inward rectifiers are expressed in epithelial and other non-excitable cell types [1]. The physiological importance of Kir channel rectification in humans will be explored next.

“Strong” inward rectifier Kir channels

Inward rectifier Kir channels exhibiting strong rectification include Kir2.x and G-protein coupled inward rectifier (GIRK) channels. Strong rectifiers are primarily expressed in excitable cells, such as the heart or neurons where they play essential roles in modulating cell excitability. The Kir2.x family is comprised of Kir2.1 (*KCNJ2*), Kir2.2 (*KCNJ12*), Kir2.3 (*KCNJ4*), Kir2.4 (*KCNJ14*) and Kir2.6 (*KCNJ18*) subunits. Kir2.x channels are expressed primarily in excitable cells such as the cardiac, neuronal and skeletal muscle cells, with lesser expression reported in the kidney and smooth muscle cells [1]. In cardiac myocytes, Kir2.x underlies constitutively active currents also known as cardiac inward rectifying current (I_{K1}), which contributes to setting the resting membrane and shaping the cardiac action potential—notably, the initial depolarization and final repolarization phases [1,10,11]. While Kir2.1 and Kir2.2 are the major forms in the ventricular cardiomyocytes [12], atrial cardiomyocytes are enriched with Kir2.3 subunits. GIRK channels are expressed predominantly in the heart and nervous system, and comprised of Kir3.1 (*KCNJ3*), Kir3.2 (*KCNJ6*), Kir3.3 (*KCNJ9*) and Kir3.4 (*KCNJ5*) subunits [1]. In the heart, GIRK channels are expressed predominantly as heteromeric complexes composed of Kir3.1 and Kir3.4 subunits, which are localized primarily in atrial myocytes [13,14]. In the nervous system, heteromeric GIRK channels are primarily formed by Kir3.1 and Kir3.2 subunits. In the absence of agonists, GIRK channels are in a “closed state” and therefore, contribute little to the resting membrane potassium conductance and potential of cells. However, the activation of G-protein coupled receptors by various neurotransmitters (e.g. acetylcholine, dopamine) induced through a pertussis toxin-sensitive pathway causes the opening of GIRK channels via the $G\beta\gamma$ of the heterotrimeric G-proteins. In the heart, M2 muscarinic receptors activation following the release of acetylcholine upon sympathetic stimulation leads to opening

of GIRK channels, resulting in potassium efflux, membrane hyperpolarization and consequently bradycardia. Defects in Kir channel functions affecting Kir2.x and GIRK channels cause various forms of cardiac arrhythmias, such as Anderson-Tawil syndrome and atrial fibrillation, as well as neurological disorders such as epilepsy and addiction [1,15]. Therefore, strong rectifiers are putative drug targets for the development of novel therapeutics for these pathological conditions. In particular, an emerging body of evidences suggests that Kir2.3 and Kir3.1/3.4, which are involved in atrial fibrillation, represent attractive targets for developing antiarrhythmic therapies without the ventricular side effects commonly associated with current therapeutics [16,17]. We have begun to investigate this possibility by identifying novel modulators of Kir2.3 and GIRK channels (see **Chapter III**).

“Weak” inward rectifier Kir channels

Inward rectifying Kir channels exhibiting weak rectification include members of the Kir1.1, Kir4.x, Kir5.1, Kir6.x and Kir7.1 families. As opposed to strong rectifiers, weak rectifiers display a high channel open probability across a wide range of membrane potentials. Consequently, weak rectifiers exhibit a relatively large current in both the inward and outward directions as compared to strong rectifiers (**Fig. 1C**).

Kir1.1: The founding member of the Kir channel family Kir1.1 (*KCNJ1*) is predominantly expressed in the kidney, although it is also reported in the brain (i.e. cortex and hippocampus) [1,18]. Kir1.1 plays a crucial role in the kidney by regulating salt and water balance, and thus blood pressure. Disease-causing mutations affecting this channel, such as autosomal recessive mutations, lead to Bartter syndrome, a condition characterized by Na⁺ and K⁺ salt wasting, excessive urination, low to normal blood pressure and metabolic alkalosis [19].

Kir1.1 represents a novel diuretic target, which has prompted the development of novel small-molecule modulators by our laboratory and others [20-22].

Kir4.x/Kir5.1: The Kir4.x family is comprised of Kir4.1 (*KCNJ10*) and Kir4.2 (*KCNJ15*) subunits. Kir4.1 is expressed predominantly in brain and spinal cord astrocytes, retinal Müller glia, stria vascularis and glia of the inner ear, and renal tubule epithelial cells. Consistent with its localization, targeted deletion of *KCNJ10* in mice produces severe motor impairment, deafness, and premature death [23-27]. In the central nervous system, Kir 4.1 functions contribute to spatial buffering (clearance) of K^+ ions in the astrocytes as the result of neuronal activity. Kir4.1 is important for Na^+ reabsorption in the distal convoluted tubule of the kidney [4]. Similarly to Kir4.1, Kir4.2 encoded by *KCNJ15* is also found in the brain and kidney. The recent discovery [28,29] of loss-of-function mutations in *KCNJ10* in patients with SeSAME (Seizures, Sensorineural deafness, Ataxia, Mental impairment, Electrolyte imbalance) or EAST (Epilepsy, Ataxia, Sensorineural deafness, salt-wasting Tubulopathy) syndrome suggests that Kir4.1 may represent a new target for the development of novel therapeutic approaches for neurological and hypertensive abnormalities. The development of in vitro assays to identify novel modulators of Kir4.1 is discussed in **Chapter IV**. Kir5.1 encoded by *KCNJ16* assembles only with Kir4.x subunits to form functional channels. It is expressed primarily in the brain and kidney.

Kir6.x: The Kir6.x family is comprised of Kir6.1 (*KCNJ8*) and Kir6.2 (*KCNJ11*) subunits. Kir6.1 and Kir6.2 form adenosine triphosphate (ATP)-sensitive Kir (K_{ATP}) channels, which modulate important functions in nerve, muscle, epithelial, and endocrine tissue physiology by integrating cellular metabolism and membrane excitability [30]. K_{ATP} channels assemble in octomeric complexes of four pore-forming Kir6.x inward rectifier K^+ (Kir) channel subunits and four regulatory SURx sulfonylurea receptor subunits [8]. SUR1 is encoded by *ABCC8*, while

SUR2A and SUR2B (*ABCC9*) are splice variants of the same gene. The three major channel subtypes created by different subunit combinations exhibit distinctive biophysical, regulatory, and pharmacological properties, as well as cell type-specific expression [1,31,32]. K_{ATP} channels are validated targets for disorder of glucose homeostasis, such as neonatal and adult-onset diabetes and hyperinsulemia, hypertension and cardiac arrhythmias [1,2]. We discussed in **Chapter V**, the discovery of a new modulator of K_{ATP} channels that could lead to the development of new therapeutics for glucose disorders, which would lack side-effects associated with common treatments.

Kir7.1: Kir7.1 encoded by *KCNJ13* is expressed in various organ systems including, the brain, eyes, thyroid, the gut and kidney [1]. As opposed to most Kir channels, Kir7.1 exhibits a low single channel conductance in the order of femtosiemens (i.e. ~50 fS). Kir7.1 channels dysfunction is associated with instance of snowflake vitreoretinal degeneration [1,3]. While our knowledge on Kir7.1 channel functions remains limited, recent evidence suggests that it could represent a novel target for post-partum hemorrhage (Jerod Denton, personal communication).

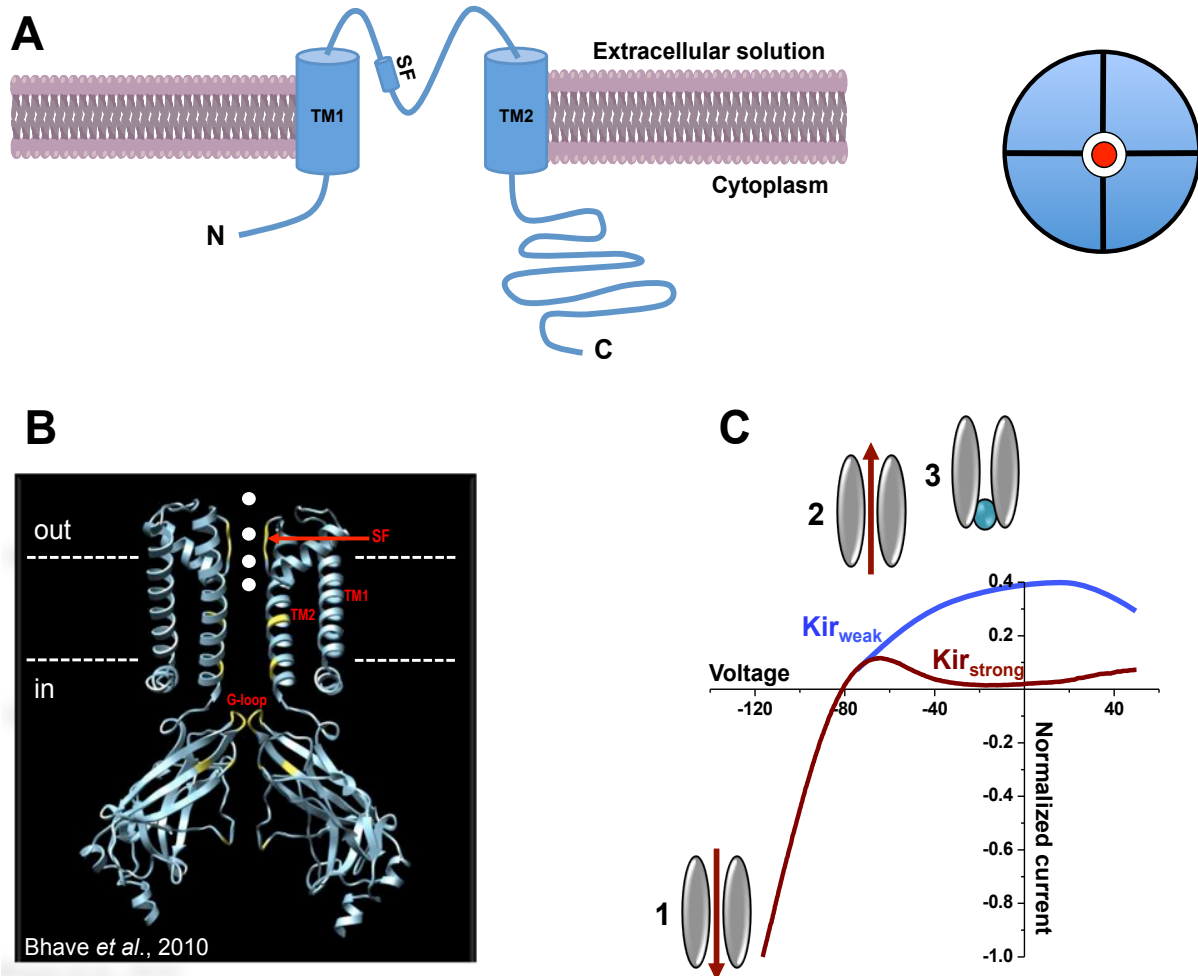


Figure 1. Overall Kir channel structure and characteristic currents. (A) *Left panel.* Schematic of a Kir channel subunit indicating the cytoplasmic N- and C-terminus domains, two transmembrane-spanning domains (TM1 and TM2) and the pore-forming loop with selectivity filter (SF). *Right panel.* Schematic of the tetrameric complex formed between homomeric Kir channel subunits. Potassium ions passing through the pore is indicated in red. (B) Homology model of the Kir1.1 channel. Two of the subunits are removed for clarity. Key structures are indicated as TM1 and TM2, SF and the G-loop. Adapted from Bhave et al., *Future Med Chem.* 2010 May;2(5):757-74. (C) Representative current-voltage relationships of Kir channel depicting currents generated by strong (red) and weak (blue) rectifiers. A schematic illustrating various stages of Kir channel current is shown as (1) inward current, (2) outward current and (3) pore block by divalent cations or polyamines.

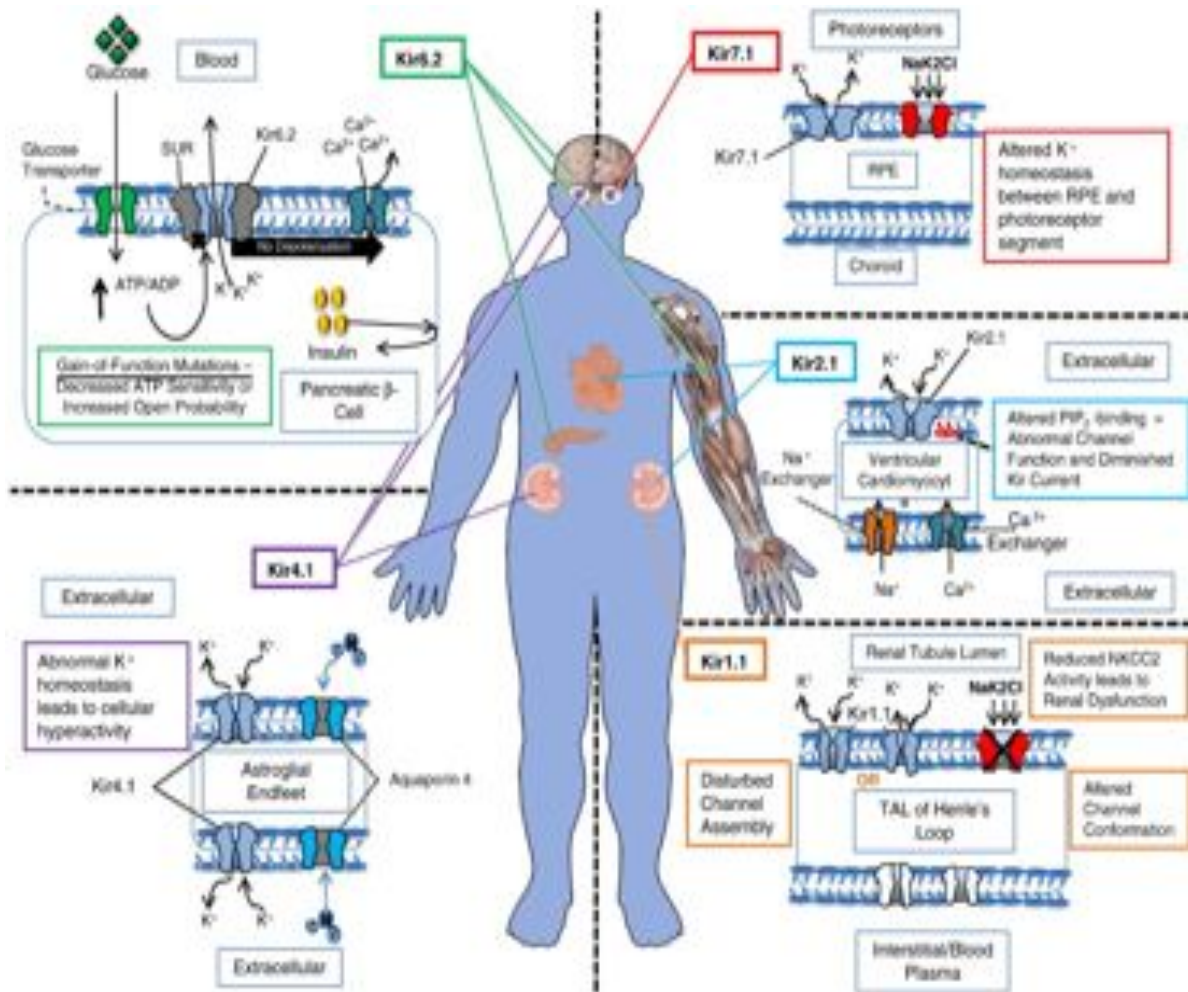
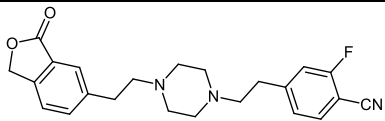
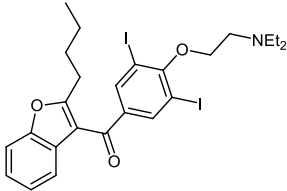
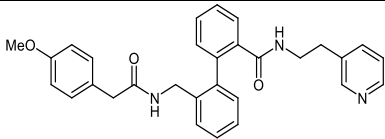
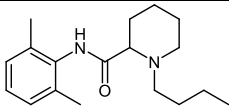
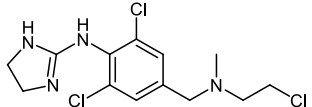
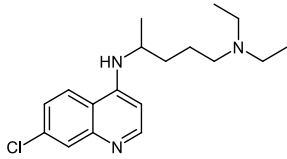
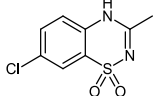


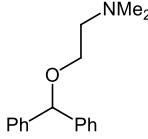
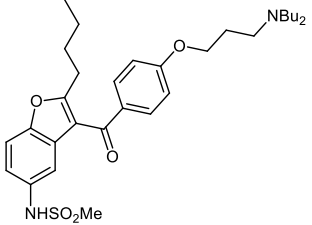
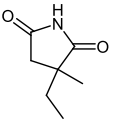
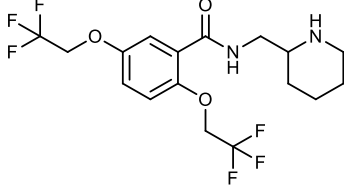
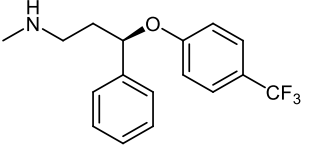
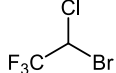
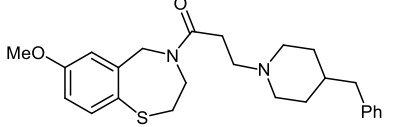
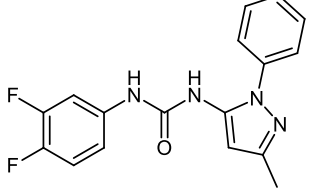
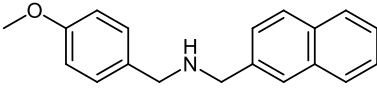
Figure 2. Tissue distribution of Kir channel subunits. The tissue-specific distribution of the Kir channels suggests that they play an important role in ion homeostasis and disease. Kir channel subunits are indicated by light blue within the membrane structure. All other possible associated channels, transporters and regulatory molecules are also shown in the membrane that controls cellular physiology. Kir channel tissue distribution along with their respective physiopathology is color-coded (Kir1.1 — orange; Kir2.1 — blue; Kir4.1 — purple; Kir6.2 — green and Kir7.1 — red). Abbreviations: Kir, inwardly rectifying potassium channel; SUR, regulatory sulfonyleurea receptor subunit; ATP, adenosine tri-phosphate; ADP, adenosine di-phosphate; RPE, retinal pigment epithelium; PIP₂, phosphatidylinositol (4,5)-bisphosphate; TAL, thick ascending limb. From Pattnaik, BR et al., *Mol Genet Metab.* 2012 Jan; **105**(1):64-72. Reproduced with authorization from Elsevier Science. License Number: 3363801001931.

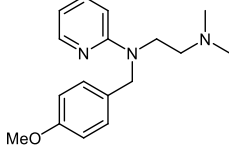
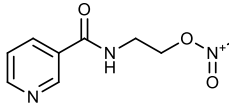
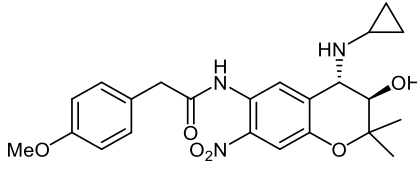
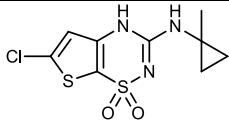
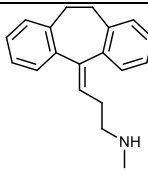
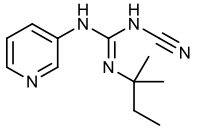
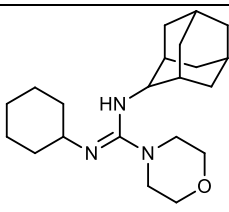
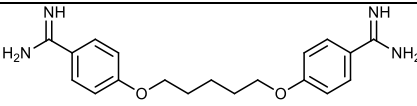
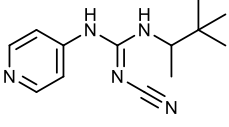
Pharmacology of Kir channels

While Kir channels have been suggested to represent important targets to for the development of novel therapeutics associated with channel dysfunction, pharmacological tools to investigate their functions and druggability are still limited. Indeed, the small-molecule pharmacology around the Kir channel family is largely comprised of weak and non-selective modulators. Shown in **Table 1** is reviewed a list, which is not exhaustive, of few modulators of Kir channels mostly representative of cardiovascular and neurological targets—exhibiting weak potency and non-tissue specific effects, as well as recently discovered small-molecules which result from high-throughput screening efforts.

Table 1. Kir channel modulators. Listed alphabetically with structure as indicated. IC₅₀ or EC₅₀ values accompanied by percent maximal inhibition/activation observed in parentheses. * indicates results obtained with heterologous expression in *Xenopus* oocytes which have been reported by some authors to yield significantly higher IC₅₀ values when compared to mammalian cells [33].**indicates results obtained from thallium flux experiments. Adapted from Bhawe G. et al., *Future Med Chem.*2010 May; 2(5): 757-74.

Compound	Structure	Kir Target	IC ₅₀ /EC ₅₀ (Max)	Selectivity	Refs.
30		Kir1.1	30-49 ^a nM	> Kir 2.1, 2.3 >> Kir4.1, Kir7.1 Known hERG blocker	[34]
Amiodarone		I _{KACH}	1.8-2.4 μM (100%)	Known voltage gated Na, K, and Ca channel blocker	[35]
AVE0118		I _{KACH}	4.5 μM (100%)	Known voltage gated K channel blocker	[36]
Bupivacaine		Kir3	22-170* μM Gβγ & voltage dependent (100%)	> Kir 1.1, 2.1 Known voltage gated Na & K channel blocker	[37]
Chloroethylclonidine		Kir2.1	37 μM (100%)	Known α ₂ adrenergic agonist	[38]
Chloroquine		Kir2.1	8.7 μM; voltage dependent (100%)	Unknown	[39]
Diazoxide (Kir activator)		Kir6.2/SUR1	31 μM (100%)	>Kir6.2/SUR2B, Kir6.2/SUR2A	[40]

Diphenhydramine		Kir2.3	689 μM^* (~80%)	> Kir 2.1 Known anti-histamine	[41]
Dronedarone		I_{KACH}	10-63 nM (100%)	Known voltage gated Na, K, and Ca channel blocker	[42]
Ethosuximide		Kir3	0.4-3.5* mM (61-76%)	> Kir 1.1, 2.1 Known voltage gated Ca & Na channel blocker	[43]
Flecainide (Kir activator)		Kir2.1	0.8 μM (22%)	>Kir2.2, Kir2.3, Kir2.1/2.2, Kir2.1/2.3	[44]
Fluoxetine		Kir3 Kir4.1	7-13* μM (58-74%) 15.2 μM (100%)	> Kir 1.1, Kir 2.1 Known SSRI	[45, 46]
Halothane		Kir3	60 μM^* (100%)	Unknown	[47]
JTV-519		I_{KACH}	0.1-2.5 μM (100%)	Known voltage gated Ca, Na, and K channel blocker	[48]
ML297 (Kir activator)		Kir3.1/3.2	0.54 μM (100%)	>Kir3.1/3.4> >Kir3.2/3.3, Kir2.1	[49]
ML133		Kir2.1	0.3 ^b -1.9 μM (100%)	> Kir2.6, 2.2, 2.3, 6.2 >>4.1, 7.1, 1.1 (>300)	[50]

Mepyramine		Kir2.3 Kir3.4	306 μM^* (~80%) < 300 μM^* (Unknown)	> Kir 2.1 Known anti-histamine	[41]
Nicorandil (Kir activator)		Kir6.2/SUR2 B	10 μM (100%)	>Kir6.2/SUR 2A	[51]
NIP-142		Kir3.1/3.4	0.64 μM (100%)	Unknown Blocks Kv1.5 with similar potency	[33]
NIP-151	Structure unavailable	Kir3.1/3.4	1.6 nM (100%)	Unknown HERG IC ₅₀ 58 μM	[52]
NN414 (Kir activator)		Kir6.2/SUR1	0.45 μM (100%)	>SUR2- containing K _{ATP}	[40]
Nortriptyline		Kir4.1	38 μM	> Kir 1.1, 2.1	[53]
P1075 (Kir activator)		Kir6.1- 6.2/SUR2B + Kir6.2/SUR2 B	0.16 μM (100%)	>Kir6.1/SUR 2A, Kir6.2/SUR1 >>Kir6.1/SU R1	[54]
PNU-37883A (Kir activator)		Kir6.1/SUR2 B Kir6.2/SUR2 B	6 μM (60%) 15 μM (80%)	>Kir6.2/SUR 1, Kir6.2/SUR2 A	[55]
Pentamidine		Kir2.1	0.2 μM (100%)	>Kir2.2, Kir2.3	[56]
Pinacidil (Kir activator)		Kir6.2/SUR2 A Kir6.2/SUR2 B	~2 μM (100%) ~10 μM (100%)	> SUR1- containing K _{ATP}	[51]

Pregnenolone sulfate (Kir activator)		Kir2.3	16 μM^* (80%)	> Kir1.1, 2.1, 3.1/3.2	[43]
SCH23390		Kir3	0.3-8 μM (100%)	Known D1 receptor antagonist	[57]
Tamoxifen		Kir2	0.3-0.9 μM (100%)	Unknown Known estrogen receptor antagonist	[58]
Tenidap (Kir activator)		Kir2.3	1.3 μM (100%)	> Kir 2.1	[59]
Thioridazine		Kir3	58 μM (92%)	Unknown Known anti- psychotic	[60]
Tricyclic Antidepressants (Nortriptyline)		Kir3 Kir4.1	18-71* μM (53-76%) 16-38 μM ; voltage dependent (100%)	> Kir 1.1, 2.1	[53, 61]
U50488H		Kir3	70 μM^* (100%)	Known κ opioid receptor agonist	[62]
VU0071063 (Kir activator)		Kir6.2/SUR1	7 μM (100%)	> Kir6.1/SUR1 >> Kir6.1/SUR2 A, Kir6.2/SUR2 A	[63]

VU573		Kir2.3 Kir3.x Kir7.1	0.8 μM (70%) 1.3 μM (80%) 0.9 μM (70%)	> Kir1.1, Kir2.1	[64]
VU590		Kir1.1	0.29 μM ** (100%)	> Kir7.1	[20]
VU591		Kir1.1	0.30 μM ** (100%)	> Kir2.1, Kir2.3, Kir4.1	[21]
VU717		Kir4.1	6-10 ** μM (100%)	Unknown	[65]
Vernakalant		I_{KACH}	10 μM (100%)	Known blocker of multiple voltage gated Na and K channels	[42]

^a At pH 8.5.

^b Obtained from $^{86}\text{Rb}^+$ assay.

Overview of Kir channels in mosquitoes

Vector-borne diseases, which are transmitted by infected female mosquitoes, such as malaria, yellow and dengue fevers or Chikungunya virus represent a major public health concern to more than half of the world's population. Current vector control strategies rely mostly on insecticide-treated bed nets and indoor residual spraying with pyrethroids, the dominant class of chemicals used as insecticides worldwide [66]. However, mounting evidences suggest that these strategies are becoming less effective because of the emergence of insecticide resistance in mosquito populations [67]. Furthermore, the efforts of public health organizations in endemic countries to curve the transmission of vector-borne diseases is greatly hindered by the fact that no new insecticides has been developed in the past 30 years [68]. Therefore, there is an urgent need to develop new and effective insecticides for implementing new control strategies.

In an effort to develop new chemicals for insecticidal use, and thus new vector control strategies, our laboratory has focused on targeting mosquito Kir channels. By engorging more than twice their own body weight in blood, mosquitoes are exposed to high physiological pressures to rapidly handle the excess fluid volume and salts (i.e. NaCl, KCl) from their hemolymph before succumbing as a result of their toxic effects. Therefore, mosquitoes possess an efficient excretory system, which include the Malpighian (renal) tubules and hindgut, involved in osmoregulation and urine excretion [69-71]. A barium sensitive-potassium conductive pathway was shown to play a critical role in fluid and salt excretion in isolated Malpighian tubules experiments [72,73]. These results suggested in part that Kir channels would be involved in osmoregulatory processes and could play other important functions in mosquito physiology. The aforementioned evidences have warranted for further investigations of the Kir channel functions in mosquitoes, and their target potential for insecticide development.

Molecular structure and functions of Kir channels

The genome of the *Aedes aegypti*, vector of the yellow and dengue fevers, contains five genes encoding putative Kir channels termed, *AeKir1*, *AeKir2A*, *AeKir2B*, *AeKir2B'* and *AeKir3*. The first *A. aegypti* Kir channels were recently cloned, notably Kir1, Kir2B and Kir3 subunits, and functionally characterized in *Xenopus laevis* oocytes [74]. Amino acid sequence alignments between human and mosquito Kir channels reveal similar conserved canonical features including two TMs and a GYG containing SF (refer to **Fig. 1**). With the exception of Kir3, both Kir1 and Kir2B form functional channels in oocytes exhibiting barium-sensitive currents. *AeKir1* expressing oocytes exhibit large inward rectifying currents (reminiscent of strong rectifiers), which are modulated by extracellular concentrations of K^+ and Na^+ ions. On the other hand, *AeKir2B* expressing oocytes exhibit weaker rectification and smaller inward rectifying currents, which are modulated by extracellular concentrations of K^+ ions (**Table 2**). To date, the mRNA expression of *A. aegypti* Kir genes has been detected using semi-quantitative RT-PCR in various tissues ranging from the Malpighian (renal) tubules, midgut, hindgut and head (**Table 2**) [75]. In vivo studies reveal that *A. aegypti* Kir channels are involved in physiological processes of osmoregulation and K^+ homeostasis. In **Chapter VII**, we discussed the cloning and functional characterization of the malaria vector, *Anopheles gambiae* Kir1 (AaKir1) channels and its possible implication in mosquito fecundity.

Table 2. Summary of qualitative assessment of *Aedes aegypti* Kir channel functions and tissue distributions. Functional expression was determined in *Xenopus laevis* oocytes as per current amplitude. Qualitative RT-PCR was used to determine tissues distribution. Functional and tissue distribution was scored as followed: +++, high; ++, moderate; +, low; –, no expression. ND, not determined; N/A, not applicable. Adapted from Piermarini PM et al, *Insect Biochem Mol Biol.* 2013 Jan; **43**(1):75-90.

Kir channels	Functional expression	Rectification property	Tissue distribution of mRNA
<i>AeKir1</i>	+++	Strong	Malpighian tubules ++
			Midgut –
			Hindgut –
			Head –
<i>AeKir2A</i>	ND	ND	Malpighian tubules +
			Midgut ++
			Hindgut ++
			Head +
<i>AeKir2B</i>	+	Weak	Malpighian tubules +++
			Midgut +++
			Hindgut ++
			Head –
<i>AeKir2B'</i>	ND	ND	Malpighian tubules +
			Midgut –
			Hindgut –
			Head +++
<i>AeKir3</i>	–	N/A	Malpighian tubules +++
			Midgut +++
			Hindgut –
			Head –

Pharmacology of Kir channels

To date, the small-molecule pharmacology for mosquitoes specific Kir channel modulators remain largely undeveloped. This lack of pharmacological tools is hampering efforts to assess the druggability of these channels for insecticide development. However, our drug discovery efforts for novel human Kir channel modulators have helped in identifying non-species selective small-molecules such as VU573 (**Chapter VI**) and mosquito specific small-molecule modulators (**Chapter VIII**) to begin to probe the integrative physiology of these channels in mosquitoes.

Objective

As summarized above, inward rectifier potassium (Kir) channels are important K^+ ion channels assuming essential physiological functions in humans. Moreover, we are beginning to uncover their physiological roles in insects, notably in mosquitoes, which we will focus in this dissertation. Therefore, Kir channels represent highly attractive molecular targets for developing not only new therapeutics for the treatment of pathologies linked to Kir channel dysfunction, but also new insecticides for controlling mosquito populations and reduce the transmission of vector-borne diseases. However, assessing the druggability of these targets has been hindered for the most part because of the lack of pharmacological tools or probe compounds with which to determine their therapeutic or insecticidal potentials. The development and implementation of high-throughput screening assays and modern drug discovery methodologies provide us with the resources to begin to fill this gap, and thus generate research tools (lead compounds) that will be used to investigate Kir channel functions both in vitro and vivo. The development of new small-molecule Kir channel modulators will ultimately benefit the research community to further probe

their integrative functions, which will guide drug discovery efforts in the setting of therapeutic and insecticide development. Subsequently, throughout the next chapters, we discuss our efforts to implement fluorescent-based high throughput screening assays for identifying and developing new small-molecule modulators of Kir channels with the goal to expand the pharmacology around this family and provide leads for therapeutic development. Furthermore, we present the first small-molecule discovery efforts aiming to investigate the insecticidal potentials of mosquito Kir channels. Lastly, using genetic tools, we begin to uncover new functions of these channels in mosquito physiology.

Notes on figures and tables

In the next chapters, the numbering of all figures and tables is specific for each chapter. For instance, “Figure 1” will be the first figure of a specific chapter, and so on. This formatting is designed to help the reader in quickly identifying visual materials of interest.

Chapter II

HIGH-THROUGHPUT SCREENING FOR SMALL-MOLECULE MODULATORS OF INWARD RECTIFIER POTASSIUM CHANNELS

This chapter was published under the same title in the *Journal of Visualized Experiments* in the January 27th, 2013 issue

Abstract

Specific members of the inward rectifier potassium (Kir) channel family are postulated drug targets for a variety of disorders, including hypertension, atrial fibrillation, and pain [76,77]. For the most part, however, progress toward understanding their therapeutic potential or even basic physiological functions has been slowed by the lack of good pharmacological tools. Indeed, the molecular pharmacology of the inward rectifier family has lagged far behind that of the S4 superfamily of voltage-gated potassium (Kv) channels, for which a number of nanomolar-affinity and highly selective peptide toxin modulators have been discovered [78]. The bee venom toxin tertiapin and its derivatives are potent inhibitors of Kir1.1 and Kir3 channels [79,80], but peptides are of limited use therapeutically as well as experimentally due to their antigenic properties and poor bioavailability, metabolic stability and tissue penetrance. The development of potent and selective small-molecule probes with improved pharmacological properties will be a key to fully understanding the physiology and therapeutic potential of Kir channels. The Molecular Libraries Probes Production Center Network (MLPCN) supported by the National Institutes of Health (NIH) Common Fund has created opportunities for academic scientists to initiate probe discovery campaigns for molecular targets and signaling pathways in need of better

pharmacology [81]. The MLPCN provides researchers access to industry-scale screening centers and medicinal chemistry and informatics support to develop small-molecule probes to elucidate the function of genes and gene networks. The critical step in gaining entry to the MLPCN is the development of a robust target- or pathway-specific assay that is amenable for high-throughput screening (HTS). Here, we describe how to develop a fluorescence-based thallium (Tl^+) flux assay of Kir channel function for high-throughput compound screening [20,21,64,82]. The assay is based on the permeability of the K^+ channel pore to the K^+ congener Tl^+ . A commercially available fluorescent Tl^+ reporter dye is used to detect transmembrane flux of Tl^+ through the pore. There are at least three commercially available dyes that are suitable for Tl^+ flux assays: BTC, FluoZin-2, and FluxOR [20,82]. This protocol describes assay development using FluoZin-2. Although originally developed and marketed as a zinc indicator, FluoZin-2 exhibits a robust and dose-dependent increase in fluorescence emission upon Tl^+ binding. We began working with FluoZin-2 before FluxOR was available [20,82] and have continued to do so [21,64]. However, the steps in assay development are essentially identical for all three dyes, and users should determine which dye is most appropriate for their specific needs. We also discuss the assay's performance benchmarks that must be reached to be considered for entry to the MLPCN. Since Tl^+ readily permeates most K^+ channels, the assay should be adaptable to most K^+ channel targets.

Video link

The video component of this chapter can be found at <http://www.jove.com/video/4209/>

Experimental Protocol

Generation of stable polyclonal cell lines

The establishment of a high quality stable cell line expressing the Kir channel of interest is an important first step toward developing a robust high-throughput screening assay. Constitutive K⁺ channel overexpression can lead to activation of cell death pathways, stable cell line degeneration and loss of assay performance. To avoid these potential problems and provide a convenient internal control for assay development (see below), a tetracycline-inducible expression system is recommended [20].

Culture the parental T-REx-HEK293 cells using standard techniques in B-medium (DMEM growth medium containing 10% FBS, 50 U/mL Penicillin, 50 µg/ml Streptomycin and 5 µg/mL Blasticidin S). Use early passage cells (*e.g.* 3-4 passages since thawing from liquid nitrogen storage) for transfection and stable clone selection.

Plate 4 million T-REx-HEK293 cells in a 75 cm² flask so that the flask is approximately 80% confluent the following day. Culture overnight in a 5% CO₂ incubator at 37 °C.

Transfect the cells using 10-15 µg of pcDNA5/TO-Kir DNA and Lipofectamine LTX/Plus reagent according to manufacturer's protocol. After 5 hours, replace the transfection medium with B-medium.

24 hr after the transfection, replace the B-medium with B-medium containing 250 µg/mL Hygromycin (BH-medium) to begin stable clone selection. Feed the cells every 2-3 days with fresh BH-medium.

Greater than 90% of the cells should die over the next 7 days, leaving behind small colonies of stably transfected cells. Allow the colonies to grow for an additional 10-14 days before splitting to a 175 cm² flask for expansion.

For cryopreservation, freeze 3 x 10⁶ cells/mL in media containing 45% conditioned BH-medium, 45% antibiotic-free, serum-containing DMEM and 10% DMSO. Freeze the cells overnight at -80 °C in a cell freezing container and then move to liquid nitrogen for long-term storage. Thaw cells from liquid nitrogen using Invitrogen's recommended protocol. Note that the viability of the cells will be lower if they are frozen from a flask that is greater than 75% confluent at the time of processing.

Generation of stable monoclonal cell lines

Wash a sub-confluent 75 cm² flask of stable polyclonal cells with divalent-free HBSS. Add 1 mL of trypsin and incubate for 3-5 min in a 5% CO₂ incubator at 37 °C. Add 5 ml of BH-medium to the flask to inhibit trypsin activity and triturate repeatedly (*e.g.*, 5 times) to fully dissociate the cells. Carefully inspect the cells under a microscope to ensure the suspension consists almost entirely of single cells. This will increase the likelihood of obtaining monoclonal cell lines.

Determine the cell density and dilute the suspension to a concentration of 0.7 cells per 20 µL. Using a multi-channel pipettor, pipette 20 µL of the cell suspension into each well of BD PureCoat amine-coated (or equivalent poly-D-lysine coated) 384-well plates. In principle, 70% of wells should receive one cell with these plating conditions. Thus, a 384-well plate should contain more than 200 clones to analyze. Continue culturing the cells in a 5% CO₂ incubator at 37 °C.

After a week, inspect the plates under a microscope for wells containing single colonies. Note their position on the lid with a permanent marker for future reference. Be sure to also note and exclude wells containing multiple colonies. These are most easily recognized by the appearance of colonies growing from multiple sides of the well. Be aware that evaporation tends to occur more quickly from wells near the edge of the plate. Add BH-medium to wells where significant evaporation has occurred. Otherwise, it is unnecessary to feed the cells.

Monitor the wells more frequently during the next 7-10 days. The cells will be ready to split when the wells of interest are at least 50% confluent.

Split the cells to duplicate 384-well plates; one plate for assaying with TI^+ flux and the other for continuing the monoclonal lines in culture. Aspirate the medium from the wells containing the cell lines of interest. Wash the cells with divalent-free HBSS, add 20 μL of trypsin to each well and transfer the plate to a 37 °C incubator for 15-20 min. After moving the plate back to the cell culture hood, add 20 μL of BH-medium to each well and triturate several times to dissociate the cells. Inspect the wells under a microscope to ensure the cells are fully dissociated. This may require multiple rounds of pipetting, as the cells will be tightly adherent. Once the cells are dissociated, transfer 10 μL of each cell suspension to duplicate wells of a new BD PureCoat amine-coated 384-well plate. Be sure to note the relationship between the source well and duplicate destination wells so that the clones exhibiting robust Kir channel activity (see below) can be traced back to the original well. Add 20 μL of BH-medium to the original source well to feed the remaining cells and continue them in culture in 5% CO_2 incubator at 37 °C.

Allow the cells in the destination plate to adhere and grow for up to a week. Once most of the clones reach at least 50% confluence, they can be assessed for Kir channel activity using the TI^+ flux assay described below.

The day before the assay, aspirate the culture medium and replace it with BH medium containing 10% dialyzed FBS. This prevents inadvertent channel expression that could arise from tetracycline contaminated serum. Induce Kir channel expression in only one of the duplicate wells for each clone by including 1 $\mu\text{g}/\text{mL}$ tetracycline. The duplicate uninduced well will serve as a "background" control. Perform the TI^+ flux assays as described next.

General TI^+ flux assay procedure

The day before a TI^+ flux experiment, dissociate the cells and quantitate the density of the cell suspension as described in sections 2.1 and 2.2. Plate 20,000 monoclonal cells stably transfected with a Kir channel gene of interest in each well of a BD PureCoat amine-coated 384-well plate using a Thermo Multidrop Combi or a multi-channel pipettor. Use BH medium containing 10% dialyzed FBS for plating. Note that some cells will be cultured overnight with 1 $\mu\text{g}/\text{mL}$ tetracycline to induce Kir channel expression, whereas others will not. The location of induced and uninduced cells will differ for each type of experiment and are shown in **Fig. 1**.

The next day, inspect the plates under a microscope to ensure that the cells are adherent and evenly distributed across the bottom of the wells. The wells should be 80-90% confluent.

Use an ELx405 Microplate Washer to replace the cell culture medium with 20 μL per well of HBSS assay buffer containing 20 mM HEPES and buffered to pH 7.3 with NaOH. Alternatively, one can use a "flick and slam" method, wherein the plate is inverted and snapped down sharply to eject the medium into a waste container, and then patted onto stacked paper towels to remove the remaining media. Immediately add back HBSS assay buffer to the plate to prevent the cells from desiccating.

Prepare the FluoZin-2, AM dye loading solution. After briefly centrifuging the tube, dissolve 50 μg of FluoZin-2 powder in 100 μL of anhydrous DMSO. At this point, aliquots of the 1,000x stock solution can be stored at $-20\text{ }^{\circ}\text{C}$ for later use. When ready to use, add 50 μL of a 20% weight per volume Pluronic F-127/DMSO solution to the dye and mix with gentle pipetting. Do not freeze the dye once Pluronic F-127 has been added, as low temperature may cause the surfactant to precipitate out of solution. Add the 150 μL volume of FluoZin-2, AM/Pluronic-F127 to 100 mL of HBSS assay buffer and mix gently to make the dye loading buffer. Using a Multidrop Combi or multi-channel pipettor, add 20 μL of dye loading buffer to each well already containing 20 μL of HBSS assay buffer. Incubate the cells at room temperature for approximately 1 hr (typically incubation has been done in the dark, although there is no direct evidence that it is necessary).

While the cells are loading with dye, prepare a TI^+ stimulus plate. Freshly dissolve 0.5 g of sodium bicarbonate in 50 ml of 5x TI^+ stimulus buffer containing 1 mM magnesium sulfate, 1.8 mM calcium sulfate, 5 mM glucose, 10 mM HEPES and 12 mM TI^+ sulfate. Alternatively, sodium bicarbonate can be replaced with sodium gluconate if, for example, the solution pH must be kept within a very narrow range and loss of carbon dioxide is a concern. Cap the tube tightly to limit the escape of carbon dioxide and invert several times until the sodium bicarbonate goes into solution. Using a multi-channel pipettor, add 50 μL of the solution to each well of a polypropylene 384-well plate (**Table 1**).

After the cells have been loaded with FluoZin-2, AM, wash the plates with an ELx405 Microplate Washer or using the "flick and slam" method, as described above in section 3.3. Depending on the type of TI^+ flux experiment to be performed, add back 20 μL or 40 μL of HBSS assay buffer to each well. The plates are now ready for experiments.

Load the cell and TI^+ plates into a Hamamatsu Functional Drug Screening System (FDSS) or equivalent kinetic imaging plate reader with integrated liquid dispensing capabilities. Use appropriate filters for fluorescein/fluorescein-based dyes such as Fluo-4.

Set up a single-add protocol so that 10 μL the 5x TI^+ series is added to the corresponding wells of the cell plate containing 40 μL of HBSS assay buffer. Record baseline fluorescence at a 1 Hz sampling frequency for at least 10 sec. The well-to-well fluorescence should be uniform and stable across the plate once optimal cell plating, washing and dye loading conditions are established. An integrated 384-channel pipettor is used to simultaneously add the TI^+ stimulus buffer to each well.

Record for at least 2 min so that the rate and peak of the TI^+ -induced increase in fluorescence is captured for off-line analysis.

Determination of optimal TI^+ concentration

TI^+ readily permeates most inward rectifier K^+ channels. To ensure that TI^+ concentrations do not exceed the dynamic range of the TI^+ reporter dye FluoZin-2, one should empirically determine the optimal TI^+ concentration to be used in a high-throughput screen. We recommend a TI^+ concentration that evokes 80% of the maximal fluorescence response (EC_{80}) under conditions where the channel is maximally activated.

Plate, dye load and wash the cells in BD PureCoat amine-coated or equivalent poly-D-lysine-coated 384-well plates as described above in section 3, leaving 40 μL of HBSS assay buffer in each well. As shown in the plate map in **Fig. 1A**, column 1 and rows A1-A23 should contain cells that have not been induced with tetracycline and therefore do not express the Kir channel of interest. The FluoZin-2 fluorescence signals from the uninduced wells will be used to

determine the level of TI^+ flux through endogenous pathways, such as the $\text{Na}^+ - \text{K}^+$ -ATPase pump and voltage gated K^+ channels, which are normally expressed in HEK-293 cells.

Use an Agilent Bravo Automated Liquid Handling Platform or manual pipetting to prepare an eleven-point TI^+ concentration dilution series in HBSS assay buffer. Typically, a 3-fold serial dilution series ranging from 100% to 0.002% TI^+ is evaluated in the assay. The series should be made up at a 5x concentration because the TI^+ solutions will be diluted 1:5 in the final assay. Prepare the dilution series by diluting the standard 5x TI^+ buffer described in section 3 with a 5x TI^+ -free buffer containing 1 mM magnesium sulfate, 1.8 mM calcium sulfate, 5 mM glucose and 10 mM HEPES. Again, freshly dissolve 0.5 g of sodium bicarbonate in 50 ml of the final TI^+ buffer immediately before plating in a polypropylene 384-well plate according to the plate map shown in **Fig. 2A**.

Load the cell and TI^+ stimulus plates into the FDSS. Set up a single-add protocol so that 10 μL the 5x TI^+ series is added to the corresponding wells of the cell plate containing 40 μL of HBSS assay buffer. Record baseline FluoZin-2 fluorescence for 10 sec before adding TI^+ to the plate. Repeat the experiment on 3 separate days to establish the reproducibility of the results.

Determination of assay sensitivity to DMSO

The small molecules interrogated in a high-throughput screen are dissolved in the organic solvent dimethyl sulfoxide (DMSO), which itself can affect the performance of the assay. Therefore, the assay's sensitivity to DMSO must first be examined to establish the highest DMSO concentration allowable in the screen.

Plate, dye load and wash the cells in BD PureCoat amine-coated 384-well plates as described above in section 3, leaving 20 μL of HBSS assay buffer in each well. The entire plate should contain cells that have been induced with tetracycline (**Fig. 3A**).

Use a Bravo Automated Liquid Handling Platform or manual pipetting to prepare an eleven-point DMSO concentration dilution series in HBSS assay buffer. Typically, a 2-fold dilution series ranging from 10% to 0.01% v/v DMSO is evaluated for activity in the assay. The series should be made up at a 2x concentration because the DMSO solutions will be diluted by half in the final assay. The dilution series should be plated in a polypropylene 384-well plate, according to the plate map shown in **Fig. 3A**.

Prepare a 5x TI^+ stimulus plate based on the EC_{80} or optimal TI^+ concentration determined above in “**Determination of optimal TI^+ concentration.**”

Load the cell, DMSO and TI^+ stimulus plates into the FDSS. Set up a two-add protocol so that 20 μL of the 2x concentration DMSO series is added to the corresponding wells of the cell plate containing 20 μL of HBSS assay buffer. Leave the DMSO on the cells for the same amount of time the cells will be exposed to small molecule vehicle during a screen. Record baseline FluoZin-2 fluorescence for at least 10 sec before adding 10 μL of 5x TI^+ buffer to each well of the cell plate. Repeat the experiment on 3 separate days to establish the reproducibility of the results.

The assay should be tolerant to DMSO concentrations of at least 0.1% v/v for a typical high-throughput screen in which compounds are tested at a concentration of 10 μM .

Determination of assay sensitivity to known pharmacological modulators

After determining the optimal TI^+ concentration and DMSO tolerance of the assay, the effects of known pharmacologically active agents on Kir channel-mediated TI^+ flux should be examined. This series of experiments will assess the assay's sensitivity, ability to rank-order compounds based on their potency, ability to categorize compounds based on their mode of efficacy (e.g. activator, inhibitor), and identify well-behaved control compounds to be used later in the assay development and screen.

Plate, dye load and wash the cells in BD PureCoat amine-coated 384-well plates as described above in section 3, leaving 20 μL of HBSS assay buffer in each well. Column 1 and rows A1-A23 should contain cells that have not been induced with tetracycline (**Fig. 4A**).

Use a Bravo Automated Liquid Handling Platform or manual pipetting to prepare an eleven-point concentration dilution series of known modulators in HBSS assay buffer. Typically, a 3-fold dilution series ranging from 100 μM to 2 nM is evaluated for activity in the assay. The series should be made up at a 2x concentration because the DMSO solutions will be diluted by half in the final assay. The dilution series should be plated in triplicate in a polypropylene 384-well plate, according to the plate map shown in **Fig. 4A**. Be sure that the dilutions are made such that the final DMSO concentrations are the same between drug treatments and less than or equal to the maximum allowable DMSO concentration defined in section 5.

Prepare a 5x TI^+ stimulus plate based on the optimal TI^+ concentration determined above in **“Determination of optimal TI^+ concentration.”**

Load the cell, compound and TI^+ stimulus plates into the FDSS. Set up a two-add protocol so that 20 μL the 2x concentration compound series is added to the corresponding wells of the cell plate containing 20 μL of HBSS assay buffer. Add the compounds to the cell plate and incubate for up to 20 min. Note that the optimal incubation time for the compounds to detect the

best signal to background ratio can be determined by running a series of experiments where couple different incubation times are chosen. Record baseline FluoZin-2 fluorescence for at least 10 sec before adding 10 μL of 5x TI^+ buffer to each well of the cell plate. Repeat the experiment on 3 separate days to establish the reproducibility of the results.

Checkerboard Analysis

In the next series of experiments, the uniformity and reproducibility of the assay will be evaluated using a "checkerboard" analysis. Typically, a control inhibitor is plated in every other well of each column and row of a 384-well plate, as shown in **Fig. 5A**. To rigorously assess the noise in the assay, an EC_{80} concentration of inhibitor should be used. DMSO is added to the other wells as a vehicle control. TI^+ flux in DMSO- and drug-treated cells is used to calculate a value for Z' prime (Z'), a statistical measure of well-to-well variability between the two populations of wells. Z' is calculated using the formula:

$$Z' = 1 - (3\text{SD}_p + 3\text{SD}_n) / |\text{mean}_p + \text{mean}_n|$$

where SD is standard deviation, p is uninhibited flux and n is fully inhibited flux values. An assay with Z' values greater than or equal to 0.5 on 3 separate days is considered suitable for high-throughput screening.

Plate, dye load and wash the cells in BD PureCoat amine-coated 384-well plates as described above in section 3, leaving 20 μL of HBSS assay buffer in each well. Note that the entire plate should be induced with tetracycline.

Make a compound/DMSO plate by pipetting into a 384-well polypropylene plate using a multi-channel pipettor, 80 μL /well of a known inhibitor of the target Kir channel at the

concentration determined in section 6.5, and 0.1% v/v DMSO vehicle as shown in **Fig. 5A**. Add the known inhibitor starting in well A1 using the multi-channel pipettor and alternate to well B2 and so on up to well B24. Repeat this procedure with DMSO starting in well B1 and so on up to well A24. The final layout of the plate should match that of a checkerboard.

Prepare a 5x TI^+ stimulus plate based on the optimal TI^+ determined above in **“Determination of optimal TI^+ concentration.”**

Load the cell, compound and TI^+ stimulus plates into the FDSS. Set up a two-add protocol so that 20 μL the 2x concentration compound series is added to the corresponding wells of the cell plate containing 20 μL of HBSS assay buffer. Add the compounds to the cell plate and incubate for up to 20 min at room temperature. Record baseline FluoZin-2 fluorescence for at least 10 sec before adding 10 μL of 5x TI^+ buffer to each well of the cell plate. Repeat the experiment on 3 separate days to establish the reproducibility of the results.

Pilot Screen

In the final stage of assay development, perform a pilot screen of a few thousand compounds to evaluate the assay's performance under conditions that will be used eventually in the large-scale high-throughput screen.

Plate, dye load and wash the cells in BD PureCoat amine-coated 384-well plates as described above in section 3), leaving 20 μL of HBSS assay buffer in each well. Note that the entire plate should be cultured overnight with tetracycline to induce Kir channel expression.

Select approximately 2,000 to 3,000 structurally diverse compounds to be tested. It is often appropriate and convenient to use compounds collections with known activities potentially enriched for ion channel modulators. Such collections include the Spectrum Collection

(MicroSource) and the LOPAC collection (Sigma). In addition, it is prudent to include known modulators of the Kir of interest in the pilot screen. Ideally, these compounds will be added to wells in a blinded fashion in order to allow an unbiased testing of the hit picking methods described later. Prepare the compounds in 384-well polypropylene plates (destination plates) using a Labcyte Echo Liquid Handler or suitable pin tool to transfer an appropriate volume of selected compounds in DMSO from the MLPCN collection (source plates) to the destination plates. Note that test compounds are only in columns 3-22; in every other well of columns 1, 2, 23, 24 add a known inhibitor at a concentration known to fully inhibit the Kir as determined in section 7. In the remaining wells of columns 1, 2, 23, and 24 add the appropriate volume of DMSO to produce DMSO concentration-matched vehicle controls. Dilute all wells with Assay Buffer using the Multidrop Combi. Typically test compounds will be 20 μ M, 2-fold above their target screening concentration.

Make TI^+ stimulus plates based on the optimal TI^+ concentration determined above in **“Determination of optimal TI^+ concentration.”**

Execute the pilot screen. Take care to stagger steps of the protocol's execution to maintain consistent timing between plates in the pilot screening run.

Once the pilot screen is completed, analyze the checkerboard wells from columns 1, 2, 23, and 24 using the Z' equation. Inspect plates that show Z' values of less than 0.5 to determine the source of poor separation of control populations. Hits can be selected using a number of methods. For pilot screens it is common to calculate the mean and standard deviation of the vehicle control population and pick hits based on wells producing values ≥ 3 standard deviations from the mean of the vehicle controls.

Following hit picking, retest selected hits in duplicate in 2 sets of plates. One set of plates contains the stable Kir cell in the absence of tetracycline and the other contains the stable Kir cell line in the presence of tetracycline. Hits that retest positive in at least one of the two retest plates and fail to show significant activity in the uninduced plates may be considered verified hits. Examine the verified hit list to determine how many of the "hidden" control samples were detected. Failure to detect the controls in the pilot screen indicates the need for further optimization of screening or hit-picking parameters.

Representative Results

The use of a tetracycline-inducible expression system provides a convenient internal control for distinguishing TI^+ flux through endogenous pathways and the Kir channel of interest. **Figure 1** shows some examples of cell plating maps used in different types of experiments. The positions of wells containing uninduced or tetracycline-induced cells are indicated with different colors. **Figure 2A** shows the source plate map used to determine the optimal TI^+ concentration for assay development and compound screening. The color gradient represents the 3- fold dilution series ranging from 100% to 0.002% TI^+ . A representative fluorescence intensity map is shown in **Fig. 2B**, with cool-to-hot colors indicating low-to-high TI^+ flux values, respectively. The cell plating map shown in **Fig. 1C** was used for this experiment. A fit of a 4-parameter logistic function to the TI^+ CRC (**Fig. 2C**) is used to determine an EC_{80} value of 15% TI^+ . **Figure 3A** shows the source plate map used to determine the DMSO tolerance of an assay. Columns 1 and 24 contain assay buffer only, whereas the color gradient indicates the 2-fold dilution series ranging from 10% to 0.01% DMSO. A representative fluorescence intensity map is shown in **Fig. 3B**, with low TI^+ flux values indicated with darker blue. The cell plating map shown in **Fig. 1B**

was used in this experiment. The average TI^+ flux values recorded from wells containing the indicated concentrations of DMSO are summarized in **Fig. 3C**. The data are plotted as the percentage of TI^+ flux recorded in the absence of DMSO. For this particular Kir channel, DMSO concentrations up to 2.5% had no effect on TI^+ flux and can therefore be used in experiments. **Figure 4A** shows the source plate map used to establish concentration-response curves for known inhibitors of a Kir channel. Each compound is indicated with a different color and is typically plated as a 3-fold dilution series. A representative fluorescence intensity map is shown in **Fig. 4B**. The cell plating map shown in **Fig. 1C** was used for this experiment. A representative experiment showing dose dependent inhibition of TI^+ flux by an inhibitor is shown in **Fig. 4C**. The robustness of an assay is determined in so-called "checkerboard" assays, which are summarized in **Fig. 5**. In the source plate map shown in **Fig. 5A**, a maximally effective concentration of an inhibitor or 0.1% DMSO as a vehicle control are plated in alternating wells. **Figure 5B** shows a representative fluorescence intensity map. A scatter plot of the peak TI^+ flux recorded from individual wells is plotted in **Fig. 5C**. The mean fluorescence values are indicated with solid line, whereas 3 standard deviations are indicated with a dotted line. The Z' value, a statistical measure of how well separated the two cell populations are separated, calculated for this plate is 0.75, which is well above the 0.5 threshold required for high-throughput screening.

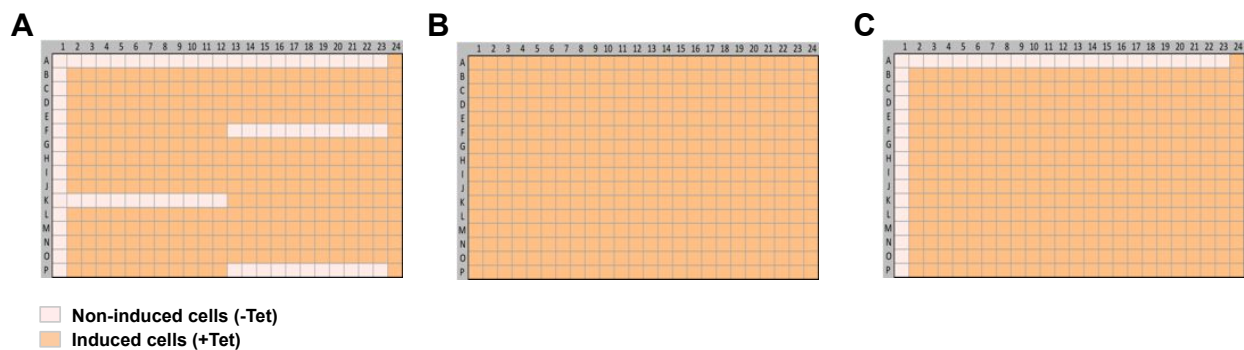


Figure 1. Cell plating maps used for TI⁺ flux assay development. (A) Cell plating map use to determine the optimal assay TI⁺ concentration. The wells in column 1, rows A1-23, K1-12, F13-23, and P13-23 contain uninduced cells (-Tet). The remaining wells contain cells that were treated with tetracycline (+Tet) to induce Kir channel expression. (B) Cell plate map use to determine the assay DMSO tolerance and perform checkerboard analysis. Note that all the wells are treated with tetracycline (+Tet). (C) Cell plate map used to determine the assay sensitivity to known pharmacological modulators. The wells in column 1 and row A1-23 contain uninduced cells (-Tet). The remaining wells contain cells that were treated with tetracycline (+Tet).

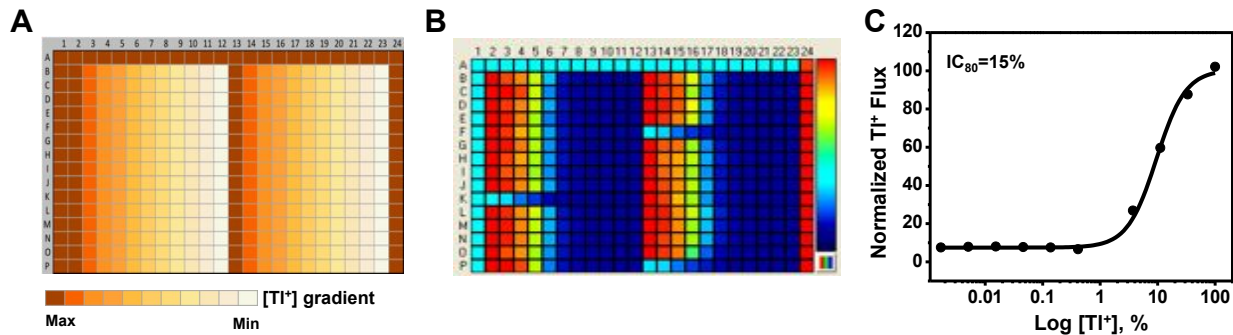


Figure 2. Determination of optimal assay TI⁺ concentration. (A) Source plate map used to determine the TI⁺ concentration that evokes approximately 80% of the maximal FluoZin-2 fluorescence increase (EC₈₀). Row A and columns 1 and 24 (yellow) contain a 5x concentration of 12 mM TI₂SO₄. The remaining rows contain a 3-fold dilution series ranging from 12 mM (100%) to 0.024 mM (0.002%) TI₂SO₄. The series is repeated in columns 2-12 and 13-23. (B) Fluorescence intensity map depicting TI⁺ flux for each well approximately 1 min after TI⁺ addition. The pseudo-color bar on the right indicates the extent of TI⁺ flux, with cooler and hotter colors representing low and high flux values, respectively. Note that the cooler colors in column 1, rows A1-23, K1-12, F13-23, and P13-23 are due to low TI⁺ flux in uninduced cells. The remaining wells, including those in column 24, contain cells that were treated with tetracycline to induce Kir channel expression (see cell plating map in Fig. 1A). (C) Mean ± SEM CRC for TI⁺-dependent changes in fluorescence (n = 3). Fitting a four-parameter logistic function to the data yielded an IC₈₀ value of 15% TI⁺.

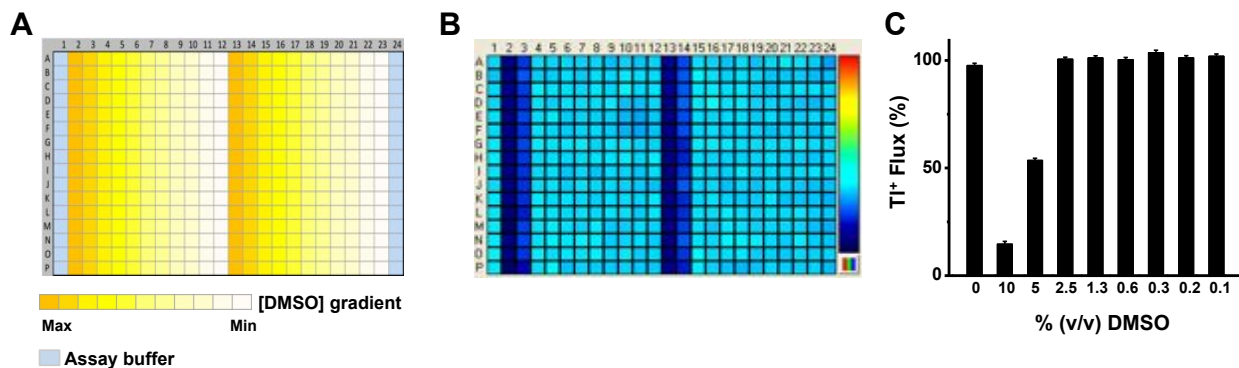


Figure 3. Assay tolerance to DMSO. (A) Source plate map used to determine assay tolerance to DMSO. Columns 1 and 24 contain HBSS assay buffer. The rows contain a 2x concentration of a 2-fold DMSO dilution series ranging from 10% to 0.01% v/v. (B) Representative fluorescence intensity map depicting Tl^{+} flux in each well recorded approximately 1 min after Tl^{+} addition. The pseudo-color bar on the right indicates the extent of Tl^{+} flux, with cooler and hotter colors representing low and high flux values, respectively. (C) Mean \pm SEM (n = 9) Tl^{+} flux normalized to that recorded in the presence of HBSS assay buffer alone.

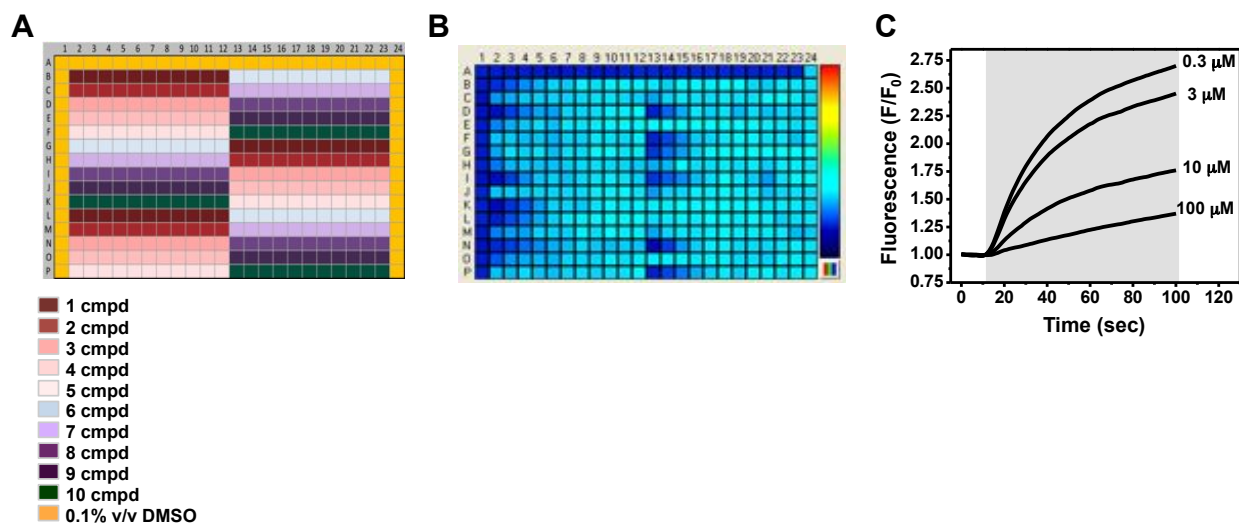


Figure 4. Assay sensitivity to known pharmacologically active compounds. (A) Source plate map used to assess the activity of known pharmacologically active compounds in the TI^+ flux assay. Row A and columns 1 and 24 contain 0.1% v/v DMSO. The plate layout allows for the testing of 10 compounds in triplicate in columns 2-23. The rows contain a 2x concentration of a 3-fold serial dilution series of compounds ranging from 100 μM to 2 nM. (B) Fluorescence intensity map depicting TI^+ flux for each well approximately 1 min after TI^+ addition. The pseudo-color bar on the right indicates the extent of TI^+ flux, with cooler and hotter colors representing low and high flux values, respectively. Note that wells in column 1 and row A1-23 contain uninduced cells. The remaining wells contain tetracycline-induced cells expressing the Kir channel of interest (See cell plate map in **Fig. 1C**). (C) Representative TI^+ -induced changes in FluoZin-2 fluorescence in wells pre-treated with the indicated concentration of a Kir channel inhibitor.

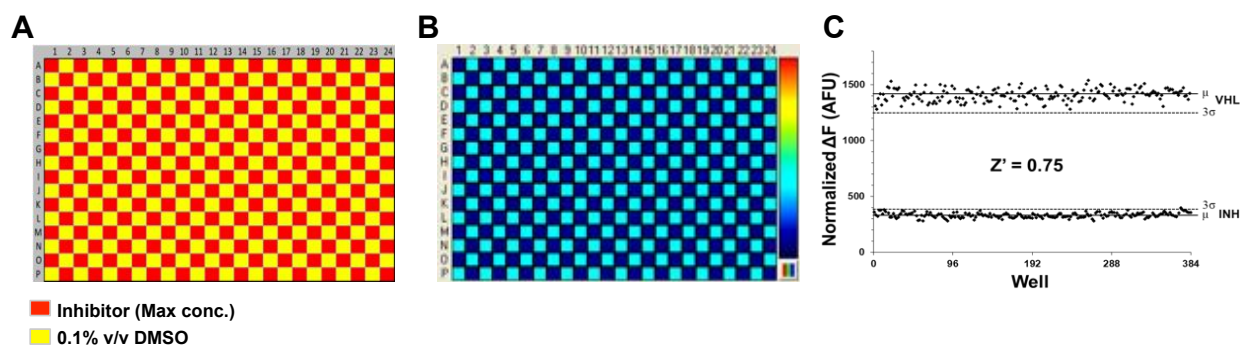


Figure 5. Determination of assay suitability for HTS. (A) Source plate map used to evaluate the well-to-well variability among wells containing 0.1% DMSO (vehicle) or a maximally effective concentration of a known inhibitor. (B) Fluorescence intensity map depicting Tl^+ flux in each well approximately 1 min after Tl^+ addition. Note that all wells contain tetracycline-induced cells expressing the Kir channel of interest (See cell plate map in **Fig. 1B**). (C) Representative scatter plot of steady-state fluorescence values obtained from vehicle- or inhibitor-treated wells. The mean fluorescence amplitude of each sample population is indicated with a solid line, 3 standard deviations from the mean is shown with a dashed line, and alternating samples for vehicle (VHL) and inhibitor (INH) are graphed as individual points.

Discussion

Once the data are collected, a common step in the analysis involves normalizing each well's fluorescence response, F , to its initial value at the beginning of the experiment, F_0 . This is commonly referred to as the "static ratio" and symbolized " F/F_0 ". In cases where F_0 is dominated by the indicator dye the static ratio operation will substantially correct for many factors such as disuniformities in illumination, signal collection, and cell number. In cases where the dye signal is weak or background fluorescence or reflections in the system are high, the static ratio will not be effective unless the background can be appropriately dealt with prior to calculating the static ratio. After data normalization, it is typical to reduce the fluorescence waveform to a single value that will be used to quantify activity and pick hits. Most commonly, this will be done by fitting the data points in the 10 seconds following addition of TI^+ to obtain an initial slope of the evoked fluorescence increase. For hit picking, a popular approach is to assume that the vast majority of compounds in the test population are inactive (the null hypothesis is in force). A mean and standard deviation is calculated for the test population and hits are selected that are three standard deviations from the mean.

For detecting Kir channel inhibitors, particularly those acting at intracellular binding sites, it may be valuable to incubate the cells with test compounds for an extended period of time (e.g. 20 min) prior to the addition of TI^+ . If the compounds are added "offline" before the assay is introduced to the plate reader, the optical properties of test compounds (e.g. fluorescence) may not be easily recognized and can adversely affect commonly used data normalization approaches such as the "static ratio" F/F_0 described above resulting in false positives and/or false negatives. To avoid this problem while simultaneously avoiding having to keep an assay plate in a reader for a long incubation, one solution is to utilize a "two read" protocol. The first read is a short (e.g.

30 sec) experiment where the compound is added after 10 seconds to allow capture of the pre-compound addition F_0 and to assess the compounds' optical effects on the system. The plate is then removed from the reader and incubated for the desired period and returned to the reader for thallium addition. After both reads are completed, the first read F_0 can be used to normalize the data from the second read thus avoiding many issues associated with adding compounds "offline" while allowing the opportunity to keep the reader busy collecting data thus improving screening throughput. The two read approach is most easily implemented when using an automated screening system. It is important to note that the two read approach will not eliminate problems caused by fluorescent compounds that saturate the detector and/or cause read-out artifacts in the CCD camera.

Not all Kir channels are maximally activated under resting conditions, thus it may be possible to design an assay that can detect small-molecule activators. In these cases, selecting an EC_{80} concentration of Tl^+ may not provide enough "headroom" for the assay to reliably detect activators. Thus, one may choose to use a lower concentration of Tl^+ (e.g. EC_{20}) in activator assays. In some cases, the assay may show low enough variability as to allow the use of an EC_{50} concentration of Tl^+ and still provide suitable resolution of both activated and inhibited channel populations. In this case, the assay may be conducted in dual activator/inhibitor mode. When available, a known activator can be used to help determine the appropriate Tl^+ concentration to maximize the chances of discovering channel activators.

There are some limitations that should be considered during the development and execution of a Tl^+ flux-based high-throughput screen. For example, the assay relies on an indirect measure of Kir channel activity using a fluorescent probe whose optical properties could be directly affected by compounds in a screen. Therefore, important observations from Tl^+ flux

experiments must be confirmed using voltage clamp electrophysiology, which is considered the "gold-standard" method for ion channel pharmacology. Furthermore, small-molecules may have direct effects on endogenous TI^+ flux pathways expressed in HEK-293 cells, leading to the identification of false-positive hits. The tetracycline-inducible system is particularly useful for distinguishing false-positive hits from Kir channel-directed modulators because the hits can be rapidly screened in uninduced cells for effects on endogenous pathways. Finally, the low solubility of TI^+ in chloride-containing buffers limit the concentration of TI^+ that can be used in an assay, requiring the use of a non-physiological TI^+ stimulus buffer that may augment the pharmacology of the target [83]. The compatibility of different buffers with the target of interest should be carefully evaluated during assay development. This can be done by establishing CRCs for known modulators using different TI^+ stimulus buffers and choosing conditions in which the pharmacology most closely matches that observed using physiological buffers.

Chapter III

DISCOVERY, CHARACTERIZATION AND STRUCTURE-ACTIVITY RELATIONSHIPS OF AN INHIBITOR OF INWARD RECTIFIER POTASSIUM (KIR) CHANNELS WITH PREFERENCE FOR KIR2.3, KIR3.X AND KIR7.1

This chapter was published under the same title in the journal *Frontiers in Pharmacology* in the November 30th, 2011 issue

Abstract

The inward rectifier family of potassium (Kir) channels is comprised of at least 16 family members exhibiting broad and often overlapping cellular, tissue or organ distributions. The discovery of disease-causing mutations in humans and experiments on knockout mice has underscored the importance of Kir channels in physiology and in some cases raised questions about their potential as drug targets. However, the paucity of potent and selective small-molecules targeting specific family members has with few exceptions mired efforts to dissect their individual physiological functions and assess their therapeutic potential. A growing body of evidence suggests that GIRK (G protein-regulated inward rectifier K) channels of the Kir3 subfamily may represent novel targets for the treatment of atrial fibrillation and pain. We therefore performed a thallium (Tl⁺) flux-based high-throughput screen (HTS) of a Kir1.1 inhibitor library for modulators of GIRK. One compound, termed VU573, exhibited 10-fold selectivity for GIRK over Kir1.1 (IC₅₀ = 1.9 μM and 19 μM, respectively) and was therefore selected for further study. In electrophysiological experiments performed on *Xenopus laevis* oocytes and mammalian cells, VU573 inhibited Kir3.1/3.2 (neuronal GIRK) and Kir3.1/3.4 (cardiac GIRK) channels with equal potency and preferentially inhibited GIRK, Kir2.3 and

Kir7.1 over Kir1.1 and Kir2.1. Thallium flux assays were established for Kir2.3 and the M125R pore mutant of Kir7.1 to support medicinal chemistry efforts to develop more potent and selective analogs. The structure-activity relationships of VU573 revealed few analogs with improved potency. However, two compounds retained most of their activity toward GIRK and Kir2.3 and lost activity toward Kir7.1. We anticipate that the VU573 series will be useful for exploring the physiology and structure-function relationships of these important potassium channels.

Introduction

Refer to **Chapter I** for a review of the inward rectifier family of potassium (Kir) channels. The founding Kir channel family member Kir1.1, commonly known as ROMK (for Renal Outer Medullary K channel), is a weak rectifier encoded by the gene *KCNJI* [84,85]. Kir1.1 is expressed almost exclusively in epithelial cells of the renal tubule where it critically regulates salt and water balance and hence blood volume and pressure [86]. Autosomal recessive mutations in *KCNJI* give rise to antenatal Bartter syndrome, a severe salt and water wasting disorder characterized by hypokalemic metabolic alkalosis and low to normal blood pressure [19]. In contrast, heterozygous carriers of *KCNJI* mutations have lower blood pressure but no overt evidence of disease [87]. These genetic data raise the intriguing possibility that Kir1.1 represents a drug target for a novel class of diuretic. Consequently, our group recently employed high-throughput screening and medicinal chemistry to develop the first publicly disclosed small-molecule inhibitors of Kir1.1 [20,21]. These, as well as inhibitors recently disclosed by investigators at Merck [22], should be instrumental in assessing the therapeutic potential of Kir1.1 for the management of hypertension. Another emerging drug target in the Kir channel

family is the G protein-coupled inward rectifier potassium (GIRK) channel, which is expressed in the heart and throughout the nervous system [1] and reviewed in **Chapter I**. In patients with chronic atrial fibrillation, GIRK channels become constitutively active in atrial cardiomyocytes through mechanisms that are incompletely understood [88-90]. This background current hyperpolarizes the membrane potential, abbreviates the action potential and increases the availability sodium channels for activation. A growing body of experimental and clinical data support the notion that electrical remodeling sets up high-frequency re-entrant current sources that perpetuate atrial fibrillation, suggesting that a specific blocker of GIRK could have antiarrhythmic actions without the ventricular side effects commonly associated with current therapies [16]. Similarly, the other Kir channel family member Kir2.3 is enriched in atrial cardiomyocytes and may also be a pharmaceutical target for atrial fibrillation [76]. As reviewed in **Chapter I** the molecular pharmacology of Kir channels remains largely undeveloped. A high-throughput screen using a voltage-sensitive dye identified analogues of amiloride (a K⁺ sparing diuretic) and propafenone (a class 1c anti-arrhythmic) that inhibit GIRK with sub-micromolar potencies [91]. These and several cardiac and neurological drugs exhibiting weak off-target activity toward GIRK [77] may be useful lead compounds for developing more specific inhibitors of GIRK. The bee venom toxin tertiapin is a nanomolar affinity GIRK antagonist that also inhibits Kir1.1 [79,92]. [93] demonstrated that administration of tertiapin to cannulated dogs terminated induced atrial fibrillation, providing some of the first experimental evidence that GIRK is a target for anti-arrhythmic therapeutics [93]. Nissan Chemical Industries developed a benzopyrane derivative, termed NIP-142, which inhibits Kir3.1/3.4 GIRK channels with sub-micromolar affinity and the cardiac Kv1.5 delayed rectifier current with equal potency [33,94]. NIP-142 has shown efficacy in terminating induced atrial fibrillation in dogs, but it is unknown

whether the improvement in sinus rhythm is due to inhibition of GIRK, Kv1.5 or both. However, the low nanomolar inhibitor NTC-801, which is highly selective for GIRK over other cardiac channels, was shown recently to be effective in several models of atrial fibrillation [95]. In an effort to further expand the molecular pharmacology of GIRK, we employed a TI^+ flux-based fluorescence assay to screen a Kir1.1 inhibitor focus library for antagonists of GIRK. One compound termed VU573 was found to preferentially inhibit GIRK (cardiac and neuronal forms), Kir2.3 and Kir7.1 over Kir1.1 and Kir2.1. We anticipate that VU573 and its analogs will be useful for investigating the physiology and structure-function relationships of inward rectifier potassium channels.

Materials and Methods

Expression vectors

Plasmids used in this study are from the following sources: rat Kir1.1 (NM_017023; Chun Jiang, Georgia State University, Atlanta, GA), human Kir2.1 (NM_000891.2; Al George, Vanderbilt University School of Medicine, Nashville, TN), human Kir7.1 (NM_002242.2; David Clapham, Harvard Medical School, Cambridge, MA). Human Kir1.1 (NM_000220), Kir3.1 (NM_002239.2), Kir3.2 (NM_002240.2), Kir3.4 (NM_000890.3) and Kir2.3 (NM_152868) were purchased from OriGene Technologies (Rockville, MD). The M125R mutant of Kir7.1 was created using the QuickChange Site-Directed Mutagenesis Kit (Agilent Technologies). The open reading frame of Kir7.1 was fully sequenced to ensure that no spurious mutations were introduced during mutation of the intended codon.

Cell lines

Monoclonal mGluR8/GIRK/HEK cells stably expressing Kir3.1/3.2, the M4 muscarinic receptor and rat mGlu8a were cultured as described previously [83]. Polyclonal stable T-REx-HEK293 cell lines expressing Kir2.3 and Kir7.1-M125R under the control of tetracycline-inducible promoter were established essentially as described in detail elsewhere [20,96]. Monoclonal Kir2.3 cell lines were isolated through limiting dilution in 384-well plates and testing for tetracycline inducible TI^+ flux, as described below. Polyclonal Kir7.1-M125R cells were used in this study. The development of monoclonal C1 T-REx-HEK293 cells expressing Kir1.1 (S44D) was described previously [20]. T-REx-HEK293 lines were cultured in DMEM growth medium containing 10% FBS, 50 U/mL Penicillin, 50 g/mL Streptomycin, 5 g/mL Blastidicin S and 250 g/mL Hygromycin.

Two-electrode voltage clamp analysis

Stage V-VI oocytes were isolated from gravid *Xenopus laevis* frogs using sterile surgical techniques under tricaine anesthesia. All methods were in accordance with the guidelines for the use of laboratory animals of Vanderbilt University School of Medicine. The oocyte follicle layer was removed by manual dissection following enzymatic treatment with 1 mg/ml collagenase (Type 1A Sigma) dissolved in calcium-free OR-2 of the following composition (in mM): 82.5 NaCl, 2 KCl, 1 MgCl₂, 5 HEPES, with pH 7.5 adjusted with NaOH. Oocytes were allowed to recover overnight at 16 °C in modified L-15 media containing gentamicin sulfate (25 mg/ml). pcDNA3.1(+) vectors carrying Kir1.1, human Kir2.1, 2.3, and 7.1 cDNA were used to synthesize channel cRNA from a T7 RNA polymerase and nucleotides provided in the mMACHINE kit (Ambion, Austin, TX) after linearization of the expression constructs. cRNA

was purified by LiCl precipitation, diluted in RNAase-free water and used for injections. The oocytes were injected with 0.5 to 10 ng of cRNA of Kir1.1, Kir2.1, Kir2.3, and Kir7.1 using a Drummond digital microdispenser. Oocytes were incubated at 16°C in modified L-15 for 24-72 h prior to Kir channel recordings. Whole-cell currents were recorded from *Xenopus* oocytes injected with Kir channel cRNA using the two-electrode voltage clamp technique. Current and voltage commands were generated with a GeneClamp 600 amplifier, a Digidata 1200 A/D converter and pClamp 8.0 software (Molecular Devices, Sunnyvale, CA). The bath was actively clamped to 0 mV using a VG-2A bath clamp (Molecular Devices). Electrodes pulled from borosilicate glass (Sutter Instruments, Novato, CA) using a PP-830 vertical puller (Narishige International, Narishige, Japan) had resistances of 0.5-5.0 MΩ when filled with 3 M KCl. The standard bath solution contained (in mM): 85 NaCl, 5 KCl, 10 HEPES, 2 MgCl₂, pH 7.4 with NaOH. After achieving stable current amplitude, VU573 was applied continuously. This was followed by application of the non-specific potassium channel blocker barium. For Kir current recordings, cells were voltage-clamped and stepped every 5 s from a holding potential of -70 to -100 mV for 200 ms, then ramped at a rate of 1.6 mV/ms to 60 mV before returning to -80 mV. All recordings were made at room temperature (20-23°C).

Whole-cell patch clamp electrophysiology

T-REx-HEK293-Kir2.3 cells were patch clamped after overnight induction with tetracycline (1 g/ml). GIRK (Kir3.1/3.2) and wild type Kir7.1 were studied in HEK-293 cells transiently co-transfected with the respective channel expression vectors and pcDNA3.1-EGFP (transfection marker) using Lipofectamine LTX/Plus reagent according to manufacturer's protocol (Invitrogen, Carlsbad, CA). The standard intracellular solution contained 135 mM KCl,

2 mM MgCl₂, 1 mM EGTA, 10 mM HEPES-free acid, and 2 mM Na₂ATP (Roche), pH 7.3, adjusted to 275 mOsmol/kg with sucrose. For Kir2.3 recordings, MgCl₂ was reduced to 1 mM to prevent channel rundown [97]. The standard bath solution contained 135 mM NaCl, 5 mM KCl, 2 mM CaCl₂, 1 mM MgCl₂, 5 mM glucose, and 10 mM HEPES-free acid, pH 7.4, 290 mOsmol/kg. In some experiments, a high-K⁺ bath was used that contained 90 mM NaCl, 50 mM KCl, 2 mM CaCl₂, 1 mM MgCl₂, 5 mM glucose, and 10 mM HEPES-free acid, pH 7.4, 290 mOsmol/kg. Kir current recordings were collected as previously described [21]. After achieving stable whole-cell currents, VU573 was applied intermittently or continuously for 2 to 10 min, followed by application of 2 mM BaCl₂. Data acquisition and analysis were performed using pClamp 9.2 software (Molecular Devices). All recordings were made at room temperature (20-23°C).

Test compound and stimulus plate preparation

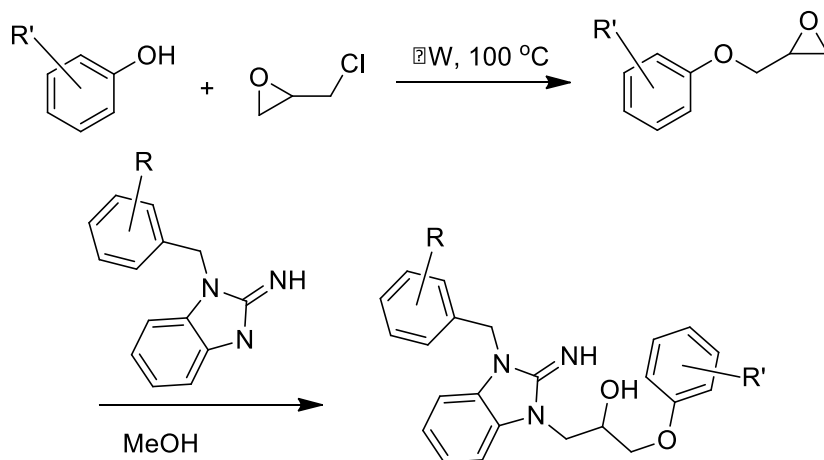
Compound master antagonist plates were created by serial diluting compounds 1:3 from 10mM stock in 100% DMSO using the BRAVO liquid handler (Agilent Technologies, Santa Clara, CA). Assay daughter plates were created using the ECHO 555 liquid handler (Labcyte, Sunnyvale, CA), transferring 240 nL from the master plate to the daughter plate for each well followed by addition of 40 µL of assay buffer resulting in antagonist compound concentration response curves starting at 60 µM (2X final concentration). Glutamate was diluted in TI⁺ buffer (125 mM sodium bicarbonate (added fresh the morning of the experiment), 1 mM magnesium sulfate, 1.8 mM calcium sulfate, 5 mM glucose, 12 mM TI⁺ sulfate, and 10 mM HEPES, pH 7.3) at 5X the final concentration to be assayed.

Kinetic imaging, data analysis, and statistics

Cells were loaded with the TI^+ sensitive fluorescent dye FluoZin-2 and plated in clear-bottom 384-well plates essentially as described previously [20,21]. Cell plates and daughter compound plates were loaded onto a kinetic imaging plate reader (FDSS 6000; Hamamatsu Corporation, Bridgewater, NJ). All recordings were made at room temperature (20-23°C). Appropriate baseline readings were taken (10 images at 1 Hz; excitation, 470 ± 20 nm; emission, 540 ± 30 nm) and 20 μL test compounds were added followed by 50 images at 1Hz additional baseline. Following a 20-min incubation period, baseline readings were taken for 30 seconds followed by addition of 10 μL Glutamate at an EC_{80} concentration. An additional 170 images were taken at 1Hz. Glutamate EC_{80} concentration was determined the day of the assay.

Data were analyzed using Excel (Microsoft Corp, Redmond, WA). Raw data were opened in Excel and each data point in a given trace was divided by the first data point from that trace (static ratio). For experiments in which antagonists were added, data were again normalized by dividing each point by the fluorescence value immediately before the glutamate addition to correct for any subtle differences in the baseline traces after the compound incubation period. The slope of the fluorescence increase beginning 5 s after TI^+ /glutamate addition and ending 15 s after TI^+ /glutamate addition was calculated. The data were then plotted in Prism software (GraphPad Software, San Diego, CA) to generate concentration-response curves after correcting for the slope values determined for baseline waveforms generated in the presence of vehicle controls. Potencies were calculated from fits using a four parameter logistic equation.

Chemical synthesis



Synthetic Scheme I:

General: All NMR spectra were recorded on a 400 MHz AMX Bruker NMR spectrometer. ^1H chemical shifts are reported in δ values in ppm downfield with the deuterated solvent as the internal standard. Data are reported as follows: chemical shift, multiplicity (s = singlet, d = doublet, t = triplet, q = quartet, br = broad, m = multiplet), integration, coupling constant (Hz). Low resolution mass spectra were obtained on an Agilent 1200 series 6130 mass spectrometer with electrospray ionization. High-resolution mass spectra were recorded on a Waters Q-TOF API-US plus Acquity system with electrospray ionization. Analytical thin layer chromatography was performed on EM Reagent 0.25 mm silica gel 60-F plates. Samples were analyzed for $\geq 95\%$ purity using LC-UV/Vis-MS. Analytical HPLC was performed on an Agilent 1200 series with UV detection at 214 nm and 254 nm along with ELSD detection. LC/MS: Method 1 = (J-Sphere80-C18, 3.0 x 50 mm, 4.1 min gradient, 5%[0.05%TFA/CH₃CN]:95%[0.05%TFA/H₂O] to 100%[0.05%TFA/CH₃CN]; Method 2 = (Phenomenex-C18, 2.1 X 30 mm, 2 min gradient, 7%[0.1%TFA/CH₃CN]:93%[0.1%TFA/H₂O] to 100%[0.1%TFA/CH₃CN]; Method 3 =

(Phenomenex-C18, 2.1 X 30 mm, 1 min gradient, 7%[0.1%TFA/CH₃CN]:93%[0.1%TFA/H₂O] to 95%[0.1%TFA/CH₃CN]. Preparative purification was performed on a custom HP1100 purification system (reference 16) with collection triggered by mass detection. Solvents for extraction, washing and chromatography were HPLC grade. All reagents were purchased from Aldrich Chemical Co. and were used without purification.

Reagents: Substituted phenols were purchased from various commercial sources, 2-Amino-1-benzylbenzimidazole and 2-Amino-1-methylbenzimidazole were purchased from Acros Organics. 1-(4-Chlorophenylmethyl)-2-aminobenzimidazole was made using published procedures [98].

General synthetic procedure: The desired phenol (2 mmol) was dissolved in 0.4 mL NaOH (5 M) and then treated with epichlorohydrin (0.32 mL, 3.7 mmol). The mixture was heated in a Biotage Initiator microwave reactor at 100 °C for a 15 min period. The reaction was cooled to ambient temperature and diluted with dichloromethane. The aqueous layer was removed and the organic layer extracted with water. The mixture was dried and solvent removed under reduced pressure. The crude mixture was then treated with the desired 2-aminobenzimidazole (3 mL, 0.2 mmol, 0.7 M MeOH) dissolved in methanol. The mixture was allowed to stir for 4 days at ambient temperature. The solvent was removed under reduced pressure and the residue was diluted with dichloromethane. The mixture was extracted with water, dried, and concentrated under reduced pressure. The crude was purified using reverse phase chromatography (C18, Acetonitrile/H₂O 0.1% TFA).

Results

VU573: A weak Kir1.1 inhibitor with preference for GIRK

We recently performed a high-throughput screen (HTS) for small-molecule modulators of Kir1.1 [20], the founding member of the inward rectifier potassium (Kir) channel family [84,99] and putative diuretic target [19,87,100]. A focus library of reproducibly active inhibitors was assembled from the primary screen, with the goal of mining the library for antagonists of other inward rectifiers. As noted in the Introduction, a growing body of evidence suggests that GIRK channels expressed in atrial cardiomyocytes may represent a viable drug target for the treatment of atrial fibrillation. Given the paucity of potent and selective small-molecule inhibitors of GIRK and therapeutic interest in the channel, we screened the focus library for GIRK modulators using a Ti^+ flux-based fluorescence assay developed recently at Vanderbilt [83]. The assay reports Ti^+ flux through heteromeric Kir3.1/3.2 channels co-expressed in HEK-293 cells with the group III metabotropic glutamate receptor mGluR8. Intracellular Ti^+ concentration is reported using the commercially available Ti^+ -sensitive fluorescent dye FluoZin-2. As shown in **Fig. 1A**, glutamate addition dose-dependently increased Ti^+ flux as GIRK channels are activated by mGluR8 stimulation. The focus library was screened at a single concentration of 10 μM using an 80% maximally effective concentration (EC_{80}) of glutamate. Several compounds were identified that preferentially inhibited GIRK over Kir1.1 (data not shown). One of these compounds, termed VU573, was selected for further study.

The chemical structure of VU573 is shown in the inset of **Fig. 1C**. The potency of VU573 was evaluated in 11-point concentration-response curves (CRC) using an EC_{80} of glutamate to activate GIRK. As shown in **Fig. 1B**, VU573 inhibited GIRK-dependent Ti^+ flux in a dose-dependent manner with a 50% inhibition concentration (IC_{50}) of approximately 1.9 μM

(Fig. 1C).

To verify that VU573 is a more potent inhibitor of GIRK than Kir1.1, a full VU573 CRC was generated using an established TI^+ flux assay for Kir1.1 [20,21]. The assay employs an inducible system in which Kir1.1 is expressed from a tetracycline-regulatable promoter. As shown in **Fig. 2A**, extracellular TI^+ addition produced a dramatic increase in FluoZin-2 fluorescence in cells cultured with tetracycline, but not in uninduced cells. Thus, most of the TI^+ flux in tetracycline-induced cells occurs through Kir1.1. VU573 exhibited weak yet dose-dependent inhibition of Kir1.1 (**Fig. 1F**), with an IC_{50} of approximately 19 μM . Whole-cell patch clamp experiments confirmed that 20 μM VU573 inhibited Kir1.1 by $49.5 \pm 0.03\%$ ($n = 5$). Thus, VU573 is a preferential inhibitor of GIRK over Kir1.1.

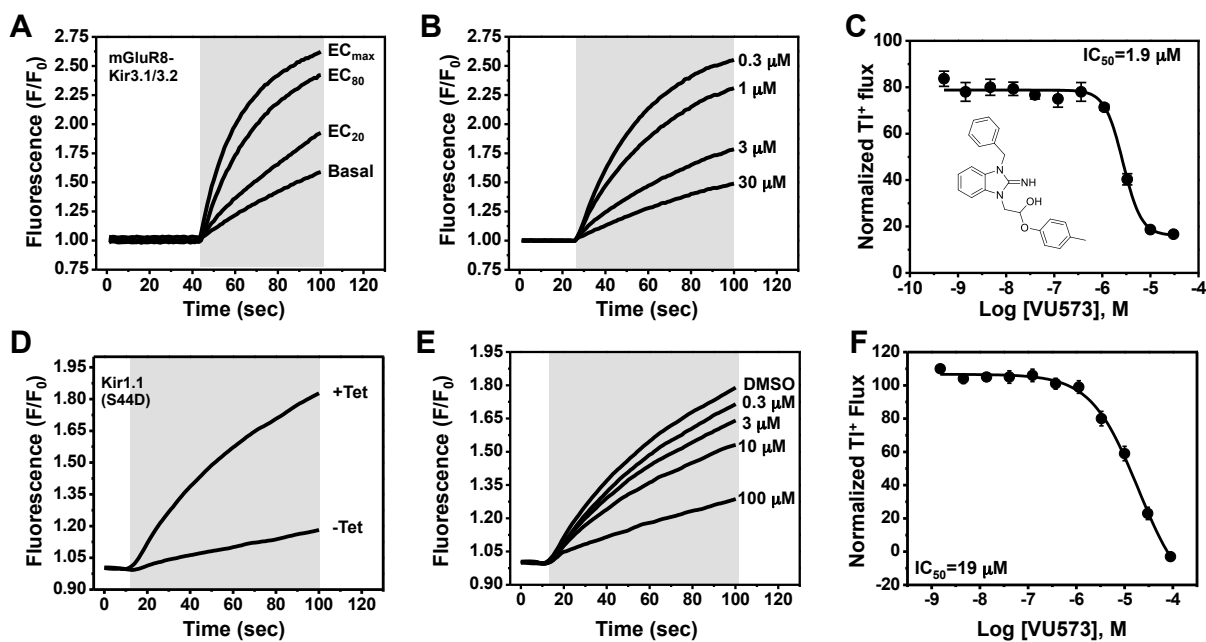


Figure 1. VU573 inhibits mGluR8-activated Kir3.1/3.2 channel activity in thallium flux assays. (A) Representative FluoZin-2 fluorescence traces recorded from HEK-293 cells stably expressing mGluR8 and Kir3.1/3.2 before and after co-application of thallium and different doses of glutamate (shaded box). From an 11-point glutamate concentration-response curve (not shown), the glutamate concentration evoking approximately 80% (EC_{80}) of the maximal response (EC_{max}) was determined and used for subsequent experiments. (B) Representative traces for changes of Tl^+ -induced FluoZin-2 fluorescence following 20 min pre-treatment of cells with the indicated concentrations of VU573 and subsequent thallium and glutamate- EC_{80} addition (shaded box). (C) Mean \pm SEM concentration-response curve for VU573-dependent inhibition of Kir3.1/3.2 ($n = 3$). The chemical structure of VU573 is shown in the inset. (D) Representative FluoZin-2 fluorescence traces recorded from monoclonal Kir1.1-S44D expressing cells cultured overnight in absence (-Tet) or presence (+Tet) of Tetracycline. (E) Representative traces for changes of Tl^+ -induced FluoZin-2 fluorescence following pre-treatment of cells with the indicated concentrations of VU573 and then exposed to thallium (shaded box). (F) Mean \pm SEM concentration-response curve for VU573-dependent inhibition of Kir1.1-S44D ($n = 3$).

VU573 shows preference for Kir2.3, GIRK and Kir7.1 over Kir1.1 and Kir2.1

To further assess the selectivity of VU573, several members of the Kir channel family were expressed in *Xenopus* oocytes and screened for VU573 sensitivity using the two-electrode voltage clamp technique (TEVC). We first tested whether VU573 discriminates between Kir3.1/3.2 and Kir3.1/3.4 channels, the predominate heterotetrameric forms of GIRK found in the nervous system and heart, respectively [1]. **Figure 3A** illustrates a typical experiment performed on an oocyte co-injected with cRNA encoding Kir3.1 and Kir3.2. Current recorded at -80 mV is shown as a function of time. The oocyte was initially bathed in a potassium-free (0K) solution and then switched to one containing 90 mM K⁺ (90K) to activate GIRK. The dramatic increase in inward current in the presence of 90K buffer was not observed in water-injected oocytes (data not shown) and therefore largely reflects current through Kir3.1/3.2 channels. Bath application of 10 μM VU573 inhibited GIRK current by approximately 50%, which was significantly lower than expected from TI⁺ flux experiments (**Fig. 1C**). The residual current was blocked by Ba²⁺. Figure 3B shows mean ± SEM % block of Kir3.1/3.2 and Kir3.1/3.4 channels by 1, 10 and 25 μM VU573 or Ba²⁺. The mean ± SEM time constant (τ) for inhibition of Kir3.1/3.2 and Kir3.1/3.4 currents by 25 μM VU573 were 28 ± 4 (n = 6) and 27 ± 5 (n = 6) sec, respectively. There were no significant (P >0.05) differences in the degree of VU573-dependent block of Kir3.1/3.2 and Kir3.1/3.4 channels at any of the concentrations.

GIRK channels are co-expressed with other members of the Kir channel family in a tissue- and cell type-specific manner. As noted in the Introduction, there is growing evidence that inhibitors of cardiac GIRK channels may be therapeutically beneficial in patients with atrial fibrillation. However, Kir2.1 and Kir2.3 are also expressed in the heart [1] and therefore represent potential off-targets for VU573 actions. GIRK, Kir2.1 and Kir2.3 are also co-expressed

in various brain regions, as is one of the newest Kir channel family members, Kir7.1 [101]. We therefore determined whether VU573 inhibits any of these channels expressed in *Xenopus* oocytes. Kir1.1 was also expressed to confirm the results from TI^+ flux experiments.

Representative TEVC recordings from oocytes expressing Kir1.1, Kir2.1, Kir2.3, or Kir7.1 are shown in **Fig. 3**. The oocytes were voltage clamped at -75 mV and stepped for 200 msec every 5 sec to -120 mV to evoke inward current. The current amplitude at -120 mV is shown as a function of time. Barium was again used at the end of each experiment as a control blocker. Consistent with the TI^+ flux data showing greater potency toward GIRK than Kir1.1, 50 μM VU573 inhibited Kir1.1 by only $4.3 \pm 1.7\%$ with a time constant of 95 ± 15 sec ($n = 8$). Kir2.1 was also relatively insensitive to VU573, and the time constant was very slow ($\tau = 735 \pm 85$ sec; $n = 4$)(**Fig. 2C**). After 25 minutes of constant bath perfusion, 50 μM VU573 inhibited Kir2.1 by only $30.2 \pm 9.4\%$. In contrast, Kir2.3 was inhibited comparatively quickly ($\tau = 154 \pm 32$ sec) by $80.9 \pm 5.0\%$ ($n = 7$). Similarly, Kir7.1 was inhibited by $66.0 \pm 6\%$ ($n = 9$) with a rapid constant of 38 ± 6 sec ($n = 8$).

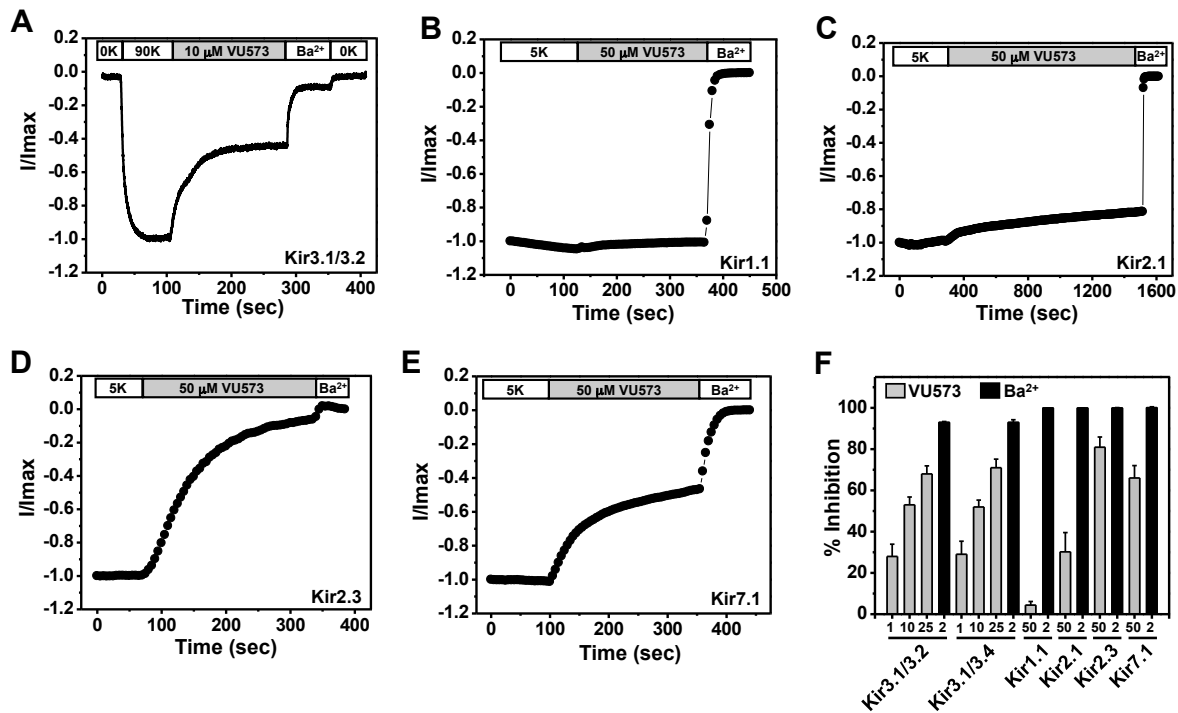


Figure 2. Effect of VU573 on Kir channels expressed in oocytes. (A) Representative Kir3.1/3.2 current traces recorded from an oocyte using the two-electrode voltage clamp technique. Oocytes were initially bathed in a potassium-free (0K) solution and then switched to one containing 90 mM potassium (90K) to activate Kir3.1/3.2. After reaching a steady state, the oocyte was exposed to 10 μ M VU573 (in 90K) bath to inhibit Kir3.1/3.2. Residual Kir3.1/3.2 currents were inhibited with 2 mM barium (Ba^{2+}). A final switch back to 0K was used to measure leak current at the end of each experiment. Representative whole-cell current traces recorded from oocytes expressing respectively (B) Kir1.1, (C) Kir2.1, (D) Kir2.3 and (E) Kir7.1 before and after application of 50 μ M VU573. Residual Kir currents were inhibited with 2 mM barium (Ba^{2+}). (F) Mean \pm SEM percent inhibition of current evoked by Kir3.1/3.2, Kir3.1/3.4, Kir1.1, Kir2.1, Kir2.3 and Kir7.1 with the indicated concentrations of VU573 (grey bars) or Ba^{2+} (black bars) (n = 4-6).

Patch clamp analysis of VU573 potency in mammalian cells

GIRK is inhibited by VU573 with an IC_{50} of approximately 2 μ M in TI^+ flux assays in HEK-293 (**Fig. 1**) cells and 10 μ M in TEVC experiments in oocytes (**Fig. 2**). To determine if the discrepancy is due to the expression system or assay type, whole-cell patch clamp techniques were used to assess the potency of VU573 toward Kir3.1/3.2 GIRK channels expressed in HEK-293 cells. The cells were voltage clamped at a holding potential of -75 mV and then stepped to -120 mV for 200 msec, after which the membrane potential was ramped between -120 mV and 120 mV at a rate of 2.4 mv/msec. As shown in Fig. 3A, GIRK activity was low in the presence of 5 mM extracellular K^+ (5K), but increased upon elevation of bath K^+ to 50 mM (50K), paralleling the behavior of GIRK observed in oocytes. Consistent with TI^+ flux data (**Fig. 1C**), bath application of 30 μ M VU573 led to a near complete inhibition of GIRK. The residual current was inhibited by barium (Ba^{2+} ; **Fig. 3B**). The mean \pm SEM time constant of inhibition was 16 ± 1 sec ($n = 5$). A fit of the CRC data (**Fig. 3C**) from patch clamp experiments yielded an IC_{50} of 1.3 μ M, which is very near that derived from TI^+ flux assays (**Fig. 1C**).

We extended our patch clamp experiments to include Kir2.3 and Kir7.1 due to their strong inhibition by VU573 in oocytes (**Fig. 2F**). A monoclonal stable T-REx-HEK293 cell line expressing Kir2.3 under the control of a tetracycline-inducible promoter was patch clamped following overnight induction with tetracycline. Kir7.1 was studied in transiently transfected HEK-293 cells (see Methods). The cells were subjected to the same voltage ramp protocol described above for GIRK. Steady state Kir2.3 and Kir7.1 currents recorded before (black line) and after (gray line) bath application of 30 μ M VU573 are shown in **Figs. 3D** and **3G**, respectively. Both channels were inhibited with a rapid time course and IC_{50} values of approximately 1 μ M (**Figs. 3F** and **3I**).

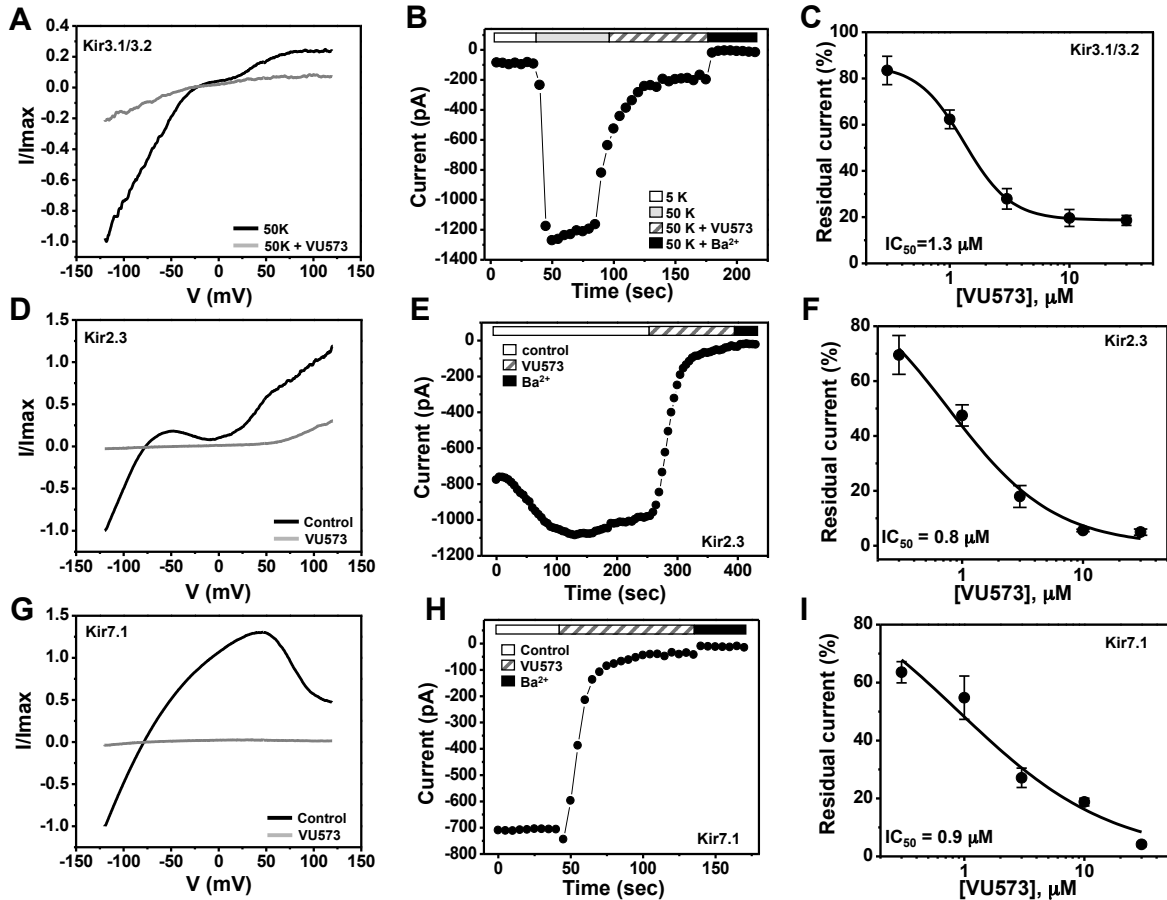


Figure 3. VU573-dependent inhibition of Kir3.1/3.2, Kir2.3 and Kir7.1 channel activity expressed in HEK-293 cells. (A, D, G) Representative whole-cell Kir3.1/3.2, Kir2.3 and Kir7.1 current traces recorded from transfected HEK-293 cells. The cell was voltage ramped every 5 sec between -120 mV and 120 mV for 200 ms from a holding potential of -75 mV. Normalized Kir3.1/3.2, Kir2.3 and Kir7.1 currents recorded before (black line) and after reaching steady-state inhibition by 30 μM VU573 (gray line) are shown. (B, E, H) Representative time course traces of VU573-dependent inhibition of Kir3.1/3.2, Kir2.3 and Kir7.1 by 30 μM VU573 using the protocol described above. After achieving whole-cell access, the current was allowed to stabilize before adding 30 μM VU573 and then 2 mM barium (Ba^{2+}) to inhibit channel activity. (C, F, I) Mean \pm SEM concentration-response curves for Kir3.1/3.2 (n = 4-7), Kir2.3 (n = 4-6) and Kir7.1 (n = 4-7), respectively.

Development of TI⁺ flux assays for Kir2.3 and Kir7.1-M125R

We next set out to employ medicinal chemistry in an effort to improve the potency and selectivity of VU573 toward GIRK, Kir2.3 and Kir7.1. Conventional electrophysiological methods are too slow and labor intensive to support a robust medicinal chemistry campaign, leading us to establish high-throughput TI⁺ flux assays for Kir2.3 and Kir7.1. As shown in **Fig. 4A**, robust tetracycline-inducible TI⁺ flux was observed in monoclonal stable T-REx-HEK-293 expressing Kir2.3. VU573 dose-dependently inhibited TI⁺ flux through Kir2.3 with an IC₅₀ of 4.7 μM, a value that is reasonably close to that derived from patch clamp experiments (**Fig. 3F**).

In contrast, despite numerous attempts on multiple polyclonal and monoclonal cell lines, we were unable to detect TI⁺ flux through Kir7.1. Western blot analysis revealed that this was not due to lack of channel protein expression (data not shown), suggesting that other channel properties were responsible. Kir7.1 is unique among Kir channels in that it has a very small unitary conductance, which has been estimated from noise analysis to be on the order of 50 femptoSiemens (fS) [101]. We reasoned that this could keep TI⁺ flux through Kir7.1 below the limit of detection of FluoZin-2. The small conductance of the channel is due at least in part to a non-conserved Methionine (M) residue at position 125 located in the pore. Mutation of the residue to Arginine (R), which occupies the homologous position in all other Kir channels (not shown), has no effect on protein expression or targeting to the plasma membrane, but increases the single channel conductance by approximately 20-fold [101]. We therefore determined if the M125R mutation would enable measurement of TI⁺ flux using FluoZin-2. As shown in **Fig. 4D**, tetracycline-induced robust TI⁺ flux in polyclonal stable T-REx-HEK-293 cells expressing Kir7.1-M125R. VU573 induced concentration-dependent inhibition of TI⁺ flux with an IC₅₀ of 4.9 μM (**Figs. 4E and 4F**). The good correlation between IC₅₀ values from patch clamp and TI⁺

flux experiments and the fact that the M125R mutation had no effect on the sensitivity to VU573 in patch clamp experiments (**Fig. 5A**) indicated that the Kir7.1-M125R assays could be used as a screening tool to support a medicinal chemistry efforts for VU573.

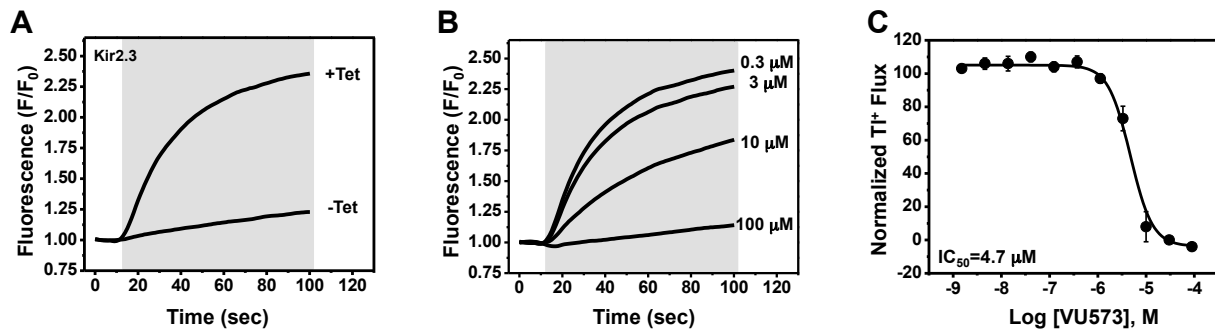


Figure 4. Development of a thallium flux assay for Kir2.3. (A) Thallium flux-dependent FluoZin-2 fluorescence recorded from monoclonal Kir2.3 T-REx-HEK-293 cells cultured overnight in absence (-Tet) or presence (+Tet) of Tetracycline. The fluorescence emission was recorded before and after the addition of extracellular thallium (shaded box). (B) Representative traces for changes of Tl^+ -induced FluoZin-2 fluorescence following 20 min pre-treatment of cells with the indicated concentrations of VU573. (C) CRC for VU573-dependent inhibition of Kir2.3 activity. Values are mean \pm SEM ($n = 3$). A fit of the CRC with a single-site four-parameter logistic function yielded IC_{50} of 4.7 μ M.

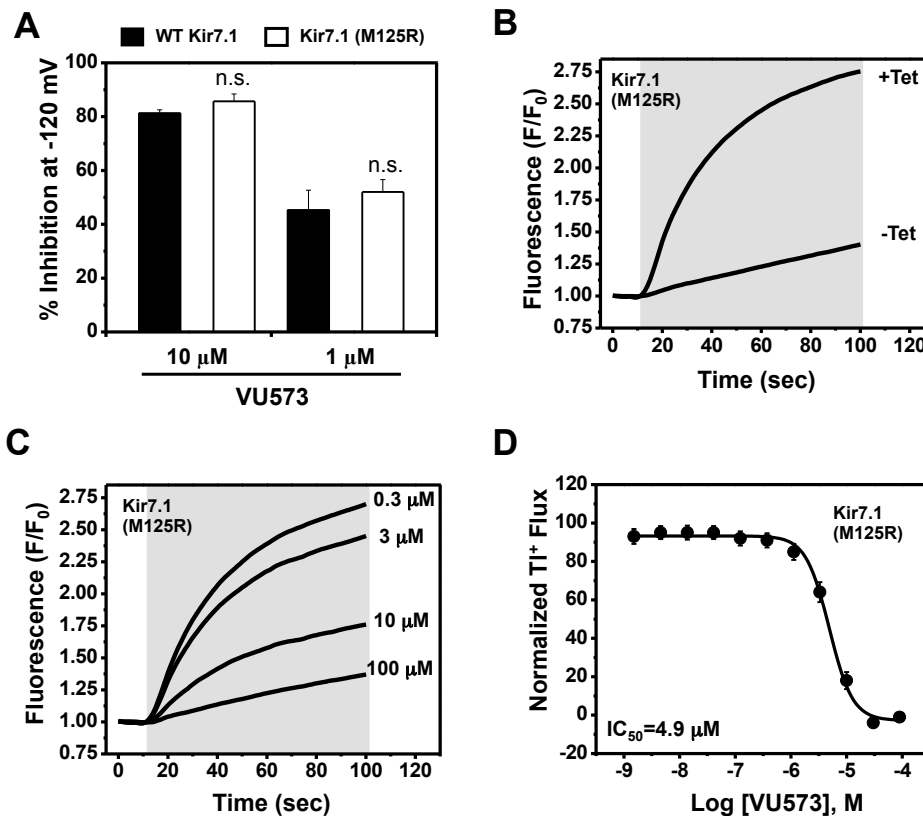
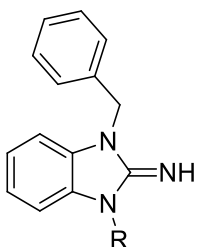
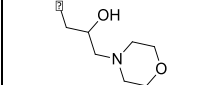
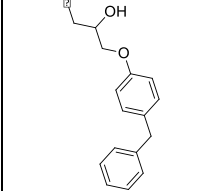
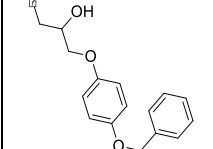
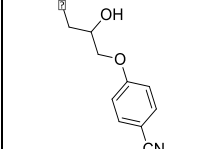
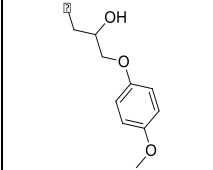
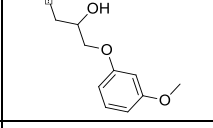
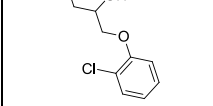
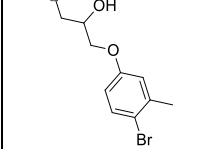
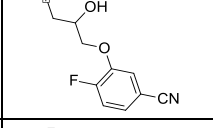
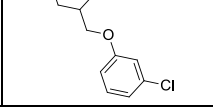
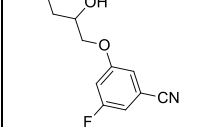


Figure 5. Development of a thallium flux assay for Kir7.1 (M125R). (A) Mean \pm SEM % inhibition of wild type (closed bars; $n = 6-7$) or M125R mutant (open bars; $n = 4-6$). Kir7.1 by the indicated concentration of VU573. Note that the wild type data are reproduced from Fig. 3. (B) Thallium flux-dependent FluoZin-2 fluorescence recorded from polyclonal Kir7.1 (M125R) T-REx-HEK-293 cells cultured overnight in absence (-Tet) or presence (+Tet) of Tetracycline. The fluorescence emission was recorded before and after the addition of extracellular thallium (shaded box). (C) Representative traces for changes of Tl⁺-induced FluoZin-2 fluorescence following 20 min pre-treatment of cells with the indicated concentrations of VU573. (D) CRC for VU573-dependent inhibition of Kir2.3 activity. Values are mean \pm SEM ($n = 3$). A fit of the CRC with a single-site four-parameter logistic function yielded IC₅₀ of 4.9 μM .

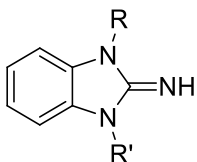
Table 1. Structure-activity relationships and lead optimization summary.



Cmpd	R	VU#/Barcode	IC ₅₀ (μM)			
			Kir2.3	Kir7.1	GIRK	Kir1.1
1		VU0160573-1/ IC4X	4.15 ± 0.35	4.77 ± 2.89	2.17 ± 0.40	10.8 ± 3.8
2		VU0403134-1/ IC3Y	5.33 ± 2.08	4.73 ± 2.57	3.20 ± 0.71	7.07 ± 2.30
3		VU0403131-1/ IC58	4.20 ± 1.25	5.17 ± 1.89	2.90 ± 1.10	6.57 ± 3.80
4		VU0340260-1/ IC38	7.53 ± 2.34	8.00 ± 3.86	4.95 ± 1.80	11.2 ± 2.8
5		VU0026784-1/ IC3L	3.43 ± 0.67	4.47 ± 2.40	1.95 ± 0.49	11.7 ± 4.1
6		VU0288495-1/ IC39	5.33 ± 1.70	4.10 ± 1.93	1.95 ± 0.07	11.9 ± 2.2
7		VU0451348-1/ R6P	3.53 ± 1.33	4.20 ± 0.95	1.40 ± 0.35	7.57 ± 2.20
8		VU0451344-1/ R80	5.03 ± 1.96	6.03 ± 1.60	3.37 ± 0.70	6.77 ± 1.70

9		VU0451342-1/ R70	24.0 ± 10.4	>100	15.3 ± 0.6	>100
10		VU0451341-1/ R7M	2.80 ± 0.99	6.07 ± 2.71	3.83 ± 1.10	6.13 ± 0.23
11		VU0451340-1/ R5C	2.33 ± 0.68	>100	3.17 ± 0.86	5.23 ± 0.59
12		VU0451339-1/ R56	11.3 ± 1.2	19.7 ± 7.4	5.27 ± 0.40	15.7 ± 2.1
13		VU0066224-6/ R7N	3.87 ± 1.40	6.70 ± 1.39	1.50 ± 0.44	12.7 ± 1.2
14		VU0451336-1/ R5B	3.13 ± 1.45	3.47 ± 0.67	1.43 ± 0.25	10.1 ± 2.9
15		VU0451333-1/ R5X	4.95 ± 1.34	5.33 ± 2.91	2.77 ± 0.60	8.60 ± 1.20
16		VU0451337-1/ R5K	5.10 ± 1.27	6.10 ± 3.12	3.43 ± 0.21	8.53 ± 1.70
17		VU0451332-1/ R7B	5.30 ± 1.56	4.33 ± 1.33	1.40 ± 0.30	8.27 ± 0.29
18		VU0451338-1/ R7I	4.45 ± 0.92	5.63 ± 2.24	2.83 ± 0.42	11.7 ± 2.1
19		VU0451330-1/ R6J	7.15 ± 0.71	8.27 ± 2.37	1.93 ± 0.21	14.3 ± 1.5

20		VU0451331-1/ RKN	3.65 ± 0.21	3.03 ± 0.68	4.33 ± 0.68	16.0 ± 2.0
21		VU0451846-2/ R87	3.60 ± 0.28	8.50 ± 2.18	5.13 ± 1.60	19.3 ± 1.5



Cmpd	R	R'	VU#/Barcode	IC ₅₀ (μM)			
				Kir2.3	Kir7.1	GIRK	Kir1.1
22			VU0401333-1/ IC4L	7.20 ± 1.73	8.93 ± 3.53	4.80 ± 1.10	14.7 ± 2.1
23			VU0403132-1/ IC48	5.70 ± 3.18	19.5 ± 28.2	3.35 ± 0.92	6.53 ± 3.90
24			VU0451343-1/ RJ4	2.80 ± 0.89	3.00 ± 0.87	4.20 ± 0.69	13.7 ± 4.4
25			VU0451335-1/ R5P	16.5 ± 0.7	25.3 ± 8.5	12.3 ± 2.5	13.0 ± 2.6
26			VU0451334-1/ R7L	4.90 ± 0.14	5.20 ± 1.82	2.87 ± 0.31	6.97 ± 2.00

Synthesis and structure-activity relationships of VU573 analogs

Lead optimization efforts directed at VU573 (**1**) to improve its potency and selectivity toward Kir2.3, GIRK and Kir7.1 were initiated by conserving the benzyl moiety and substituting the R group (**Table 1**). Structure-activity relationships revealed few analogs with channel selectivity. Replacement of the phenoxy moiety with a morpholino group to the VU573 scaffold resulted in compound (**9**), which lost activity (IC_{50} values $>100 \mu\text{M}$) for Kir7.1 and Kir1.1. The IC_{50} values for Kir2.3 and GIRK were 24 and 15.3 μM , respectively. Substitution of the R group of the VU573 scaffold with a phenoxy benzyloxy functional group led to an analog (**11**), which was equipotent for Kir2.3 and GIRK, but loss activity toward Kir7.1 (IC_{50} values $>100 \mu\text{M}$). An alternate functional group for the VU573 scaffold, a 4-cyanophenyl (**12**), led to an analog compound with moderate selectivity for GIRK ($IC_{50} = 5.27 \mu\text{M}$) and weak inhibition of Kir2.3 and Kir7.1, with IC_{50} values of 11.3 and 19.7 μM , respectively. All other analogs in which substitutions were made at both R and R' groups led to similar potency among the Kir2.3, Kir7.1 and GIRK channels as compared to VU573, but with weak inhibition for Kir1.1. The development of two VU573 analogs, R70 and R5C (**Table 1**), that retain activity toward GIRK and Kir2.3 but have lost activity toward Kir7.1 suggest that chemically optimized analogs based on the VU573 scaffold can be developed to increase their selectivity.

To determine if the apparent loss of activity is an artifact of the TI^+ flux assay or the use of the M125R mutant, we examined the effects of the VU573 analog R70 on wild type Kir7.1 currents in whole-cell patch clamp experiments. The cells were voltage clamped between -120 mV and 120 mV in 20 mV increments from a -75 mV holding potential (**Fig. 6E**). As illustrated in the average current traces recorded before (**Fig. 6A**) or during bath application of 10 μM R70 (**Fig. 6B**), the analog had no effect on wild type Kir7.1 activity. In contrast, subsequent addition of 10 μM VU573 led to a near complete inhibition of the channel. The mean \pm SEM current-voltage relationships recorded in the three conditions are shown in **Fig. 6D**.

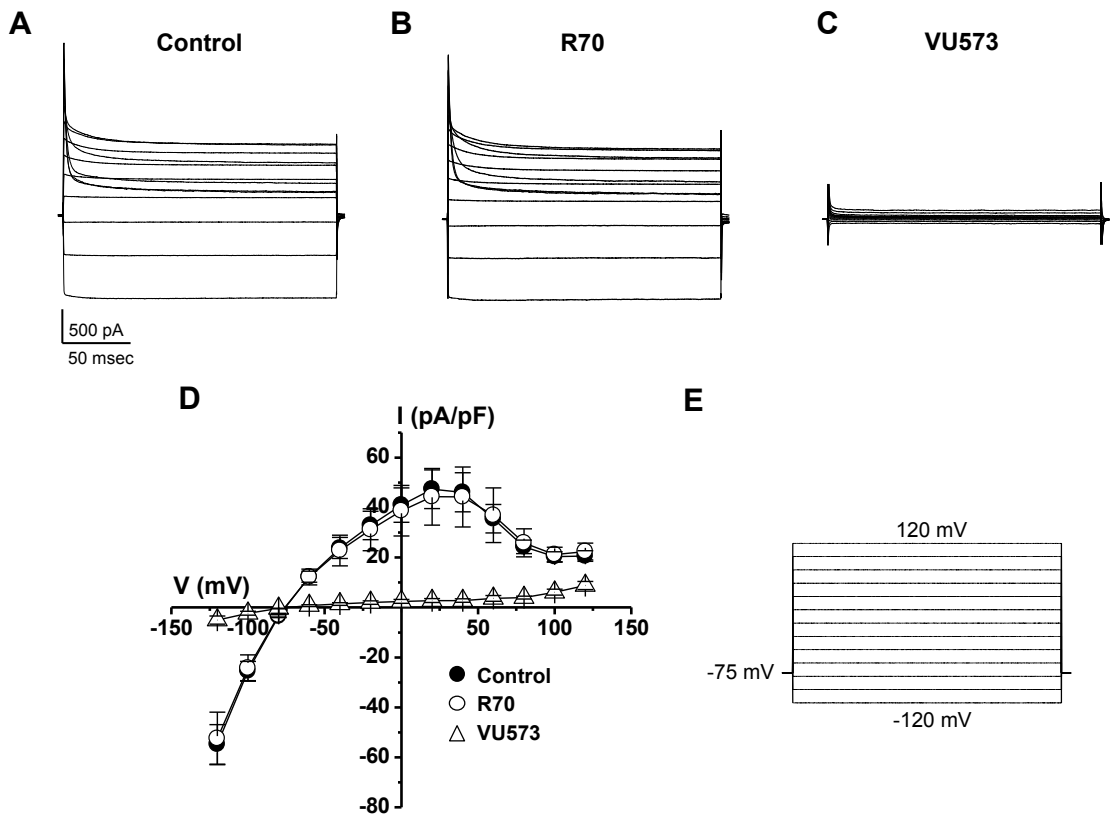


Figure 6. Lack of effect of R70 on wild type Kir7.1 activity. Average Kir7.1 current traces ($n = 4$ each) recorded in the absence (**A**) or presence of (**B**) $10 \mu\text{M}$ R70 or (**C**) $10 \mu\text{M}$ VU573. (**D**) Mean \pm SEM ($n = 4$) current-voltage Kir7.1 relationships recorded in the indicated conditions using the voltage-clamp protocol shown in (**E**).

Discussion

The Tl^+ flux assay developed by [82] and subsequently commercialized by Invitrogen under the FluxOR[®] label has had a major impact on high-throughput screening for potassium channels. The assay takes advantage of the fact that Tl^+ readily permeates most K^+ channel pores. With the exception of wild type Kir7.1, the assay seems to be particularly well suited for inward rectifier K^+ channels due to their high open probability near the resting membrane potential of a cell. This obviates the need, for example, of depolarizing the cell with a high-potassium step to open voltage-gated K^+ channels. To date, Tl^+ flux assays have been reported for the inward rectifiers Kir1.1 [20], Kir2.1 [102], Kir2.3 (this study), Kir3.1/3.2 [83], and Kir7.1-M125R (this study). Thallium flux assays have also been developed for some ligand- and voltage-gated potassium channels, including SK3 and KCNQ2 [82], KCNQ4 [103] and hERG [104-107]. A Tl^+ flux assay was used to screen for modulators of the potassium-chloride co-transporter KCC2 [108]. This is notable because KCC2 is electroneutral and therefore cannot be screened using voltage-sensitive dyes. Thus, the Tl^+ flux assay appears to be broadly adaptable to both electrogenic and electroneutral K^+ transport proteins.

In the present study, Tl^+ flux- and electrophysiological-based counterscreens revealed a preferential inhibitor of GIRK, Kir2.3 and Kir7.1. It is unclear why IC_{50} values are lower in oocytes compared to mammalian cells, but likely reflects differences in membrane properties or intracellular factors between the two cell types. VU573 inhibits GIRK independent of GPCR stimulation and does not discriminate between cardiac (Kir3.1/3.4) and neuronal (Kir3.1/3.2) forms of the channel. The latter observation suggests that the VU573 binding site is located within the Kir3.1 subunit, which is common to both heteromeric forms, or is shared between all three subunits. Pharmacology experiments on homotetrameric Kir3.1, Kir3.2 and Kir3.4

channels should help resolve the issue. Given the broad tissue distribution and important physiological functions of GIRK channels in the periphery and central nervous system, the development of sub-type selective modulators may be important for developing, for example, cardiac-specific drugs to treat atrial fibrillation without toxic side effects on the nervous system. The availability of high-resolution crystal structures of the GIRK cytoplasmic domain [109], GIRK-bacterial Kir channel chimeras [110] and now full-length mammalian Kir2.2 [7] should be helpful in guiding and interpreting experiments to define the molecular binding site for VU573 and other GIRK antagonists. The relatively flat SAR of VU573 against GIRK, Kir2.3 and Kir7.1 suggests that the VU573 scaffold may be amenable to the addition of diazirine or other reactive moieties for photoaffinity labeling of the channels for identification of the binding site using mass spectrometry. A detailed understanding of both unique and overlapping binding sites will provide novel insights into the molecular architecture of GIRK and should facilitate the development of subtype-specific inhibitors.

Members of the Kir2.X sub-family, including Kir2.1, Kir2.2, Kir2.3, Kir2.4 and Kir2.6, are broadly expressed in neurons, cardiac, skeletal and smooth muscle cells, endothelial cells, macrophages and epithelial cells [111]. Much of our understanding of the physiology of Kir2.X channels comes from studies of disease-causing mutations in humans [112,113] and knockout mice [114]. While it is clear from this work that Kir2.X channels are essential in many organ systems, pinpointing their individual roles has been difficult due to their overlapping expression profiles, propensity to form Kir2.X heterotetramers and poorly developed pharmacology. The development of sub-type selective Kir2.X inhibitors would undoubtedly bolster efforts to understand the physiology and druggability of Kir2.X homo- and heteromeric channels. To date, however, the inhibitor pharmacology of Kir2.X channels is limited to barium, cesium and a

handful of non-specific drugs such as chloroquine [39], mefloquine [115], quinacrine [116], carvedilol [117], tamoxifen [58] and pentamidine [56]. Pregnenolone sulfate [43] and flecainide [44] are activators of Kir2.3 and Kir2.1, respectively. Like VU573 (this study), mefloquine, quinacrine, tamoxifen and carvedilol preferentially inhibit Kir2.3 over Kir2.1. Electrophysiological analysis of mutagenized channels suggests that chloroquine and pentamidine are cytoplasmic pore blockers, whereas mefloquine and carvedilol appear to disrupt channel interactions with the activating membrane phospholipid phosphatidylinositol 4,5-bisphosphate (PIP₂). There is evidence that quinacrine has a complex mechanism of action involving both pore block and disruption of channel-PIP₂ interactions. In this regard, studies are underway to determine the blocking mechanism of VU573. Because VU573 is also a preferential inhibitor of Kir2.3, we are currently testing if it shares a common mechanism of action and binding site(s) with these drugs. Looking ahead, it will be important to determine whether VU573 or any of the aforementioned drugs show preference for homomeric versus heteromeric Kir2.X channels. These studies may help inform medicinal chemistry efforts to develop subtype-specific inhibitors of Kir2.X channels.

To our knowledge, VU573 is only the second and most potent Kir7.1 inhibitor available. We recently reported that the ~300 nM Kir1.1 inhibitor 7,13-*Bis*[(4-nitrophenyl)methyl]-1,4,10-trioxa-7,13-diazacyclopentadecane dihydrochloride, or VU590, inhibits Kir7.1 with an IC₅₀ of approximately 8 μM, making VU590 the first publically disclosed small-molecule inhibitor of both Kir1.1 and Kir7.1 [20]. In the present study, we found that VU573 preferentially inhibits Kir7.1 (IC₅₀ ~1 μM) over Kir1.1 (IC₅₀ ~19 μM).

Kir7.1 is widely expressed in the brain, retinal pigment epithelial cells of the eye, the choroid plexus, and epithelial cells of the intestine, nephron and inner ear [101,118-121]. Very

little is known about the physiology of Kir7.1 due in part to the unusually small (i.e. ~50 fS) single-channel conductance of the channel. This precludes the use of single channel recording techniques to study its activity in native cell types, where other inward rectifiers with larger unitary conductances are often co-expressed. Whole-cell patch clamp recordings could conceivably be used to dissect out the relative contributions of Kir7.1 and other Kir channels to the macroscopic current provided that specific blockers were available. This scenario highlights the need for better pharmacological modulators of Kir7.1 and other members of the Kir channel family. The development of a Kir7.1 cell line that is sensitive to thallium is a significant headway for the identification of such modulators. The discovery of VU573 and its inactive analogs represent important steps toward filling this gap. Furthermore, and importantly, the development of a robust Tl^+ flux assay using the Kir7.1-M125R mutant will enable HTS for chemically diverse modulators of the channel.

Interestingly, heritable mutations in the Kir7.1-encoding gene *KCNJ13* were recently found in patients with two forms of retinal disease [122,123]. These findings confirm the importance of Kir7.1 in retinal pigmented epithelia of the eye and raise important questions regarding the physiological roles of this channel in other organ systems. The development of potent and selective Kir7.1 antagonists will greatly facilitate those efforts.

Chapter IV

DEVELOPMENT AND VALIDATION OF FLUORESCENCE- AND AUTOMATED PATCH CLAMP-BASED FUNCTIONAL ASSAYS FOR THE INWARD RECTIFIER POTASSIUM CHANNELS KIR4.1

This chapter was published under the same title in the journal *ASSAY and Drug Development Technologies* in the November/December 2013 issue

Abstract

The inward rectifier potassium (Kir) channel Kir4.1 plays essential roles in modulation of neurotransmission and renal sodium transport and may represent a novel drug target for temporal lobe epilepsy and hypertension. The molecular pharmacology of Kir4.1 is limited to neurological drugs, such as fluoxetine (Prozac®), exhibiting weak and nonspecific activity toward the channel. The development of potent and selective small-molecule probes would provide critically needed tools for exploring the integrative physiology and therapeutic potential of Kir4.1. A fluorescence-based thallium (Tl^+) flux assay that utilizes a tetracycline-inducible T-Rex-HEK293-Kir4.1 cell line to enable high-throughput screening (HTS) of small-molecule libraries was developed. The assay is dimethyl sulfoxide tolerant and exhibits robust screening statistics ($Z' = 0.75 \pm 0.06$). A pilot screen of 3,655 small molecules and lipids revealed 16 Kir4.1 inhibitors (0.4% hit rate). 3,3-Diphenyl-N-(1-phenylethyl)propan-1-amine, termed VU717, inhibits Kir4.1-mediated thallium flux with an IC_{50} of $\sim 6 \mu M$. An automated patch clamp assay using the IonFlux HT workbench was developed to facilitate compound characterization. Leak-subtracted ensemble "loose patch" recordings revealed robust tetracycline-inducible and Kir4.1 currents that were inhibited by fluoxetine ($IC_{50} = 10 \mu M$), VU717 ($IC_{50} = 6 \mu M$), and structurally

related calcium channel blocker prenylamine ($IC_{50} = 6 \mu M$). Finally, we demonstrate that VU717 inhibits Kir4.1 channel activity in cultured rat astrocytes, providing proof-of-concept that the TI^+ flux and IonFlux HT assays can enable the discovery of antagonists that are active against native Kir4.1 channels.

Introduction

Refer to **Chapter I** for a review of the inward rectifier family of potassium (Kir) channels. Kir4.1 (*KCNJ10*) plays important roles in humans as underscored by loss-of-function mutations leading to SeSAME/EAST syndrome (reviewed in **Chapter I**), and thus may represent a druggable target for epilepsy and hypertension.

Kir4.1 constitutes the major K^+ conductance in brain and spinal cord astrocytes and contributes to a large negative membrane potential in these cells. It is generally believed that K^+ released into the extracellular space during trains of action potentials moves down its electrochemical gradient and into astrocytes via Kir4.1. The large negative membrane potential generated by Kir4.1 also contributes to glutamate uptake by astrocytes. Accordingly, knockout of *KCNJ10* depolarizes the astrocyte membrane potential and slows the rate of K^+ and glutamate uptake [26,27]. The loss of spatial buffering likely accounts, at least in part, for the reduced seizure threshold in SeSAME/EAST syndrome [28,29]. However, the severity of the SeSAME/EAST syndrome may be due in part to gliosis, aberrant myelination, and neuronal death during embryological development [24,27]. The development of selective small-molecule antagonists that are active in vivo would provide important tools for exploring the “druggability” of Kir4.1 and dissecting the relative contributions of acute versus chronic Kir4.1 loss-of-function in SeSAME/EAST syndrome. Furthermore, small-molecule activators of Kir4.1 may facilitate spatial buffering and lower the seizure threshold in epilepsy patients.

The renal consequences of SeSAME/EAST syndrome include polyuria, hypokalemia, and metabolic alkalosis, and are consistent with impaired NaCl reabsorption in the distal convoluted tubule (DCT). In the DCT, NaCl absorption is mediated by the thiazide diuretic-sensitive NaCl cotransporter (NCC), which is located in the apical membrane of this nephron segment. Heteromeric Kir4.1/5.1 channels expressed in the basolateral membrane of the DCT 1) recycle K^+ across the basolateral membrane to help maintain the activity of the $Na^+-K^+-ATPase$, and 2) hyperpolarize the basolateral membrane potential to facilitate the electrogenic exit of Cl^- ions. Knockout of *KCNJ10* in mice recapitulates the salt-wasting phenotype of subjects with SeSAME/EAST syndrome [28]. However, deletion of the Kir5.1-encoding gene *KCNJ16* paradoxically increases renal NaCl reabsorption [124]. As alluded to earlier, unlike homomeric Kir4.1 channels, Kir4.1/5.1 is critically regulated by intracellular pH (pHi) and is partially inhibited at physiological pHi. A loss of this negative regulation in *KCNJ16*-knockout mouse leads to an increase in Kir4.1 activity and NaCl reabsorption in the DCT [29]. Kir4.1/5.1 antagonists would be expected to mimic thiazide diuretics by indirectly inhibiting NCC-mediated NaCl reabsorption. However, they could offer some important advantages over conventional diuretics due to the localization of the channel on the basolateral membrane [125-127]. Loop and thiazide diuretics must first be secreted by renal proximal tubule cells before reaching their sites of action on the apical membrane [128-131]. Interactions between diuretics and other secreted drugs, including antibiotics, NSAIDs, antivirals, as well as organic acid in the setting of renal failure, can limit their secretion and natriuretic effects. Kir4.1/5.1 inhibitors acting directly on the basolateral membrane should circumvent this limitation. Furthermore, Zaika *et al.* (2013) reported recently that dopamine inhibits Na^+ reabsorption in the cortical collecting duct (CCD) through inhibition of Kir4.1 homomeric and Kir4.1/5.1 heteromeric channels [132]. Conceivably,

Kir4.1/5.1 antagonists would exhibit greater clinical efficacy than thiazide diuretics due to inhibition of sodium reabsorption in multiple nephron segments, unlike conventional diuretics that tend to work on single segments. Identifying subtype-selective modulators active against Kir4.1 or Kir4.1/5.1 channels will be essential for investigating the druggability of Kir4.1 as an anti-hypertensive target.

Loss-of-function mutations in the methyl CpG binding protein 2 (*MECP2*) gene give rise to Rett syndrome, a neurological disorder characterized by difficulties with communication, learning, and motor coordination. Of relevance to the present discussion, the *MECP2*-null mouse exhibits increased expression of Kir4.1 in the locus coeruleus, a brainstem region involved in regulation of respiratory activity by carbon dioxide (CO₂) [133]. Zang *et al.* (2011) proposed that an increase in CO₂/pH-insensitive Kir4.1 homotetrameric channels and loss of CO₂/pH-sensitive Kir4.1/5.1 heteromeric channels leads to a blunted respiratory response to CO₂ and dysregulation of respiratory rhythmogenesis in Rett syndrome patients. If this is correct, and barring untoward general effects on neurotransmission, then small-molecule antagonists of homotetrameric Kir4.1 channels may help correct breathing abnormalities in Rett syndrome patients [134,135].

Evaluating the therapeutic potential of Kir4.1 awaits the development of potent, specific, and bioavailable small-molecule modulators, as the molecular pharmacology of Kir4.1 is limited to a small number of neurological drugs (e.g. selective serotonin reuptake inhibitors and tricyclic antidepressants) exhibiting weak off-target activity toward the channel. Here we report the development and validation of a fluorescence-based thallium (Tl⁺) flux assay to enable high-throughput library screening and an automated patch clamp electrophysiology assay that utilize an IonFlux HT workstation to facilitate hit validation and characterization.

Materials and Methods

Molecular biology and stable cell line generation

The human Kir4.1 channel open reading frame was purchased from OriGene Technologies (NM_002241.4; Origene) and sub-cloned into pcDNA5/TO (Life Technologies) using standard molecular biology techniques. Polyclonal T-REx-HEK293 cell lines stably transfected with pcDNA5/TO-Kir4.1 were established essentially as described previously [20,136]. Monoclonal cell lines were isolated through limiting dilution in 384-well plates and tested for tetracycline inducible TI^+ flux, as outlined below. The cell lines were maintained in DMEM growth medium containing 10% FBS, 50 U/ml Penicillin, 50 μ g/mL Streptomycin, 5 μ g/mL Blasticidin S and 250 μ g/mL Hygromycin in a 5% CO_2 incubator at 37 °C.

Manual patch clamp electrophysiology

T-REx-HEK293-Kir4.1 cells were used for patch clamp analysis following overnight induction with tetracycline (1 μ g/mL). The standard pipette solution contained (in mM): 135 KCl, 2 $MgCl_2$, 1 EGTA, 10 HEPES-free acid, and 2 Na_2ATP (Roche), pH 7.2, 275 mOsmol/kg. The standard bath solution contained (in mM): 135 NaCl, 5 KCl, 2 $CaCl_2$, 1 $MgCl_2$, 5 glucose, and 10 HEPES-free acid, pH 7.4, 290 mOsmol/kg. Electrodes pulled from capillary glass had resistances of 3.0-3.5 $M\Omega$ when filled with pipette solution. Voltage and current signals were generated and acquired using an Axopatch 200B amplifier and Digidata 1322A analog-to-digital converter (Molecular Devices). Data acquisition and analysis were performed using pClamp 9.2 software (Molecular Devices). All recordings were made at room temperature (20-23°C).

Western blot analysis

Monoclonal T-REx-HEK293-Kir4.1 cells were plated at a density of 1×10^5 cells/cm² and cultured overnight in the absence or presence of tetracycline (0.01-1.0 µg/mL), washed three times with ice-cold phosphate-buffered saline (PBS) and solubilized in ice-cold RIPA buffer containing (in mM): 150 NaCl, 100 NaF, 50 Tris-HCl (pH 8.0), 35 sodium deoxycholate, 5 EDTA, 1% Triton X-100, 0.1% SDS and 1X Protease Inhibitor Cocktail. Cell lysates were scraped into Eppendorf tubes, sonicated, rotated end-over-end for 30 min at 4°C, and then centrifuged for 10 min to pellet insoluble material. The protein concentration of cleared lysates was quantitated using BCA reagent (Thermo Scientific). Cell lysates were either used immediately or frozen as single-use aliquots at -80°C for subsequent immunoblot analysis.

Proteins were separated electrophoretically using 10% Bis-Tris NuPAGE gels (Life Technologies) and transferred to 0.45 µm pore nitrocellulose membranes (BioRad, Hercules, CA) for immunoblot analysis. Membranes were blocked overnight at 4°C in Tris-buffered saline (25 mM Tris, 1.3 mM KCl and 137 mM NaCl) containing 0.1% TWEEN-20 (TBST) and 5% nonfat milk. Membranes were incubated for 1 h at room temperature in polyclonal Kir4.1 antiserum (Alomone Labs) diluted 1:500 in milk-TBST and subsequently for 1 h at room temperature in milk-TBST containing HRP-conjugated secondary antiserum diluted 1:40,000. Protein bands were visualized on film using enhanced chemiluminescence detection methods (Thermo Scientific). Membranes were stripped in buffer containing 100 mM 2-mercaptoethanol, 62.5 mM Tris-HCl (pH 6.7) and 2% SDS (50°C for 30 min) and reprobed with β-actin antiserum.

Tl⁺ flux assay development and library screening

A Tl⁺ flux assay of Kir4.1 function was developed essentially as described previously [137]. Briefly, T-REx-HEK293-hKir4.1 cells (20,000 cells/20 μ L per well) were plated in clear-bottomed, amine-coated, black-walled 384-well plates (BD Biosciences) and cultured overnight in DMEM containing 10% dialyzed FBS, 50 U/mL Penicillin, 50 μ g/mL Streptomycin, 5 μ g/mL Blasticidin S and 250 μ g/mL Hygromycin and 1 μ g/mL tetracycline (assay media) at 37 °C in the presence of 5% CO₂. The following day, a dye stock was prepared fresh by dissolving 50 μ g Fluozin-2 (Life Technologies) in 100 μ L of anhydrous DMSO. To prepare the dye loading solution, 50 μ L of 20% pluronic acid is added to the above dye stock and the dye stock was diluted to 2 μ M with Assay Buffer (AB) (Hanks Balanced Salt Solution + 20 mM HEPES, pH 7.3). Twenty microliters was added to each well containing cells. The cells were incubated for 60 min at room temperature (RT), followed by automated washing using the ELx405 plate washer (BioTek) primed with AB. A final aspiration step resulted in 20 μ L residual volume. The plate was loaded into the Functional Drug Screening System 6000 (FDSS6000; Hamamatsu) to obtain an initial baseline image (F₀)–10 images at 1 Hz (excitation, 470 \pm 20 nm; emission, 540 \pm 30 nm). The FDSS's integrated 384-channel pipettor simultaneously added 20 μ L of DMSO vehicle control, fluoxetine or test compounds to each plate for final concentrations of 0.1 %, 100 and 10 μ M, respectively. Test compounds in 40 μ L of AB were prepared by transferring 80 nL into a 384 well polypropylene plate using the ECHO 550 acoustic formatter (Labcyte) from a 10 mM stock (BioFocus DPI). Four columns in each plate were filled with DMSO vehicle control or fluoxetine-containing buffer for determination of Z' (e.g. Fig. 3B), while the remaining 20 columns were used for compound screening. The compounds were allowed to incubate on the cells for 20 min at RT; then, the plate was reloaded into the FDSS and a second baseline

acquired. The FDSS's integrated pipettor added 10 μ L of thallium stimulus (125 mM sodium gluconate, 12 mM thallium sulfate, 1 mM magnesium sulfate, 1.8 mM calcium gluconate, 5 mM glucose, 10 mM HEPES, pH 7.3) while imaging of the flux continued at 1 Hz for 4 min total sampling time.

Concentration-response curves

Compound master plates were created by serial diluting compounds 1:3 from 10 mM stock in 100% DMSO using the BRAVO liquid handler (Agilent Technologies). Assay daughter plates were created using the ECHO 555 liquid handler (Labcyte), transferring 240 nL from the master plate to the daughter plate for each well followed by addition of 40 μ L of AB resulting in antagonist compound concentration-response curves (CRCs) starting at 60 μ M (2X final concentration). Concentration-response series were done in triplicate in the daughter plate. Cell plates and daughter compound plates were loaded onto an FDSS 6000. Baseline readings were taken (10 images at 1 Hz; excitation, 470 ± 20 nm; emission, 540 ± 30 nm) and 20 μ l of test compounds was added followed by 50 images at 1 Hz additional baseline. Following a 20-min incubation period, baseline readings were taken for 30 seconds followed by addition of Tl^+ stimulus buffer, followed by a 4-min read.

Data were analyzed using Excel (Microsoft Corp.). Raw data were opened in Excel and each data point in a given trace was divided by the first data point from that trace (static ratio). For experiments in which antagonists were added, data were again normalized by dividing each point by the fluorescence value immediately before the thallium addition to correct for any subtle differences in the baseline traces after the compound incubation period. The slope of the fluorescence increase beginning 5 s after Tl^+ addition and ending 15 s after Tl^+ addition was

calculated. The data were then plotted in Origin software (OriginLab Software, Inc.) to generate concentration-response curves after correcting for the slope values determined for baseline waveforms generated in the presence of vehicle controls. Potencies were calculated from fits using a four-parameter logistic equation.

Automated patch clamp electrophysiology

T-REx-HEK293-Kir4.1 cultured cells were induced overnight with 0.1 $\mu\text{g/ml}$ tetracycline prior to IonFlux automated electrophysiology. For cell isolation, cultured cells were washed with Ca- and Mg-free HBSS buffer, followed by Detachin™ solution (Genlantis) to detach them. The cells were resuspended in extracellular solution at 3×10^6 cells/ml. The extracellular solution contained (mM): 135 NaCl, 5 KCl, 2 CaCl₂, 1 MgCl₂, 5 glucose, and 10 HEPES-free acid, pH 7.4, 290 mOsmol/kg. The intracellular solution for the whole cell voltage clamp contained (mM): 5.4 CaCl₂, 1.8 MgCl₂, 120 KCl, 4 Na₂ATP, 10 HEPES, and 10 EGTA, pH 7.2 with KOH. The cell suspension in extracellular solution was dispensed into an IonFlux plate for recording. The IonFlux plate has been described previously [138,139]. In brief, the IonFlux HT plate consists of 32 unique experimental patterns with each experimental pattern being comprised of 12 wells in the form of an SBS standard 384-well plate with a unique microfluidic bottom. Within a 12-well experimental pattern, two wells, referred to as “traps” are filled with intracellular solution, eight wells are designated for compounds which can be applied at any time during the experiment, one well is filled with cell suspension in extracellular solution and the remaining, “waste” well contains the solution outflow during the experimental run. For each experimental pattern, there are two recordings. Each recording is from an ensemble of 20 cells patched in parallel on a single “trap”, such that the current measured is the sum of all 20 cells of the ensemble. Given

the variability in the quality of the seal for each given cell, the ensemble recording ends up being similar to “loose seal” recording conditions.

For recording Kir4.1 current, cells were voltage-clamped at -80 mV (which is near E_K for the solution pair used) and stepped to -120 mV then ramped at 0.5 mV/s to +120 mV, and finally stepped back to -80 mV. Given that the cells are being held near E_K , the current flow at the holding potential is primarily non-specific leak current, due in large part to the “loose seal” recording conditions. Kir4.1-specific current was estimated using the following formula:

$$I_{\text{Kir4.1}} = I_{-120 \text{ mV}} - (I_{-80 \text{ mV}} * 1.5)$$

This equation is based on the assumption that the current measured at -80 mV is exclusively, nonspecific leak. Data analysis and graphical presentation were performed using a combination of IonFlux, Excel and Origin software.

Animals

Experiments were performed on Sprague-Dawley rats and were approved by the University of Alabama Institutional Animal Care and Use Committee.

Astrocyte cultures

Spinal cord astrocytes were cultured in phenol red-free medium as described previously [26]. Briefly, postnatal day 0 (P_0) pups were decapitated and spinal cords were dissected into ice-cold serum-free EMEM (Gibco) containing 20 mM glucose. Once the meninges were stripped and cords were minced and placed into an O_2 saturated papain solution (Worthington)

for 20 min. The tissue was washed twice with spinal cord astrocyte media (EMEM supplemented with 10% fetal calf serum, 20 mM glucose, and penicillin/streptomycin) and then triturated. Cells were plated at a density of 1.0×10^6 cells/mL on polyornithine- and laminin-coated coverslips. The medium was changed every day for the first 3 days and then every fourth day thereafter. Electrophysiology was performed on astrocytes that had been in culture for 7-10 days.

Astrocyte electrophysiology

Whole-cell voltage-clamp recordings were made as described previously [26]. Coverslips were transferred to a Zeiss Observer D1 microscope (Zeiss) equipped with DIC optics. Signals were acquired using an Axopatch 200B amplifier, controlled by Clampex 10.2 software via a Digidata 1320 interface (Axon Instruments). Signals were filtered at 2 kHz and digitized at 5 kHz. Data acquisition and storage were conducted with the use of pClamp 10.2 (Axon Instruments). Whole-cell capacitance and series resistances were measured directly from the amplifier, with the upper limit for series resistance being 12 M Ω and series resistance compensation adjusted to 80% to reduce voltage errors. Coverslips were continuously perfused with artificial cerebral spinal fluid (ACSF) containing (in mM): 120 NaCl, 3 KCl, 1 MgCl₂, 2 CaCl₂, 26.2 NaHCO₃, 11 glucose and 5 HEPES, bubbled with 95% O₂ and 5% CO₂. The pipette solution contained (in mM) 125 K-gluconate, 10 KCl, 10 HEPES, 10 creatine phosphate, 2 MgATP, 0.2 NaGTP and 0.5 EGTA. Drugs were diluted in DMSO to a stock concentration and added directly to the bathing solution at a concentration of 1 μ L per milliliter (1:1,000).

Results

Cell line characterization

A monoclonal T-REx-HEK293 cell line expressing Kir4.1 from a tetracycline-inducible promoter was developed and characterized. Tetracycline-inducible cell lines are useful because 1) they can limit potential cell line degeneration and loss of assay performance due to K⁺ channel overexpression, and 2) they provide a convenient internal control for distinguishing effects of pharmacologically active compounds on endogenous TI⁺ flux pathways versus the overexpressed Kir channel of interest. Manual whole-cell patch clamp electrophysiology was used to characterize the functional and pharmacological properties of Kir4.1 channels expressed in T-REx-HEK293 cells. Under current clamp conditions, the resting membrane potential of cells cultured overnight in the absence or presence of tetracycline (1 µg/mL) was -23.8 ± 3.9 mV (n = 8) and -72.5 ± 0.6 mV (n = 5), respectively. The cells were voltage clamped at -75 mV, and then stepped between -120 mV and +120 mV in 10-mV increments for 250 ms to evoke whole-cell currents. Uninduced cells exhibited relatively small-amplitude outward currents at positive test potentials (**Fig. 1A**) carried by voltage-gated K⁺ and Cl⁻ channels endogenously expressed in HEK293 cells [140][141]. In sharp contrast, tetracycline induced the expression of large-amplitude inward and outward currents exhibiting weak rectification at positive test potentials (**Fig. 1B**). The current was inhibited by barium (not shown) as well as the selective serotonin reuptake inhibitor (SSRI) fluoxetine (**Fig. 1C**), as reported by Kurachi and colleagues [46,142]. The mean \pm SEM current-voltage (I-V) relationships recorded from uninduced cells (open circles; n = 5) or induced cells in the absence (closed circles; n = 8) or presence (open triangles; n = 4) of 100 µM fluoxetine are shown in **Fig. 1D**. Fluoxetine also inhibited the endogenous outward current in HEK cells (**Fig. 1C-D**), consistent with reports the drug inhibits other ion

channels [143-145]. Thus, overnight induction with tetracycline gives rise to robust, fluoxetine-inhibitable Kir4.1 channel activity in this stable cell line. As shown in **Fig. 1E**, western blot analysis revealed that overnight incubation with tetracycline led to the dose-dependent induction of Kir4.1 channel expression that reached a maximum level with 0.1 $\mu\text{g}/\text{mL}$ tetracycline. No Kir4.1-immunoreactive bands were observed in lysates prepared from nontransfected “parental” T-REx cells, indicating that the antiserum is specific for Kir4.1.

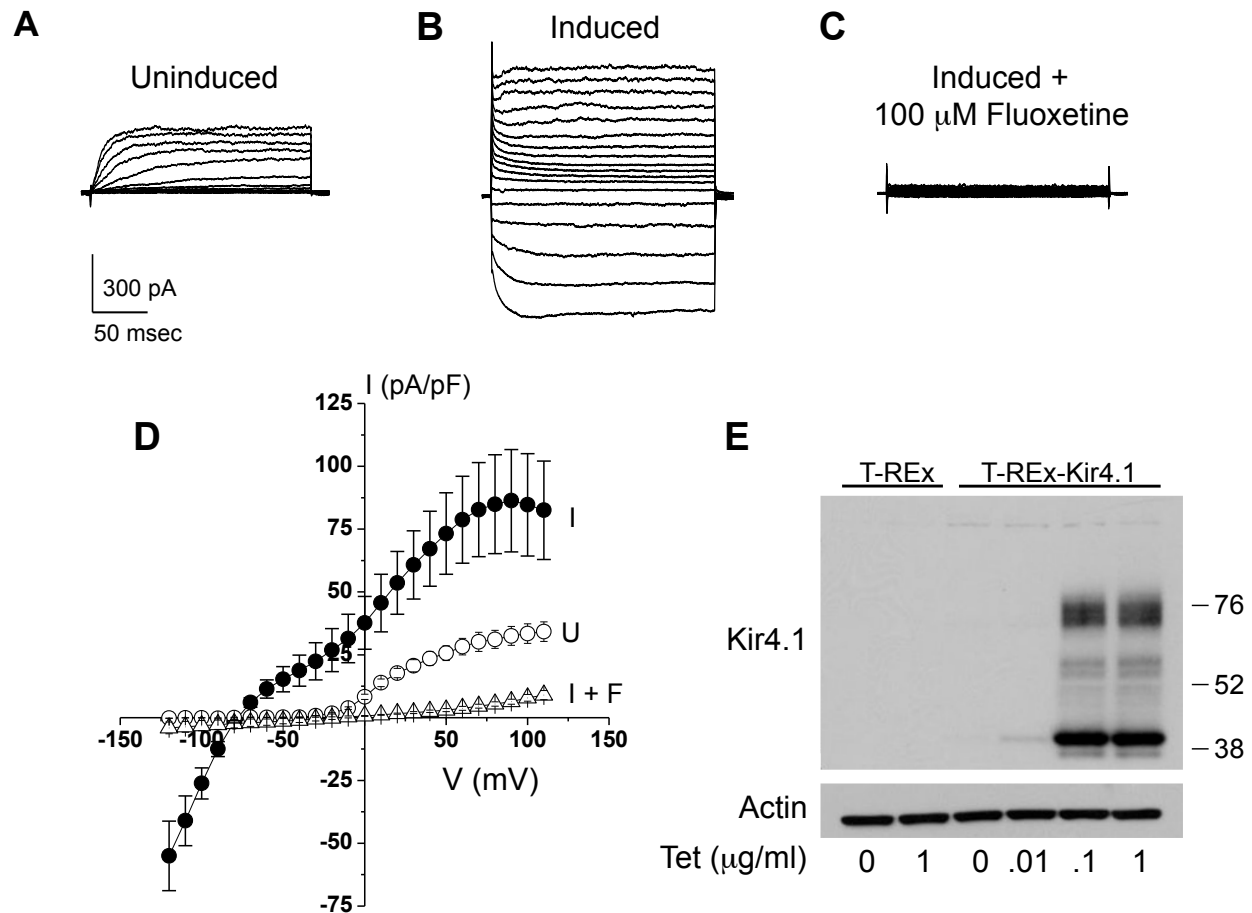


Figure 1. Tetracycline-inducible Kir4.1 expression in stably transfected T-REx-HEK293 cells. (A, B, C) Representative whole-cell currents recorded from monoclonal T-REx-HEK293-Kir4.1 cells cultured without tetracycline (A), or with tetracycline before (B) and after (C) bath addition of the Kir4.1 channel blocker fluoxetine. Cells were voltage clamped between -120 mV and +120 mV for 500 ms in 10mV increments from a holding potential of -75 mV. (D) Mean \pm SEM current-voltage (I-V) relationships from uninduced (U) or induced cells bathed in control buffer (I) or buffer containing 100 μ M fluoxetine (I + F). Current amplitude was normalized to cell capacitance and is expressed as pA/pF ($n = 5-6$). (E) Western blot analysis of Kir4.1 expression in lysates prepared from parental T-REx or T-REx-Kir4.1 cells cultured overnight with the indicated concentrations of tetracycline. Tet (0.1 and 1 μ g/mL) induced in T-REx-Kir4.1 cells, but not in the parental cells (T-REx), the expression of a prominent \sim 42 kDa band and higher-molecular-weight bands corresponding to differentially glycosylated forms of the channel. The membrane was stripped and reprobed for β -actin to ensure equal protein loading.

Tl⁺ flux assay

A quantitative Tl⁺ flux assay was developed to enable high-throughput screening (HTS) for small-molecule Kir4.1 modulators. The assay employs the fluorescent dye FluoZin-2 to report the inwardly directed movement of the K⁺ congener Tl⁺ through the channel pore, as reported by us for other Kir channels previously [20,21,64,137]. Monoclonal T-REx-HEK293-hKir4.1 cells were plated in clear-bottomed 384-well plates, cultured overnight in the absence or presence of tetracycline, and used in Tl⁺-flux assays the following day (see Materials and Methods for details). **Figures 2A** and **2B** show FluoZin-2 fluorescence emission traces recorded from wells containing uninduced or induced cells, respectively, before and after addition of various Tl⁺ concentrations (arrow; see below). The Tl⁺-induced fluorescence increase in uninduced cells (**Fig. 2A**) was relatively small, reflecting the movement of the cation through endogenous pathways. However, induction of Kir4.1 expression led to a dramatic increase in the rate and extent of Tl⁺ flux (**Fig. 2B**). Indeed, we were concerned that Tl⁺ flux was so high that the indicator dye may become saturated and limit the assay's ability to detect weak inhibitors or agonists, and therefore established a Tl⁺ concentration-response curve (CRC) to identify a submaximal concentration that still provided a robust signal window. The inset of **Fig. 2B** shows that mean \pm SEM change in FluoZin-2 fluorescence exhibited a sigmoidal, dose-dependent relationship that saturated around 2 mM Tl⁺. The concentration required to evoke ~80% of the maximal response was determined from the fit of a four-parameter logistic function to be 0.84 mM. This concentration was used for assay development and the pilot screen to provide "headroom" for identifying small-molecule activators of Kir4.1.

The sensitivity of the assay to the small-molecule solvent DMSO was determined by assessing Tl⁺ flux across a 2-fold dilution series of DMSO ranging from 0.1% to 5% v/v. As

shown in **Fig. 2C**, TI^+ flux was unaffected at concentrations up to 0.3% v/v, but it dropped off dose-dependently at higher concentrations. DMSO had no effect on Kir4.1-mediated TI^+ flux at the screening concentrations of 0.1% and 0.3% v/v (see below).

“Checkerboard” assays were performed on 3 separate days to determine the well-to-well uniformity within a plate and day-to-day reproducibility. Every other well of a 384-well plate containing tetracycline-induced T-REx-HEK-293-Kir4.1 cells was treated for 20 min with DMSO (vehicle) or 100 μM Fluoxetine (nonspecific blocker) before initiating TI^+ flux. In **Figure 2D**, TI^+ -induced FluoZin-2 fluorescence from each well of one plate is plotted, with the mean fluorescence and 3 standard deviations from the mean indicated with a μ and 3σ , respectively. The assay conditions afforded clear separation of the two cell populations, yielding a mean \pm SEM Z' value for 9 plates on 3 separate days of 0.75 ± 0.06 . Thus, the assay is robust, reproducible, and suitable for HTS.

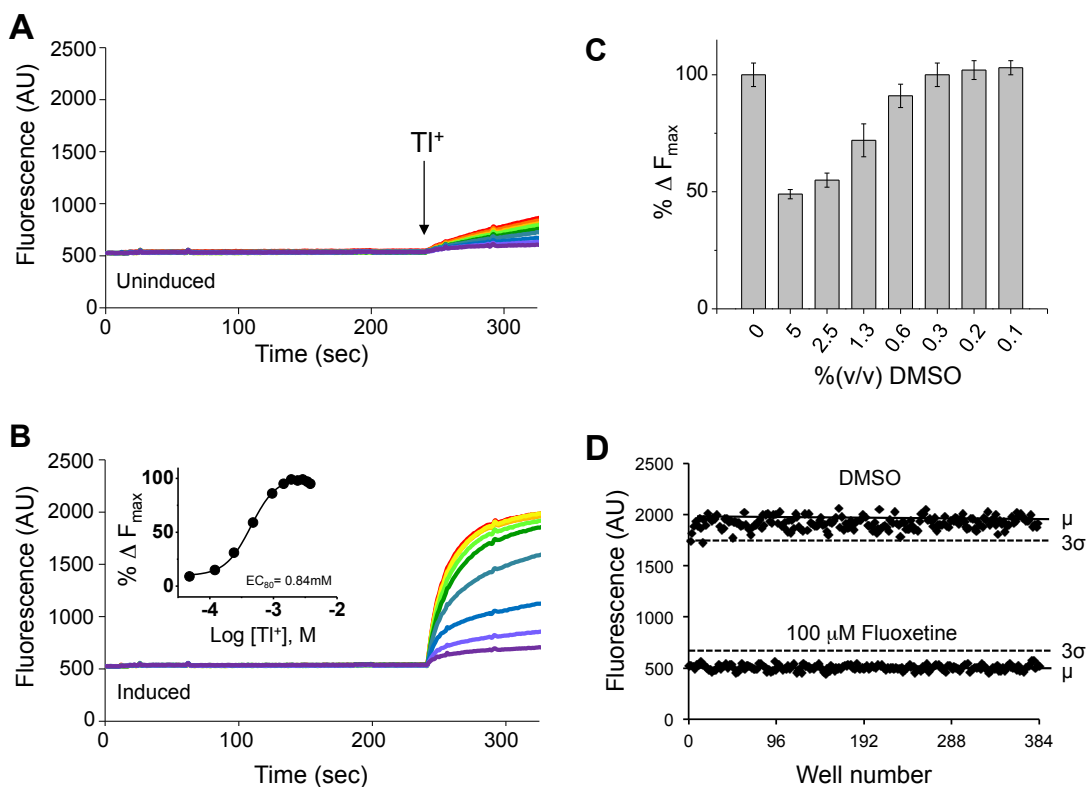


Figure 2. Thallium flux reporter assay of Kir4.1 channel function. (A, B) Representative Tl^+ -induced changes in FluoZin-2 fluorescence recorded from T-REx-HEK293-Kir4.1 cells cultured overnight without (A) or with (B) tetracycline. Baseline fluorescence was recorded for 4 min before Tl^+ addition (arrow). Mean \pm SEM ($n = 3$) concentration–response curve (CRC) and 4-parameter logistic fit for Tl^+ flux recorded from tetracycline-induced cells is shown in the inset of panel (B). (C) Dimethyl sulfoxide (DMSO) tolerance of Kir4.1-mediated Tl^+ flux. Data are means \pm SEM Tl^+ flux normalized to that recorded in the presence of DMSO ($n = 9$). (D) Representative checkerboard assay using DMSO (vehicle) or 100 μ M fluoxetine. The mean peak fluorescence amplitude of each sample population is indicated with a solid line. Three standard deviations from the mean are shown with a dashed line. The mean \pm SD Z' calculated over nine plates on 3 separate days was 0.75 ± 0.06 .

Discovery of a novel Kir4.1 inhibitor

The assay was validated with a screen of 3,655 small molecules and bioactive lipids at the Vanderbilt HTS center. Small molecules and lipids were tested at a nominal concentration of 10 μM (0.1% DMSO) and 3 μM (0.3% DMSO), respectively. The mean Z' for the entire 19-plate run, calculated from the peak fluorescence amplitude in vehicle or fluoxetine-treated wells, was 0.82 ± 0.04 . The hit rate was 0.4% (16/3,655 compounds). All of the hits were inhibitors, none of which were lipids. The most potent inhibitor identified was 3,3-diphenyl-*N*-(1-phenylethyl) propan-1-amine, which we termed VU717. The chemical structure is shown in **Fig. 3A**. In TI^+ flux assays, VU717 dose-dependently inhibited Kir4.1 activity with an IC_{50} of 6.3 μM and Hill coefficient of 4.5 (**Figs. 3B-C**).

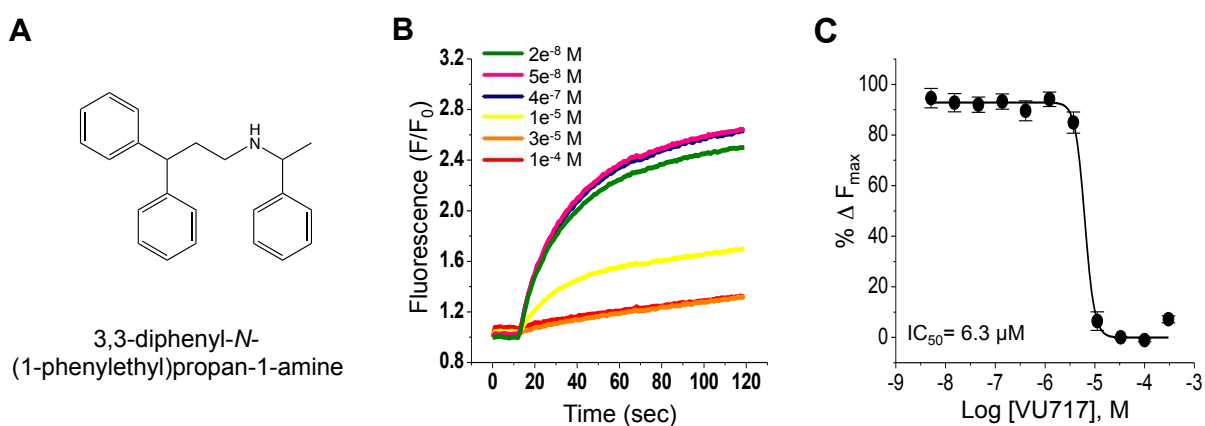


Figure 3. Discovery of a novel Kir4.1 channel inhibitor in a TI^+ flux-based pilot screen. (A) Chemical structure of 3,3-diphenyl-*N*-(1-phenylethyl) propan-1-amine (VU717). (B) Representative FluoZin-2 fluorescence traces recorded from induced T-REx-HEK293-Kir4.1 cells treated with the indicated doses of VU717. (C) Mean \pm SEM CRC for VU717-dependent inhibition of Kir4.1-mediated TI^+ flux. Data are from three independent experiments performed in triplicate.

Development of an automated patch clamp assay for Kir4.1 using the IonFlux HT

Patch clamp electrophysiology is the gold standard technique for interrogating the pharmacology of ion channels. However, manual patch clamping is low-throughput and thus imposes a considerable bottleneck. We therefore set out to develop an automated patch clamp assay to minimize this bottleneck and facilitate the development of Kir4.1 channel modulators.

We first established the time required to induce Kir4.1 channel expression and function in T-REx-HEK293-Kir4.1 cells following induction with tetracycline. **Figure 4A** shows a representative Western blot of Kir4.1 (top panel) or actin (bottom panel, loading control) expression in lysates prepared from cells cultured with tetracycline (1 $\mu\text{g/ml}$) for 0, 2, 4, 6, or 18 h. Kir4.1 expression was time dependent and reached a maximum following 18 h of induction.

We then assessed Kir4.1 channel activity in cells induced for the same time period using an IonFlux HT automated patch clamp workstation. The IonFlux HT utilizes a network of microfluidic channels that enables fully automated cell introduction, trapping, sealing, whole-cell formation, and voltage clamp using 64 independent voltage clamp amplifiers. Recordings are made in the “loose patch” configuration from an ensemble of 20 cells per channel. This approach has the advantage of increasing the robustness and throughput of recordings, but may suffer from significant “leak” current introduced by sub-Giga-Ohm-resistance seals. We therefore employed Ba^{2+} to discriminate Kir4.1-mediated current from leak current. Cells were voltage clamped at a holding potential of -80 mV, which is near the calculated Nernst equilibrium potential for K^+ , and then stepped to a test potential of -120 mV. Currents were leak-subtracted as described in Material and Methods. The mean \pm SEM of Ba^{2+} -sensitive current at -120 mV is shown in **Fig. 4B**. In contrast to the Western blot results showing abundant Kir4.1 protein expression after only 6 h of tetracycline induction, no Ba^{2+} -sensitive currents were detectable at this time point.

Following 18 h of induction, however, robust Ba²⁺-inhibitable were clearly observed. Cells were therefore induced overnight with tetracycline in all subsequent experiments.

Figure 4C shows representative, leak-subtracted current traces recorded in the absence or presence of 300 μM Ba²⁺ from cells subjected to a voltage ramp between -120 mV and +120 mV. In control solution, the current exhibited a steep voltage-dependent relationship between -120 mV and +50 mV, a plateau around +60 mV, and rectification at potentials more positive than +70 mV. This current waveform is similar to that recorded from T-REx-HEK293-Kir4.1 cells using the manual patch clamp technique (**Fig. 1D**). The inward current was abolished by 300 μM Ba²⁺.

Figure 5A summarizes the current amplitudes recorded in the absence or presence of Ba²⁺ from an entire 384-well format plate on two separate days. Each plate consists of 32 “experimental patterns”, each containing 2 cell “traps”. Each data point represents the average current amplitude from two daughter traps. The mean \pm SD current amplitudes in control and Ba²⁺-treated cells were, respectively, -5857 ± 1438 pA and 886 ± 478 pA. Out of 64 patterns tested, 59 of these led to successful cell trapping, whole-cell formation, and recordings of Ba²⁺-inhibitable Kir4.1 channel activity (92% success rate).

The mean \pm SEM Ba²⁺ CRC recorded on two separate days are shown in **Fig. 5B**. The IC₅₀ values derived from 4-parameter logistic functions for days 1 and 2 were 3.59 ± 0.12 μM and 2.37 ± 0.12 μM , respectively. Taken together, these data indicate that robust Kir4.1-dependent channel activity can be readily measured using the IonFlux HT workstation.

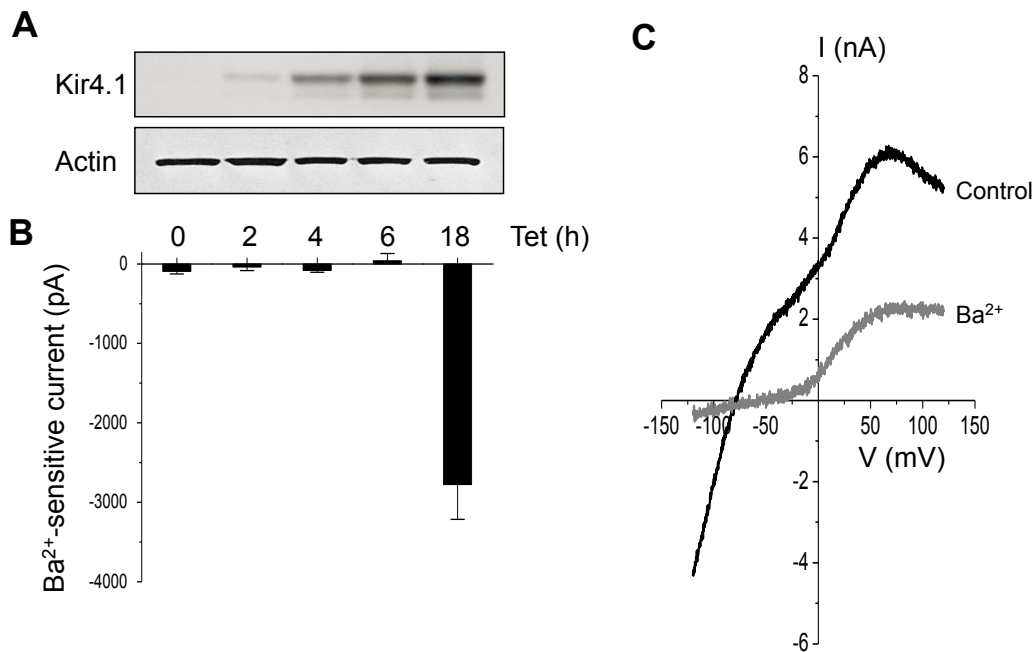


Figure 4. Automated patch clamp electrophysiology assay for Kir4.1. (A) Time-course of Kir4.1 protein expression in lysates prepared from cells cultured for the indicated times with tetracycline (0.1 $\mu\text{g}/\text{mL}$). β -actin was used as a loading control. (B) Corresponding time-course analysis of Ba²⁺-inhibitable Kir4.1 current amplitude at -120 mV recorded using an IonFlux HT automated patch clamp workstation. Following overnight induction with tetracycline, the cells were voltage clamped at a holding potential of -80mV and then ramped between -120 mV and +120 mV in the absence (control) and presence of 300 μM barium (Ba²⁺). Data are mean \pm SEM current amplitude at -120 mV. (C) Representative leak-subtracted (see the ‘‘Materials and Methods’’ section), whole-cell currents recorded in the absence or presence of Ba²⁺.

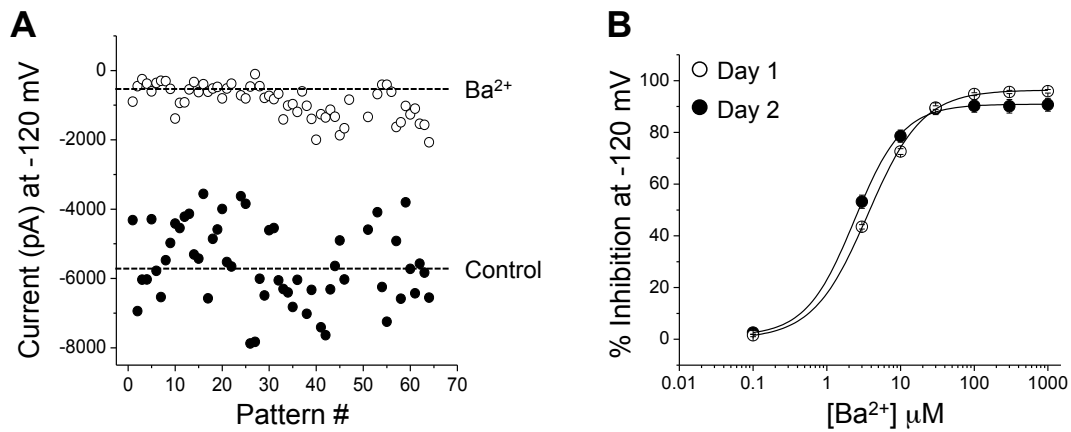


Figure 5. The IonFlux HT assay is reproducible. (A) Leak-subtracted whole-cell current amplitude recorded at -120 mV from individual microfluidic patterns in the absence or presence of 300 μM Ba²⁺. Data recorded on two separate days are shown. (B) Mean ± SEM Ba²⁺ CRC recorded on two separate days (n = 10–30).

Characterization of small-molecule Kir4.1 antagonists with the IonFlux HT

VU717 and fluoxetine share some chemical features that likely contribute to their activity toward Kir4.1, including two hydrophobic benzene rings and an ionizable secondary amine group (**Fig. 6A**). In an effort to identify other inhibitors of Kir4.1, a search of the National Center for Biotechnology Information PubChem database for structurally related substances revealed that the calcium channel blocker prenylamine (3,3-diphenyl-N-(1-phenylpropan-2-yl)propan-1-amine), shares these chemical features (**Fig. 6A**). Prenylamine was formerly used clinically as a vasodilator in the treatment of angina pectoris, but was discontinued because of its propensity to induce *torsades de pointes* by blocking hERG channels [146]. The potencies of VU717, prenylamine, and fluoxetine were compared across a 3-fold dilution series ranging from 300 nM to 100 μ M. The mean \pm SEM CRCs for the three compounds are shown in **Fig. 6B**. The IC_{50} values for VU717 (n = 6-43), prenylamine (n = 4-20), and fluoxetine (n = 2-17) were 6.0 ± 1.3 μ M, 6.2 ± 1.0 μ M, and 10.4 ± 3.2 μ M, respectively, and the Hill coefficients were 1.9, 2.0, and 2.3, respectively. For comparison, CRCs were established in Kir4.1 Tl^+ flux assays for VU717, prenylamine, and fluoxetine, which yielded IC_{50} values of 9.72 ± 2.0 μ M, 14.8 ± 1.9 μ M, and 22.8 ± 0.9 μ M, respectively. Thus, although the potencies derived from electrophysiology and Tl^+ flux assays differ by ~ 2.5 -fold, the Tl^+ flux assay assigned the correct rank-order potency across this series.

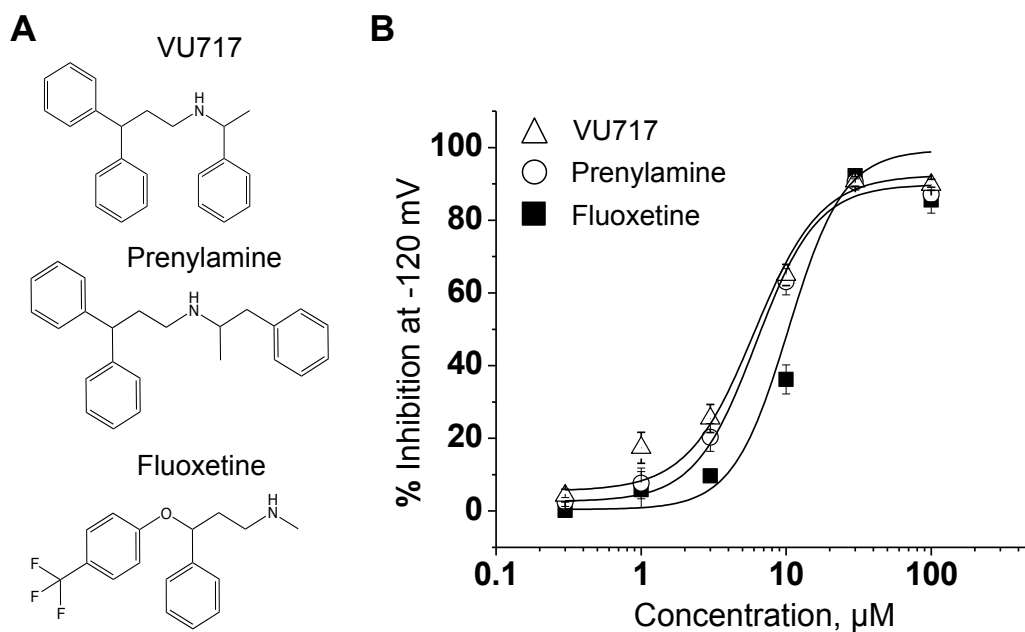


Figure 6. Characterization of small-molecule Kir4.1 inhibitors using the IonFlux HT. (A) Chemical structures of VU717, prenylamine, and fluoxetine. (B) Mean \pm SEM CRCs for VU717 (triangle, $n = 6-43$), prenylamine (circle, $n = 4-20$), and fluoxetine (square, $n = 2-17$). A fit of the CRC with a single-site four-parameter logistic function yielded IC_{50} values of 6.0 ± 1.3 , 6.2 ± 1.0 , and $10.4 \pm 3.2 \mu\text{M}$, respectively, for VU717, prenylamine, and fluoxetine.

VU717 inhibits native Kir4.1 channels in astrocytes

Given that VU717 was discovered in a screen against a heterologously expressed channel, we assessed the effects of the compound on astrocyte currents to determine if VU717 is active against native Kir4.1 channels. Astrocytes exhibiting significant arborization were selected under DIC microscopy for voltage clamp recording (**Fig. 7A**, inset). In response to a linear voltage ramp (-160 mV to +160 mV over 300 ms) these cells responded with a large amplitude current that reversed at -80 mV (**Fig. 7B**). This current was nearly completely inhibited in the presence of 250 μM Ba^{2+} containing ACSF, identifying this current as Kir4.1 mediated current as previously described [26,147]. Barium was then washed off and the currents quickly returned to baseline. ACSF containing 10 μM or 30 μM VU717 was then applied to the voltage clamped cell until maximum inhibition was achieved. **Figure 7B** shows that 10-30 μM VU717 inhibited approximately 90% of the whole-cell current at -120 mV, which is nearly identical to that blocked by 250 μM barium. This is comparable to that observed in conventional patch clamp recordings from Kir4.1-expressing HEK293 cells in which VU717 inhibited $94 \pm 1.8\%$ ($n = 5$) of current at -120 mV. This data clearly indicates that the TI^+ flux assay is capable of identifying inhibitors of native Kir4.1 channels.

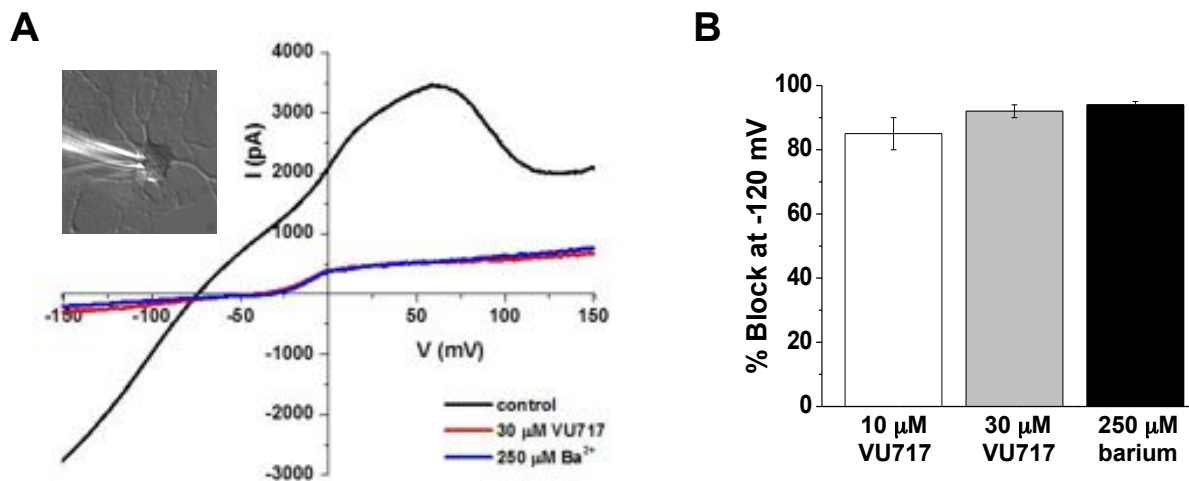


Figure 7. VU717 inhibition of native Kir4.1 activity channels in astrocytes. (A, B) Representative I-V relationships recorded by voltage ramping a cell from -160 mV to +160 mV in control artificial cerebral spinal fluid (ACSF) or ACSF containing 30 μM VU717 or 250 μM Ba²⁺. A DIC image of a cultured astrocyte is shown in the inset. (B) Mean ± SEM % inhibition of astrocyte whole-cell current at -120 mV by VU717 (10 and 30 μM; n = 5, n = 6, respectively) or Ba²⁺ (250 μM; n = 16).

Discussion

The assays developed herein should support a robust small-molecule probe discovery effort for Kir4.1. The TI^+ flux assay developed originally by Weaver *et al.* (2003) and later commercialized by Invitrogen and TEFlabs under the FluxOR[®] and Thallos labels, respectively, has now been used to establish fluorescence-based functional assays for a variety potassium channels, including Kir1.1, Kir2.1, Kir2.3, Kir3.1/3.2, Kir7.1, hERG, KCNQ4 [20,21,50,64,82,83,85,148-150], as well as the potassium-chloride co-transporter KCC2 [108]. Most Kir channels are well suited for the TI^+ flux assay, because they typically exhibit a large open probability near the resting membrane potential of the cell and therefore do not require activation by depolarization or an agonist. This is not true of G protein-coupled Kir3 channels, which require activation with a Gi/o-coupled receptor before TI^+ addition [64,83].

Like most of the TI^+ flux assays developed by our group [20,21,64,137], the Kir4.1 assay employs a tetracycline-inducible HEK293 cell expression system. This offers a number of experimental advantages over constitutive expression systems for assay development and HTS. For example, the ability to quantitate “background” TI^+ flux through endogenous pathways and a K^+ channel target of interest is useful for selecting stably transfected clones affording the most robust signal window for screening. Dozens of clones cultured in the absence or presence of tetracycline can be assayed simultaneously, and those exhibiting the strongest tetracycline-inducible signal can be selected for assay development. In the absence of suitable reference compounds (e.g. fluoxetine used in this study), uninduced cells could be included in assay plates as a “blocked” control for calculating Z' scores. Finally, false-positive hits acting on endogenous TI^+ flux pathways, as opposed to the K^+ channel target, can be rapidly identified and triaged in screens against uninduced cells. As shown in **Figs. 2A** and **2B**, Kir4.1-mediated TI^+ flux

dominates the signal window, which increases the ability of the assay to identify specific Kir4.1 modulators.

In pilot experiments, we noted that the fluorescence emission of FluoZin-2 approached its asymptotic value within ~60 sec of adding TI^+ to the cell plate. Such robust TI^+ flux was not surprising given that 1) the cell line was selected for high Kir4.1 expression and function, and 2) Kir4.1 is a “weak rectifier” exhibiting a high open-state probability across a broad range of membrane potentials, unlike some voltage-gated K^+ channels that require depolarization for channel opening and TI^+ flux [82]. However, the robustness of TI^+ flux raised concerns that the dye would become saturated and fail to report subtle changes in Kir4.1 activity caused by pharmacologically weak modulators in a screen. We reasoned that using a lower TI^+ concentration would prevent saturation, increase the sensitivity of the assay, and provide “headroom” for identifying activators. From dose-response experiments, an EC_{80} concentration of 0.84 mM was determined, which represents only 15% of that used previously by our group [20,21,64,137]. Despite the use of lower TI^+ concentrations, which tended to slightly increase the well-to-well variability in fluorescence and reduce the mean Z' score (data not shown), the assay generated robust screening statistics indicating that it is suitable for HTS of chemical libraries. Our studies of VU717 show that the assay is clearly capable of identifying a ~6 μM IC_{50} inhibitor of Kir4.1 in a primary screen, which is a reasonable starting point to developing a submicromolar inhibitor suitable for in vitro and ideally in vivo pharmacology.

With an anticipated hit rate of 0.4%, it would take several weeks to characterize a hit collection from a large compound screen using “gold standard” manual patch clamp electrophysiology techniques. We therefore evaluated the IonFlux HT as an automated patch clamp workstation for characterizing Kir4.1 modulators in a shorter time frame while

maintaining fidelity. The IonFlux platform technology is based on the Fluxion's proprietary microfluidic system, which enables ensemble cell recording in a continuous manner. While already validated for the study of ligand-gated, voltage-gated, sodium and hERG channels pharmacology [138,139], this is the first study to show that the IonFlux platform can be adapted for the study of Kir channel pharmacology. Kir4.1 is considered a "weak rectifier" since a decrease in channel conductance (i.e. rectification) is only observed at relatively large positive potentials (e.g. **Fig. 4A**). This presented a challenge for discriminating Kir4.1-derived current in "loose patch" recordings contaminated by "leak" current, because both channel-mediated and leak currents exhibit Ohmic (linear) current-voltage relationships across most of the voltage range tested. To circumvent this problem, we reasoned that all of the Kir4.1-mediated current would reverse directions at the Nernst equilibrium potassium for potassium (E_K), which was approximately -80 mV under the recording conditions used as opposed to 0 mV for leak-mediated currents. Leak current, defined as the offset current at -80 mV multiplied by 1.5 (i.e. -80 mV x 1.5 = -120 mV), was subtracted from the whole-cell current amplitude at -120 mV to yield values for leak-subtracted Kir4.1 current amplitude. The results suggest that this platform is sufficiently robust (> 90% success rate) to provide an initial electrophysiological characterization of small molecule inhibitors of Kir4.1. With a runtime of ~30 min per plate and the ability to characterize up to 30 compounds along with controls on a given plate the system will be capable of producing CRCs for hundreds of compounds per day.

In conclusion, we have developed and validated a robust TI^+ flux assay to support a primary screen for small-molecule modulators of Kir4.1. A pilot screen of 3,655 small-molecules and lipids and a subsequent structural homology search led to the discovery of the novel Kir4.1 antagonists VU717 and prenylamine. In addition, we demonstrated for the first time that Kir4.1

channel pharmacology can be characterized in automated loose patch clamp electrophysiology assays using the IonFlux HT workstation. The development of small-molecule Kir4.1 modulators using these assay platforms will provide critically needed tools for investigating the integrative physiology and therapeutic potential of Kir4.1 in temporal lobe epilepsy and hypertension.

Chapter V

DIRECT ACTIVATION OF β -CELL K_{ATP} CHANNELS WITH A NOVEL XANTHINE DERIVATIVE

This chapter was reprinted with permission of the American Society for Pharmacology and Experimental Therapeutics. All rights reserved.

Abstract

ATP-regulated potassium (K_{ATP}) channel complexes of Kir6.2 and SUR1 critically regulate pancreatic islet beta-cell membrane potential, calcium influx, and insulin secretion, and consequently, represent important drug targets for metabolic disorders of glucose homeostasis. The K_{ATP} channel opener diazoxide is used clinically to treat intractable hypoglycemia caused by excessive insulin secretion, but its use is limited by off-target effects due to lack of potency and selectivity. Some progress has been made in developing improved Kir6.2/SUR1 agonists from existing chemical scaffolds and compound screening, but there are surprisingly few distinct chemotypes that are specific for SUR1-containing K_{ATP} channels. Here we report the serendipitous discovery in a high-throughput screen of a novel activator of Kir6.2/SUR1, termed VU0071063. The xanthine derivative rapidly and dose-dependently activates Kir6.2/SUR1 with a half-effective concentration (EC₅₀) of approximately 7 μ M, is more efficacious than diazoxide at low micromolar concentrations, directly activates the channel in excised membrane patches, and is selective for SUR1- over SUR2A-containing Kir6.1 or Kir6.2 channels, as well as Kir2.1, Kir2.2, Kir2.3, Kir3.1/3.2, and Kv2.1. Finally, we show that VU0071063 activates native Kir6.2/SUR1 channels, thereby inhibiting glucose-stimulated calcium entry in isolated mouse pancreatic beta-cells. VU0071063 represents a novel tool/compound for investigating beta-cell

physiology, K_{ATP} channel gating, and a new chemical scaffold for developing improved activators with medicinal chemistry.

Introduction

By integrating cellular metabolism, membrane potential (V_m), and excitability, ATP-sensitive K^+ (K_{ATP}) channels carry out fundamental roles in nerve, muscle, epithelial, and endocrine tissue physiology [30]. The molecular structure of K_{ATP} channels is reviewed in **Chapter I**.

Pancreatic islet β -cell K_{ATP} channels are validated drug targets for type 2 diabetes and severe hypoglycemia resulting from excessive insulin secretion [2]. Increases in blood glucose induce MgATP-dependent Kir6.2/SUR1 channel inhibition, V_m depolarization, Ca^{2+} influx through L-type voltage-dependent Ca^{2+} channels (VDCC), and secretion of insulin, which, in turn, acts on a myriad of target tissues to promote glucose uptake and utilization [151]. Sulfonylurea drugs (e.g. glibenclamide, tolbutamide) that directly inhibit Kir6.2/SUR1 and stimulate insulin secretion are used clinically to help manage glycemic levels in type 2 diabetic patients. In contrast, K_{ATP} channel activators (e.g. diazoxide) are used to treat disorders of severe hypoglycemia, such as congenital hyperinsulinism and insulin-producing pancreatic tumors [151,152]. The major K_{ATP} channel subtype in cardiomyocytes consists of Kir6.2 and SUR2A [32], and potassium channel opener (KCO) activation of sarcolemmal K_{ATP} channels and V_m hyperpolarization affords cardioprotection from subsequent ischemia-reperfusion injury [153]. Activation of vascular smooth muscle Kir6.1/SUR2B with pinacidil or diazoxide leads to vasodilation and a reduction in blood pressure [31], but can also result in pathological edema and

other cardiovascular pathologies reminiscent of those found in Cantu syndrome, which results from gain-of-function mutations in SUR2 [32].

Given the broad tissue distribution of K_{ATP} channels, their important physiological roles, and therapeutic as well as pathological potential in various conditions, there is considerable interest in the continued development of pharmacological modulators for targeting specific subtypes of K_{ATP} channels [154]. Here, we report the serendipitous discovery of a novel xanthine derivative that directly activates heterologously expressed Kir6.2/SUR1 channels and native pancreatic β -cell K_{ATP} channels. The activator, termed VU0071063, is more potent and efficacious than diazoxide and is selective for SUR1-containing K_{ATP} channels. VU0071063 represents a new tool compound for interrogating Kir6.2/SUR1 channel physiology and structure-function relationships of K_{ATP} channel gating.

Materials and Methods

Expression vectors

The following vectors were used in this study: pcDNA5/TO-Kir6.2 (NM_010602), pcDNA5/TO-Kir6.1 (NM_004982), pcDNA3.1-SUR1 (L40623.1), pCMV6c-SUR2A (D83598.1), pcDNA5/TO-Kir2.1 (NM_000891.2), pcDNA5/TO-Kir2.2 (NM_021012), pcDNA5/TO-Kir2.3 (NM_152868).

Cell lines and transfections

T-REx-HEK293 cells were transfected with pcDNA5/TO-Kir6.2 using Lipofectamine 2000 (Life Technologies) and cultured with Blasticidin and Hygromycin to select stably

transfected cells as previously described [20,64]. After confirming they exhibited tetracycline-inducible Kir6.2 expression by Western blot analysis (**Fig. 1A**), the cells were co-transfected with pcDNA3.1-SUR1 and grown in G418-containing medium to select cells carrying stably integrated plasmids for both K_{ATP} channel subunits. Monoclonal lines were isolated by limiting dilution, expanded, and tested for tetracycline-inducible thallium (Tl^+) flux, as described below. One cell line exhibiting robust Tl^+ flux was selected for assay development and small-molecule screening. Monoclonal T-REx-HEK293 cell lines expressing other mammalian Kir channels were generated as described previously [20,64]. Monoclonal mGluR8/GIRK/HEK293 cells stably expressing Kir3.1/3.2, the M4 muscarinic receptor and rat mGluR8a were cultured as described previously [83]. For transient transfections, HEK293T cells were transfected with 1 μ g of Kir6.x, 2 μ g SURx, and 0.5 μ g of pcDNA3.1-EGFP (transfection marker) using Lipofectamine LTX Plus according to the manufacturer's instructions.

Western blot analysis

Western blot analysis of Kir6.2 expression was performed following 24-h induction with tetracycline essentially as described previously [20]. Goat polyclonal Kir6.2 antiserum (SC-11226) and donkey anti-goat HRP-conjugated antiserum (SC-2020) were purchased from Santa Cruz.

Tl^+ flux assays

Tl^+ flux assays were performed essentially as described previously [137]. Briefly, stably transfected T-Rex-HEK-293 cells expressing Kir6.2/SUR1 channels were cultured overnight in

384-well plates (20,000 cells/20 μ L/well black-walled, clear-bottomed PureCoat amine-coated plates; BD, Bedford, MA) with a plating media containing DMEM, 10% dialyzed FBS and 1 μ g/mL tetracycline. On the day of the experiment, the cell culture medium was replaced with dye-loading solution containing assay buffer (Hanks Balanced Salt Solution with 20 mM HEPES, pH 7.3), 0.01% (w/v) Pluronic F-127 (Life Technologies, Carlsbad, CA), and 1.2 μ M of the thallium-sensitive dye Thallo-AM (TEFlabs, Austin, TX). Following 1 hr incubation at room temperature, the dye loading solution was washed from the plates and replaced with 20 μ L/well of assay buffer. The plates were transferred to a Hamamatsu Functional Drug Screening System 6000 (FDSS6000; Hamamatsu, Tokyo, Japan) and 20 μ L/well of test compounds in assay buffer (as prepared below) was added. After a 20 minute incubation period, a baseline recording was collected at 1 Hz for 10 s (excitation 470 ± 20 nm, emission 540 ± 30 nm) followed by addition of TI^+ stimulus buffer (10 μ L/well) and data collection for an additional 4 min. The TI^+ stimulus buffer contains in (mM) 125 NaHCO_3 , 1.8 CaSO_4 , 1 MgSO_4 , 5 glucose, 1.8 TI_2SO_4 , 10 HEPES, pH 7.4. For TI^+ flux assay on Kir3.1/3.2 expressing cells, the thallium stimulus buffer contains 12 mM TI_2SO_4 and either an EC_{20} or EC_{80} of glutamate (Sigma-Aldrich, St. Louis, MO).

Test compounds from the Vanderbilt Institute of Chemical Biology (VICB) library were dispensed into in polypropylene 384-well plates (Greiner Bio-One, Monroe, NC) using an Echo555 liquid handler (Labcyte, Sunnyvale, CA) diluted in assay buffer to 2X final concentrations to generate 4- or 11-point 3-fold serial dilution series. The K_{ATP} channel inhibitors glibenclamide and tolbutamide were resuspended in assay buffer containing VU0071063 or diazoxide. TI^+ flux assays on Kir2.1, Kir2.2, Kir2.3, and Kir3.1/3.2 were performed as described previously [64].

Tl⁺ flux data were analyzed as previously [137] described using a combination of Excel (Microsoft Corp, Redmond, WA) with XLfit add-in (IDBS, Guildford, Surrey, UK) and OriginPro (OriginLab, Northampton, MA) software. Each data point in a given trace was divided by the first data point from that trace (static ratio) followed by subtraction of data points from control traces generated in presence of vehicle controls. The slope of the fluorescence increase beginning 5 s after Tl⁺ addition and ending 15 s after Tl⁺ addition was calculated. The data were then plotted in Prism software (GraphPad Software, San Diego, CA) to generate concentration-response curves (CRCs). Potencies were calculated from fits to CRC data using a four parameter logistic equation.

Patch clamp electrophysiology

Transfected cells were dissociated with trypsin, plated on poly-L-lysine-coated glass coverslips, and allowed to recover for at least 1 h before experiments. Coverslips were transferred to a small-volume perfusion chamber and mounted on the stage of an inverted microscope. Patch electrodes were pulled from 1.5-mm outer diameter glass capillaries and had resistances ranging from 3-5 M Ω when filled with the following intracellular solution (in mM): 135 KCl, 2 MgCl₂, 1 EGTA, 10 HEPES, and 3 Na₂ATP, pH 7.3. The standard bath solution contained (in mM): 135 NaCl, 5 KCl, 2 CaCl₂, 1 MgCl₂, 5 glucose, and 10 HEPES, pH 7.4. Whole-cell currents were recorded under voltage-clamp conditions using an Axopatch 200B amplifier (Molecular Devices). The cells were voltage-clamped and stepped every 5 s from a holding potential of -75 to 120 mV for 200 ms, then ramped at a rate of 2.4 mV/ms from -75 to 120 mV before returning to -75 mV. Electrophysiological data were collected at 5 kHz and

filtered at 2 kHz. Data acquisition and analysis were performed using pClamp 9.2 software (Molecular Devices).

For excised-patch clamp measurements, COSm6 cells were transiently transfected with Kir6.2, SUR1, and EGFP for 24 hours before patch-clamp analysis. Transfected cells were identified by GFP fluorescence and membrane patches were voltage-clamped. The pipette (resistance 1-2.5 M Ω) and bath solutions were (in mM): 140 KCl, 10 HEPES and 1 EGTA and 0.5 free Mg²⁺, pH 7.35). After sealing, the membrane patch was excised to the inside-out configuration. Currents were recorded at a membrane potential of -50 mV using pClamp 8.2 software.

Calcium imaging

Islet-cell intracellular calcium ([Ca²⁺]_i) was measured using Ca²⁺ sensitive dye fura-2 (Life Technologies) as previously described [155]. Briefly, mouse islets were dissociated in 0.005% trypsin, plated on glass coverslips, and cultured for 16 h in RPMI-1640 medium supplemented with 10% fetal calf serum (FCS), concentrations of glucose specified, 100 IU mL⁻¹ penicillin, and 100 mg mL⁻¹ streptomycin. Cells were dye-loaded for 20 min at 37°C with 2 μ M fura-2-AM in solution containing (in mM): NaCl, 119; CaCl₂·[(H₂O)₆], 2.5; KCl, 4.7; Hepes, 10; MgSO₄, 1.2; KH₂PO₄, 1.2; glucose, 2; pH 7.35. Fluorescence imaging was performed using a Nikon Eclipse TE2000-U microscope equipped with an epifluorescent illuminator (Sutter instruments, Novato, CA), a CoolSNAP HQ2 camera (Photometrics, Tucson, AZ) and Nikon Elements software (Nikon, Japan). The [Ca²⁺]_i ratios of emitted fluorescence intensities at excitation wavelengths of 340 and 380 nm (*F*₃₄₀/*F*₃₈₀) were determined every 5 s with background subtraction. Cells were perfused at 37°C at a flow of 2 mL/min; the solutions

utilized during the experiments are the loading solution with various glucose concentrations and VU0071063, as indicated.

Measurement of complex II activity

Mitochondria were isolated from four mouse hearts using differential centrifugation in sucrose-based buffer as previously described [156,157]. Complex II enzymatic activity was measured spectrophotometrically at 600 nm as previously described [156,158].

Chemicals

VU0071063 was purchased from AldrichCPR (Sigma-Aldrich, LLC, Milwaukee, WI). Diazoxide, glibenclamide, and tolbutamide were purchased from Sigma-Aldrich. All compounds were dissolved in anhydrous dimethyl sulfoxide (DMSO, Fisher Scientific, Pittsburgh, PA, USA) and diluted in bath solution before use. The final concentration of DMSO used was less than or equal to 0.3% (v/v).

Results

Serendipitous discovery of the Kir6.2/SUR1 activator VU0071063

A TI^+ flux assay of Kir6.2/SUR1 K_{ATP} channels was developed to assess the specificity of inhibitors of a mosquito Kir channel identified in a high-throughput screen (Raphemot, Denton, unpublished). The assays employ stably transfected T-REx-HEK293 cells expressing Kir6.2 from a tetracycline-inducible promoter and SUR1 constitutively (**Fig. 1B**). Kir6.2/SUR1 is

inhibited in T-REx-HEK293 cells under control conditions and must be activated by metabolic poisoning (data not shown) or the SUR1-prefering K_{ATP} channel opener diazoxide to mediate TI^+ flux. While testing approximately 300 mosquito Kir1 antagonists for selectivity, diazoxide was inadvertently excluded from one plate, revealing a dose-dependent increase in TI^+ flux in wells I3, I4, I5, and I6 containing 30, 10, 3, and 1 μ M of a mosquito Kir1 antagonist, respectively (**Fig. 2B-C**). The small-molecule added to these wells, which we termed VU0071063, was re-ordered as a powder, freshly dissolved in DMSO, and characterized in TI^+ flux and electrophysiological assays.

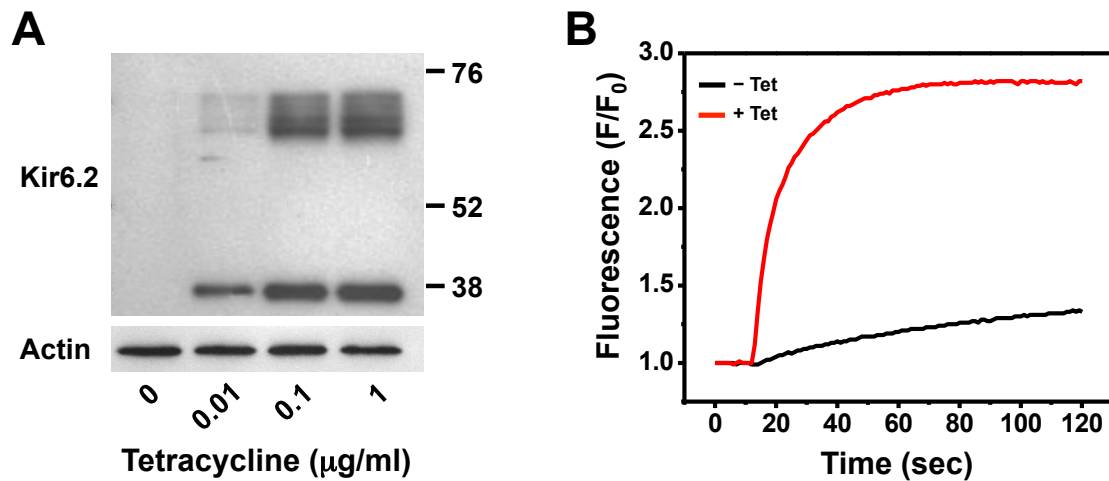


Figure 1. T-REx-HEK293-Kir6.2/SUR1 cell line characterization. (A) Cells were cultured overnight with the indicated concentration of tetracycline and subjected to Western blot analysis of Kir6.2 expression in whole-cell lysates. Membranes were stripped and re-probed for b-actin as a loading control. (B) Representative TI^+ flux experiment in cells cultured overnight with (red) or without (black) tetracycline and then pre-treated with 250 μM diazoxide for 20 min before TI^+ (12 mM TI_2SO_4) addition.

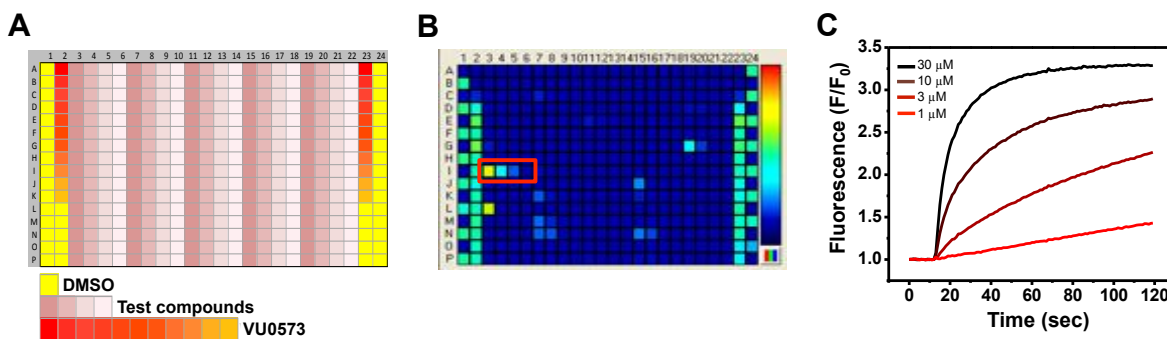


Figure 2. Discovery of VU0071063 in a TI^+ flux assay of Kir6.2/SUR1. (A) Plate map used in CRC analyses. DMSO (solvent) and broad-spectrum Kir channel inhibitor VU0573 (Raphemot et al., 2011) were used as controls. 4-point test compound CRCs were distributed horizontally, whereas 11-point VU0573 CRCs were distributed vertically. (B) Fluorescence heat map recorded from the assay plate containing 4 doses of VU0071063 (red box). Fluorescence intensity is indicated by the pseudocolored scale (right), with cooler (blue) to hotter (red) colors corresponding to low high TI^+ flux, respectively. (C) Representative time versus normalized (F/F_0) fluorescence intensity in wells containing the indicated concentrations of VU0071063.

Effects of VU0071063 on pancreatic Kir6.2/SUR1 K_{ATP} channels

The activity of VU0071063 on Kir6.2/SUR1 was compared to diazoxide and the SUR2-preferring opener pinacidil in 11-point CRCs in TI⁺ flux assays. The chemical structures of the three agonists are illustrated in **Fig. 3A**. Tetracycline-induced T-REx-HEK293-Kir6.2/SUR1 cells were treated with the agonists for 20-min prior to TI⁺ addition to allow full activation of the channel. As shown in the representative fluorescence traces in **Fig. 3B**, 30 μ M VU0071063 led to a slightly greater steady-state activation of Kir6.2/SUR1-dependent TI⁺ flux than did 250 μ M diazoxide. VU0071063 and diazoxide led to a dose-dependent activation of TI⁺ flux, whereas pinacidil was predictably inactive against Kir6.2/SUR1 (**Fig. 3C**). Half-maximal effective concentrations (EC₅₀) derived from logistical fits to CRC data for VU0071063 and diazoxide were 10.3 μ M (95% CI: 9.5-11 μ M) and greater than 100 μ M (EC₅₀~120 μ M), respectively (n = 4-6 independent experiments). To confirm that TI⁺ flux is dependent on Kir6.2/SUR1 channels, and not endogenous TI⁺ flux pathways, the dose-dependent effects of K_{ATP} channel inhibitors glibenclamide and tolbutamide were evaluated. The cells were pre-treated with EC₈₀ doses of VU0071063 (20 μ M) or diazoxide (250 μ M) and 3-fold dilutions of glibenclamide or tolbutamide ranging from 2 nM to 90 μ M. Similar to published half-maximal inhibitory concentration (IC₅₀) values, the IC₅₀ for glibenclamide and tolbutamide in VU0071063-treated cells were 5.60 nM (95% CI: 5-6 nM) and 3.07 μ M (95% CI: 2-5 μ M), respectively. These values are similar to those of diazoxide-treated cells (glibenclamide IC₅₀ = 16.6 nM [95% CI: 15-18 nM]; tolbutamide IC₅₀ = 1.60 μ M [95% CI: 1.4-2 μ M]).

Whole-cell patch clamp electrophysiology was used to further characterize the effects of VU0071063 and diazoxide on Kir6.2/SUR1. Bath application of VU0071063 rapidly (**Fig. 4A**) and dose-dependently (**Fig. 4C**) activated Kir6.2/SUR1 currents, with a maximal activation of

1077 ± 87% at a dose of 50 μM. In contrast, diazoxide activated Kir6.2/SUR1 more slowly (**Fig. 4B**) and with significantly (T-test P = 0.01) lower efficacy (maximal activation 580 ± 105% at 50 μM) than VU0071063. As shown in **Fig. 4B**, following steady-state activation with 50 μM diazoxide, bath addition of 50 μM VU0071063 led to further Kir6.2/SUR1 activation. These data show that at low micromolar concentrations, VU0071063 is a more potent activator of Kir6.2/SUR1 than diazoxide.

To exclude the possibility that VU0071063 might be activating channels in intact cells by altering cell metabolism, currents were recorded from COSm6 cells expressing Kir6.2 and SUR1, in inside-out membrane patches. In the presence of 0.1 mM MgATP, which inhibits WT channels ~90%, both 10 μM and 20 μM of VU0071063 markedly increased the patch current (**Fig. 5**).

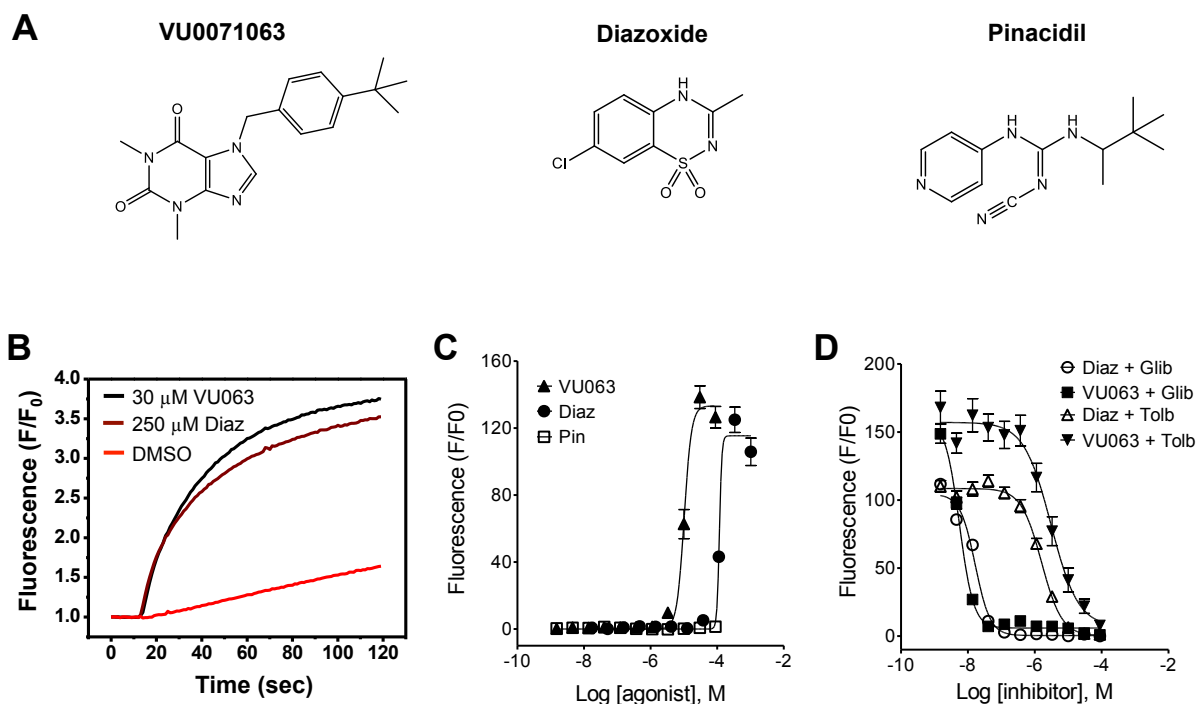


Figure 3. Characterization of VU0071063 activity against Kir6.2/SUR1 in Ti^+ flux assays. (A) Chemical structures of VU0071063 (VU063), diazoxide, and pinacidil. (B) Representative Ti^+ flux experiment demonstrating activation of Kir6.2/SUR1 by 30 μM VU0071063 or 250 μM diazoxide, but not the vehicle control DMSO (0.3%). Fluorescence data have been normalized (F/F_0) to baseline values recorded before Ti^+ addition. (C) Dose-dependent activation of Kir6.2/SUR1 by VU0071063 and diazoxide, but not pinacidil ($n = 4$ -6 independent experiments, each performed in triplicate). (D) Dose-dependent inhibition of VU0071063- and diazoxide-dependent Ti^+ flux by glibenclamide and tolbutamide ($n = 3$ independent experiments, each performed in triplicate).

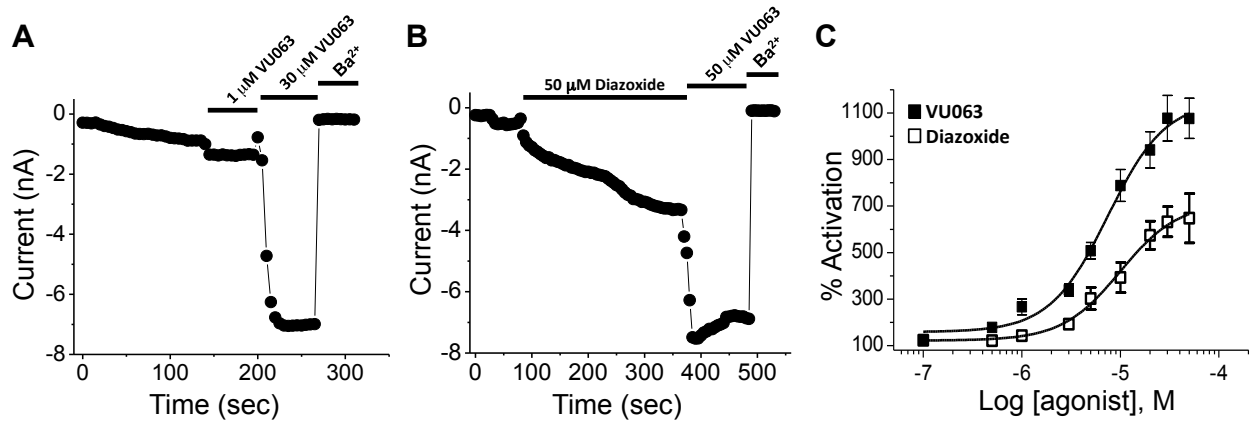


Figure 4. Characterization of VU0071063 activity against Kir6.2/SUR1 with patch clamp electrophysiology. (A) Transfected cells expressing Kir6.2/SUR1 were voltage clamped at -75 mV and stepped every 5 sec to -120 mV to elicit inward current. Minor current run-up was observed following establishment of the whole-cell configuration and dialysis with the pipette solution. Addition of 1 μ M or 30 μ M VU0071063 led to rapid activation of inward current. (B) In contrast, addition of 50 mM diazoxide activated Kir6.2/SUR1 slowly. After achieving steady-state activation, addition of 50 μ M VU0071063 led to further activation of Kir6.2/SUR1. Inward currents were blocked with 2 mM Ba²⁺. (C) Mean \pm SEM dose-response data fitted with 4-parameter logistic functions to derive EC₅₀ values of 7 μ M and 11 μ M for VU0071063 (closed square) and diazoxide (open square), respectively (n = 5 – 10 per concentration). Data are normalized and expressed as percent (%) activation from baseline current in the absence of agonist.

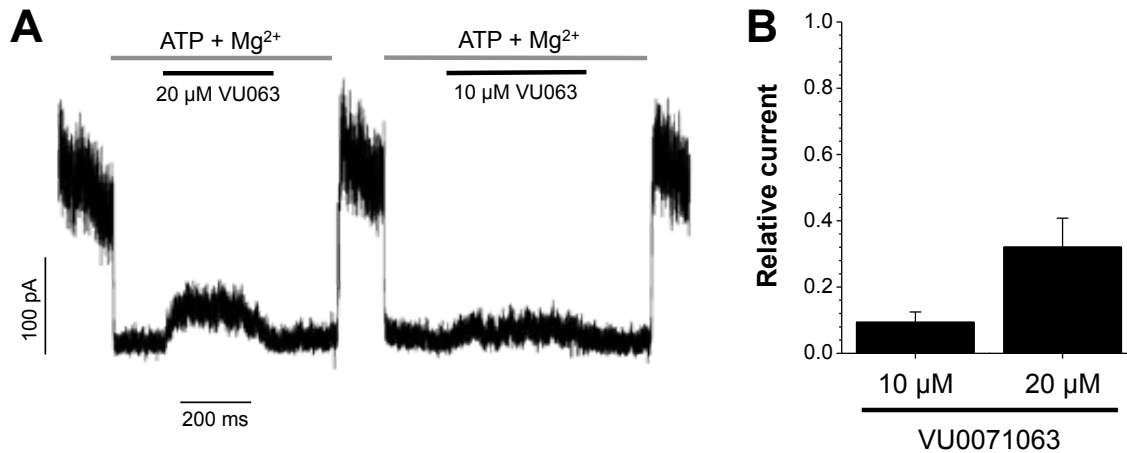


Figure 5. VU0071063 activates Kir6.2/SUR1 in excised inside-out patches. (A) Representative inside-out membrane patch of COS cells transiently expressing Kir6.2 and SUR1. Membrane potential held at -50mV. Patches were excised in ATP-free K-internal (150 mM-KCl, 10 mM-HEPES, 1 mM-EGTA) solution and then exposed to 0.1 mM-MgATP followed by 0.1 mM-Mg-ATP + VU0071063 (10 μM or 20 μM) solutions as indicated by solid lines above the representative trace. (B) The relative current in 0.1 mM Mg-ATP + VU0071063 (10 μM or 20 μM) with respect to current in ATP-free solution averaged from all recordings (n = 4).

VU0071063 is selective SUR1-containing K_{ATP} channels

The pharmacological selectivity of known K_{ATP} channel agonists is achieved through interactions with the SUR subunit. To determine if VU0071063 activity is also dependent on the SUR, we tested its effects on Kir6.2 or Kir6.1 channels containing SUR1 or SUR2A using patch clamp electrophysiology. Diazoxide and pinacidil were used as positive controls for SUR1- and SUR2A-containing channels, respectively. As shown in the representative timecourse experiment in **Fig. 6A**, and summary data (mean ± SEM; n = 7) in **Fig. 6C**, bath application of 50 μM VU0071063 rapidly and reversibly activated Kir6.2/SUR1 to a greater extent than an equal concentration of diazoxide. Qualitatively similar results were observed in cells transfected with Kir6.1/SUR1 (**Fig. 6D**). In striking contrast, VU0071063 had no effect on Kir6.2/SUR2A (**Figs. 6B, 6E**) or Kir6.1/SUR2A (**Fig. 6F**), whereas pinacidil activated both channel subtypes. Dose-response experiments revealed that VU0071063 had no appreciable effects on Kir6.2/SUR2A at concentrations up to 150 μM (**Fig. 7**), which is 15-fold higher than the IC₅₀ for Kir6.2/SUR1.

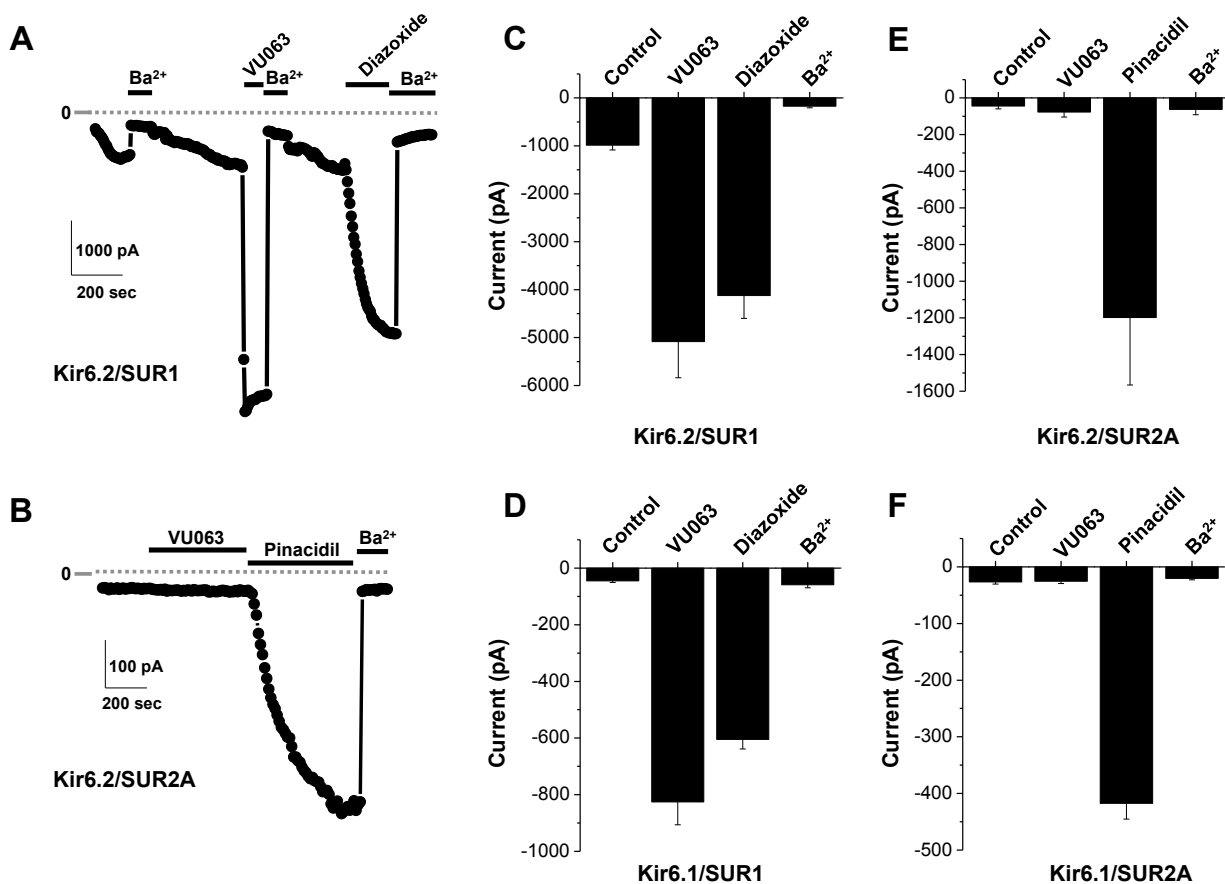


Figure 6. VU0071063 is selective for SUR1-containing KATP channels. (A) Representative whole-cell patch clamp experiment showing the effects of 50 μM VU0071063, 50 μM diazoxide, and 2 mM Ba^{2+} on Kir6.2/SUR1 current at -120 mV. Note the differences in the kinetics of activation of VU0071063 and diazoxide. (B) Representative recording showing effects of 50 μM VU0071063, 50 μM pinacidil, and 2 mM Ba^{2+} on Kir6.2/SUR2A currents. (C, E, D, F) Mean \pm SEM current at -120 mV recorded from cells transfected with Kir6.2/SUR1, Kir6.1/SUR1, Kir6.2/SUR2A, or Kir6.1, SUR2A, respectively (n = 4-7).

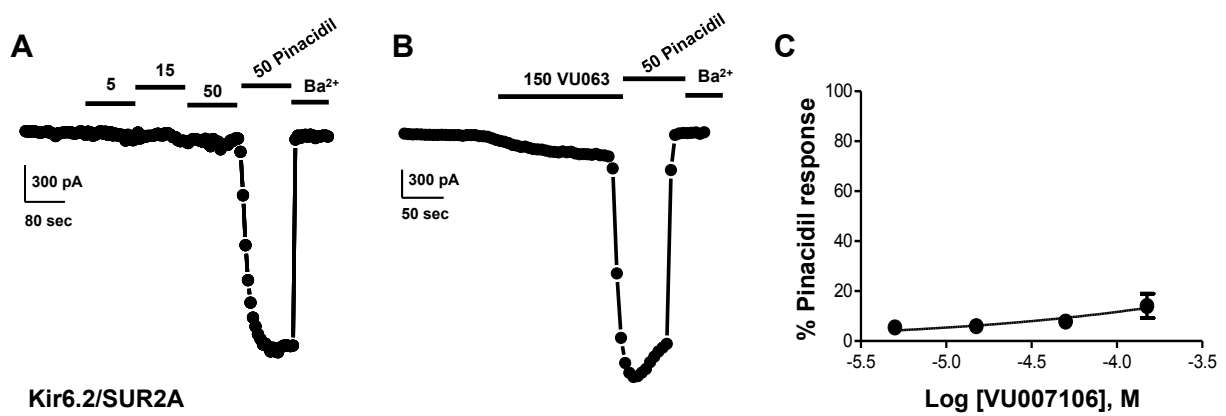


Figure 7. Lack of effect of VU0071063 on Kir6.2/SUR2A channels. (A) Whole-cell Kir6.2/SUR2A currents were measured every 5 sec at -120 mV before and after addition of 5, 15, or 50 μ M VU007106 or 50 μ M pinacidil (positive control), followed by application of 2 mM Ba²⁺. (B) Single-dose exposure to 150 μ M VU0071063 has only a modest effect on Kir6.2/SUR2A channel activity. (C) VU0071063 CRC data normalized to 50 μ M pinacidil response. Data are means \pm SEM (n = 4 at each dose).

VU0071063 inhibits glucose-stimulated β -cell Ca^{2+} influx

Glucose-stimulated closure of β -cell K_{ATP} channels results in membrane potential depolarization, activation of voltage-dependent Ca^{2+} channels (VDCC), Ca^{2+} influx, and Ca^{2+} -induced insulin secretion. We therefore tested whether VU0071063 activates native Kir6.2/SUR1 channels by measuring the effect of the activator on β -cell Ca^{2+} influx during glucose-stimulation. Treatment of β -cells with high (14 mM) glucose induced a significant rise in Ca^{2+} as determined by the fluorescent Ca^{2+} indicator fura-2, which shows an increase in the fluorescent ratio of Ca^{2+} bound to Ca^{2+} unbound dye in response to glucose (red cells, **Fig. 8**). Activation of β -cell K_{ATP} channels with VU0071063 in the presence of high (14 mM) glucose resulted in inhibition of β -cell Ca^{2+} influx and reduction in Ca^{2+} levels back to those observed in low (2 mM) glucose conditions (green cells, **Fig. 8**). The reduction in Ca^{2+} influx mediated via K_{ATP} activation is reversible following removal of VU0071063, which results in a return of β -cell Ca^{2+} levels to high (14 mM) glucose levels (red cells, **Fig. 8**). This data indicates that VU0071063 activates native β -cell K_{ATP} channels and thereby reduces VDCC activation and Ca^{2+} influx.

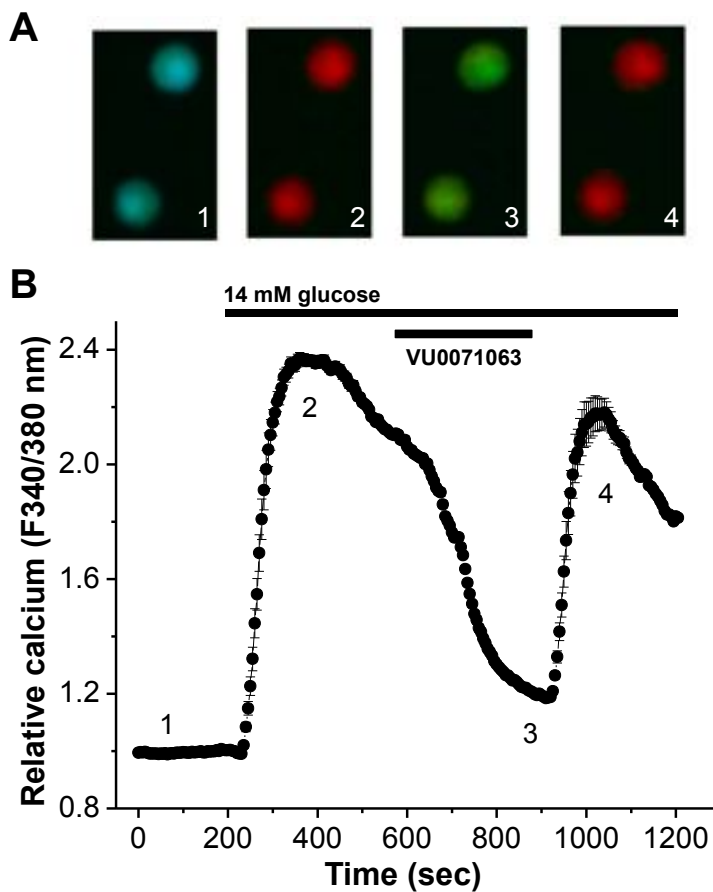


Figure 8. VU0071063 inhibits glucose-stimulated β -cell calcium entry. (A) Two representative β -cells loaded with FURA-2; displayed as a fluorescent ratio (340/380 nm) in response to 2mM glucose (1), 14 mM glucose (2), 14 mM glucose + 10 μ M VU0071063 (3), and 14 mM glucose (4). (B) Relative calcium responses of mouse islet-cells following treatment with 2mM glucose and as indicated by the conditions labeled above (black lines, n = 239 islet-cells over 3 days and 13 plates of cells).

Kir6.2/SUR1 activation by VU0071063 is not mediated by a PDE inhibitory pathway

Vascular smooth muscle K_{ATP} channels are activated by cAMP/PKA- and cGMP/PKG-dependent pathways following phosphodiesterase (PDE) inhibition with theophylline (see discussion). Because VU0071063 contains a theophylline moiety (**Fig. 9A**), we tested whether theophylline could activate Kir6.2/SUR1 in Tl^+ flux assays under conditions identical to those used to discover VU0071063. However, as shown in **Fig. 9B**, theophylline at a concentration of 250 μ M had no effect on Kir6.2/SUR1-dependent Tl^+ flux.

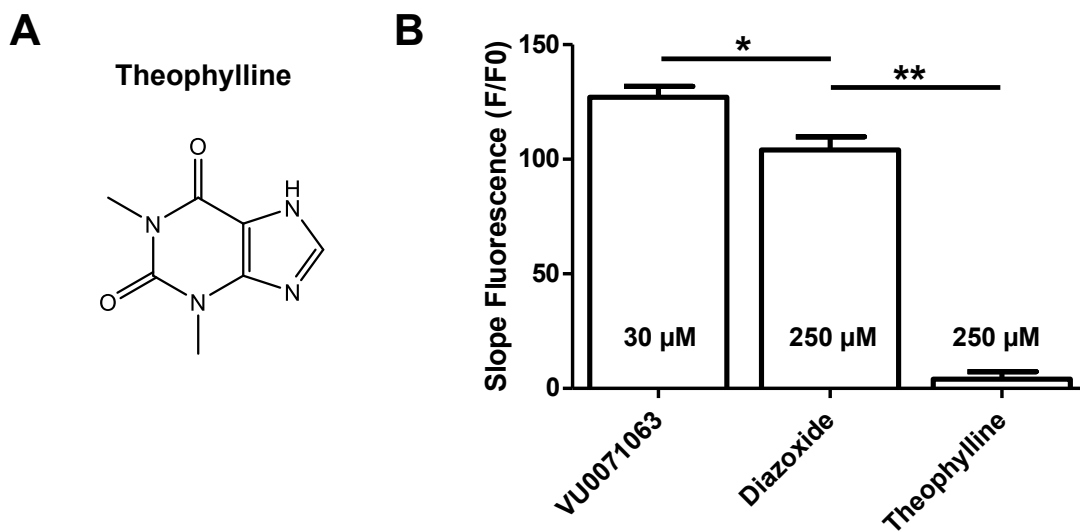


Figure 9. Lack of effect of theophylline on Kir6.2/SUR1-dependent TI^+ flux. (A) Chemical structure of theophylline. (B) Mean \pm SEM slope fluorescence recorded from wells treated with 30 μ M VU0071063, 250 μ M diazoxide, or 250 μ M theophylline for 20 min before TI^+ addition. Data are from 2 independent experiments performed in triplicate. Significance * $P = 0.03$, ** $P = 0.003$, unpaired Students t-test.

Ancillary Pharmacology

The selectivity of VU007106 was evaluated in 11-point CRCs in TI^+ flux assays against Kir2.1, Kir2.2, Kir2.3, and Kir3.1/3.2. VU0071063 was inactive against Kir2.1 and Kir2.2 ($\text{IC}_{50} > 100 \mu\text{M}$) and showed weak inhibitor activity against Kir3.1/3.2 ($\text{IC}_{50} = 65 \mu\text{M}$) and Kir2.3 ($\text{IC}_{50} = 91 \mu\text{M}$)(**Fig. 10**). Patch clamp electrophysiology was used to determine whether VU0071063 acts on the voltage-gated K^+ channel Kv2.1, which contributes to action repolarization in pancreatic β -cells [159,160]. Cells were voltage clamped at a holding potential of -75 mV and stepped to +50 mV every 5 seconds. Bath application of 10 μM VU0071063 led to a $7.8 \pm 0.9 \%$ ($n = 4$) reduction in outward Kv2.1 current at 40 mV that was fully reversible (**Fig. 11**).

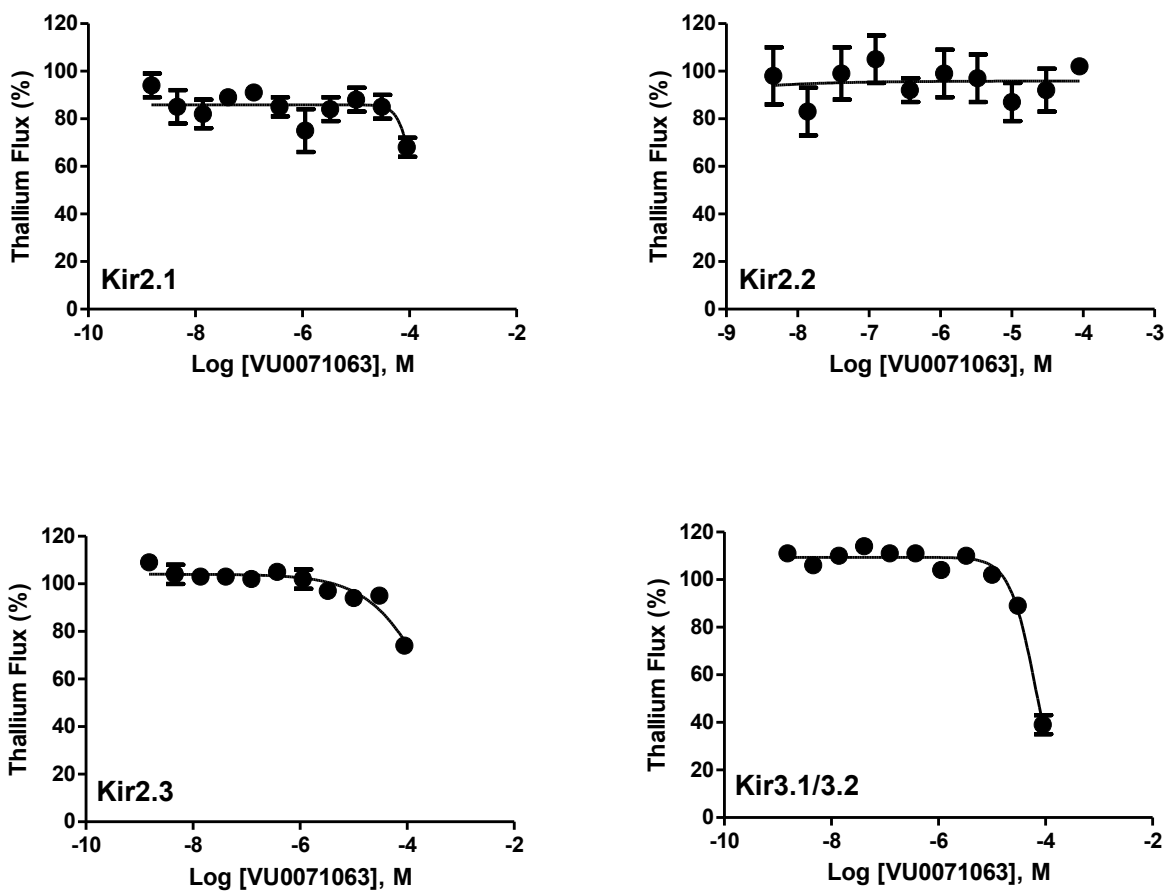


Figure 10. Selectivity of VU0071063 among members of the Kir channel family. 11-point CRC of VU0071063 were established for Kir2.1, Kir2.2, Kir2.3, and Kir3.1/3.2 expressing cell lines (n = 2 independent experiments performed in triplicate per cell line).

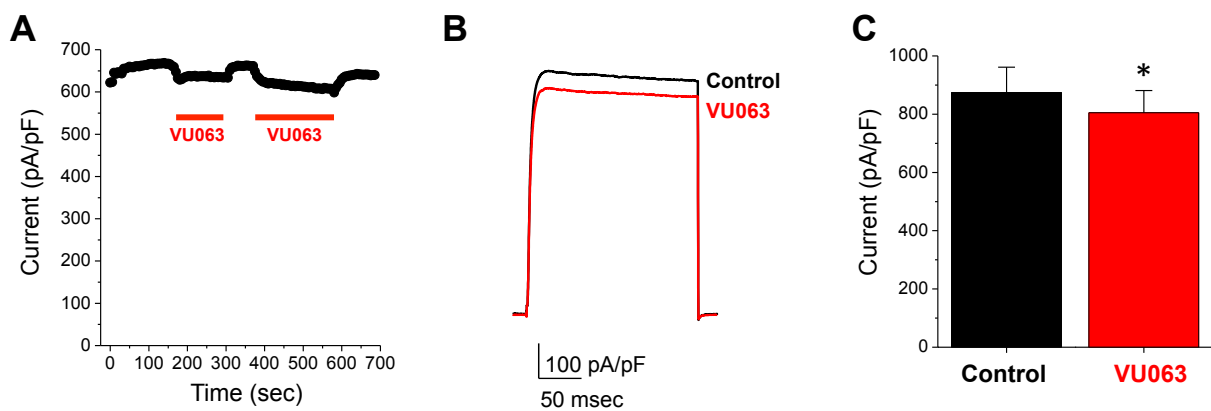


Figure 11. Effects of VU0071063 on heterologously expressed Kv2.1. (A) Time versus current amplitude plot illustrating the rapid and reversible inhibition of Kv2.1 current at 40 mV by 10 μ M VU0071063. (B) Representative current traces recorded at 40 mV before and during bath perfusion with 10 μ M VU0071063. (C) Mean \pm SEM current amplitude at 40 mV in the absence (control) or presence of 10 μ M VU0071063. *P = 0.01, paired Students t-test.

Discussion

Pancreatic K_{ATP} channels are validated drug targets for intractable hypoglycemia due to insulinoma and congenital hyperinsulinism, and therefore considerable efforts have been made to develop specific activators of Kir6.2/SUR1 channels [154,161,162]. Diazoxide is the best known SUR1-preferring opener and has been used clinically for more than 50 years. However, its use has been limited by a lack of potency and selectivity, leading to undesirable side effects such as low blood pressure, blurred vision, reduced urination, fluid retention, and hirsutism, mimicking the effects of Cantu Syndrome, which results from gain-of-function in the cardiovascular SUR2 isoform [32], and reflecting enhanced opening of vascular smooth muscle K_{ATP} channels and potentially effects on mitochondrial respiration [163]. In an effort to develop openers with fewer side effects, several groups have synthesized analogs from existing lead compounds that show improved potency and selectivity toward Kir6.2/SUR1. Structural modifications to the diazoxide scaffold have led to several new series with sub-micromolar potency and selectivity for pancreatic over smooth muscle K_{ATP} channels (de Tullio et al., 2011; Pirotte et al., 2010). One analog, termed NN414 [40], shows favorable activity in obese rats [164,165], as well as healthy and type 2 diabetes patients [166,167]. Clinical trials were initiated but later suspended due to drug-induced elevations of key liver enzymes [154]. Analogs of the SUR2-preferring openers cromakalim and pinacidil that exhibit selectivity for pancreatic K_{ATP} channels [168-173] have also been developed, showing that is possible to switch SUR preference with chemical modifications to the scaffold. To our knowledge, the only unique pancreatic K_{ATP} channel activator chemotypes reported in the last 2 decades were identified in screens of small-molecule libraries. These include the 4-sulfamoylphenylbenzamide and nitropyrazole series of K_{ATP} activators. A 4-sulfamoylphenylbenzamide derivative was shown to activate heterologously

expressed Kir6.2/SUR1 channels and inhibit glucose-stimulated insulin secretion from primary rat islets with sub-micromolar efficacy; the activity toward SUR2-containing channels was not reported [174]. One nitroprazole analog exhibits nanomolar-affinity toward Kir6.2/SUR1 and at least 15-fold selectivity over SUR2A and SUR2B-containing channels [175]. No in vivo efficacy of either series has been published.

To our knowledge, VU0071063 is only the third publically disclosed SUR1-preferring chemotype identified with compound screening and therefore provides an important starting point for the development of new channel openers. The discovery of VU0071063 underscores the value of mining focused libraries from primary screens for modulators of diverse inward rectifier K⁺ channels. VU0071063 is slightly more potent than diazoxide, and activates the channel with a faster timecourse. The reason for the discrepancy in IC₅₀ values derived from TI⁺ flux and patch clamp experiments is unclear, but likely reflects 1) differences in the behavior of TI⁺ and K⁺ in the K_{ATP} channel pore, and 2) the slower kinetics of diazoxide action compared to that of VU0071063 (e.g. **Fig. 6**). In an effort to avoid the latter issue, T-REX-HEK293-Kir6.2/SUR1 cells were incubated with compounds for 20 min before adding TI⁺ stimulus buffer, however we still observed a rightward shift in the EC₅₀ value for diazoxide.

VU0071063 is selective for Kir6.2/SUR1 over Kir6.2/SUR2A and Kir6.1/SUR2A, as well as Kir3.1/3.2, Kir2.1, Kir2.2, Kir2.3, and Kv2.1. Kv2.1 was tested for VU0071063 sensitivity because it plays important roles in the electrophysiology of pancreatic β-cells by modulating action potential repolarization, Ca²⁺ influx through VDCC, and insulin secretion. At the same dose shown to reduce high glucose-induced Ca²⁺ influx in pancreatic β-cells, 10 μM VU0071063 significantly inhibited Kv2.1 currents by approximately 10%. Inhibition of Kv2.1 would be expected to prolong the action potential depolarization and increase, not decrease, Ca²⁺

influx through VDCC, excluding a potential role of Kv2.1 in the VU0071063 mechanism of action. Specific effects of VU0071063 on the electrical excitability and underlying ion channels in β -cells will be examined in future studies. Furthermore, the selectivity of VU0071063 suggests the binding site is located within SUR1, which belongs to the ABC superfamily of transporters. Considering that the ABC transporter family member CFTR is inhibited at high concentrations ($IC_{50} = 250 \mu\text{M}$;[176]) of diazoxide, future studies should address whether VU0071063 inhibits CFTR or other members of this superfamily. Finally, although VU0071063 does not activate SUR2A-containing channels, potential effects on SUR2B-containing channels and hence vascular smooth muscle tone should be considered before using VU0071063 as an *in vivo* probe of SUR1-containing K_{ATP} channels. Despite several attempts and different experimental conditions, we were unable to measure the activity of SUR2B-containing K_{ATP} channels in our expression system and could not determine the effect of VU0071063 on these channels (unpublished observations).

VU0071063 is structurally related to the xanthine derivative KMUP-1, which induces smooth muscle relaxation and vasodilation through activation of the cGMP and cAMP pathways. KMUP-1 induces the accumulation of cGMP and cAMP in part by inhibiting their degradation by phosphodiesterase (PDE) enzymes. Pharmacological agents that prevent cGMP accumulation predictably suppress KMUP-1-induced dilation. Inhibitors of several different families of K^+ channels, including tetraethylammonium, 4-aminopyridine, iberiotoxin, charybdotoxin, and glibenclamide, blunt the vasodilatory effects of KMUP-1, indicating an important role of the membrane potential in its mechanism of action [177-179]. However, this does not appear to involve direct K^+ channel activation. For example, [180] found that KMUP-1 activates large-conductance Ca^{2+} -activated K^+ (BK) currents in cerebral smooth muscle cells, but this was

dependent on cGMP generation. Although the effects of KMUP-1 on K_{ATP} currents have not been reported, cGMP is known to activate vascular K_{ATP} channels [181]. The PDE-inhibitory activity of KMUP-1 is likely mediated through the theophylline moiety, since the addition of theophylline, a non-specific PDE inhibitor, recapitulates the effects of KMUP-1 on cGMP levels and vascular tone [180]. As noted earlier, VU0071063 also contains a theophylline group, raising the possibility that PDE inhibition and cGMP or cAMP accumulation contributes to Kir6.2/SUR1 activation. However, theophylline at a concentration of 250 μ M had no effect on Kir6.2/SUR1-mediated TI^+ flux following 20-min incubation. This, together with the observation that VU0071063 directly activates Kir6.2/SUR1 in excised membrane patches (**Fig. 5**), suggests that PDE inhibition and cyclic nucleotides are not essential components of its mechanism of action.

There are several important questions regarding VU0071063 and its mechanism of action remaining to be answered. KMUP-1 and VU0071063 differ only in the structure of their side-chains that project off a common theophylline moiety, yet only VU0071063 appears to be a direct SUR1/Kir6.2 channel activator. Determination of VU0071063 structure-activity relationships with medicinal chemistry will inform a deeper understanding of pharmacophore requirements for activation of SUR1- and SUR2-containing K_{ATP} channels and may lead to the development of improved xanthine-based activators. Do VU0071063 and diazoxide activate Kir6.2/SUR1 through common molecular mechanisms? For instance, do they share the same receptor binding site in SUR1, and does VU0071063 require ATP hydrolysis for channel activation like diazoxide [182]? It is well established that diazoxide has direct effects on mitochondrial respiration, although the underlying mechanisms are a matter of ongoing debate [163]. At least some of the effects of diazoxide in cardiac and smooth muscle cells are mediated

through inhibition of mitochondrial complex II [183,184], which has made it difficult to ascribe beneficial and undesirable effects of the drug to K_{ATP} channel-mediated effects or other mechanisms. Importantly, VU0071063 (< 100 μ M) had no effect on complex II activity (**Table 1**). It will be important to determine whether VU0071063 action is limited to plasma membrane SUR1-containing channels or also has off-target effects on mitochondrial respiration and potentially other signaling pathways. The activation of K_{ATP} channels are linked to signaling pathways that can protect a cellular against stress [185]. While the location of the channel that mediates protection (e.g. canonical surface K_{ATP} vs. mitochondrial K_{ATP} channels) remains elusive [185-187], VU0071063 may prove to be a valuable tool to investigate the role of K_{ATP} channels in stress responses.

Table 1. Percent inhibition of Complex II activity in response to VU0071063 and diazoxide. Mitochondria isolated from mouse hearts underwent three cycles of freeze-thaw and subject to the complex II enzymatic activity assay. Complex II activity was measured and expressed as percent inhibition. Control complex II activity was 88.0 ± 3.1 nmol/min/mg protein. Data are mean \pm S.E.M. percent inhibition. N = 4 independent mitochondria preparations.

[Compound] μ M	Complex II activity (% inhibition)	
	VU0071063	Diazoxide
1	1.5 ± 3.5	-
3	-2.2 ± 4.5	-
10	2.4 ± 2.7	7.6 ± 2.5
30	0.0 ± 4.3	14.9 ± 6.0
100	4.9 ± 2.9	24.2 ± 4.3
300	-	36.0 ± 3.5
600	-	41.6 ± 0.7

In conclusion, VU0071063 is a novel xanthine derivative that directly and selectively activates K_{ATP} channels containing SUR1. Despite K_{ATP} channels being validated drug targets for numerous diseases, VU0071063 is only the third SUR1-preferring chemotype discovered using small-molecule library screening. We anticipate that the TI^+ flux assay described here will enable the discovery of additional small-molecule modulators of Kir6.2/SUR1 and other K_{ATP} channel subtypes.

Chapter VI

ELICITING RENAL FAILURE IN MOSQUITOES WITH A SMALL-MOLECULE INHIBITOR OF INWARD-RECTIFYING POTASSIUM CHANNELS

This chapter was published under the same title in the journal *PLoS One* in the May 29th, 2013 issue

Abstract

Mosquito-borne diseases such as malaria and dengue fever take a large toll on global health. The primary chemical agents used for controlling mosquitoes are insecticides that target the nervous system. However, the emergence of resistance in mosquito populations is reducing the efficacy of available insecticides. The development of new insecticides is therefore urgent. Here we show that VU573, a small-molecule inhibitor of several mammalian inward-rectifying potassium (Kir) channels, inhibits a Kir channel cloned from the renal (Malpighian) tubules of *Aedes aegypti* (*AeKir1*). Injections of VU573 into the hemolymph of adult female mosquitoes (*Ae. aegypti*) render them incapacitated (flightless or dead) within 24 hours by disrupting their production and excretion of urine in a manner consistent with channel block of *AeKir1*. Moreover, the toxicity of VU573 in mosquitoes (*Ae. aegypti*) is exacerbated when hemolymph potassium levels are elevated. Our study demonstrates that renal failure is a promising mechanism of action for killing mosquitoes, and motivates the discovery of selective small-molecule inhibitors of mosquito Kir channels for use as insecticides.

Introduction

Mosquitoes are vectors of debilitating diseases that take an immense toll on global health. Anopheline mosquitoes transmit pathogenic protozoans (*Plasmodium* sp.) that cause malaria. On an annual basis, there are an estimated hundreds of millions of episodes of malaria, which claim nearly one million lives; ~85% of the victims are children under 5 years of age [188]. Culicine mosquitoes transmit viral pathogens that cause chikungunya, dengue, West Nile, and yellow fevers. Of the estimated 50-100 million individuals infected with dengue each year, hundreds of thousands require hospitalization and tens of thousands die [189]. These protozoan and viral pathogens are transmitted to humans solely by adult female mosquitoes, which feed on vertebrate blood to obtain nutrients for developing eggs.

The primary chemical agents currently in use for controlling mosquitoes are insecticides that target the nervous system. Although the development of insecticides such as DDT and pyrethroids, which modulate the activity of ion channels in the central nervous system of insects, offered promise for the eradication of mosquitoes in the 20th century, the emergence of resistance in mosquito populations has reduced their efficacy [190,191]. Currently, there are not many alternatives, because no new insecticides for public-health use have been developed in over 30 years [68]. Thus, the discovery of chemicals that target novel physiological processes and molecular targets in mosquitoes are urgently needed [68,192].

A physiological process in the mosquito that has not yet been targeted by insecticides is the excretion of urine. The renal (Malpighian) tubules generate urine via the transepithelial secretion of NaCl, KCl, other solutes, and water from the extracellular fluid (hemolymph) to the tubule lumens [193,194]. The tubules empty their secretions into the hindgut where solute and/or water is removed or added to the final urine before it is ejected via muscular contractions

of the hindgut. Thus, inhibiting the function of Malpighian tubules—i.e., causing renal failure—is expected to disrupt extracellular fluid homeostasis with detrimental consequences to normal functions in the mosquito. Female mosquitoes would be particularly vulnerable to renal failure, because they would not be able to excrete the unwanted salt and water ingested during a blood meal [195-197].

The aim of the present study is to elicit renal failure in adult female mosquitoes (*Aedes aegypti*) using a small-molecule inhibitor of inward-rectifying potassium (Kir) channels. The molecular structure of Kir channels in mosquitoes is review in **Chapter I**. In mosquito Malpighian tubules, Kir channels of the basolateral membrane are considered one of the two major routes for the uptake of K^+ into the epithelium [74,198]. The Malpighian tubules of *Ae. aegypti* express three cDNAs encoding Kir channel subunits (*AeKir1*, *AeKir2B*, *AeKir3*), which we have cloned and functionally characterized [74]. *AeKir1* mediates robust K^+ currents when expressed in *Xenopus* oocytes, whereas *AeKir2B* and *AeKir3* produce relatively small and nominal K^+ currents, respectively [74]. Thus, we focused on inhibiting *AeKir1* in the present study.

Materials and Methods

Expression vectors and sub-cloning

The open-reading frame of the *AeKir1* cDNA cloned from Malpighian tubules of adult female *Ae. aegypti* [74] was subcloned into a pcDNA5/TO expression vector (Invitrogen, Carlsbad, CA) using BamHI and XbaI restriction sites. The accuracy of the resulting *AeKir1*-pcDNA/TO vector was confirmed by sequencing it in both the 5' and 3' directions.

Stable cell line generation

Stably transfected polyclonal T-REx-HEK293 cell lines expressing *AeKir1* under the control of a tetracycline-inducible promoter were established as described previously [20,136]. Monoclonal cell lines were isolated through limiting dilution in 384-well plates and tested for tetracycline inducible TI^+ flux, as described below. T-REx-HEK293 lines were cultured in DMEM growth medium containing 10% FBS, 50 U/mL Penicillin, 50 $\mu\text{g/mL}$ Streptomycin, 5 $\mu\text{g/mL}$ Blasticidin S and 250 $\mu\text{g/mL}$ Hygromycin.

Whole-cell patch clamp electrophysiology

T-REx-HEK293-*AeKir1* cells were voltage clamped in the whole-cell configuration of the patch clamp technique after overnight induction with tetracycline (1 $\mu\text{g/mL}$). Patch electrodes were pulled from silanized 1.5 mm outer diameter borosilicate microhematocrit tubes using a Narishige PP-830 two-stage puller. Electrode resistance ranged from 2.5 to 3.5 $\text{M}\Omega$ when filled with the following intracellular solution (in mM): 135 KCl, 2 MgCl_2 , 1 EGTA, 10 HEPES free acid, 2 Na_2ATP (Roche, Indianapolis, IN), pH 7.3, 275 mOsm. The standard bath solution contained (in mM): 135 NaCl, 5 KCl, 2 CaCl_2 , 1 MgCl_2 , 5 glucose, 10 HEPES free acid, pH 7.4, 290 mOsm. The high- K^+ bath contained (in mM): 90 NaCl, 50 KCl, 2 CaCl_2 , 1 MgCl_2 , 5 glucose, and 10 HEPES-free acid, pH 7.4, 290 mOsmol. Whole-cell currents were recorded under voltage-clamp conditions using an Axopatch 200B amplifier (Molecular Devices, Sunnyvale, CA). Electrical connections to the amplifier were made using Ag/AgCl wires and 3 M KCl/agar bridges. Electrophysiological data were collected at 5 kHz and filtered at 1 kHz. Data acquisition and analysis were performed using pClamp 9.2 software (Axon Instruments).

After achieving stable whole-cell currents, VU573 or VU342 was applied intermittently or continuously for 2 to 10 min, followed by application of 2 mM BaCl₂. All recordings were made at room temperature (20-23°C).

Test compound and stimulus plate preparation

Compound master antagonist plates were created by serial diluting compounds 1:3 from 30mM stocks in 100% DMSO using the BRAVO liquid handler (Agilent Technologies, Santa Clara, CA). Assay daughter plates were created using the ECHO 555 liquid handler (Labcyte, Sunnyvale, CA), transferring 240 nl from the master plate to the daughter plate for each well followed by addition of 40 µl of assay buffer resulting in antagonist compound concentration response curves starting at 200 µM (2X final concentration). Tl⁺ stimulus buffer contained (in mM): 125 sodium bicarbonate (added fresh the morning of the experiment), 1 magnesium sulfate, 1.8 calcium sulfate, 5 glucose, 12 Tl⁺ sulfate, and 10 HEPES, pH 7.3 at 5X the final concentration to be assayed.

Thallium flux assays

Cells were loaded with the Tl⁺ sensitive fluorescent dye FluoZin-2(acetoxymethyl ester form) and plated in clear-bottom 384-well plates essentially as described previously [20,21]. Cell plates and daughter compound plates were loaded onto a kinetic imaging plate reader (FDSS 6000; Hamamatsu Corporation, Bridgewater, NJ). All recordings were made at room temperature (20-23°C). Appropriate baseline readings were taken (10 images at 1 Hz; excitation, 470 ± 20 nm; emission, 540 ± 30 nm) and 20 µl test compounds were added followed by 50

images at 1Hz additional baseline. Following a 20 minute incubation period, baseline readings were taken for 10 seconds followed by addition of 10 μL of Ti^+ stimulus buffer. An additional 240 images were taken at 1 Hz.

Chemical synthesis

The methods for synthesizing VU573, VU342, and other analogs are described in detail elsewhere [64].

Mosquito colonies

The following reagents were obtained through the MR4 as part of the BEI Resources Repository, NIAID, NIH: *Aedes aegypti* LVP-IB12, MRA-735, deposited by M.Q. Benedict, and *Aedes albopictus* ALBOPICTUS, MRA-804, deposited by Sandra Allan. Eggs from both *Aedes* species were raised to adults as described previously [199]. Adult female mosquitoes of *Anopheles gambiae* (Mbita strain) and *Culex pipiens* (Buckeye strain) were provided by the laboratories of Drs. Woody A. Foster and David L. Denlinger, respectively (the Ohio State University). For all experiments described below, only adult females of 3-10 days post-emergence were used.

Mosquito toxicology experiments

Mosquitoes were first anesthetized on ice and then injected with 69 nL of fluid (see below) using a pulled-glass capillary attached to a nanoliter injector (Nanoject II, Drummond Scientific Company, Broomall, PA). The injected fluid was a sodium-based phosphate-buffered saline (Na⁺-PBS) containing 15% DMSO and various concentrations of VU573 or VU342 to deliver the doses indicated in **Figs. 2A, 2C, and S3**. The Na⁺-PBS consisted of the following in mM: 137 NaCl, 2.7 KCl, 10 Na₂HPO₄, and 2 KH₂PO₄ (pH 7.5). After injection, the mosquitoes were placed in a small cage (10 females per cage) within a rearing chamber (28°C, 80% relative humidity, 12:12 light:dark) and allowed free access to a solution of 10% sucrose. The mosquitoes were observed 24 h after injection.

A similar approach was used to determine the toxicity of VU573 after a stress to hemolymph Na⁺ or K⁺ homeostasis (**Fig. 2F**). However, in these experiments, each mosquito was injected with 900 nL of fluid (100 nl/s) and the mosquitoes were not given access to sucrose. The injected fluid was a Na⁺-PBS or K⁺-PBS containing 1.1% DMSO and 0.77 mM of VU573. Vehicle controls received the respective PBS with DMSO alone. The K⁺-PBS consisted of the following in mM: 2.7 NaCl, 137 KCl, 2 Na₂HPO₄, and 10 KH₂PO₄ (pH 7.5).

Isolated Malpighian tubule experiments

Fluid secretion assays. Fluid secretion rates from isolated Malpighian tubules (*Ae. aegypti*) were measured in vitro using the method described in [200], which is modified from that of Ramsay [201]. In brief, isolated tubules were bathed in a 50 µL drop of a mosquito Ringer solution with elevated K⁺ (see composition below), which was then covered with light

mineral oil. A glass hook was used to pull the open proximal end of the tubule into the mineral oil where fluid was secreted. The diameter of the droplet was measured to calculate the secreted volumes.

In one set of tubules, the initial spontaneous rate of fluid secretion was calculated during the first 30 min (control). In another set of tubules, the rates of fluid secretion were determined 2 h after adding one of the following to the peritubular bath: the vehicle (0.05% DMSO), VU573 (10 μ M), or VU342 (10 μ M). The Ringer solution consisted of the following in mM: 119.4 NaCl, 34 KCl, 25 HEPES, 1.8 NaHCO₃, 1.7 CaCl₂, and 1.0 MgSO₄, pH 7.1.

Electrophysiology. The basolateral membrane voltage (V_{bl}) and input resistance (R_{pc}) of principal cells were measured in isolated Malpighian tubules using two-electrode voltage clamping, as described previously [202]. In each experiment, a single principal cell near the distal (blind) end of the tubule was impaled with two glass microelectrodes: one measured V_{bl} and the other injected current (I_m). The R_{pc} of the impaled cell was calculated from current-voltage plots that were generated via voltage clamping (see ref. [200] for details). After recording a steady-state V_{bl} and R_{pc} (control) from the impaled cell, either VU573 (10 μ M) or BaCl₂ (5 mM) was added to the peritubular bath. The resulting V_{bl} and R_{pc} (treatment) were measured again upon reaching a new steady-state (usually 1-2 min later).

Mosquito excretion experiments

Urine excretion rates from intact mosquitoes (*Ae. aegypti*) were measured using a method modified from the laboratory of Hansen [203]. After anesthetizing mosquitoes on ice they were injected as described above with 900 nL of fluid (100 nL/s). The injected fluid was one of two

HEPES-buffered saline (HBS) solutions containing 1.8% DMSO with 0.77 mM VU573 or 0.77 mM VU342. Vehicle controls received the respective HBS with DMSO alone. The Na⁺-HBS consisted of the following in mM: 146 NaCl, 4.2 *N*-methyl-D-glucammonium (NMDG)-Cl, and 25 HEPES (pH 7.5). The K⁺-HBS consisted of the following in mM: 10 NaCl, 75 KCl, 65.2 NMDG-Cl, and 25 HEPES (pH 7.5). After injection, mosquitoes were placed immediately in a graduated, packed-cell volume tube (MidSci, St. Louis, MO; 3 mosquitoes per tube) at room temperature. The mosquitoes were removed from the tubes with forceps after 2 h and the excreted urine was centrifuged into the graduated column of the tube for measurement. Uninjected control mosquitoes were handled exactly as above sans the injection step.

Statistical analyses

TI⁺-flux assays. Data were analyzed using Excel (Microsoft Corp, Redmond, WA). Raw data were opened in Excel and each data point in a given trace was divided by the first data point from that trace (static ratio). The slope of the fluorescence increase beginning 5 s after TI⁺ addition and ending 15 s after TI⁺ addition was calculated. The data were then plotted in Prism software (GraphPad Software, San Diego, CA) to generate concentration-response curves after correcting for the slope values determined for baseline waveforms generated in the presence of vehicle controls. Potencies were calculated from fits using a four parameter logistic equation.

Mosquito toxicology and urine excretion. Data were analyzed using Prism 5 for Windows (Graphpad Software). To generate a dose-response curve for VU573, the doses (x-axis) were log transformed and then a non-linear curve was fitted to the data using the ‘log(agonist) vs. response’ algorithm. An ED₅₀ was calculated from this curve. To compare 1) the incapacitating effects among the vehicle, VU573, and VU342 treatments, and 2) the rates of

urine excretion among the control, vehicle, VU573, and VU342 treatments, one-way ANOVAs were performed with Newman-Keuls posttests. To compare the incapacitating effects between the vehicle and VU573 within each mosquito species, a paired t-test was used.

Malpighian tubule experiments. Data were analyzed using Prism 5 for Windows (Graphpad Software) and Excel (Microsoft Corp). To compare the rates of fluid secretion among control, vehicle, VU573, and VU342 treatments, a one-way ANOVA was performed with a Newman-Keuls posttest. To compare the V_{bl} and R_{pc} values of principal cells between control and treatment periods a paired t-test was performed.

Results and Discussion

With few exceptions, the small-molecule pharmacology of the Kir channel family is undeveloped [204]. In an effort to reveal new modulators of human Kir1.1, we previously performed a high-throughput screen of approximately 225,000 small molecules from the National Institutes of Health Molecular Libraries Small-Molecule Repository [20]. The screen discovered compound VU573 (**Fig. 1A**), which inhibits several human Kir channels [64]. Thus, we tested whether VU573 also inhibits the mosquito Kir channel, *AeKir1*.

The tetracycline-induced expression of *AeKir1* in a human cell line (T-REx-HEK-293 cells) produces robust, barium-sensitive, inward-rectifying K^+ currents in whole-cell patch clamp recordings (**Fig. 2**). Bath application of VU573 inhibits the *AeKir1*-mediated currents in a dose-dependent manner (**Fig. 1B, C**) with an IC_{50} of 5.14 μ M (**Fig. 1C**); this IC_{50} is similar to that observed for human Kir2.3, Kir3.x, and Kir7.1 [64].

To facilitate our search for derivatives of VU573 with an improved potency for *AeKir1* over human Kir channels, we developed a high-throughput, fluorescence-based assay to measure

AeKir1 activity in T-REx-HEK-293 cells. The assay uses thallium (Tl^+) as a surrogate of K^+ [20,21,64,204]. The flux is inhibited in a dose-dependent manner by VU573 with an IC_{50} of 15 μM (**Fig. 1D, E**). The slightly higher IC_{50} of VU573 calculated via the Tl^+ -flux assay vs. patch clamp recordings is consistent with results of our previous study on the inhibition of human Kir2.3 and Kir7.1 channels by VU573 [64], and likely reflects different channel permeabilities to Tl^+ and K^+ [85].

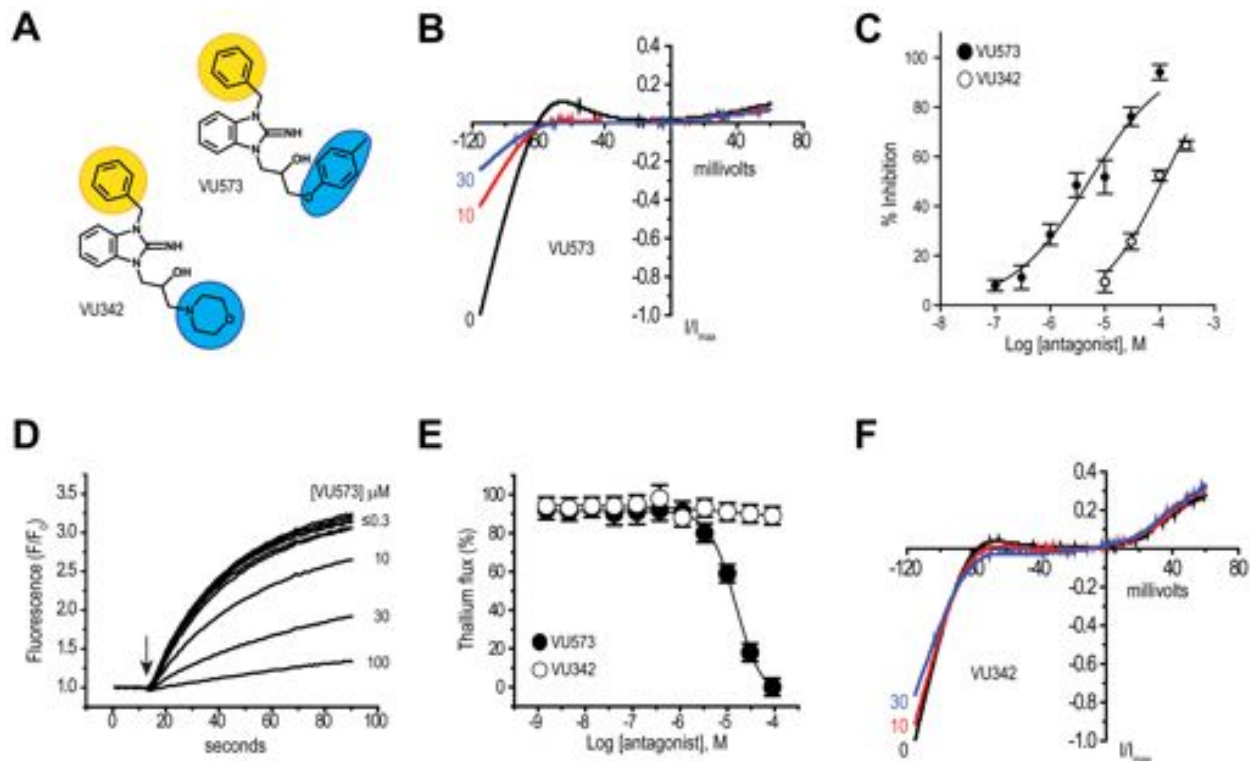


Figure 1. Small-molecule probes of *AeKir1* expressed in T-REx-HEK-293 cells. (A) Chemical structures 3 of the *AeKir1* antagonist VU573 and inactive analog VU342. The ‘northern’ and ‘southern’ groups are indicated by yellow and blue shading, respectively. (B) Normalized *AeKir1* current-voltage (*I*-*V*) relationships illustrating VU573-dependent inhibition at 0, 10, and 30 μM . Cells were voltage clamped at -75 mV and ramped between -120 mV and $+60$ mV. (C) Concentration-response curves of VU573 (filled circles) and VU342 (open circles) derived from patch clamp experiments ($n = 4-9$). The IC_{50} of VU573 and VU342 are 5.14 ± 1.2 μM and 112 ± 1.1 μM , respectively. (D) Dose-dependent inhibition of the *AeKir1*-mediated TI^+ flux by VU573 ranging in concentrations from ≤ 0.3 to 100 μM . The arrow indicates when TI^+ was added to the extracellular bath. (E) Concentration-response curves of VU573 (filled circles) and VU342 (open circles) derived from TI^+ flux assays. $n = 2-3$ independent experiments, each performed in triplicate. (F) Representative *I*-*V* relationships showing minimal effects of VU342 on the *AeKir1*-mediated currents at concentrations of 0, 10, and 30 μM . Values in panels C and E are means \pm SEM.

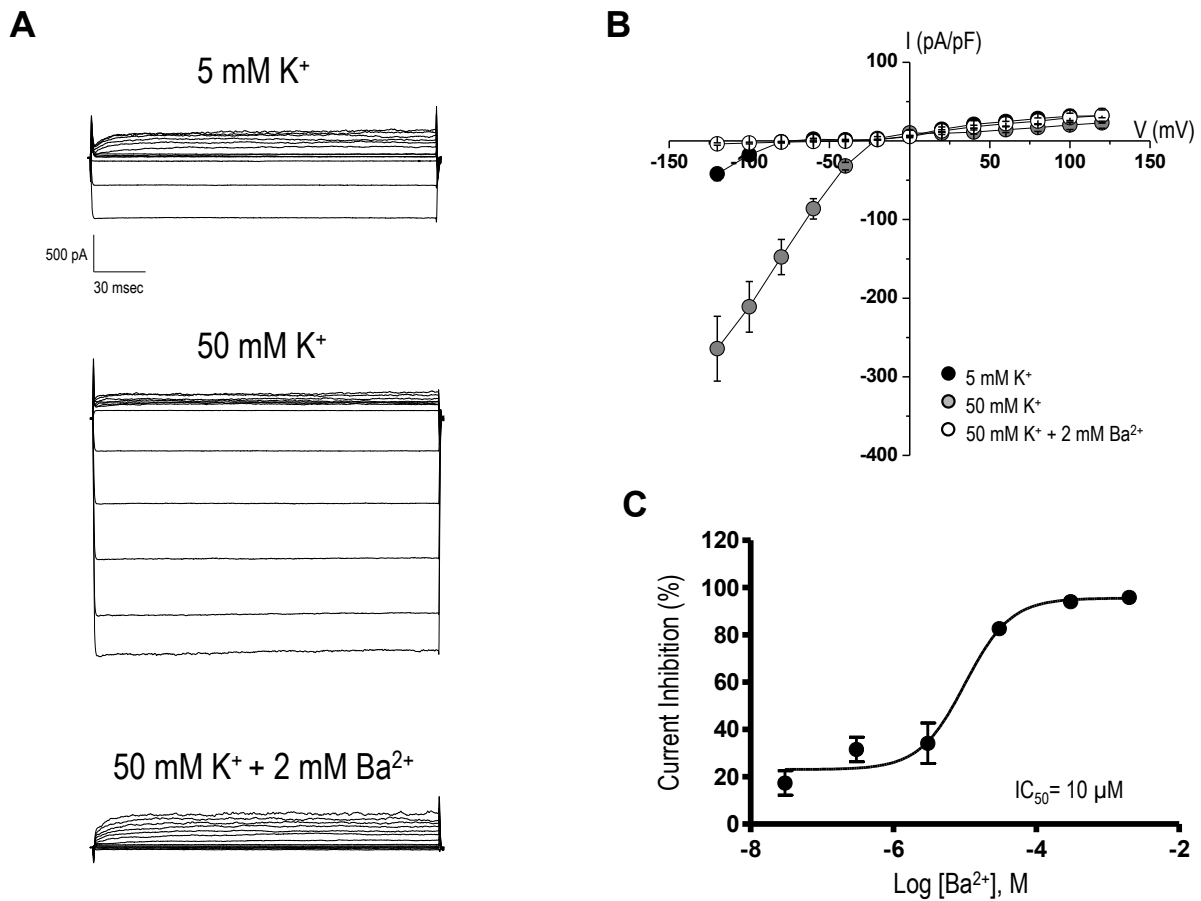
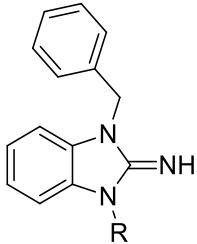
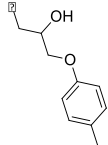
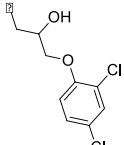
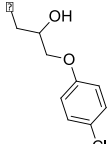
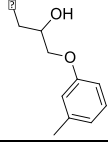
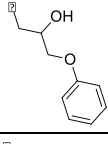
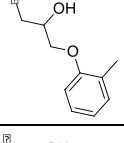
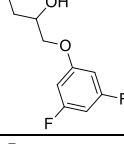
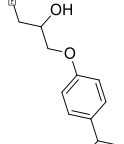
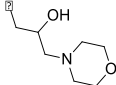
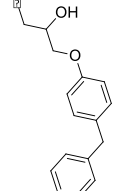
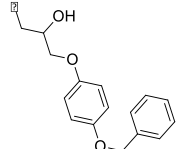
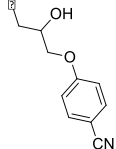
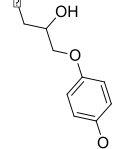
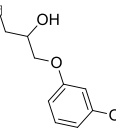
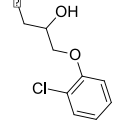
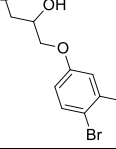
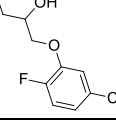
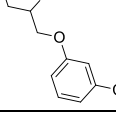
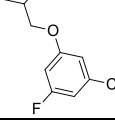


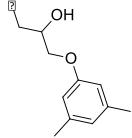
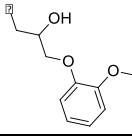
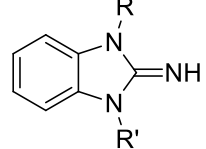
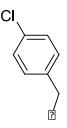
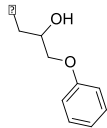
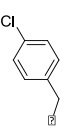
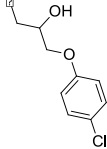
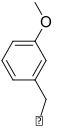
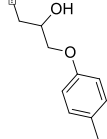

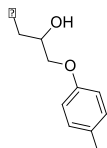

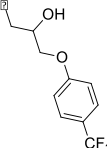
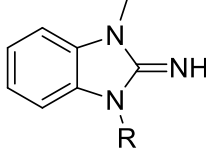
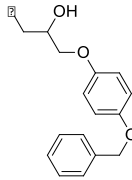
Figure 2. Functional expression of *AeKir1* in T-REx-HEK293 cells and its inhibition by barium (Ba²⁺). (A) Representative current traces recorded from stably transfected cells cultured overnight in the presence of tetracycline to induce channel expression of *AeKir1*. Recordings were made from a cell superfused with 5 mM K⁺ (top panel), 50 mM K⁺ (middle panel), or the control blocker 2 mM Ba²⁺ in 50 mM K⁺ (bottom panel). (B) Current-voltage (I-V) relationships for *AeKir1* bathed in 5 mM K⁺ (dark circle), 50 mM K⁺ (grey circle), or 50 mM K⁺ plus 2 mM Ba²⁺ (white circle). n = 3–7. (C) Concentration-response curve of Ba²⁺-dependent inhibition of *AeKir1* with a 50% inhibition concentration (IC₅₀) of 10 μM. Data are means ± SEM (n = 4–6).

We used the TI^+ -flux assay to assess the structure-activity relationships of 47 analogs of VU573 (**Table 1**), focusing on the ‘northern’ benzyl and ‘southern’ aryl-ether of VU573 (**Fig. 1A, Table 1**) (see [64] for synthesis). Modification of the northern or the southern group of VU573 did not produce analogs with improved potency for *AeKir1* (**Table 1**). However, the replacement of the southern aryl ether with a morpholine moiety produced compound VU342 (**Fig. 1A; Compound 9 in Table 1**), which nominally inhibits the *AeKir1*-mediated TI^+ flux ($\text{IC}_{50} > 100 \mu\text{M}$; **Fig. 1E**). When assessed in whole-cell patch-clamp experiments of T-REx-HEK-293 cells, VU342 is 22-times less potent than VU573 at inhibiting *AeKir1* ($\text{IC}_{50} = 112 \mu\text{M}$; **Fig. 1C, F**); the maximal inhibition of *AeKir1* is only ~65% and requires a concentration of 300 μM (**Fig. 1C**). Accordingly, in subsequent experiments, we used VU342 as a negative control.

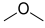
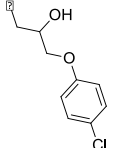
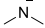
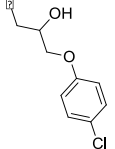
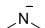
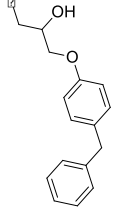
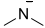
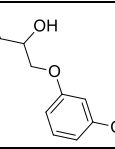
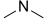
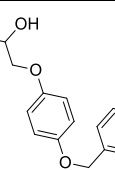
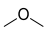
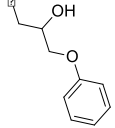
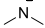
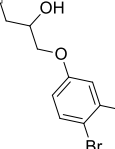
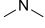
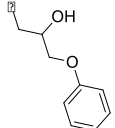
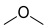
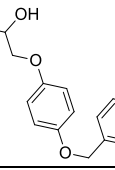
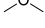
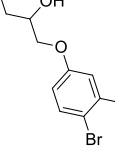
Table 1. Structure-activity relationships for VU573 and its analogs. Values are means \pm SEM (n = 1-3 independent TI^+ flux experiments in triplicate).

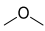
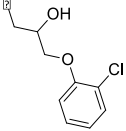
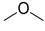
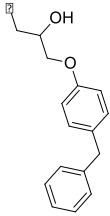
				
Compound	R	R'	VU#/Barcode	IC ₅₀ (μM)
1 (VU573)		N/A	VU0160573-1/ IC4X	15 \pm 1.2
2		N/A	VU0403134-1/ IC3Y	13 \pm 3.7
3		N/A	VU0403131-1/ IC58	10 \pm 0.0
4		N/A	VU0340260-1/ IC38	20 \pm 2.00
5		N/A	VU0026784-1/ IC3L	11 \pm 2.1
6		N/A	VU0288495-1 IC39	12 \pm 0.5
7		N/A	VU0451348-1/ R6P	9.4 \pm 0.3
8		N/A	VU0451344-1/ R80	14 \pm 0.5

9 (VU342)		N/A	VU0451342-1/ R70	>100
10		N/A	VU0451341-1/ R7M	11 ± 1.2
11		N/A	VU0451340-1/ R5C	13 ± 3.7
12		N/A	VU0451339-1/ R56	10 ± 0.0
13		N/A	VU0066224-6/ R7N	20 ± 2.00
14		N/A	VU0451336-1/ R5B	11 ± 2.1
15		N/A	VU0451333-1/ R5X	12 ± 0.5
16		N/A	VU0451337-1/ R5K	9.4 ± 0.3
17		N/A	VU0451332-1/ R7B	14 ± 0.5
18		N/A	VU0451338-1/ R71	>100
19		N/A	VU0451330-1/ R6J	12 ± 2.1

20		N/A	VU0451331-1/ RKN	18 ± 4.0
21		N/A	VU0451846-2/ R87	19 ± 3.0
				
Compound	R	R'	VU#/Barcode	IC ₅₀ (μM)
22			VU0401333-1/ IC4L	16 ± 1.5
23			VU0403132-1/ IC48	>100
24			VU0451343-1/ RJ4	18 ± 2.0
25			VU0451335-1/ R5P	24 ± 0.5
26			VU0451334-1/ R7L	8.0 ± 0.5
				
Compound	R	R'	VU#/Barcode	IC ₅₀ (μM)
27		N/A	VU0467122-1/ 1CQH	7.9 ± 1.1

28		N/A	VU0467123-1/ 15L2	33 ± 2.9
29		N/A	VU0467128-1/ 15ND	8.4 ± 1.1
30		N/A	VU0467127-1/ 15NC	30 ± 1.1
31		N/A	VU0467126-1/ 15LR	7.6 ± 1.2
32		N/A	VU0467125-1/ 15KQ	12 ± 1.1
33		N/A	VU0467124-1/ 15LD	17 ± 1.2
34		N/A	VU0026649-2/ 1LTK	26
35		N/A	VU0027181-2/ 1LR8	17
Compound	R	R'	VU#/Barcode	IC ₅₀ (μM)
36			VU0469204-1/ 1LTW	>100

37			VU0469203-1/ 1LTH	>100
38			VU0035129-2/ 1LRM	30
39			VU0469202-1/ 1MCF	>100
40			VU0469201-1/ 1MDX	22
41			VU0094518-2/ 1MCC	>100
42			VU0469200-1/ 1LTU	>100
43			VU0469194-1/ 1LTG	>100
44			VU0469195-1/ 1LT7	>100
45			VU0469199-1/ 1LU7	>100
46			VU0469198-1/ 1LU6	>100

47			VU0469197-1/ 1LRW	>100
48			VU0469196-1/ 1LTT	>100

We next assessed the effects of VU573 in adult female mosquitoes (*Ae. aegypti*). VU573 was dissolved in a phosphate-buffered saline (PBS) containing 15% DMSO and delivered directly to the hemolymph via intrathoracic microinjection (69 nL per mosquito). The injection of VU573 renders mosquitoes incapacitated (flightless or dead) within 24 hours in a dose-dependent manner ($ED_{50} = 53.6$ pmol; **Fig. 3A**). Of the mosquitoes incapacitated by VU573, 92.3% were flightless while 7.7% were dead. Some of the incapacitated mosquitoes (3.6%) also exhibited greatly distended abdomens consistent with the retention of fluid in the absence of renal functions ('bloated' in **Fig. 3B**). Parallel experiments in adult females of other important mosquito vectors (*Anopheles gambiae*, *Aedes albopictus*, *Culex pipiens*) show that injection of VU573 also incapacitates these mosquitoes (**Fig. 4**).

To determine if the effects of VU573 on mosquitoes are associated with its inhibition of *AeKir1*, we compared the efficacy of VU573 to incapacitate mosquitoes (*Ae. aegypti*) with that of the inactive analog VU342. **Figure 2C** shows that nearly 100% of the mosquitoes injected with VU573, but less than 20% of those injected with the vehicle or VU342, are incapacitated within 24 hours. Furthermore, 10% of the mosquitoes injected with VU573 were bloated (e.g., **Fig. 3B**), while none of the vehicle or VU342-injected mosquitoes retained fluid. Thus, the incapacitation of mosquitoes by VU573 likely arises from the inhibition of Kir channels—presumably those in the renal excretory system.

To assess whether VU573 inhibits the production of urine by Malpighian tubules we used the method of Ramsay [201]. As shown in **Fig. 3D**, isolated Malpighian tubules bathed in a high-potassium Ringer solution (control) spontaneously secrete fluid at a rate of ~0.6 nL/min in the first 30 min. The addition of VU573 to the peritubular bath (10 μ M final concentration) significantly inhibits the rate of fluid secretion to 0.26 nl/min after 2 hours (**Fig. 3D**), whereas

the addition of the vehicle (0.05% DMSO) or VU342 (10 μ M) has no effect on the rate of fluid secretion after 2 hours (**Fig. 3D**). Thus, VU573 inhibits the first step in urine formation at the level of the Malpighian tubules.

To confirm the inhibition of Kir channels by VU573, we used two-electrode voltage clamping to measure the basolateral membrane voltage (V_{bl}) and input resistance (R_{pc}) of principal cells of isolated Malpighian tubules [202]. Peritubular application of VU573 (10 μ M) significantly hyperpolarizes the V_{bl} by 7.0 mV while increasing the R_{pc} by 5.7 k Ω (Table 1); these changes are consistent with the blockade of Kir channels in the basolateral membrane of Malpighian tubules [202]. By comparison, peritubular application of barium at 5 mM, which is a generic blocker of potassium channels including Kir channels (e.g., **Fig. 2**), also significantly hyperpolarizes the V_{bl} while increasing the R_{pc} . The channel block by Ba^{2+} is significantly greater than that of VU573, which is to be expected given that it is less selective than VU573 (**Table 2**).

Table 2. Effects of VU573 (10 μ M) and barium (5 mM) on the basolateral membrane voltage (V_{bl}) and input resistance (R_{pc}) of principal cells in isolated Malpighian tubules.

	V_{bl} (mV)	R_{pc} (k Ω)
Control ($n = 5$)	-45.4 ± 3.6	249.6 ± 15.2
VU573 ($n = 5$)	-52.4 ± 4.5 <i>b</i>	255.3 ± 15.4 <i>a</i>
Control ($n = 6$)	-47.4 ± 4.2	199.2 ± 30.4
Barium ($n = 6$)	-59.3 ± 3.3 <i>c</i>	322.8 ± 31.0 <i>d</i>

a,b,c,d indicate $P < 0.02, 0.003, 0.008,$ and $0.0003,$ respectively (paired t-test). Values are means \pm SEM.

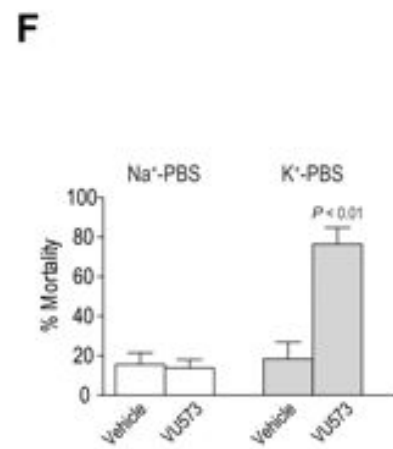
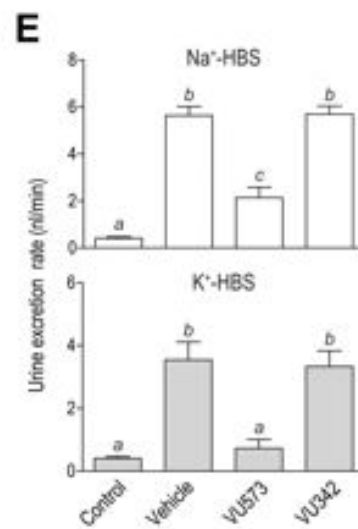
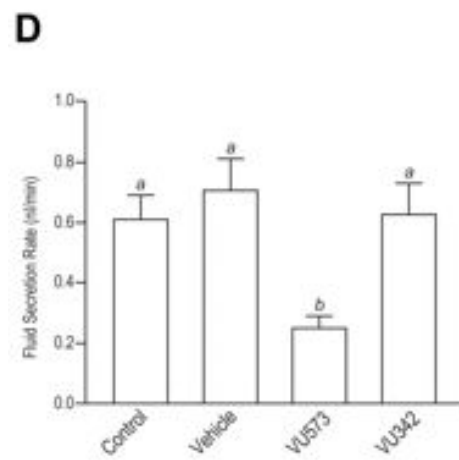
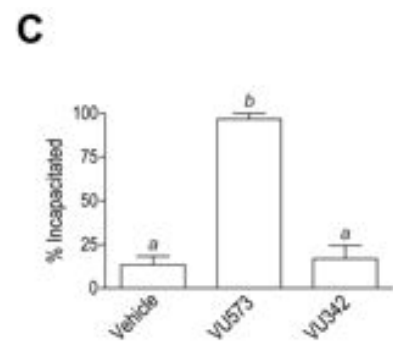
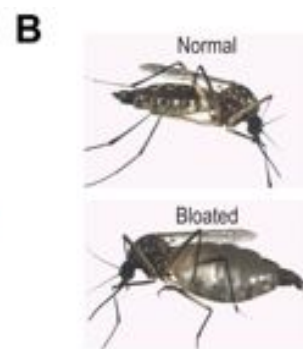
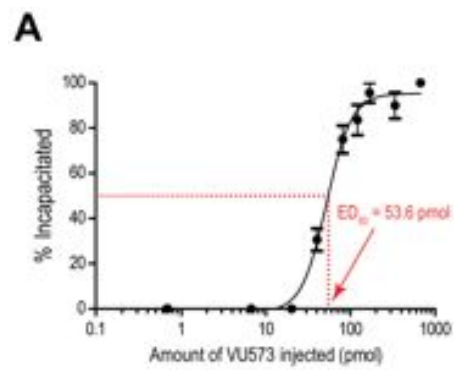
To determine whether the VU573-mediated inhibition of fluid secretion by isolated Malpighian tubules causes renal failure in intact mosquitoes, we measured urine excretion rates using a method modified from the laboratory of Hansen [203]. Mosquitoes fed on a sucrose solution ad libitum (control) excrete urine at a rate of 0.41 nL/min (**Fig. 3E**, top), whereas those injected with 900 nL of a Na⁺-HEPES-buffered saline (HBS)—a volume 30% less than that ingested with a blood meal [195]—excrete urine at a significantly higher rate of 5.64 nL/min ('vehicle' in **Fig. 3E**, top). The rate of urine excretion is significantly dampened to 2.14 nL/min if the Na⁺-HBS contains VU573 (0.77 mM), whereas the rate is unaffected (5.7 nL/min) if the Na⁺-HBS contains VU342 (**Fig. 3E**, top).

A more pronounced inhibition of urine excretion by VU573 is observed when 900 nl of a K⁺-HBS is injected (**Fig. 3E**, bottom). Mosquitoes injected with the K⁺-HBS alone (vehicle) excrete urine at a significantly higher rate (3.54 nL/min) than the controls (**Fig. 3E**, bottom), but if the injected K⁺-HBS contains VU573 (0.77 mM) then the rate of urine excretion is markedly reduced to 0.73 nL/min (**Fig. 3E**, bottom). Urine excretion is unaffected if the K⁺-HBS contains VU342 (**Fig. 3E**, bottom). Thus, VU573 inhibits both the production of urine in Malpighian tubules in vitro (**Fig. 3D**) and the excretion of urine in vivo (**Fig. 3E**). The more effective inhibition of urine excretion by VU573 in the presence of elevated hemolymph K⁺ is expected with the block of Kir channels in Malpighian tubules [74]. Taken together, the above findings suggest that VU573 incapacitates mosquitoes by interfering with K⁺ homeostasis.

In view of the above results, we sought to determine if the incapacitating effects of VU573 are enhanced by K⁺ in *Ae. aegypti*. In the control experiment, the injection of 900 nL of Na⁺-PBS with VU573 (0.77 mM) into the thoracic hemolymph of mosquitoes does not significantly increase mortality compared to those injected with the Na⁺-PBS vehicle alone (**Fig.**

3F), but still renders them flightless within 24 hours. In contrast, the injection of K^+ -PBS with VU573 (0.77 mM) significantly increases mortality compared to the vehicle (**Fig. 3F**). This finding mirrors the more pronounced effects of VU573 on the urine excretion rates of mosquitoes injected with K^+ -HBS vs. Na^+ -HBS (**Fig. 3E**), suggesting that the lethal effects of VU573 stem from the disruption of hemolymph K^+ homeostasis. Accordingly, the above findings indicate that VU573 would be most toxic to female mosquitoes after feeding on vertebrate blood, which presents a K^+ load to the hemolymph [195-197]. In *Ae. aegypti*, about 30 min after feeding, the digestion of blood cells releases as much K^+ for absorption into the hemolymph as that in the injection of K^+ -PBS [195]. Thus, soon after feeding on blood, a female mosquito is expected to succumb to the effects of VU573, which are amplified by elevated hemolymph K^+ levels.

Figure 3. Effects of VU573 and VU342 on adult female mosquitoes (*Aedes aegypti*). (A) Dose-response curve of the incapacitating effects of VU573 on mosquitoes with an effective dose 50% (ED₅₀) of 53.6 pmol. ‘% Incapacitated’ refers to the proportion of mosquitoes that are flightless or dead within 24 h after injection. Each mosquito was injected with 69 nL of PBS/15% DMSO containing an appropriate concentration of VU573 to deliver the dose indicated. The ED₅₀ was determined by fitting a non-linear curve to the data ($R^2 = 0.95$). n = 3-5 trials of 10 mosquitoes per dose. (B) Representative images of *Ae. aegypti* exhibiting ‘Normal’ and ‘Bloated’ abdomens. (C) Incapacitating effects resulting 24 h after injecting mosquitoes (69 nL each) with PBS containing the vehicle (15% DMSO), VU573 (10 μM), or VU342 (10 μM). n = 6 trials of 10 mosquitoes per treatment. Lower-case letters indicate statistical categorization of the means as determined by a one-way ANOVA and a Newman-Keuls posttest ($P < 0.05$). (D) Effects of VU573 and VU342 on the in vitro secretion of fluid by isolated Malpighian tubules. Tubules were bathed in a peritubular Ringer solution (control) to which one of the following was added: vehicle (0.05% DMSO), VU573 (10 μM), or VU342 (10 μM). Secretion rates of the controls were calculated for the first 30 min, whereas those of the vehicle and small molecules were calculated 2 h after their addition. n = 7 tubules for control, vehicle, and VU342; n = 5 tubules for VU573. Lower-case letters indicate statistical categorization of the means as determined by a one-way ANOVA and a Newman-Keuls posttest ($P < 0.05$). (E) Effects of VU573 and VU342 on the in vivo rates of urine excretion in intact mosquitoes. Mosquitoes were either uninjected (control) or injected with a Na⁺ or K⁺ HBS (900 nL) containing the vehicle (1.8% DMSO), VU573 (0.77 mM) or VU342 (0.77 mM). n = 8 trials of 3 mosquitoes for controls; n = 10 and n = 8 trials of 3 mosquitoes for Na⁺-HBS and K⁺-HBS, respectively. Lower-case letters indicate statistical categorization of the means as determined by a one-way ANOVA and a Newman-Keuls posttest ($P < 0.05$). (F) Effects of injecting a Na⁺ or K⁺ PBS (900 nL) with the vehicle (1.1% DMSO) or VU573 (0.77 mM) on mosquito mortality. n = 5 trials of 10 mosquitoes each. Statistical differences between the vehicle and VU573 are determined with a paired t-test for each PBS. Values shown in all panels are means ± SEM.



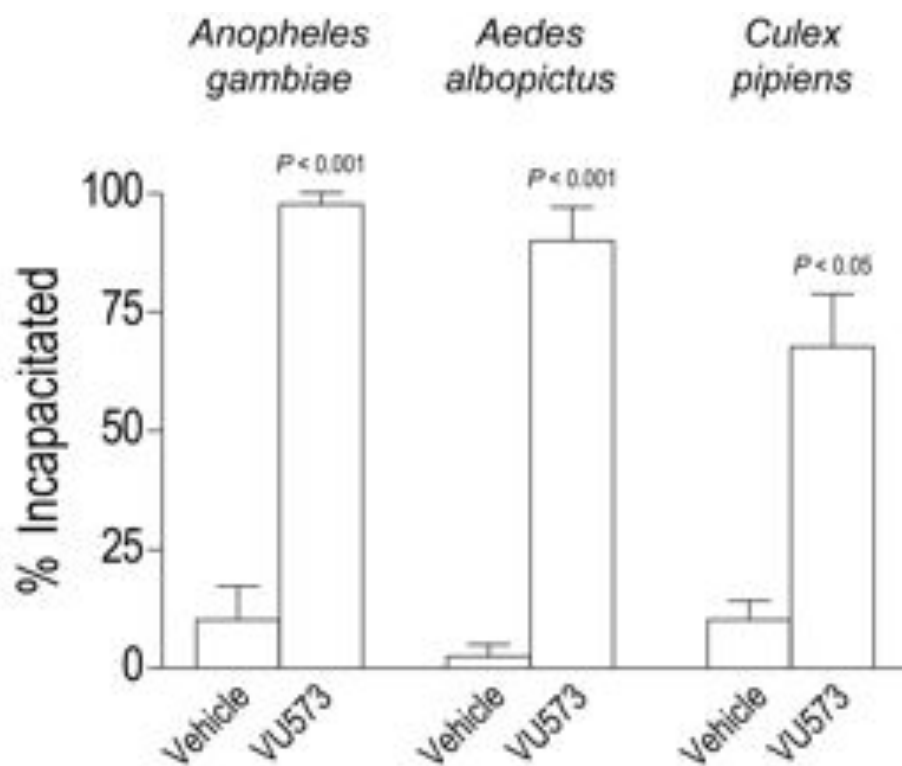


Figure 4. Incapacitating effects of VU573 in three species of mosquitoes. Adult female mosquitoes were injected with Na⁺- PBS (69 nL) containing the vehicle (15% DMSO) or VU573 (10 mM). ‘% Incapacitated’ refers to the proportion of mosquitoes that are flightless or dead within 24 h after injection. Values are means ± SEM (n = 4 independent trials of 10 mosquitoes). Statistical differences between vehicle and VU573-treated mosquitoes were determined by a paired t-test for each species. *Anopheles gambiae* is the primary vector of malaria; *Aedes albopictus* is a vector of emerging arboviruses, such as dengue and Chikungunya fevers; *Culex pipiens* is a vector of West Nile virus and lymphatic filariasis.

In conclusion, we have demonstrated that a small-molecule inhibitor of Kir channels elicits renal failure in female mosquitoes, which would decrease their reproductive output and ability to transmit pathogens by limiting the number of vertebrate blood meals they could consume. Therefore, such inhibitors could be considered as a potential new class of insecticides to be further developed for combatting the emerging problem of insecticide resistance in mosquitoes. The challenges that lay ahead are the development of: 1) small molecules that inhibit Kir channels of mosquitoes with greater potency than those of humans and beneficial insects, and 2) an efficient and effective system to deliver the inhibitors to mosquitoes. The high-throughput screening assay for *AeKir1* established in the present study will expedite the former effort.

Chapter VII

MOLECULAR AND FUNCTIONAL CHARACTERIZATION OF ANOPHELES GAMBIAE INWARD RECTIFIER POTASSIUM (KIR1) CHANNELS: A NOVEL ROLE IN EGG PRODUCTION

Abstract

Inward rectifier potassium (Kir) channels play essential roles in regulating diverse physiological processes. Although Kir channels are encoded in mosquito genomes, their functions remain largely unknown. In this study, we identified the members of the *Anopheles gambiae* Kir gene family and began to investigate their function. Notably, we sequenced the *A. gambiae Kir1 (AgKir1)* gene and showed that it encodes all the canonical features of a Kir channel: an ion pore that is composed of a pore helix and a selectivity filter, two transmembrane domains that flank the ion pore, and the so-called G-loop. Heterologous expression of *AgKir1* in *Xenopus* oocytes revealed that this gene encodes a functional, barium-sensitive Kir channel. Quantitative RT-PCR experiments then showed that relative *AgKir1* mRNA levels are highest in the pupal stage, and that *AgKir1* mRNA is enriched in the adult ovaries. Gene silencing of *AgKir1* by RNA interference did not affect the survival of female mosquitoes following a blood meal, but decreased their egg output. These data provide evidence for a new role of Kir channels in mosquito fecundity, and further validates them as promising molecular targets for the development of a new class of mosquitocides to be used in vector control.

Introduction

A reviewed of mammalian Kir channels is discussed in **Chapter I**. In comparison to mammals, relatively little is known about Kir channels in insects, with most of our understanding coming from the model insect, *Drosophila melanogaster*. The *D. melanogaster* genome encodes three members of the Kir gene family, which are named *Kir1*, *Kir2*, and *Kir3* [205]. Experiments using heterologous expression systems have demonstrated that *Kir1* and *Kir2* encode functional inward rectifier K⁺ channels, whereas *Kir3* does not [205]. In embryos, *Kir2* and *Kir3* are expressed in the hindgut and the Malpighian (renal) tubules, respectively [205], whereas in adult flies all *Kir* encoding genes are expressed in the Malpighian tubules [206]. Thus, given their spatial expression it has been hypothesized that Kir channels may play a role in osmoregulatory processes [205,206]. Kir channels also appear to be involved in development; a recent study by Dahal et al. (2012) showed that genetic disruption of *Kir2* expression causes wing-patterning defects as a result of dysregulation of bone morphogenetic protein (BMP) signaling.

The genome of the yellow-fever vector mosquito *Aedes aegypti* encodes five members of the Kir channel family, named *Kir1*, *Kir2A*, *Kir2B*, *Kir2B'* and *Kir3* [74]. Similar to the *Drosophila* Kir family, *A. aegypti* *Kir1* and *Kir2B*, but not *Kir3*, encode functional channels when heterologously expressed [74]. Also similar to *D. melanogaster*, the expression of *Kir1*, *Kir2B*, and *Kir3* is enriched in Malpighian tubules, consistent with the hypothesis that these genes play important roles in osmoregulation and urine production. Indeed, we recently reported that pharmacologically inhibiting *A. aegypti* *Kir1* channels using a small-molecule antagonist reduces urine output, disrupts K⁺ homeostasis, and leads to a flightless or dead phenotype within 24 hours of treatment. That study showed that Kir channels are essential for proper renal

physiology and suggests that inhibiting Kir channels could be a novel insecticidal mechanism for the control of mosquito disease vectors [207].

The biology of Kir channels in the African malaria vector *Anopheles gambiae* remains unexplored. Here, we identified the members of the *A. gambiae* Kir gene family and began to explore their expression, function, pharmacology, and integrative physiology. Most notably, we found that the expression of *A. gambiae* Kir1 (*AgKir1*) is enriched in the ovaries and that RNAi-mediated knockdown of the channel decreases the number of eggs laid by female mosquitoes.

Materials and Methods

Mosquito rearing

Anopheles gambiae Giles *sensu stricto* (G3 strain; Diptera: Culicidae) were reared and maintained in an environmental chamber set to 27°C and 75% humidity as previously described [208]. Briefly, eggs were hatched in distilled water and larvae were fed a mixture of koi food and yeast daily. Upon eclosion, adults were fed a 10% sucrose solution *ad libitum*. All experiments were carried out on adult female mosquitoes.

Sequencing of *Anopheles gambiae* Kir1 from Malpighian tubule cDNA

As described in previous studies [74,209,210], the GeneRacer Kit (Life Technologies, Carlsbad, CA) was used to generate two independent pools of single-stranded cDNA (designated as 5'-cDNA and 3'-cDNA) from Malpighian tubule total RNA (derived from ~50 females). The 5'-cDNA was used as the template for 5'-rapid amplification of cDNA ends (RACE), whereas the 3'-cDNA was used as the template for 3'-RACE.

The 5'- and 3'-RACE reactions were assembled in volumes of 25 μ l as recommended by the manufacturer. Each reaction consisted of (1) a GeneRacer Kit primer (5'-Primer or 3'-Primer), (2) a gene-specific primer (designed using the bioinformatic prediction of *AgKir1*), (3) 5'- or 3' RACE library cDNA, and (4) Platinum PCR Supermix HF (Life Technologies). A “touchdown” thermocycling protocol was used for all RACE reactions as outlined by the GeneRacer Kit. The amplification products of the RACE reactions were visualized by 1% agarose gel electrophoresis, TA-cloned (Life Technologies), and chemically transformed into *Escherichia coli* (Zymo Research, Irvine, CA), as described previously [74,209,210]. Plasmid DNA from the resulting *E. coli* colonies was sequenced at the Molecular and Cellular Imaging Center of the Ohio State University Ohio Agricultural Research and Development Center (Wooster, OH). A consensus sequence for *AgKir1* was generated after aligning the DNA sequences of the 5'-RACE, 3'-RACE, and full-length PCR products. After assembly, sequences were graphically visualized using Artemis software (Wellcome Trust Sanger Institute, Cambridge, UK). The primers used to determine the full-length sequence of *AgKir1* are presented in **Table 1** and the positions and lengths of *AgKir1* exons and introns in the Agamp3 assembly of the *A. gambiae* genome are shown in **Table 2**.

The predicted AgKir1 protein mass was calculated using the Compute pI/Mw tool in the ExPASy Bioinformatics Resource Portal (http://web.expasy.org/compute_pi/), and a search for a signal peptide was done using the SignalP 4.0 server [211]. The membrane-associated domains were predicted using the Eukaryotic Linear Motif server (<http://www.elm.eu.org>), and ExPASy ProtScale (<http://web.expasy.org/protscale/>) was used to plot hydrophobicity using the Rao and Argos scale [212]. Prediction of the selectivity filter was done by searching for the canonical T-

X-G-Y(F)-G sequence [1], the pore helix was identified by alignment to AeKir1 [74], and alignment with human Kir sequences was used to predict the G-loop [213].

Table 1. Primers used for cloning and sequencing *Anopheles gambiae* Kir1 (*AgKir1*).

Name	Sequence (5' -3')	PCR reaction
1R	GCCACTAGCCGGTTGATCTTTCATTCGT	5'-RACE (initial)
2R	CAGCTGACGAGCACTGCACAGAGGAGTA	5'-RACE (initial)
3R	TAAATAGCTGCTGCGTGCTTGCCTGGT	5'-RACE (nested)
4R	CTCCATGGCTCAGGGCGATCAGGTA	5'-RACE (initial)
5R	ACTCGCTTCCGAATACGTCTGGAGCTGT	5'-RACE (nested)
1F	GTGGTGGAATCGACCGGTATGAC	3'-RACE (initial)
2F	TCCGATACCGATGAATCCGACACAT	3'-RACE (initial)
3F	CCCGTTCGTCGTCCAGTGCCAGTGGT	3'-RACE (nested)
FL_3F	CAGCAGCAGCAGACGACTT	Full-length
FL_4F	GCGGTGTCGTTGGAATAAG	Full-length (nested)
FL_1R	TTCTGCAACCACTGGCACT	Full-length
FL_2R	GAAGTGAACGGGAGGATGTG	Full-length (nested)

Table 2. Positions and lengths of *Anopheles gambiae* Kir1 exons and introns in the *Anopheles* genome

Exon	Chromosome	Start Position	Stop Position	Length of Exon	Length of Following Intron	
1	2R	2,201,198	2,201,335	1,037	5,805	
2	2R	2,207,081	2,207,547	407	56,200	*Start codon (51-53)
3	2R	2,263,718	2,263,834	115	282	
4	2R	2,264,117	2,264,258	142	68	
5	2R	2,264,327	2,264,410	84	75	
6	2R	2,264,486	2,264,760	275	77	
7	2R	2,264,838	2,264,838	190	69	
8	2R	2,265,097	2,265,221	125	66	
9	2R	2,265,288	2,265,396	109	67	
10	2R	2,265,464	2,265,758	295	2,745	*Stop codon (267-269)
11	2R	2,268,504	2,269,189	673	n/a	

Protein alignment and phylogenetic analysis

Protein sequences of Kir channels from *Aedes aegypti*, *Anopheles gambiae*, *Culex quinquefasciatus*, *Drosophila melanogaster* and *Microcoleus vaginatus* were retrieved from the National Center for Biotechnology Information protein database website (<http://www.ncbi.nlm.nih.gov/pubmed/>) or VectorBase (<https://www.vectorbase.org/>), with accession IDs shown in **Table 3**. Protein sequences were aligned with the ClustalW algorithm using Geneious Pro v4.8.5 software (<http://www.geneious.com>; Biomatters, Auckland, New Zealand), and amino acid similarities were calculated using the Blosum62 score matrix (threshold = 0). The LG+I+G+F model of amino acid substitution according to the Akaike information criterion was then identified with ProtTest 2.4 [214], and used to construct a maximum likelihood tree (1000 replicates) in PhyML 3.0 [215], as implemented in the T-REX web server [216]. The phylogenetic tree was visualized and edited with FigTree v1.4.0 (<http://tree.bio.ed.ac.uk/software/figtree/>). The amino acid sequence of Ion transport 2 domain protein (a putative Kir channel) from the cyanobacterium *M. vaginatus* was used as the outgroup.

Table 3. Accession numbers of *A. aegypti*, *A. gambiae*, *C. quinquefasciatus*, *D. melanogaster* and *M. vaginatus* Kir channel sequences.

Protein name	VectorBase ID
AeKir1	AAEL008932
AeKir2A	AAEL008928
AeKir2B	AAEL008931
AeKir2B'	AAEL013373
AeKir3	AAEL001646
AgKir1	AGAP001280
AgKir2A	AGAP001281
AgKir2A'	AGAP001283
AgKir2B	AGAP001284
AgKir3A	AGAP007818
AgKir3B	AGAP028144
CqKir1	CPIJ017135
CqKir2A	CPIJ017138
CqKir2B	CPIJ017140
CqKir3A	CPIJ000961
CqKir3B	CPIJ000962

Protein name	GenBank ID
DmKir1	NP_001262861.1
DmKir2	ACL85253.1
DmKir3	NP_001137835.1
MvKir	WP_006634522.1

Heterologous expression and electrophysiology in *Xenopus* oocytes

To express *AgKir1* in *Xenopus* oocytes, the open-reading frame of *AgKir1* was subcloned into a pGH19 plasmid and the synthesized complementary RNA (cRNA) was injected into stage IV-V defolliculated *Xenopus laevis* oocytes as previously described [74]. The oocytes were injected with either 7.5 or 15 ng of cRNA to induce *AgKir1* channel expression, and cultured for 3-7 days in OR3 media as described [74,209,217]. Oocytes that had been injected with nuclease-free H₂O served as controls.

Whole-cell *AgKir1* currents were recorded using the two-electrode voltage clamp technique as previously described [74]. Current and voltage commands were generated with a Digidata 1440A Data Acquisition System (Molecular Devices, Sunnyvale, CA) and the Clampex module of pCLAMP software (version 10, Molecular Devices). For current recordings, an oocyte was transferred to the holding chamber under superfusion with a control solution and was impaled with two conventional-glass microelectrodes backfilled with 3M KCl (resistances of 0.5–1.5 MΩ). The control solution (ND96) contained (in mM): 96 NaCl, 0 NMDG-Cl, 2 KCl, 1 MgCl₂, 1.8 CaCl₂, and 5 HEPES, with pH adjusted to 7.5 with NMDG-OH. For some experiments, a low-K⁺ solution was used, which contained (in mM): 0.5 NaCl, 97.5 NMDG-Cl, 0.5 KCl, 1 MgCl₂, 1.8 CaCl₂, and 5 HEPES. Alternately, a high-K⁺ solution was used, which contained (in mM): 0.5 NaCl, 48 NMDG-Cl, 50 KCl, 1 MgCl₂, 1.8 CaCl₂, and 5 HEPES. *AgKir1* currents were inhibited with Ba²⁺ (1 mM), a non-specific K⁺ channel blocker [84,218,219]. For current-voltage (I-V) recordings, oocytes were voltage clamped near their spontaneous membrane potential (V_m) and stepped from -140 mV to + 40 mV in 20 mV increments for 100 ms each. All recordings were performed at room temperature, and the I-V plots were generated using the Clampfit module of pCLAMP.

RNA isolation, cDNA synthesis, and quantitative real-time PCR

Total RNA was isolated from whole adult female mosquitoes as previously described [220]. Briefly, RNA extracted from 10 to 20 mosquitoes was isolated using TRIzol® Reagent (Life Technologies, Carlsbad, CA) and purified using the RNeasy kit (Qiagen, Valencia, CA). First-strand cDNA was synthesized from poly(A)+ RNA using the SuperScript® III First-Strand Synthesis System for RT-PCR (Life Technologies) according to manufacturer instructions. Real-time quantitative PCR (qRT-PCR) was then done using Power SYBR® Green PCR Master Mix (Applied Biosystems, Foster City, CA) on an ABI 7300 Real-Time PCR System. Relative quantification was carried out using the $2^{-\Delta\Delta CT}$ method [221], and the ribosomal protein S7 (*rps7*) was used as the reference gene [222,223].

AgKir1 mRNA levels, and the mRNA levels of other *A. gambiae* Kir genes, were measured by real-time quantitative PCR (qRT-PCR) essentially as described [208]. To quantify *AgKir1* mRNA levels in different developmental stages, cDNA was synthesized from RNA purified from ~200 eggs, 50 second instar larvae, 40 third instar larvae, 30 fourth instar larvae, 20 pupae (callow or black) or 15 adults (24 h, 5 days or 10 days old). Two biological replicates were conducted and each was analyzed in duplicate. The graphed output displays the average fold-change in mRNA levels relative to eggs.

To quantify *A. gambiae* Kir gene expression in different body segments, cDNA was synthesized from RNA purified from 10 whole bodies, 20 heads, 20 thoraces or 20 abdomens from adult mosquitoes at 4 days post-eclosion. To quantify *A. gambiae* Kir gene expression in dissected tissues, cDNA was synthesized from RNA purified from midguts, Malpighian tubules, ovaries and fat bodies. Tissues were collected from ≥ 25 mosquitoes as previously described [208], except that in this study the Malpighian tubules were separated from the midgut and

processed separately. These are standard methods of tissue dissection, although the procedure for fat body collection suffers from the fact that other cell types are collected as well, including the dorsal vessel, other muscle, the ventral nerve cord, pericardial cells, and sessile hemocytes [224,225]. The body segment and tissue experiments were conducted in parallel, with three independent trials being performed and each being analyzed in duplicate. The graphed output of body segment and tissue analyses displays the average fold-difference in mRNA levels relative to whole bodies. The primers used for qRT-PCR are presented in **Table 4**.

RNA interference (RNAi)-based gene silencing

An RNAi-based strategy was used to silence gene expression. A 492 bp double stranded RNA (dsRNA) construct specific to *A. gambiae Kir1* was synthesized using the MEGAscript® kit (Life Technologies, Carlsbad, CA) as described earlier [222]. As a control, a 214 bp dsRNA construct specific to *bla(Ap^R)*, the ampicillin-resistant gene that is encoded in Novagen's pET-46 Ek/LIC vector (EMD Chemicals, Gibbstown, NJ), was synthesized from DNA purified from BL21(DE3) *Escherichia coli* cells containing the pET-46 plasmid.

To knockdown mRNA levels, approximately 500 ng of *AgKir1* dsRNA or *bla(Ap^R)* dsRNA was intrathoracically injected into 3-day-old female mosquitoes. To verify knockdown efficiencies, ≥ 10 mosquitoes were collected at days 4, 8, and 11 post-injection, total RNA was purified, cDNA was synthesized, and relative gene expression was quantified by qRT-PCR. For each timepoint, 2-3 biological replicates were conducted, and each was assayed in duplicate. Gene silencing data are presented as mRNA levels relative to the *bla(Ap^R)* dsRNA-injected control groups. The primers used for RNAi and gene expression are presented in **Table 4**.

Table 4. Primer sequences used for amplification of Kir channel genes for expression analyses and RNA interference.

Gene	Vectorbase ID ^a (Application)	Primer name	Primer sequence (5'-3') ^b	Amplicon Length (bp)
<i>AgKir1</i>	AGAP001280 (qRT-PCR)	<i>Ag_Kir1_02F</i>	TCCTCTGTGCAGTGCTCGTC	168
		<i>Ag_Kir1_02R</i>	TACTGCGTGAAGCGAAG	
<i>AgKir1</i>	AGAP001280 (dsRNA synthesis)	<i>Ag_Kir1_T702F</i>	<u>TAATACGACTCACTATAGGGCGATGAAAGTCACAAAC</u>	519 ^c
		<i>Ag_Kir1_T702R</i>	<u>TAATACGACTCACTATAGGGCTATCCCGATCGATCTTG</u>	
<i>AgKir2A</i>	AGAP001281 (qRT-PCR)	<i>Ag_Kir2A_03F</i>	GAGACGCACTCCGTCGATAC	153
		<i>Ag_Kir2A_03R</i>	ACATACGCAAACGGTCAACA	
<i>AgKir2A'</i>	AGAP001283 (qRT-PCR)	<i>Ag_Kir2A'_02F</i>	GTTACATCTGCCCGATAACC	217
		<i>Ag_Kir2A'_02R</i>	CACTATGCCAACCATGAACG	
<i>AgKir2B</i>	AGAP001284 (qRT-PCR)	<i>Ag_Kir2B_01F</i>	GTCAGGTGTATTGCTTACGC	178
		<i>Ag_Kir2B_01R</i>	GCGGGGTTTCTTGTACCCAG	
<i>AgKir3A</i>	AGAP007818 (qRT-PCR)	<i>Ag_Kir3_01F</i>	CGTGTGGTGAACAAGATTGG	193
		<i>Ag_Kir3_01R</i>	GAATCAGATCACCGTGAGCG	
<i>rpS7</i>	AGAP010592 (qRT-PCR)	<i>rpS7_02F</i>	GACGGATCCCAGCTGATAAA	132
		<i>rpS7_02R</i>	GTTCTCTGGGAATTCGAACG	
<i>bla(Ap^R)</i>	Bacterial gene (dsRNA synthesis)	<i>blaApr_T7_01F</i>	TAATACGACTCACTATAGGGCCGAGCGCAGAAGTGGT	214 ^c
		<i>blaApr_T7_01R</i>	<u>TAATACGACTCACTATAGGGAACCGGAGCTGAATGAA</u>	

^a Vectorbase IDs were obtained from the AgamP3 assembly in www.vectorbase.org.

^b Underlined sequences are specific to the T7 RNA polymerase promoter sites needed for dsRNA synthesis.

^c dsRNA amplicon length includes the T7 promoter sequence tags.

Antibody production

An affinity purified, polyclonal rabbit antibody raised against a synthetic peptide (SRRIRKRVIFKQGDC) corresponding to a putative fragment of the cytosolic NH₂-terminal domain of AgKir1 (S128-C142) was developed by 21st Century Biochemicals (Marlboro, MA).

Western blotting

To prepare protein lysates, whole mosquitoes were homogenized in a 10% Ringer solution. After determining the protein concentration using the Bradford reagent, the lysates were diluted by addition of one volume of high-urea buffer that was composed of the following: 6 M Urea, 15 mM TrisHCl, 0.3% SDS and 0.25 mM NaCl at pH 7.4 [209]. The high-urea lysates were mixed with an appropriate volume of a 5X Laemmli gel loading buffer (60 mM Tris-HCl, 25% glycerol, 2% SDS, 0.5% β -mercaptoethanol, 0.1% bromophenol blue) and incubated at 100°C for 5 minutes. Approximately 30 μ g of protein was separated by SDS-PAGE on a denaturing 12% polyacrylamide resolving gel (with a 4% stacking gel; ProtoGel[®]Quick-Cast, National diagnostics, Atlanta, GA) using an XCell SureLock Mini Cell electrophoresis unit (Life Technologies). After electrophoresis, the stacking gel was discarded and the separated proteins were transferred to a polyvinylidene difluoride (PVDF) membrane (Thermo Scientific, Rockford, IL) using an XCell II blot module (Life Technologies) according to the manufacturer's protocol.

To detect AgKir1 immunoreactivity, the PVDF membrane was washed three times with Tris-buffered saline containing 0.01% Tween 20 (TBST; 10 mM TrisHCl, 150 mM NaCl, and 0.01% Tween 20, pH 7.4), blocked for 30 min with 5% nonfat dry milk dissolved in TBST (blocking buffer), and incubated overnight at 4°C with the anti-AgKir1 antibody (1:1000 dilution) in blocking buffer. The following day, the PVDF membrane was washed three times (5

min each) with TBST, incubated for 1 h with a horseradish peroxidase (HRP)-conjugated goat anti-rabbit IgG (1:20,000 dilution; Pierce Biotechnology, Thermo Scientific, Rockford, IL) in blocking buffer, and washed three times (5 min each) with TBST. To visualize AgKir1 immunoreactivity, a luminescent substrate of HRP (DuraWest Chemiluminescent, Pierce Biotechnology) was applied to the PVDF membrane, and the signal was detected with a ChemiDocVersatile Document Imager (Bio-Rad Laboratories, Hercules, CA).

Survival assays

For survival assays, 3-day-old adult female mosquitoes were intrathoracically injected with *bla(Ap^R)* dsRNA or *AgKir1* dsRNA and then returned to the environmental chamber and provided with 10% sucrose. At day 8 following the dsRNA injections, the mosquitoes were allowed to blood-feed on mice anesthetized with a mixture of ketamine and xylazine for approximately 30 min, and subsequently maintained on 10% sucrose. Beginning with the time of blood feeding, mosquito survival was recorded daily for 19 days, and the graphed output represents the mean percent survival from the three biological replicates (24-27 mosquitoes per group in each trial).

Fecundity assays

For the fecundity assays, 3-day-old adult female mosquitoes were intrathoracically injected with *bla(Ap^R)* dsRNA or *AgKir1* dsRNA and allowed to blood feed 8 days later. Forty-eight hours after blood-feeding, fully engorged mosquitoes were individually transferred to *Drosophila* vials (Fisher Scientific, Pittsburgh, PA) containing 2-3 mL of distilled water and

capped with a cotton ball. Mosquitoes were monitored for the next 3 days, and eggs were counted once oviposition had taken place. A total of 5 biological replicates were performed.

Results

Anopheles gambiae Kir1 gene structure

Reciprocal tblastn searches of the AgamP3 assembly of the *A. gambiae* genomic sequence and the AaegL2 assembly of the *A. aegypti* genomic sequence in www.vectorbase.org revealed that *A. gambiae* AGAP001280 and *A. aegypti* AAEL008932 are 1:1 orthologs (reciprocal E-values = 0.0). Thus, because AAEL008932 is named *AeKir1* [74], we named AGAP001280 *AgKir1*.

To determine the complete mRNA sequence of *AgKir1*, the entire transcript was sequenced by 5' and 3' RACE. Assembly of the RACE sequences revealed that the *AgKir1* mRNA is 3,452 nucleotides (base pairs; bp) in length, and is composed of a 1,085 bp 5' untranslated region (UTR), a 1,668 bp open reading frame (ORF) and a 669 bp 3' UTR (**Fig. 1**; GenBank ID: Pending). Alignment of the mRNA sequence and the chromosome 2R genomic sequence revealed that the *AgKir1* gene is composed of 11 exons that span 68,906 bp of genomic sequence. Although initially predicted as AGAP001280, the mRNA sequence is significantly larger than the prediction. Starting at the 5' end, *AgKir1* spans the predictions of AGAP013159 and AGAP001280. Thus, these two VectorBase gene IDs should be merged into a single entry.

Conceptual translation of the full-length mRNA revealed that *AgKir1* encodes a 555 amino acid (aa) protein with a predicted mass of 62.1 kDa. As expected of an ion channel, the ORF does not encode a signal peptide. The ORF, however, does encode all of the characteristic features of inward rectifier potassium channels (Kirs). Specifically, ELM analysis predicts three

membrane-associated domains, located in aa positions 171-193, 213-235, and 248-270. The first and third predictions are the classical transmembrane domains seen in Kir channels [1]. The second prediction is the ion pore, which includes the pore helix (aa 219-230; 100% identity with the predicted pore helix in AeKir1; [74]) and the selectivity filter TIGYG (aa 232-236; [1]). A hydrophobicity plot of the conceptual translation of AgKir1 supports the prediction of the two transmembrane domains and the ion pore (**Fig. 2**). Finally, alignment of AgKir1 with human Kir5.1 [213] predicts that aa 390-400 form the so-called G-loop.

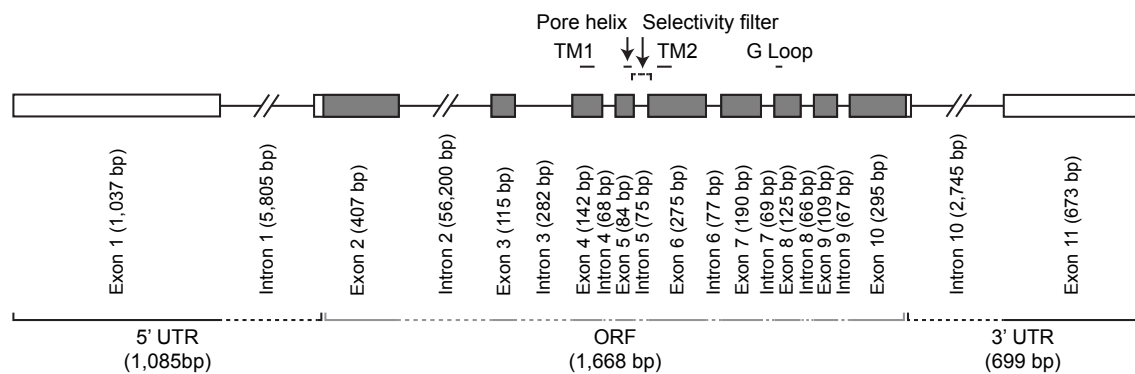


Figure 1. Gene structure of *Anopheles gambiae* *AgKir1*. The open reading frame (ORF) is the gray boxes, the untranslated regions (UTRs) are the white boxes, and the introns are the horizontal lines. The locations that encode the transmembrane domains (TM1 and TM2), pore helix, selectivity filter and G-loop are marked, and the sizes (in bp) of the UTRs, ORF, exons and introns are provided.

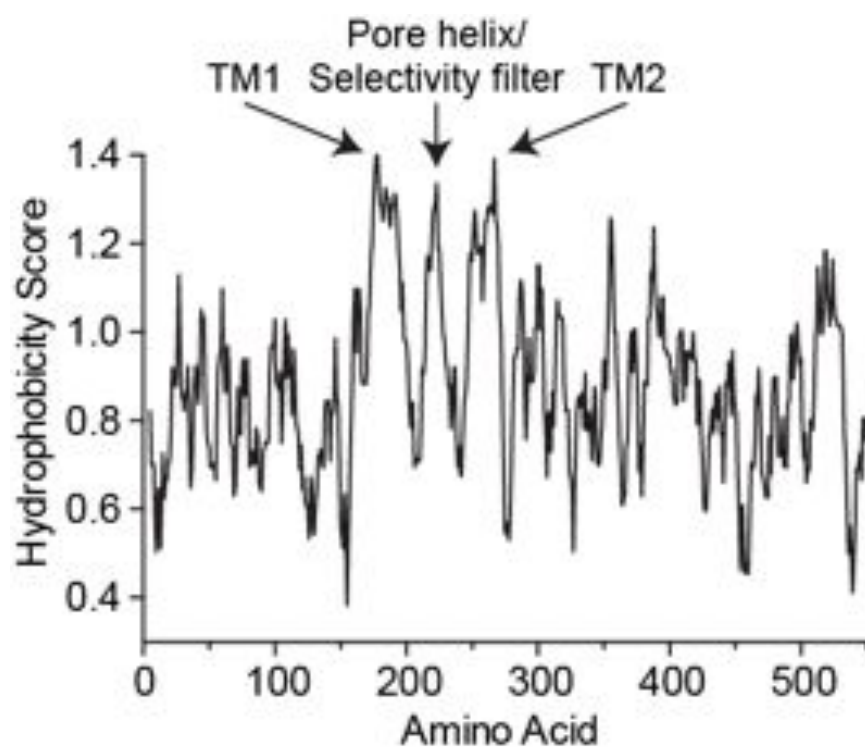


Figure 2. Hydrophobicity plot of AgKir1. Hydrophobicity plot showing the three major hydrophobic regions of AgKir1: the two transmembrane domains (TM1 and TM2) and the ion pore (composed of the pore helix and the selectivity filter). Higher values indicate higher hydrophobicity.

Phylogenetic analysis of AgKir channels

A tblastn search of the AgamP3 assembly of the *A. gambiae* genomic sequence and the CpipJ1 assembly of the *C. quinquefasciatus* genomic sequence in www.vectorbase.org using *AgKir1* as the query sequence, followed by the identification of characteristic features of Kir channels, identified five additional members of the *A. gambiae* Kir gene family (for a total of six Kir genes), and five members of the *C. quinquefasciatus* Kir gene family. Based on sequence alignment and a phylogenetic analysis (see below), the *A. gambiae* genes were named *AgKir2A*, *AgKir2A'*, *AgKir2B*, *AgKir3A* and *AgKir3B*, and the *C. quinquefasciatus* genes were named *CqKir1*, *CqKir2A*, *CqKir2B*, *CqKir3A* and *CqKir3B*.

For the *A. gambiae* Kir genes, alignment of the conceptual translation of *AgKir1* with the putative amino acid sequences of *AgKir2A*, *AgKir2A'*, *AgKir2B*, *AgKir3A* and *AgKir3B* revealed several characteristic features of Kir channels, including a pore-forming domain containing the signature “TIGYG” K⁺ selectivity filter (STGYG in the case of the two *AgKir3* genes), two transmembrane-spanning domains (TM1 and TM2), and the G-loop (**Figs. 1-3**) [1,213]. The core region (between filled circles in **Fig. 3**; [205]) of *AgKir1* shares approximately 60% amino acid sequence identity with *AgKir2* subtypes, but only about 40% identity with *AgKir3* subtypes. Finally, it is interesting that all mosquito (*Anopheles*, *Aedes* and *Culex*) Kir3 genes encode a non-canonical form of the selectivity filter, whereas *DmKir3* contains the canonical form. Given that *AeKir3* and *DmKir3* do not encode a functional channel [74,205], it is possible that the *A. gambiae* and *C. quinquefasciatus* Kir3 genes do not encode functional channels as well (for an alignment of the selectivity filters of dipteran and human Kir channels see **Fig. 4**).

A maximum likelihood tree of dipteran Kir channels using Ion transport 2 domain protein (a putative Kir channel) of *M. vaginatus* as the outgroup shows that Kir genes can be divided into two major clades: Kir1/Kir2 and Kir3 (**Fig. 5**). Consistent with the neighbor-joining analysis of Piermarini et al. [74], the Kir1/Kir2 clade can be subdivided into Kir1 and Kir2 groups, and the Kir2 group can be further subdivided into Kir2A and Kir2B subgroups. Interestingly, whereas *D. melanogaster* only encodes three Kir genes (Kir1, Kir2 and Kir3), the Kir gene family has expanded in the mosquito lineage. That is, the genomes of all three mosquito species encode at least two Kir2 genes, and the genomes of *A. gambiae* and *C. quinquefasciatus* encode two Kir3 genes.

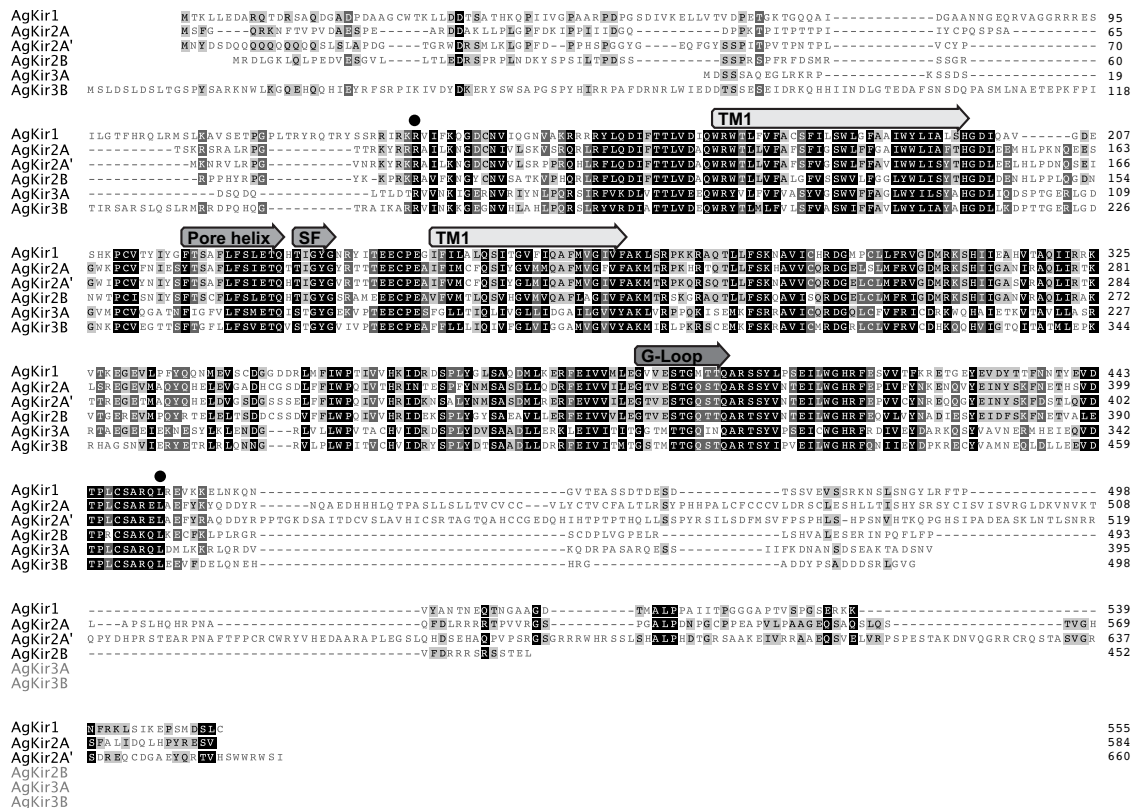


Figure 3. Amino acid sequence alignment of *Anopheles gambiae* Kir channels. ClustalW alignment of the conceptual translations of the RACE sequenced *AgKir1* and the other predicted members of the *A. gambiae* Kir gene family. The transmembrane domains (TM1 and TM2), the pore-helix, the selectivity filter and the G-Loop are indicated. The core region is flanked by filled circles. Shadings denote the amino acid similarity at a given position, with black highlight, dark grey highlight, light grey highlight, and no highlight indicating 100%, 80-99%, 60-79% and <60% similarity, respectively.

				SF			
				←→			
Dipteran Kir1 channels	AeKir1	215	FSLETQH	TIGYGNR	228		
	AgKir1	225	FSLETQH	TIGYGNR	238		
	CqKir1	113	FSLETQH	TIGYGNR	126		
	DmKir1	124	YSVETQT	TIGYGNR	137		
Dipteran Kir2 channels	AeKir2A	185	FSIETQH	TIGYGNR	198		
	AeKir2B	182	FSLETQH	TIGYGNR	195		
	AeKir2B'	127	FSLETQH	TIGYGNR	140		
	AgKir2A	181	FSIETQT	TIGYGNR	194		
	AgKir2A'	184	FSIETQH	TIGYGNR	197		
	AgKir2B	172	FSLETQH	TIGYGNR	185		
	CqKir2A	121	FSIETQH	TIGYGNR	134		
	CqKir2B	172	FSLETQH	TIGYGNR	185		
Dipteran Kir3 channels	DmKir2	195	FSIETQH	TIGYGNR	208		
	AeKir3	121	FSIETQV	STGYGAK	134		
	AgKir3A	127	FSMETQI	STGYGAK	140		
	AgKir3B	244	FSVETQV	STGYGVI	257		
	CqKir3A	107	FSIESQV	STGYGTW	120		
Human Kir channels	CqKir3B	213	FSIETQV	TGFGDK	226		
	DmKir3	210	YSVETQT	TGFGDK	223		
	HsKir1.1	134	FSLETQV	TIGYGNR	147		
	HsKir2.1	135	FSIETQT	TIGYGNR	148		
	HsKir2.2	136	FSIETQT	TIGYGNR	149		
	HsKir2.3	127	FSVETQT	TIGYGNR	140		
	HsKir2.4	140	FALETQT	SIGYGNR	153		
	HsKir2.6	136	FSIETQT	TIGYGNR	149		
	HsKir3.1	136	FFIETEAE	TIGYGNR	149		
	HsKir3.2	145	FSIETEET	TIGYGNR	158		
	HsKir3.3	113	FSIETEET	TIGYGNR	126		
	HsKir3.4	142	FSIETEET	TIGYGNR	155		
	HsKir4.1	121	FSLESQT	TIGYGNR	134		
	HsKir4.2	120	FSLESQT	TIGYGNR	133		
	HsKir5.1	124	FSLETQT	TIGYGNR	137		
HsKir6.1	133	FSIEVQV	TGFGGR	146			
HsKir6.2	36	FSIEVQV	TGFGGR	49			
HsKir7.1	122	FSLETQL	TIGYGNR	125			
MvKir	89	FSVQTMAT	TIGYGNR	102			

Figure 4. ClustalW protein sequence alignment of the K⁺-selectivity filter (TXGY[F]G) from *Aedes aegypti*, *Anopheles gambiae*, *Culex quinquefasciatus*, *Drosophila melanogaster*, *Homo sapiens* and *Microcoleus vaginatus* Kir channels. The Kir3 genes of *Aedes aegypti*, *Anopheles gambiae* and *Culex quinquefasciatus* encode a non-canonical selectivity filter. The GenBank accession numbers used in this analysis were the following: *Homo sapiens* (Hs): NP_000211.1; NP_000882.1; NP_066292.2; NP_690607.1; NP_037480.1; NP_001181887.2; NP_002230.1; NP_002231.1; NP_004974.2; NP_000881.3; NP_002232.2; NP_733932.1; NP_061128.1; NP_004973.1; NP_000516.3; NP_002233.2. Refer to Table S1 for VectorBase and GenBank accession numbers for dipteran Kir channels (*Aedes aegypti*, Ae; *Anopheles gambiae*, Ag; *Culex quinquefasciatus*, Cq; *Drosophila melanogaster*, Dm) and the cyanobacterium *Microcoleus vaginatus*, Mv.

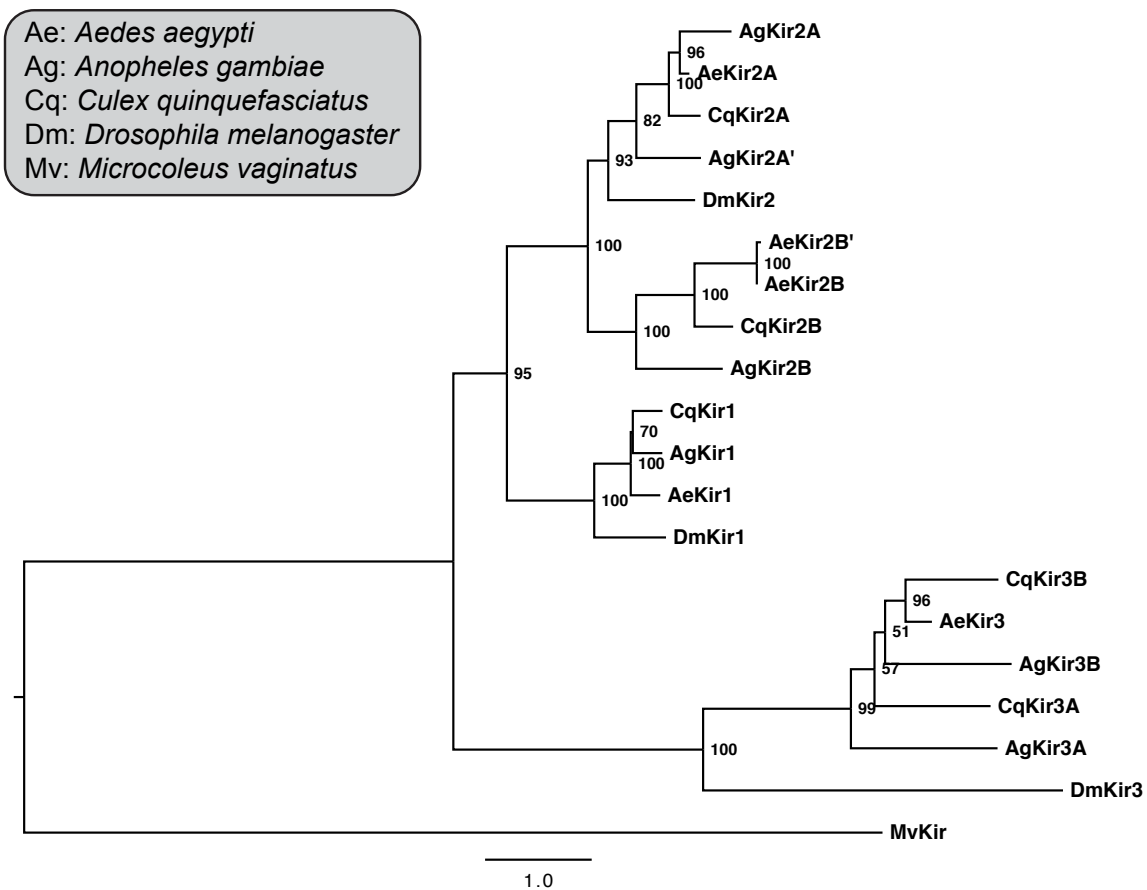


Figure 5. Phylogenetic analysis of the *Anopheles gambiae*, *Aedes aegypti*, *Culex quinquefasciatus*, and *Drosophila melanogaster* Kir channel families. Proteins sequences were aligned by ClustalW and the maximum likelihood tree computed with PhyML 3.0. A putative Kir channel from the cyanobacterium *M. vaginatus* was used as the outgroup, and bootstrap support for the clades are shown for each node. The proportion of amino acid changes among the proteins is indicated by the branch length. The gene IDs are presented in **Table 3**.

Functional characterization of AgKir1 channels in *Xenopus* oocytes

We have shown that a small molecule inhibitor of AeKir1 (VU573) (1) incapacitates adult females of several mosquito species (*A. aegypti*, *A. albopictus*, *A. gambiae* and *C. pipiens*) and (2) disrupts the excretory physiology of at least *A. aegypti* [207]. Thus, because of the important role that AeKir1 plays in renal physiology, our first assessment of Kir gene function in *A. gambiae* focused on *AgKir1*. As shown in **Fig. 6A**, when bathed in a control (ND96) solution, heterologous expression of AgKir1 channels in *Xenopus* oocytes gave rise to functional channels exhibiting spontaneous large inward and small outward currents between -140 mV and -80 mV. Moreover, the spontaneous resting membrane potential of the AgKir1-expressing oocytes (-96.9 ± 1.3 mV) was (1) hyperpolarized compared to the H₂O-injected oocytes (-42.0 ± 2.5 mV), and (2) close to the estimated Nernst potential for K⁺ (-102 mV). As shown in **Fig. 6B**, the inward AgKir1 channel currents increase with increased extracellular K⁺ concentrations and are inhibited by barium. These functional characteristics are canonical of most animal Kir channels, and very similar to those of AeKir1 [207]. Thus, AgKir1 functions as an inward rectifier K⁺ channel.

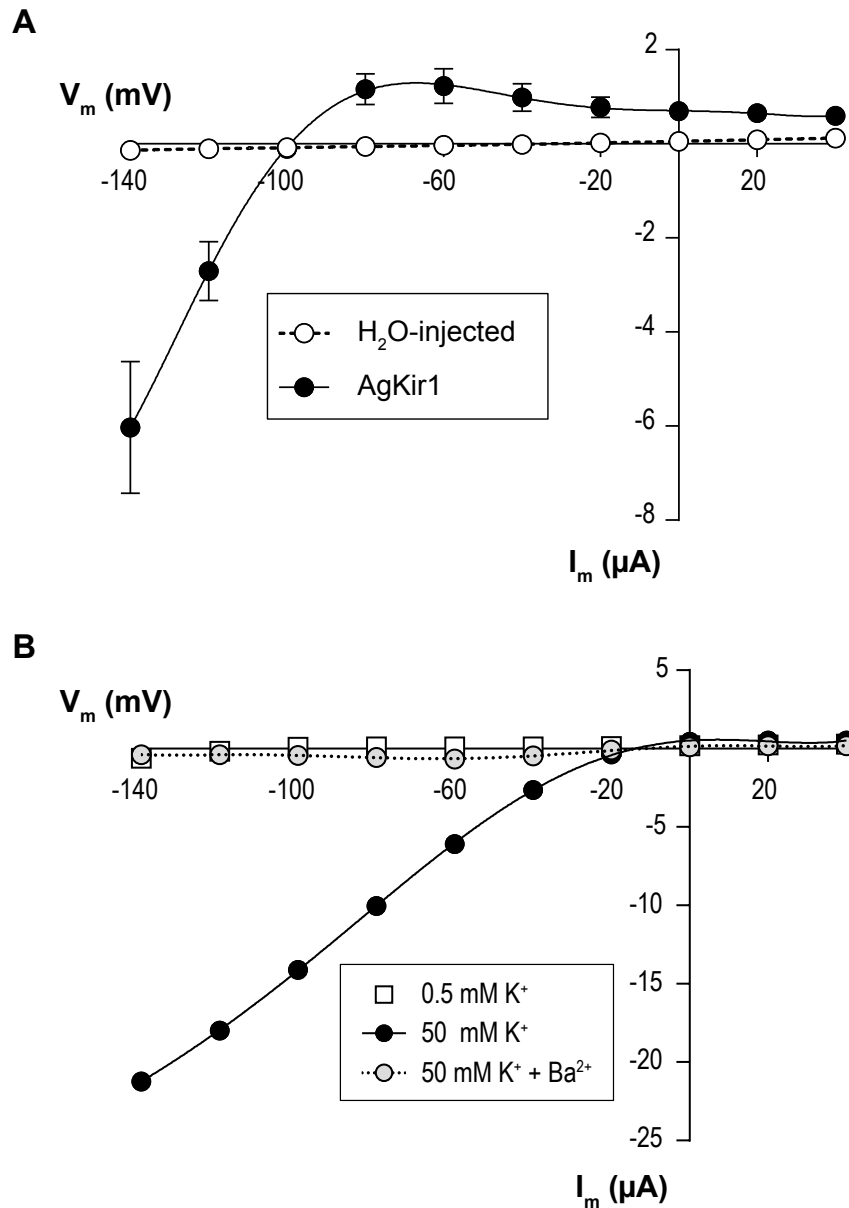


Figure 6. Current-voltage (I-V) relationships of AgKir1 channels in *Xenopus* oocytes. (A) The I-V relationship of AgKir1 channel-expressing oocytes (filled circles; $n = 6$) reveals robust inward rectifying currents when bathed in the control (ND96) solution, whereas those of H₂O-injected oocytes (open circles; $n = 8$) exhibit nominal currents. Data are mean \pm SEM. (B) Barium (1 mM) blocks inward-rectifying K⁺ currents in AgKir1 channel expressing oocytes. Oocytes were bathed consecutively in the following solutions: (1) low-K⁺ solution (open squares), (2) high-K⁺ solution (filled circles), (3) high-K⁺ solution with Ba²⁺ (open circles). Shown is a representative I-V plot from an oocyte. V_m , membrane voltage; I_m , membrane current.

Developmental and tissue distribution of *Kir1* in *Anopheles gambiae*

To gain insight into the possible in vivo functions of AgKir1, we analyzed the expression patterns of *AgKir1* at different life stages. Quantitative RT-PCR analyses revealed that *AgKir1* is ubiquitously expressed in all mosquito life stages, with transcript levels being highest in the pupal stage and lowest in third instar larval stage (**Fig. 7**; ANOVA $P = 0.0003$). Specifically, relative to eggs, there is a trend for *AgKir1* mRNA levels to decrease by half during the larval and then increase between 2- and 3-fold in the early (callow) and late (black) pupal stages. After eclosion, *AgKir1* mRNA levels return to levels similar to those observed in eggs and remain unchanged through the 10th day following adult emergence (the last timepoint assayed).

To determine the locations of *AgKir1* transcription, we analyzed the expression pattern of *AgKir1* in different body segments and tissues of 4-day-old adult female mosquitoes. Quantitative RT-PCR analyses revealed that *AgKir1* mRNA levels are detectable in all body segments and in all tissues assayed (**Fig. 8**). Specifically, mRNA levels in the head, thorax, abdomen and Malpighian tubules are comparable to the levels detected in the mosquito whole body. *AgKir1* mRNA levels trended to be lower in the midgut and fat body tissues when compared to the whole body, a finding that is in agreement with the *Kir1* gene expression profile reported in MozAtlas [226]. However, of all the tissues examined, we observed the significant enrichment of *AgKir1* mRNA in the ovaries: levels were almost 2.5-fold higher than those found in the whole body (ANOVA $P = 0.0008$). Furthermore, when compared to other *Anopheles* Kir genes, enrichment of Kir mRNA in the ovaries was only observed for *AgKir1* (**Fig. 9**). This finding suggested a potentially novel role of Kir channels in mosquito fecundity.

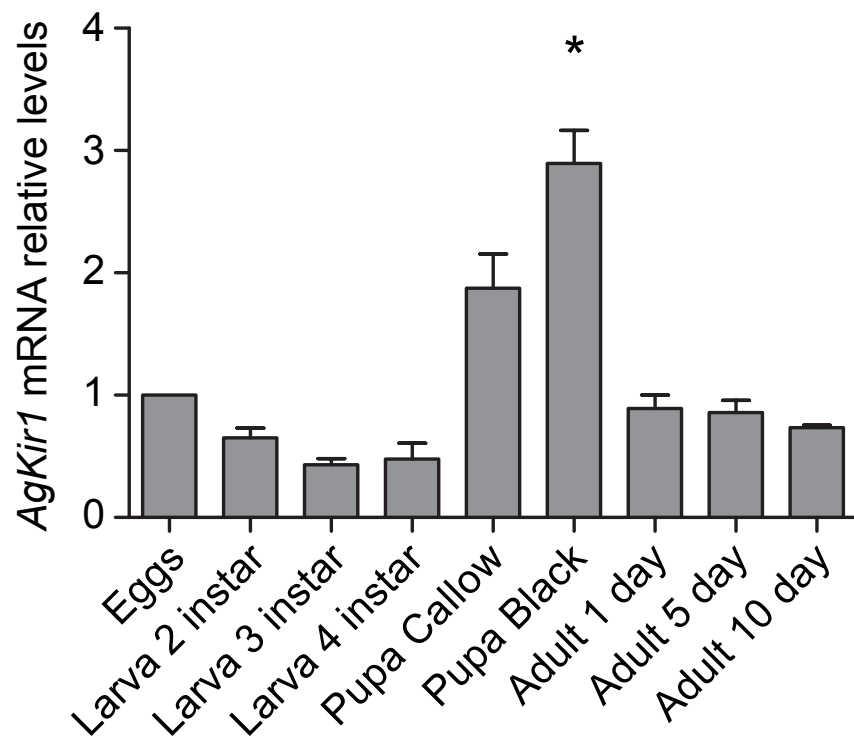


Figure 7. Quantitative RT-PCR analysis of the expression of *A. gambiae* *AgKir1* in different developmental stages. Transcript levels were measured in eggs, developing first instar larvae, second through fourth instar larvae, callow (early) and black (late) pupae, and adults at 24 h, 5 days and 10 days after eclosion. Data are mean \pm SEM fold-difference (two biological replicates) in mRNA levels relative to eggs, using *RPS7* as the reference gene. ANOVA $P = 0.0003$, and the asterisk indicates $P < 0.05$ when compared to eggs (Tukey's test).

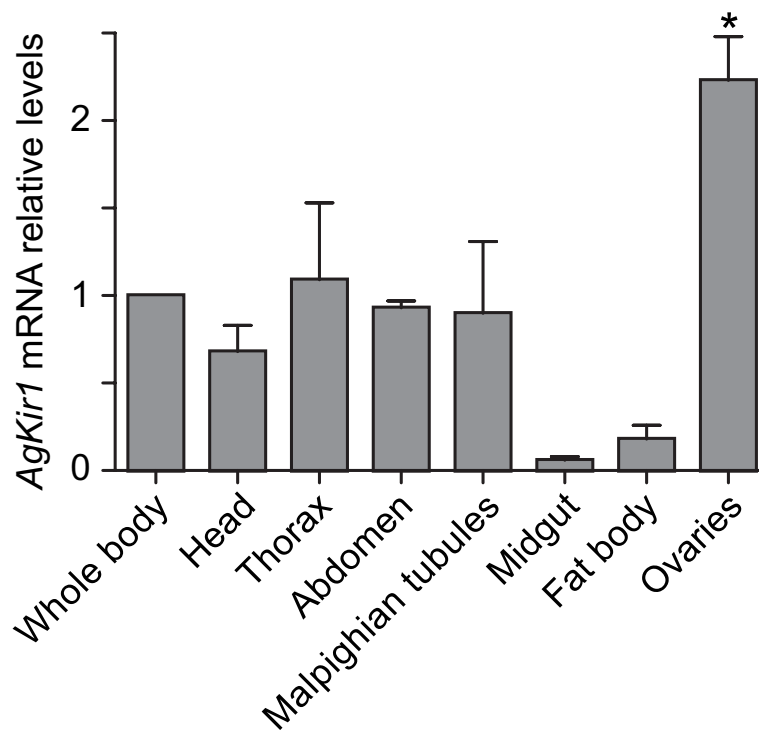


Figure 8. Quantitative RT-PCR analysis of the expression of *A. gambiae* *AgKir1* in different body segments and tissues. Transcript levels were measured in the whole body, head, thorax, abdomen, Malpighian tubules, midgut, fat body and ovaries. Data are mean ± SEM fold-difference (three biological replicates) in mRNA levels relative to the whole body, using *RPS7* as the reference gene. ANOVA $P = 0.0008$, and the asterisk indicates $P < 0.05$ when compared to whole body (Tukey's test).

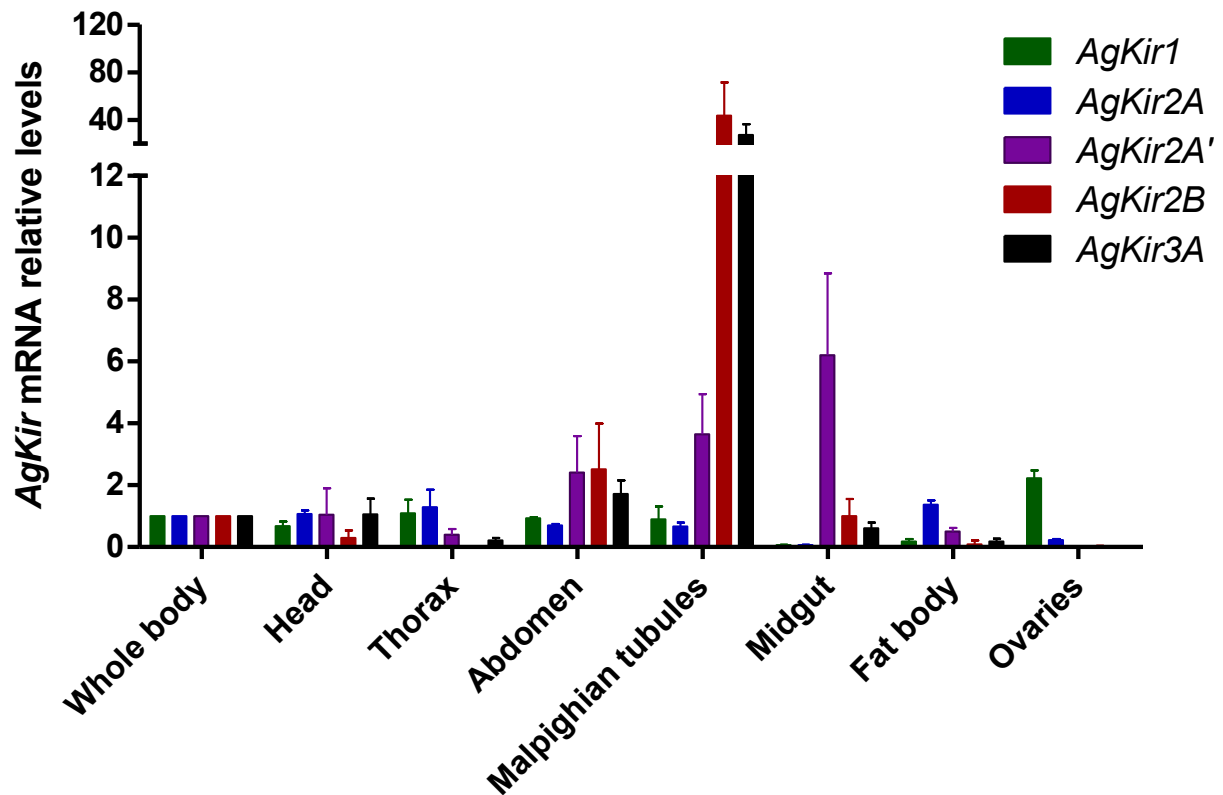


Figure 9. Quantitative RT-PCR analysis of the expression of *A. gambiae* Kir genes in different body segments and tissues. Transcript levels were measured in the whole body, head, thorax, abdomen, Malpighian tubules, midgut, fat body and ovaries. Data are mean \pm SEM fold-difference (three biological replicates) in mRNA levels relative to the whole body, using *RPS7* as the reference gene.

***AgKir1* knockdown does not affect survival**

We have shown that injection of a small-molecule inhibitor of AeKir1 (VU573) into the hemocoel of adult female mosquitoes (*A. aegypti*, *A. albopictus*, *A. gambiae*, *C. pipens*) induces incapacitation and/or death [207]. Moreover, VU573 disrupts renal excretory physiology and hemolymph K⁺ homeostasis in at least *A. aegypti* [207]. These findings suggest that Kir channels are essential regulators of physiological events affecting osmoregulation. Thus, we sought to determine whether AgKir1 is important for mosquito survival following a blood meal, which is a period when mosquitoes face extreme stresses to hemolymph Na⁺, K⁺, Cl⁻, and water homeostasis [69,70]

Toward this goal, we developed methods for knocking down *AgKir1* mRNA levels by RNA interference. Relative to the *bla(Ap^R)* dsRNA controls, injection of *AgKir1* dsRNA significantly reduced *AgKir1* mRNA levels by 24% (P = 0.3487) and 58% (P = 0.0108) at 4 and 8 days post-treatment, respectively (**Fig. 10A**). To determine if *AgKir1* knockdown affects survival following blood feeding, we blood fed mosquitoes 8 days after injecting *AgKir1* dsRNA or *bla(Ap^R)* dsRNA, discarded the mosquitoes that were not fully engorged, and monitored their survival over the next 19 days. Surprisingly, in three independent trials, knockdown of *AgKir1* had no effect on mosquito survival as compared to the control *bla(Ap^R)* group (Logrank P values = 0.6500, 0.8523 and 0.9288; **Fig. 11**). In fact, the slopes and R-square values of the survival curves of the *AgKir1* dsRNA (y = -3.43; R² = 0.985) and *bla(Ap^R)* dsRNA (y = -3.17; R² = 0.941) groups were nearly identical.

Engorged mosquitoes usually take 2-3 days to digest their meal. To ensure that *AgKir1* remained suppressed at that time, we measured *AgKir1* mRNA and protein levels at 72 hrs post-blood feeding, which also represented 11 days post-injection of dsRNA. As shown in **Fig. 10**,

AgKir1 mRNA levels were decreased by >95% (P = 0.0014) relative to the *bla(Ap^R)* dsRNA control group, and AgKir1 protein was reduced considerably, but not completely. These findings suggest that a partial knockdown of *AgKir1* (1) might not be sufficient to affect mosquito survival following a single naïve blood meal, (2) that the function of AgKir1 may be redundant with other Kir channels, or (3) that the functional role(s) of Kir1 may differ between the anopheline and culicine lineages.

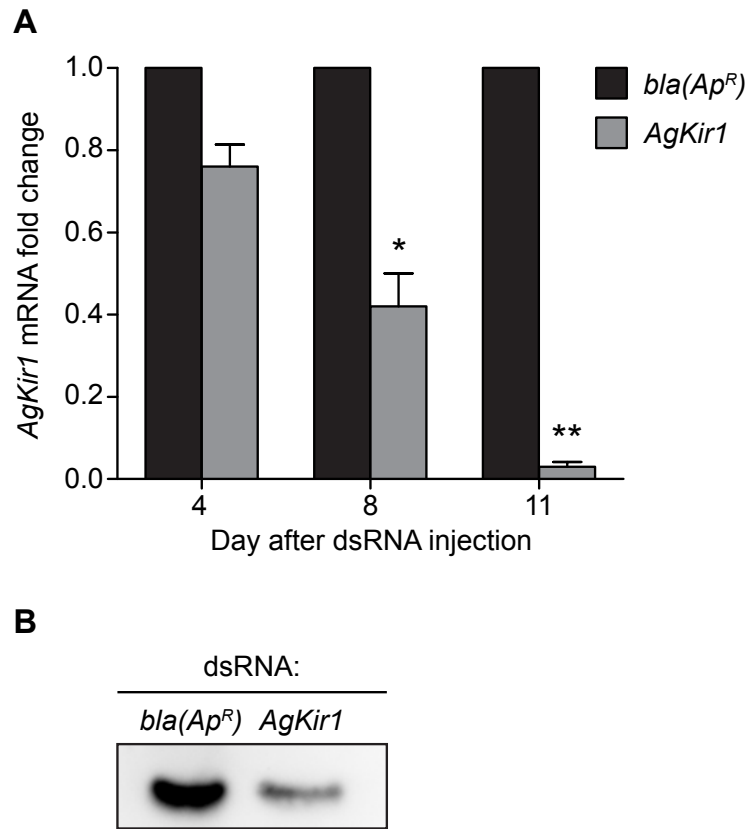


Figure 10. Quantitative RT-PCR and western blot analyses showing *AgKir1* RNAi-based knockdown efficiencies. (A) Quantitative RT-PCR analysis demonstrating the efficiency of *AgKir1* RNAi-based knockdown at 4, 8 and 11 days post-dsRNA injection. Data are mean \pm SEM fold-difference (two or three biological replicates) in mRNA levels relative to the *bla(Ap^R)* dsRNA control group. ANOVA $P = 0.0023$, and asterisks (*, **) indicate $P < 0.05$ or $P < 0.01$ respectively when compared to the *bla(Ap^R)* dsRNA group (Tukey's test). (B) Western blot analysis demonstrating the partial knockdown of *AgKir1* protein levels in *A. gambiae* mosquitoes at 11 days post *bla(Ap^R)* dsRNA or *AgKir1* dsRNA injection.

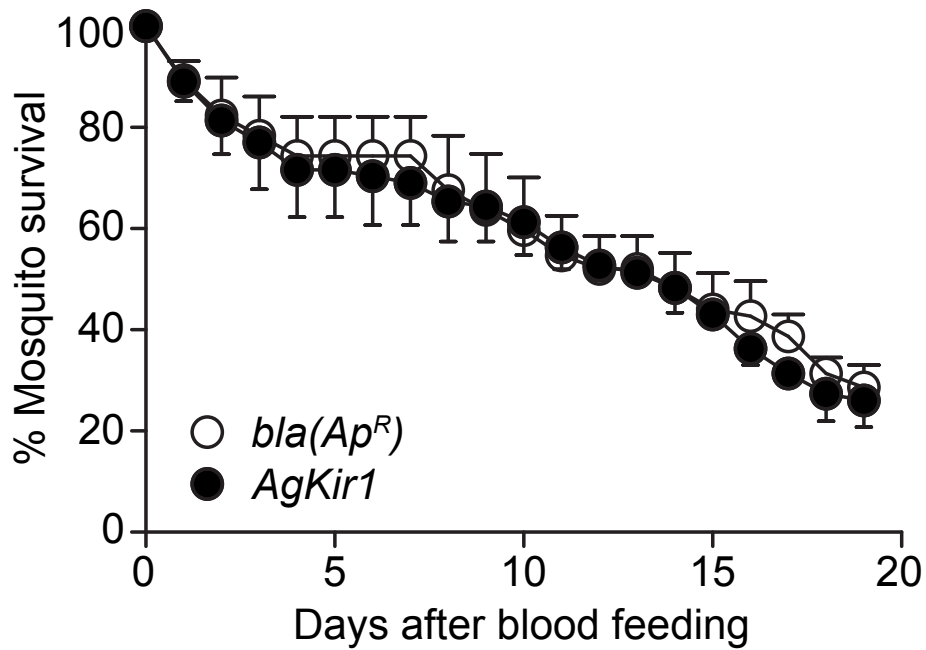


Figure 11. *AgKir1* knockdown does not affect mosquito survival after a blood meal. Paired cohorts composed of 24-27 *A. gambiae* each were injected with *bla(Ap^R)* dsRNA or *AgKir1* dsRNA, provided a blood meal 8 days later, and the survival was tracked for the next 19 days. Data are mean \pm SEM of 3 biological replicates.

***AgKir1* knockdown decreases fecundity**

Because *AgKir1* is enriched in the ovaries (**Fig. 8**), we hypothesized that it could be involved in fecundity. Therefore, we investigated the effect of *AgKir1* RNAi-based knockdown on egg production using a similar protocol to that used for survival experiments, except that the mosquitoes were placed in an oviposition environment at 48 hrs post-blood feeding, and egg laying was monitored for up to three days thereafter. As shown in **Fig. 12**, mosquitoes that were treated with *AgKir1* dsRNA oviposited an average of 21.41 eggs whereas the mosquitoes that were treated with *bla(Ap^R)* dsRNA oviposited an average of 30.11 eggs (n = 151 for both groups; Mann-Whitney P = 0.0485). Furthermore, the number of mosquitoes that laid any eggs in the *AgKir1* dsRNA and *bla(Ap^R)* dsRNA was 32% and 42%, respectively. Together, these data indicate that silencing of *AgKir1* significantly impairs a mosquito's ability to produce and oviposit eggs.

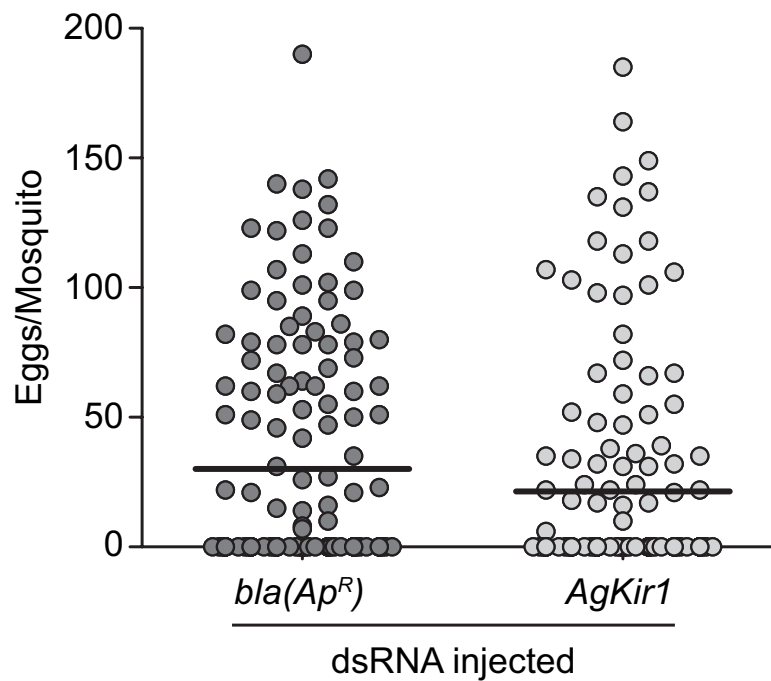


Figure 12. *AgKir1* knockdown decreases mosquito fecundity. Paired cohorts of *A. gambiae* were injected with *bla(Ap^R)* dsRNA or *AgKir1* dsRNA, provided a blood meal 8 days later, and allowed to oviposit. The circles represent the number of eggs laid by each female (n = 151), the horizontal line marks the mean, and the whiskers the SEM. The two groups were statistically different (*, Mann–Whitney P = 0.0485).

Discussion

The large volume of blood that is commonly ingested by mosquitoes represents a major physiological challenge, thereby necessitating an efficient excretory system that rapidly off-loads excessive weight, water, and solutes [69,70]. In a previous study, we showed that pharmacological inhibition of Kir1 (1) incapacitates adult female mosquitoes of several species (*A. aegypti*, *A. albopictus*, *A. gambiae*, *C. pipiens*) and (2) reduces urine production/excretion and disrupts the maintenance of hemolymph K^+ homeostasis in at least *A. aegypti* [207]. That study, besides showing that Kir channels are essential for proper renal excretory physiology in mosquitoes, suggested that inhibiting Kir channels could be used to control mosquito populations, and by extension, mosquito-borne diseases. However, the two major mosquito lineages, the Culicinae (e.g., *Aedes* sp., *Culex* sp.) and the Anophelinae (e.g., *Anopheles* sp.), diverged approximately 200 million years ago [227], and many physiological differences are known to exist between these two groups [223,228-230]. In the present study, we began the characterization of the Kir gene family in the African malaria mosquito, *Anopheles gambiae*. Among other things, we identify the members of the *A. gambiae* Kir gene family, describe their developmental and tissue expression, and show that silencing *AgKir1* reduces mosquito fecundity.

Whereas the genome of *Drosophila melanogaster* encodes three Kir genes, the genomes of *A. aegypti*, *A. gambiae* and *C. quinquefasciatus* encode between five and six Kir genes. This gene expansion in mosquitoes may reflect an increase in the molecular complexity of homomeric or heteromeric Kir channel complexes that are required to regulate unique physiological processes. Indeed, the importance of functional complexity was demonstrated in *Drosophila*, where disruption of Kir channel heteromerization results in the dysregulation of BMP signaling,

which causes major developmental defects [231]. Thus, by encoding six Kir genes, *A. gambiae* have potentially increased the diversity of heteromeric and homomeric complexes available to carry out a multitude of diverse physiological processes.

Using heterologous expression in *Xenopus* oocytes, we show that *AgKir1* encodes a canonical inward-rectifying K⁺ channel with similar properties as *AeKir1* [74]. That is, the channel mediates strong inward K⁺ currents that are blocked by barium. Moreover, the electrophysiological properties of *AgKir1*-expressing oocytes in ND96 solution (i.e., resting membrane potentials and I-V relationships) closely resemble those of *AeKir1*-expressing oocytes [74].

AgKir1 is transcribed in all developmental stages. Peak expression of *AgKir1* occurs in pupae, which suggests a role for *AgKir1* during post-embryonic development, and more specifically, metamorphosis. Interestingly, a reciprocal pattern of expression for at least *Kir2A* occurs in the development of *A. aegypti*, where *Kir2A* abundance is elevated in larvae and adults but is decreased in pupae [232]. The reorganizations associated with metamorphosis are known to result in changes in membrane excitability. As pertains to Kirs, earlier studies have implicated a role for K⁺ channels in regulating membrane potential during post-embryonic development of motor neurons in the fruit fly, *Drosophila melanogaster* [233], and the tobacco hornworm, *Manduca sexta* [234,235]. Further supporting a role for Kirs in development, a recent study showed that *D. melanogaster* *DmKir2* is required for normal wing development, and that Kir channel involvement occurs through the regulation of BMP signaling [231].

AgKir1 is expressed in all adult tissues and body segments. Interestingly, *AgKir1* expression was enriched in the ovaries. This enrichment suggested that Kir channels could be involved in fecundity. Previous studies have demonstrated a role for ionic currents in the maturation of

oocytes. For example, ionic currents such as inward rectifying K^+ currents undergo dynamic modulation (i.e., K^+ current amplitude decreases with oocyte maturation) upon in vitro hormone-stimulation in maturing starfish oocytes [236]. Moreover, ion channel currents (e.g. calcium currents) are involved in oocyte maturation and fertilization in vertebrate and invertebrate animals [237,238]. Therefore, given that *AgKir1* expression is enriched in the ovaries and that *AgKir1* gene silencing reduces fecundity, it is possible that *AgKir1* may participate in the regulation of mosquito oocyte maturation by modulating membrane excitability in these tissues. In insects, oocyte maturation is generally arrested during meiotic cell division and resumes in a fertilization independent manner that requires a mechanical stimulus, such as oviduct passage or rehydration [239,240]. Thus, future studies should investigate whether *AgKir1* plays a role in oogenesis.

Although we detected a role for *AgKir1* in fecundity, we originally anticipated that, based on our previous findings in *A. aegypti* and *A. gambiae* [207], gene silencing of *AgKir1* would result in a dead or flightless phenotype following blood feeding. However, no significant increase in post-blood feeding mortality was observed between *AgKir1* dsRNA and *bla(Ap^R)* dsRNA-treated groups, and the flightless phenotype was not observed either. The fact that we did not observe an obvious phenotype following gene silencing may reflect the difference in efficiency between pharmacologic and reverse-genetic approaches. For example, acute pharmacological inhibition of protein function is expected to yield an extreme phenotype (e.g., death or bloating), whereas partial gene silencing by RNAi may not sufficiently reduce protein levels to produce an obvious effect. Alternatively, it is possible that (1) other Kir channels expressed in the Malpighian tubules of *A. gambiae* can compensate for the reduced levels of *AgKir1*, (2) Kir1 performs different functions in the Malpighian tubules of *A. gambiae* and *A.*

aegypti, or (3) RNAi efficiency is markedly different between tissues [241]. Nevertheless, our survival experiment is consistent with studies in *D. melanogaster*, where there is no apparent lethal effect following Kir1 knockdown, but rather a sub-lethal effect on immune function [242].

In conclusion, here we present the first evidence that Kir channels play a role in mosquito fecundity, which together with their important roles in mosquito renal physiology [207], further validates them as promising molecular targets for the development of a new class of mosquitocides to be used in vector control.

Chapter VIII

DISCOVER AND CHARACTERIZATION OF A POTENT AND SELECTIVE INHIBITOR OF Aedes Aegypti INWARD RECTIFIER POTASSIUM CHANNELS

Abstract

Vector-borne diseases such as dengue fever and malaria, which are transmitted by infected female mosquitoes, affect nearly half of the world's population. The emergence of insecticide-resistant mosquito populations is reducing the effectiveness of conventional insecticides and threatening current vector control strategies, which has created an urgent need to identify new molecular targets against which novel classes of insecticides can be developed. We previously demonstrated that small molecule inhibitors of mammalian Kir channels are promising chemicals for new mosquitocide development. In this study, high-throughput screening of approximately 30,000 chemically diverse small-molecules was employed to discover potent and selective inhibitors of *Aedes aegypti* Kir1 (*AeKir1*) channels heterologously expressed in HEK293 cells. Of 283 confirmed screening 'hits', the small-molecule inhibitor VU625 was selected for lead optimization and in vivo studies based on its potency and selectivity toward *AeKir1*, and tractability for medicinal chemistry. In patch clamp electrophysiology experiments of HEK293 cells, VU625 inhibits *AeKir1* with an IC_{50} value of 96.8 nM, making VU625 the most potent inhibitor of *AeKir1* described to date. Furthermore, electrophysiology experiments in *Xenopus* oocytes revealed that VU625 is a weak inhibitor of *AeKir2B*. Surprisingly, injection of VU625 failed to elicit significant effects on mosquito behavior, urine excretion, or survival. However, when co-injected with probenecid, VU625 inhibited the excretory capacity of mosquitoes and was toxic, suggesting that the compound is

detoxified and/or excreted by organic anion and ATP-binding cassette (ABC) transporters. Interestingly, the dose-toxicity relationship of VU625 (when co-injected with probenecid) is biphasic, which is consistent with the molecule inhibiting both *AeKir1* and *AeKir2B* with different potencies. This study demonstrates proof-of-concept that potent and highly selective inhibitors of mosquito Kir channels can be developed using conventional drug discovery approaches. Furthermore, it reinforces the notion that the physical and chemical properties that determine a compound's bioavailability in vivo will be critical in determining the efficacy of Kir channel inhibitors as insecticides.

Introduction

Mosquitoes are vectors of protozoan, filarial nematode, and viral pathogens that cause numerous human diseases, including malaria, lymphatic filariasis, and dengue fever. These diseases impose an enormous burden on global health and profoundly impair socioeconomic advancement in developing countries [243]. The overuse of pyrethroid insecticides targeting mosquito voltage-gated sodium channels in nerve cells has led to the emergence of insecticide-resistant populations of mosquitoes, which is hampering the effectiveness of vector control strategies [190,244]. Consequently, there is an urgent need to identify new molecular targets against which insecticides can be developed and deployed.

An emerging body of evidence from our group supports the idea that inward rectifier potassium (Kir) channels represent viable targets for insecticide development. Kir channels are tetrameric proteins that conduct K^+ ions across the cell membrane and thereby generate an ionic current that underlies various cellular functions. In mammals, for example, Kir channels regulate the electrical excitability of neurons and cardiac cells, hormone secretion, and transport of K^+

ions across epithelial tissues of the kidney and gut [1]. Missense mutations that perturb the activity of Kir channels cause human diseases of the heart, nervous system, pancreas, and kidney [2,3,245].

The functions of Kir channels in mosquitoes and other insects is less clear, although several recent studies have begun to shed light on the molecular physiology of this important gene family. Dipterans possess three major Kir channel subtypes, denoted Kir1, Kir2 and Kir3. In *Drosophila melanogaster*, Kir channels are known to play important physiological roles in osmoregulation, immunity, and development [205,206,231,242].

The genome of *Aedes aegypti* encodes five Kir channel genes (*AeKir1*, *AeKir2A*, *AeKir2B*, *AeKir2B'* and *AeKir3*), which are expressed in various body segments and tissues such as the carcass (thorax and abdomen), head, Malpighian tubules, midgut and hindgut [74,232]. We showed previously in vitro that the *A. aegypti* Kir1 (*AeKir1*) channel mediates strong inward rectifying K⁺ currents that are blocked by barium and the small molecule inhibitor, VU573 (companion paper) [74,207]. Furthermore, we demonstrated in vivo that VU573 induces a reduction in urine production and excretion in isolated Malpighian tubules and intact mosquitoes, respectively, and incapacitates and/or kills mosquitoes within 24 h [207]. In the companion paper, we show that VU590, a small molecule inhibitor of *AeKir1* that is structurally distinct from VU573, also inhibits urine excretion and kills mosquitoes. Taken together, these studies indicate that Kir channels represent promising molecular targets for insecticides.

Although the above 'tool' compounds allowed us to establish proof-of-concept, they are not suitable for insecticide development, in part, because they inhibit mammalian Kir channels with greater potency than *AeKir1*. Here, we aim to discover new chemical probes of *AeKir1* channels that exhibit improved potency and selectivity compared to the tool compounds by optimizing and

validating an existing fluorescent thallium (Tl^+) flux-based assay of *AeKir1* function [207] for high-throughput screening (HTS) of small molecule libraries. Screening approximately 30,000 small molecules from the chemical library of the Vanderbilt Institute of Chemical Biology (VICB) resulted in the identification of 283 compounds with activity against *AeKir1* channels. We focus on the in vitro and in vivo activity of one of these compounds, N-(3-methoxyphenyl)-2-methyl-1-propionylindoline-5-sulfonamide (VU625), which exhibits nanomolar affinity and selectivity for *AeKir1* over mammalian Kir channels.

Materials and Methods

Tl^+ flux assays

Tl^+ flux assays were performed essentially as described previously [137,246,247]. Briefly, stably transfected T-Rex-HEK-293 cells expressing *AeKir1* channels were cultured overnight in 384-well plates (20,000 cells/20 μ L/well black-walled, clear-bottomed BD PureCoat amine-coated plates (BD, Bedford, MA) with a plating media containing DMEM, 10% dialyzed FBS and 1 μ g/mL tetracycline. The next day, the cell culture medium was replaced with a dye-loading solution containing assay buffer (Hanks Balanced Salt Solution with 20 mM HEPES, pH 7.3), 0.01% (w/v) Pluronic F-127 (Life Technologies, Carlsbad, CA), and 1.2 μ M of the thallium-sensitive dye Thallos-AM (TEFlabs, Austin, TX). Following 1 hr incubation at room temperature, the dye-loading solution was washed from the plates and replaced with 20 μ L/well of assay buffer.

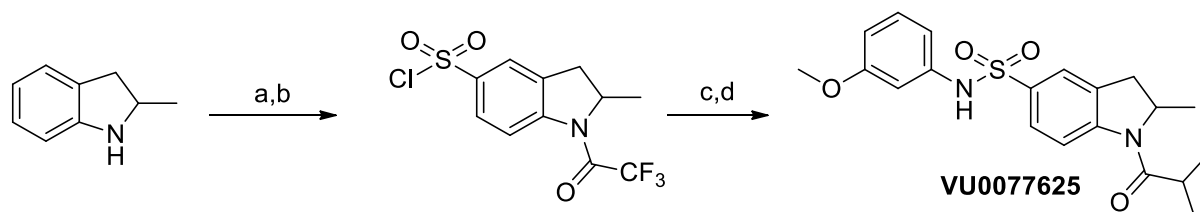
The plates were transferred to a Hamamatsu Functional Drug Screening System 6000 (FDSS6000; Hamamatsu, Hamamatsu (or Bridgewater, NJ), Japan) where 20 μ L/well of test

compounds in assay buffer (as prepared below) were added and allowed to incubate with the cells for 20 min. After the incubation period, a baseline recording was collected at 1 Hz for 10 s (excitation 470 ± 20 nm, emission 540 ± 30 nm) followed by a thallium stimulus buffer addition (10 μ L/well) and data collection for an additional 4 min. The Tl^+ stimulus buffer contains in (mM) 125 $NaHCO_3$, 1.8 $CaSO_4$, 1 $MgSO_4$, 5 glucose, 12 Tl_2SO_4 , 10 HEPES, pH 7.4. For Tl^+ flux assays on Kir2.x, Kir4.1 and Kir6.2/SUR1 expressing cells, the Tl^+ stimulus buffer contained 1.8 mM Tl_2SO_4 . Also, Tl^+ flux assays on Kir3.1/3.2/mGlu8 expressing cell, required addition of an EC_{80} concentration of glutamate (Sigma-Aldrich, St. Louis, MO) with the thallium stimulus buffer [64].

The test compounds were transferred to daughter polypropylene 384-well plates (Greiner Bio-One, Monroe, NC) using an Echo555 liquid handler (Labcyte, Sunnyvale, CA), and then diluted into assay buffer to generate a 2X stock in 0.6% DMSO (0.3% final). For Tl^+ flux assays on Kir6.2/SUR1 expressing cells, test compounds were diluted in assay buffer containing diazoxide (250 μ M final) to induce channel activation. Concentration-response curves (CRCs) were generated by screening compounds at 3-fold dilution series in 4-point (1 μ M - 30 μ M) or 11-point (1 nM - 30 μ M) CRCs.

Tl^+ flux data were analyzed as previously described [65,83,137,246] using a combination of Excel (Microsoft Corp, Redmond, WA) with XLfit add-in (IDBS, Guildford, Surrey, UK) and OriginPro (OriginLab, Northampton, MA) software. Raw data were opened in Excel and each data point in a given trace was divided by the first data point from that trace (static ratio) followed by subtraction of data points from control traces generated in presence of vehicle controls. The slope of the fluorescence increase beginning 5 s after Tl^+ addition and ending 15 s after Tl^+ addition was calculated.

Compound synthesis



Scheme 1. Reagents and conditions: (a) TFAA, pyridine, 0 °C; (b) ClSO₃H, 40 °C, 1 h; PCl₅, rt; (c) 3-methoxyaniline, DIEA, rt; MeOH:THF:10% NaOH (1:1:1); (d) pyridine, CH₂Cl₂, ClCOCH₂CH₃

2,2,2-trifluoro-1-(2-methylindolin-1-yl)ethan-1-one: To a round bottom flask equipped with a magnetic stir bar 2-methylindoline (4.8 mL, 37 mmol, 1 eq.) and pyridine (46 mL) were added. The reaction mixture was cooled to 0 °C and trifluoroacetic anhydride (6.3 mL, 44 mmol, 1.2 eq.) was added dropwise. The reaction mixture was allowed to warm to room temperature and was stirred an additional 2 hours. The reaction was quenched with water (50 mL) and diluted with DCM (100 mL). The organic layer was separated and washed subsequently with water (50 mL) and brine (50 mL), dried over Na₂SO₄, and concentrated under reduced pressure. The crude material (8.33g, 98%) was used without purification. LCMS: R_T = 0.785 min, [M + H]⁺ = 229.6; >98%.

2-methyl-1-(2,2,2-trifluoroacetyl)indoline-5-sulfonyl chloride: Chlorosulfonic acid (22 mL, 330 mmol, 9 equiv.) was added to a 100 mL round bottom flask equipped with a reflux condenser, cooled to 0 °C. To this, 2,2,2-trifluoro-1-(2-methylindolin-1-yl)ethan-1-one, (8.5 g, 37 mmol, 1 eq.) was added dropwise. The reaction mixture was removed from the ice bath. The vial was heated to 40 °C for 1 hour. The reaction was subsequently cooled to room temperature and PCl₅ (7.7 g, 37 mmol, 1 equiv.) was added slowly. After gas evolution ceased, the reaction mixture was heated to 80 °C for 1 hour. The reaction mixture was cooled to room temperature

and then placed in an ice bath. Water was added very slowly to the reaction mixture. Subsequently, DCM was added and the reaction was filtered through a phase separator. The organic layer was concentrated under reduced pressure and used without subsequent purification (6.46 g, 53%).

N-(3-methoxyphenyl)-2-methylindoline-5-sulfonamide: 2-methyl-1-(2,2,2-trifluoroacetyl)indoline-5-sulfonyl chloride (2.5 g, 7.6 mmol, 1 eq.) was diluted with DCM (10 mL). 3-methoxyaniline (1.71 mL, 15.2 mmol, 2 eq.) followed by *N,N*-Diisopropylethylamine (5.3 mL, 31 mmol, 4 eq.) was added to the reaction. Reaction progress was monitored by LCMS. Once the reaction was deemed complete, it was diluted with DCM (40 mL) and washed with water (2x, 50 mL) and brine (50 mL). The organic layer was dried over Na_2SO_4 and concentrated under reduced pressure. Purification by flash chromatography (0%-100% EtOAc in Hexanes) afforded the desired product (2.66 g, 85%). LCMS: $R_T = 0.800$ min., $[\text{M} + \text{H}]^+ = 414.7$; >98% @ 220 and @ 254 nm. The trifluoroacetate was removed by stirring in a 1:1:1 mixture of MeOH, THF, and 10% NaOH affording the title compound (782 mg, 38%). LCMS: $R_T = 0.665$ min., $[\text{M} + \text{H}]^+ = 318.8$; >98% @ 220 and @ 254 nm.

N-(3-methoxyphenyl)-2-methyl-1-propionylindoline-5-sulfonamide (VU0077625): N-(3-methoxyphenyl)-2-methylindoline-5-sulfonamide (11 mg, 0.035 mmol, 1 eq.) was diluted with DCM (0.3 mL). To this reaction, pyridine was added (0.011 mL, 0.14 mmol, 4 eq.) followed by propionyl chloride (0.003 mL, 0.05 mmol, 1.5 eq.). Reaction progress was monitored by LCMS. Once the reaction was deemed complete it was concentrated under forced air and heat and was subsequently purified on preparative HPLC (3 mg, 26%). ^1H NMR (400.1 MHz, CDCl_3) δ (ppm): 8.17 (bs, 1 H); 7.67 (dd, $J = 1.69, 8.72$ Hz, 1 H); 7.58 (s, 1 H); 7.16 (t, $J = 8.25$ Hz, 1 H);

6.69-6.57 (m, 4 H); 4.58 (bs, 1 H); 3.74 (s, 3 H); 3.38-3.32 (m, 1 H); 2.66-2.47 (m, 4 H); 1.29-1.22 (m, 5 H). HRMS (TOF, ES⁺) C₁₉H₂₃N₂O₄S [M + H]⁺ calc'd for 375.1379, found 375.1381.

Patch clamp electrophysiology

T-REx-HEK293-*AeKir1* cells were voltage clamped in the whole-cell configuration of the patch clamp technique after overnight induction with tetracycline (1 mg/ml) essentially as described earlier [207]. Briefly, patch electrodes were pulled from silanized 1.5 mm outer diameter borosilicate microhematocrit tubes using a Narishige PC-10 two-stage puller. Electrode resistance ranged from 3.5 to 5.5 MΩ when filled with the following intracellular solution (in mM): 135 KCl, 2 MgCl₂, 1 EGTA, 10 HEPES free acid, 2 Na₂ATP (Roche, Indianapolis, IN), pH 7.3, 275 mOsm. The standard bath solution contained (in mM): 135 NaCl, 5 KCl, 2 CaCl₂, 1 MgCl₂, 5 glucose, 10 HEPES free acid, pH 7.4, 290 mOsm. Whole-cell currents were recorded under voltage-clamp conditions using an Axopatch 200B amplifier (Molecular Devices, Sunnyvale, CA). Electrical connections to the amplifier were made using Ag/AgCl wires and 3 M KCl/agar bridges. Electrophysiological data were collected at 5 kHz and filtered at 1 kHz. Data acquisition and analysis were performed using pClamp 9.2 software (Axon Instruments). All recordings were made at room temperature (20–23°C).

Heterologous expression of *AeKir1* and *AeKir2B* in *Xenopus* oocytes

AeKir1 and *AeKir2B* proteins were expressed heterologously in *Xenopus laevis* oocytes as described previously [74]. In brief, defolliculated *Xenopus* oocytes (Ecocyte Bioscience, Austin, TX) were injected with 10 ng (0.35 ng/nL) of either *AeKir1* or *AeKir2B* cDNA and

cultured for 3–7 days in OR3 media at 18°C. Oocytes injected with 28 nl of nuclease-free H₂O served as controls.

Electrophysiology of *Xenopus* oocytes

All electrophysiological experiments on *Xenopus* oocytes were performed at room temperature. The compositions of the solutions used in these experiments are shown in Table 1. When present, VU625 was dissolved in solution *III* to a final concentration of 0.1, 1, 5, 15, or 50 μ M (0.05% DMSO). All solutions were delivered by gravity to a RC-3Z oocyte chamber (Warner Instruments, Hamden, CT) via polyethylene tubing at a flow rate of \sim 2 ml/min. Solution changes were made with a Rheodyne Teflon 8-way Rotary valve (Model 5012, Rheodyne, Rohnert Park, CA).

Table 1. Compositions (in mM) of solutions used in *Xenopus* oocyte electrophysiology.

Solution #	<i>I</i>	<i>II</i>	<i>III</i>
NaCl	96	88.5	88.5
NMDG-Cl	0	9.5	0
KCl	2	0.5	10
MgCl₂	1.0	1.0	1.0

pH = 7.5 adjusted with NMDG-OH (NMDG = N-methyl-D-glucamine).
Osmolality = 190 mOsm kg⁻¹ H₂O (\pm 5 mOsm kg⁻¹ H₂O)

In brief, each oocyte was transferred to the holding chamber under superfusion with solution *I* and impaled with two conventional-glass microelectrodes backfilled with 3 M KCl (resistances of 0.5–1.5 M Ω) to measure membrane potential (V_m) and whole-cell membrane current (I_m), respectively. Current-voltage (I-V) relationships of oocytes were acquired as described in the companion paper. In brief, the oocytes were subject to a voltage-stepping

protocol consisting of 20 mV steps from -140 mV to +40 mV (100 ms each). After the conclusion of the voltage-stepping protocol, the clamp was turned off and a new solution was superfused through the chamber for ~90 s before acquiring another I-V relationship. All V_m and I_m values were recorded by a Digidata 1440A Data Acquisition System (Molecular Devices) and the Clampex module of pCLAMP. The I-V plots were generated using the Clampfit module of pCLAMP.

To evaluate the inhibition of Kir1 and Kir2B activity by VU625, we focused on the maximal inward currents elicited by the voltage-stepping protocol, which occur at a voltage of -140 mV. The background, inward currents in solution *II* (i.e., low K^+) were subtracted from those in 1) solution *III* (i.e., elevated K^+) to calculate the total inward current for an oocyte before exposure to VU625 (I_A), and 2) solution *III* with VU625 to calculate the inward current after exposure to the small molecule (I_B). The percent inhibition of the inward current was calculated by subtracting I_B from I_A and then dividing by I_A .

Mosquito colony

The *Aedes aegypti* eggs were obtained through the MR4 as part of the BEI Resources Repository, NIAID, NIH: *Aedes aegypti* LVPIB12, MRA-735, deposited by M.Q. Benedict. The eggs were raised to adults as described previously [210], and all experiments described were conducted with adult females 3–10 days post-emergence.

Mosquito toxicology experiments

Mosquitoes for injection were anesthetized on ice and impaled through the metapleuron using a pulled-glass capillary attached to a nanoliter injector (Nanoject II, Drummond Scientific Company, Broomall, PA). A single injection delivered 69 nL of solution. The injection solution consisted of a potassium-rich phosphate buffered saline (K^+ -PBS), 15% DMSO, 1% β -cyclodextrin, 0.1% Solutol, and various concentrations of VU625 to deliver the desired doses. When needed, water-soluble probenecid (Biotium, Hayward CA) was present at 50 mM. The K^+ -PBS solution consisted of the following in mM: 92.2 NaCl, 47.5 KCl, 10 Na_2HPO_4 , and 2 KH_2PO_4 (pH 7.5). After injection, the mosquitoes were placed into small cages (10 females per cage) within a rearing chamber (28°C, 80% relative humidity, 12:12 light:dark) and allowed free access to a solution of 10% sucrose. The mosquitoes were observed at 2 h or 24 hr after injection.

Mosquito excretion experiments

Urine excretion rates were measured as described in the companion paper. In brief, after anesthetizing mosquitoes on ice, they were injected as described above with 900 nL of a K^+ -PBS vehicle containing 1.15% DMSO, 0.077% β -cyclodextrin, and 0.008% Solutol, or the vehicle containing VU625 (0.77 mM). When needed, the vehicle was supplemented with water soluble probenecid (3.08 mM). After injection, the mosquitoes were placed immediately in a graduated, packed-cell volume tube (MidSci, St. Louis, MO; 5 mosquitoes per tube) and held at 28°C. In a previous study [207], the mosquitoes remained in a single tube for 2 h and were then removed from the tubes with forceps. The excreted urine was centrifuged into the graduated column of

the tube for measurement and the total excreted volume after 2 h was measured. In the present study, preliminary experiments were conducted to better resolve the time-course of urine excretion. That is, mosquitoes were transferred to a new tube every 30 minutes and the amount of urine excreted was measured. We found that ~95% of the total volume excreted by the mosquitoes in 120 min is voided within the first 60 min. Thus, we used a 60 min end point for the excretion measurements in the present study.

Statistical analyses

TI⁺ flux assay. The *Z'* value was calculated as described earlier [137], using the following formula:

$$Z' = 1 - (3SD_p + 3SD_n) / |\text{mean}_p + \text{mean}_n|$$

where SD is standard deviation, p and n are vehicle control and compound inhibited flux values respectively.

To compare the effect of DMSO on *AeKir1*-mediated TI⁺ flux, a one-way ANOVA was performed with a Tukey's multiple comparison test. Prism software (GraphPad Software) was used to generate CRC from TI⁺ flux: Half-inhibition concentration (IC₅₀) values were calculated from fits using a four parameter logistic equation.

Mosquito toxicology and urine excretion. Prism (Graphpad Software) was used to generate a dose-response curve for the toxicity of VU625; the doses (x-axis) were first log transformed and then the mortality data was fitted using a 'biphasic' algorithm (<100 constraint) to calculate potencies (ED₂₅ and ED₇₅ values). To compare the toxic effects among the vehicle, probenecid,

VU625, and VU625 + probenecid treatments, and the excretory capacity among the vehicle, probenecid, VU625, and VU625 + probenecid treatments, one-way ANOVAs were performed with Newman-Keuls posttests.

Results

Discovery of novel *AeKir1* inhibitors via high-throughput screening

In an effort to discover mosquito-specific inhibitors of *AeKir1*, we optimized a TI^+ flux assay for high-throughput screening (HTS) of large libraries of chemically diverse small molecules. The assay utilizes a monoclonal T-REx-HEK293 cell line that expresses *AeKir1* from a tetracycline-inducible promoter [207]. The fluorescent dye, ThalloS, is used to report the inward flux of TI^+ through the *AeKir1* channel pore in a population of cells plated in individual wells of a 384-well plate. As shown in **Fig. 1A**, overnight induction of *AeKir1* expression with tetracycline leads to a robust TI^+ flux compared to control cells that were not treated with tetracycline. This assay enables more than 300 compounds to be tested simultaneously in a single plate, and thousands of compounds to be tested daily, for effects on *AeKir1* activity.

The assay was validated for HTS by meeting a series of performance benchmarks. First, the assay was tested for its tolerance to the small-molecule vehicle DMSO at screening concentrations up to 0.3% v/v. As shown in **Fig. 1B**, the TI^+ -flux mediated by *AeKir1* is unaffected by DMSO concentrations up to 1.3% v/v as compared to the 0% DMSO control (one-way ANOVA, $P < 0.0001$). Next, the assay was tested for uniformity and reproducibility of HTS performance. As shown in **Fig. 1C**, the average Z' statistic for these experiments was 0.69 ± 0.05

($Z' \geq 0.5$ is suitable for HTS), indicating that the assay is robust and will enable modulators of *AeKir1* to be identified in HTS with a low false-positive rate.

Approximately 30,000 compounds from the VICB library were screened at a nominal concentration of 10 μM for inhibition of *AeKir1*. From this primary screen and following confirmation testing in tetracycline-induced and uninduced T-REx-HEK293-*AeKir1* cells (see Methods), 283 authentic channel-dependent modulators were selected for further study. Because our ultimate goal is to develop Kir channel inhibitors that are active against mosquitoes and not humans, these ‘hits’ were subsequently tested for dose-dependent activity against a panel of mammalian Kir channels, including Kir1.1, Kir2.1, Kir2.2, Kir2.3, Kir3.1/3.2, Kir4.1, Kir7.1(M125R), and Kir6.2/SUR1 [20,64,137]. Four-point concentration response curves (CRCs) were generated for the 283 compounds, resulting in 17 inhibitors with 11 unique chemical scaffolds that exhibited dose-dependent inhibition of *AeKir1* with IC_{50} values below 5 μM and little to no activity ($\text{IC}_{50} \geq 30 \mu\text{M}$) against mammalian Kir channels (data not shown). These compounds were purchased from commercial vendors, freshly dissolved in DMSO, and assayed in 11-point CRCs against *AeKir1*. In TI^+ flux assays, one compound—N-(3-methoxyphenyl)-2-methyl-1-propionylindoline-5-sulfonamide, termed VU625—was found to inhibit *AeKir1* in 11-point CRCs with an IC_{50} of 0.32 μM (95% CI: 0.25 – 0.39 μM) and a Hill coefficient value of 0.98 (95% CI: 0.8 – 1.2) (**Figs. 2A-C**).

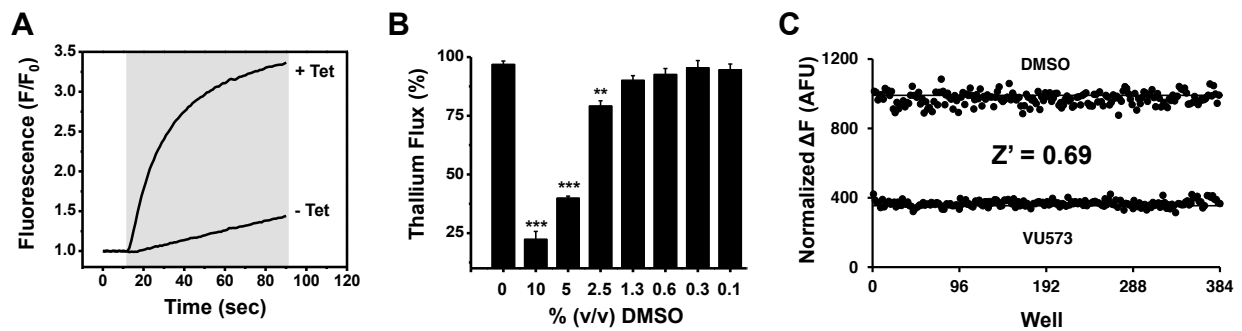


Figure 1. TI⁺ flux assay of *AeKir1* channel activity for high-throughput screening. (A) Representative TI⁺-induced changes in Thallos fluorescence in T-Rex-HEK293-*AeKir1* cells cultured overnight with (+Tet) or without (-Tet) tetracycline. The shaded box indicates the cell exposure to TI⁺. (B) DMSO concentrations up to 1.3% v/v DMSO have no effect on TI⁺ flux through *AeKir1*. Data are means \pm SEM ($n = 3$). One-way ANOVA $P < 0.0001$, and asterisks (**, ***) indicate $P < 0.01$ or $P < 0.001$ respectively, when compared to 0% DMSO (Tukey's test). (C) Representative checkerboard analysis using 100 μ M VU573 or 0.1% v/v DMSO as the vehicle control. The mean peak fluorescence amplitude of each sample population is indicated with a solid line and alternating samples for DMSO (top) and VU573 (bottom) are graphed as individual points. The mean \pm SD Z' calculated over 6 plates on 3 separate days was 0.69 ± 0.05 .

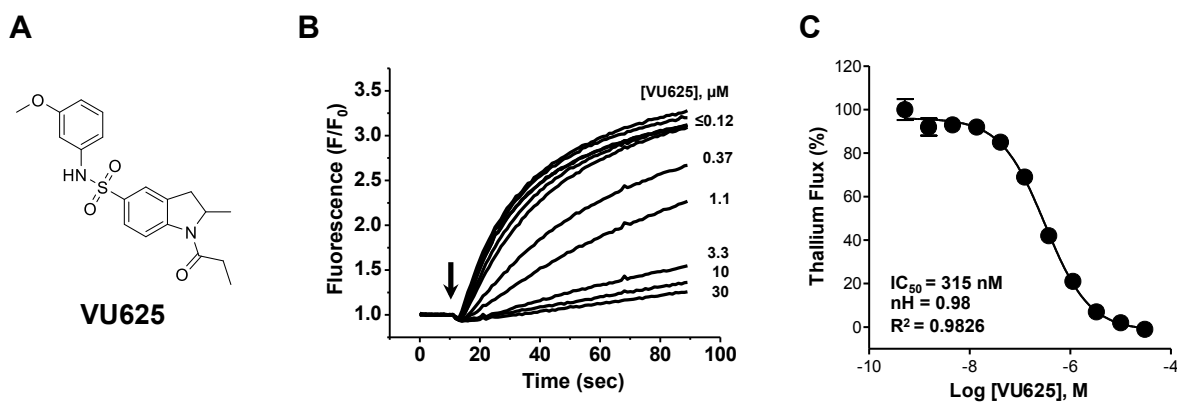


Figure 2. VU625 is a potent inhibitor of *AeKir1* in Tl⁺ flux assays. (A) Chemical structure of VU625. **(B)** Dose-dependent inhibition of the *AeKir1*-mediated Tl⁺ flux by VU625 with concentrations ranging from ≤ 0.12 to 30 μM . The arrow indicates when Tl⁺ was added to the extracellular bath. **(C)** Concentration-response curves of VU625 derived from Tl⁺ flux assays. The IC₅₀ and Hill-coefficient (nH) values are 315 nM (95% CI: 254.4 - 390.2 nM) and 0.98 respectively. Data are mean \pm SEM. n = 4 independent experiments performed in triplicate.

VU625 is a potent and preferential inhibitor of *Ae*Kir1

From TI^+ flux experiments, we found that VU625 had no significant effects on the mammalian Kir channels assayed with the exception of G-protein coupled Kir channels comprised of Kir3.1/3.2 subunits ($\text{IC}_{50} = 8.6 \mu\text{M}$; **Table 2**). Furthermore, in radioligand displacement assays against 68 mammalian GPCR's, ion channels, and transporters, $10 \mu\text{M}$ VU625 was active (>50% displacement) against only three targets: adenosine A1 receptor (76% displacement), melatonin MT1 receptor (56% displacement) and 5-HT_{2B} receptor (69% displacement) (**Table 3**).

Table 2. Selectivity of VU625 against human Kir channels assessed in TI^+ flux assays. $n= 2$ independent experiments in triplicate

Kir channel	Inhibition of TI^+ flux (IC_{50} , μM)
Kir1.1	>30
Kir2.1	>30
Kir2.2	>30
Kir2.3	>30
Kir3.1/3.2	8.6
Kir4.1	>30
Kir6.2/SUR1	>30
Kir7.1(M125R)	>30

Table 3. Summary of results obtained from the activity of the VU625 compound in radioligand binding assays. The significant results are highlighted in grey.



Experimental Results

Cat #	Assay Name	Batch*	Spec.	Rep.	Conc.	% Inh.
Compound: VU625, PT #: 1171820						
200510	Adenosine A ₁	335760	hum	2	10 µM	76
200610	Adenosine A _{2A}	335761	hum	2	10 µM	13
200720	Adenosine A ₃	335848	hum	2	10 µM	18
203100	Adrenergic α _{1A}	335762	rat	2	10 µM	7
203200	Adrenergic α _{1B}	335763	rat	2	10 µM	-3
203400	Adrenergic α _{1D}	335814	hum	2	10 µM	3
203630	Adrenergic α _{2A}	335764	hum	2	10 µM	24
204010	Adrenergic β ₁	335765	hum	2	10 µM	-9
204110	Adrenergic β ₂	335943	hum	2	10 µM	2
285010	Androgen (Testosterone) AR	335851	rat	2	10 µM	31
212510	Bradykinin B ₁	335859	hum	2	10 µM	9
212620	Bradykinin B ₂	335857	hum	2	10 µM	12
214510	Calcium Channel L-Type, Benzothiazepine	335860	rat	2	10 µM	6
214600	Calcium Channel L-Type, Dihydropyridine	335768	rat	2	10 µM	19
216000	Calcium Channel N-Type	335817	rat	2	10 µM	2
217030	Cannabinoid CB ₁	335769	hum	2	10 µM	23
219500	Dopamine D ₁	335770	hum	2	10 µM	12
219700	Dopamine D _{2S}	335771	hum	2	10 µM	16
219800	Dopamine D ₃	335861	hum	2	10 µM	28
219900	Dopamine D _{4,2}	335862	hum	2	10 µM	0
224010	Endothelin ET _A	335872	hum	2	10 µM	1
224110	Endothelin ET _B	335847	hum	2	10 µM	-1
225510	Epidermal Growth Factor (EGF)	335842	hum	2	10 µM	-12
226010	Estrogen ERα	335815	hum	2	10 µM	5
226600	GABA _A , Flunitrazepam, Central	335773	rat	2	10 µM	-5
226500	GABA _A , Muscimol, Central	335772	rat	2	10 µM	-1
228610	GABA _{B1A}	335856	hum	2	10 µM	9
232030	Glucocorticoid	335865	hum	2	10 µM	9
232700	Glutamate, Kainate	335873	rat	2	10 µM	13
232810	Glutamate, NMDA, Agonism	335858	rat	2	10 µM	-1
232910	Glutamate, NMDA, Glycine	335874	rat	2	10 µM	13
233000	Glutamate, NMDA, Phencyclidine	335774	rat	2	10 µM	14
239610	Histamine H ₁	335775	hum	2	10 µM	28
239710	Histamine H ₂	335843	hum	2	10 µM	2

Note: Items meeting criteria for significance (≥50% stimulation or inhibition) are highlighted.

* Batch: Represents compounds tested concurrently in the same assay(s).

ham=Hamster; hum=Human

Experimental Results

Cat #	Assay Name	Batch*	Spec.	Rep.	Conc.	% Inh.
239820	Histamine H ₃	335816	hum	2	10 µM	0
241000	Imidazoline I ₂ , Central	335776	rat	2	10 µM	10
243520	Interleukin IL-1	335870	mouse	2	10 µM	5
250460	Leukotriene, Cysteinyl CysLT ₁	335866	hum	2	10 µM	11
251600	Melatonin MT ₁	335844	hum	2	10 µM	58
252610	Muscarinic M ₁	335867	hum	2	10 µM	21
252710	Muscarinic M ₂	335777	hum	2	10 µM	6
252810	Muscarinic M ₃	335778	hum	2	10 µM	8
257010	Neuropeptide Y Y ₁	335845	hum	2	10 µM	1
257110	Neuropeptide Y Y ₂	335822	hum	2	10 µM	1
258590	Nicotinic Acetylcholine	335779	hum	2	10 µM	-9
258700	Nicotinic Acetylcholine α1, Bungarotoxin	335780	hum	2	10 µM	-7
260130	Opiate δ ₁ (OP1, DOP)	335783	hum	2	10 µM	2
260210	Opiate κ (OP2, KOP)	335782	hum	2	10 µM	4
260410	Opiate μ (OP3, MOP)	335781	hum	2	10 µM	-2
264500	Phorbol Ester	335784	mouse	2	10 µM	6
265010	Platelet Activating Factor (PAF)	335850	hum	2	10 µM	26
265600	Potassium Channel [K _{ATP}]	335785	ham	2	10 µM	14
265900	Potassium Channel hERG	335786	hum	2	10 µM	26
268420	Prostanoid EP ₄	335787	hum	2	10 µM	24
268700	Purinergeric P2X	335854	rabbit	2	10 µM	5
268810	Purinergeric P2Y	335818	rat	2	10 µM	-3
270000	Rolipram	335937	rat	2	10 µM	39
271110	Serotonin (5-Hydroxytryptamine) 5-HT _{1A}	335819	hum	2	10 µM	7
271700	Serotonin (5-Hydroxytryptamine) 5-HT _{2B}	335789	hum	2	10 µM	69
271910	Serotonin (5-Hydroxytryptamine) 5-HT ₃	335820	hum	2	10 µM	15
278110	Sigma σ ₁	335790	hum	2	10 µM	19
279510	Sodium Channel, Site 2	335791	rat	2	10 µM	6
255520	Tachykinin NK ₁	335868	hum	2	10 µM	13
285900	Thyroid Hormone	335871	rat	2	10 µM	2
220320	Transporter, Dopamine (DAT)	335846	hum	2	10 µM	11
226400	Transporter, GABA	335864	rat	2	10 µM	34
204410	Transporter, Norepinephrine (NET)	335767	hum	2	10 µM	16
274030	Transporter, Serotonin (5-Hydroxytryptamine) (SERT)	335853	hum	2	10 µM	3

Note: Items meeting criteria for significance (≥50% stimulation or inhibition) are highlighted.

* Batch: Represents compounds tested concurrently in the same assay(s).

ham=Hamster; hum=Human

To further confirm the activity of VU625 obtained from TI^+ -flux assays, we used patch-clamp electrophysiology to assay the inhibition of *AeKir1*. In whole-cell patch clamp recordings, VU625 inhibited *AeKir1* channel activity with an IC_{50} of 96.8 nM (95% CI: 75.4 - 124.2 nM) and a Hill coefficient value of 1.02 (95% CI: 0.8 – 1.3) (**Figs. 3A, B**). In **Appendix A**, we demonstrated that VU573 and VU590 have distinct pharmacological effects on *AeKir1* and *AeKir2B* channel functions. Thus, we sought to determine the effects of VU625 on *AeKir2B*. We evaluated VU625 activity on *Xenopus* oocytes heterologously expressing *AeKir2B*, using *AeKir1* expressing oocytes as positive controls. As shown in **Fig. 3C**, VU625 inhibits *AeKir1*- and *AeKir2B*-mediated K^+ currents with IC_{50} values of 3.8 μM (95% CI: 2.3 – 6.3 μM), and 45.1 μM (95% CI: 31.7 – 64.2 μM), respectively. Thus, VU625 inhibits both *AeKir1* and *AeKir2B* channels, albeit with greater affinity for *AeKir1*. Because of its potency, relatively clean ancillary pharmacology and chemical tractability, VU625 was selected for lead optimization.

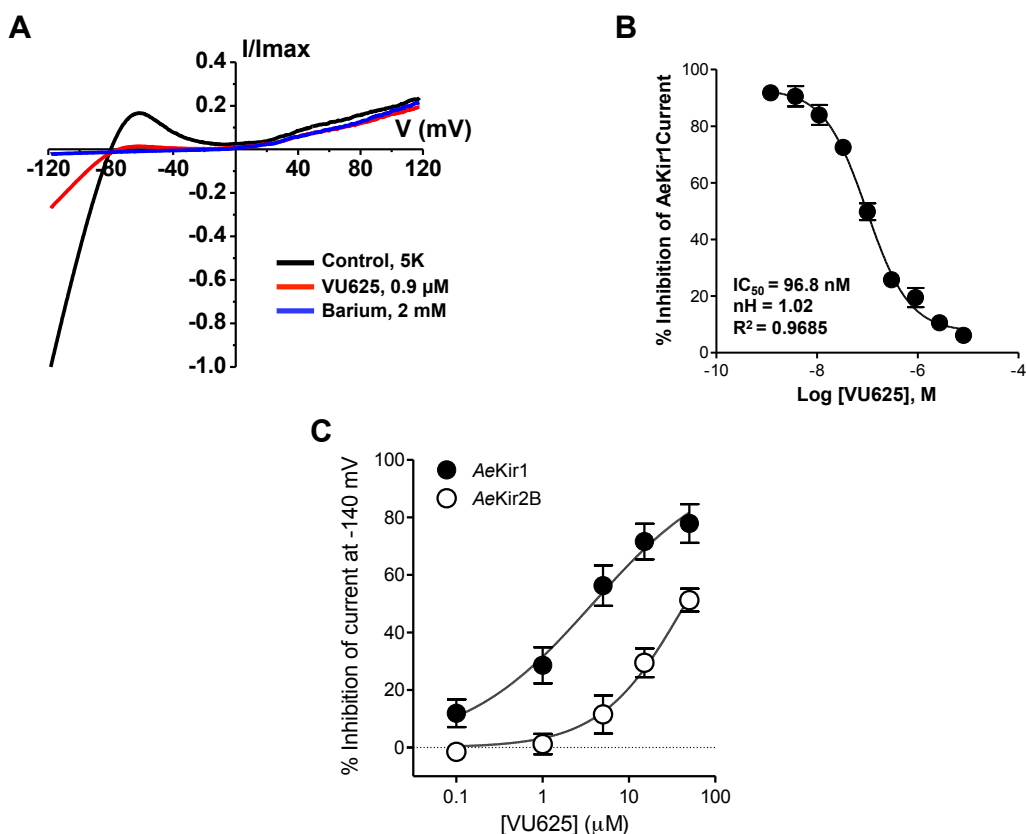


Figure 3. VU625 is preferential inhibitor of *AeKir1* over *AeKir2B* in whole-cell electrophysiology. (A) Normalized *AeKir1* current-voltage relationships obtained from heterologous expression in T-Rex-HEK293 cells, illustrating VU625-dependent inhibition before (control) and after addition of 0.9 μ M VU625. Residual *AeKir1* currents were inhibited with 2 mM barium. Cells were voltage clamped at -75 mV and ramped between -120 mV and +60 mV. (B) Concentration-response curve of VU625 derived from patch clamp experiments ($n = 4-6$). The IC_{50} of VU625 is 96.8 nM (95% CI: 75.4 - 124.2 nM). (C) Concentration-response curves of current inhibition mediated by heterologous expression in *Xenopus* oocytes of *AeKir1* (filled circles) and *AeKir2B* (open circles) channels after bath application of VU625. $n = 4-5$ oocytes per concentration. The calculated IC_{50} values of VU625 for *AeKir1* and *AeKir2B* current inhibition are 3.8 μ M (95% CI: 2.3 - 6.3 μ M) and 45.1 μ M (95% CI: 31.7 - 64.2 μ M), respectively.

Chemical lead optimization and structure-activity relationships

For the lead optimization of VU625 (**3a**, **Table 4**), we partitioned the compound into three areas for SAR exploration denoted as the sulfonamide, central core, and southern amide portions (**Fig. 4A**). The first generation libraries held the sulfonamide and the central core sections constant and diversified the southern amide portion (**Table 4**). The synthetic scheme (**Fig. 4B**) for this portion was straightforward and started with protection of the amine with trifluoroacetamide (TFAA, pyridine) followed by sulfonyl chloride formation (ClSO₃, PCl₅). Next, the sulfonamide was formed, the protecting group was removed, and either the amide or sulfonamide was formed (see Methods for details). Little tolerance for steric bulk was seen in this portion of the molecule. That is, the trifluoroacetamide (VU0477197, **3b**, **Table 4**) retained potency (0.58 μM), however, larger aromatic amides were much less active (**3c-g**, **Table 4**). The same trend was observed for the sulfonamide compounds, with smaller sulfonamides retaining nanomolar activity (VU0477691, **3k**, 0.76 μM; VU0477692, **3l**, 0.82 μM) and the larger aromatic group leading to less activity (**3h**, **Table 4**).

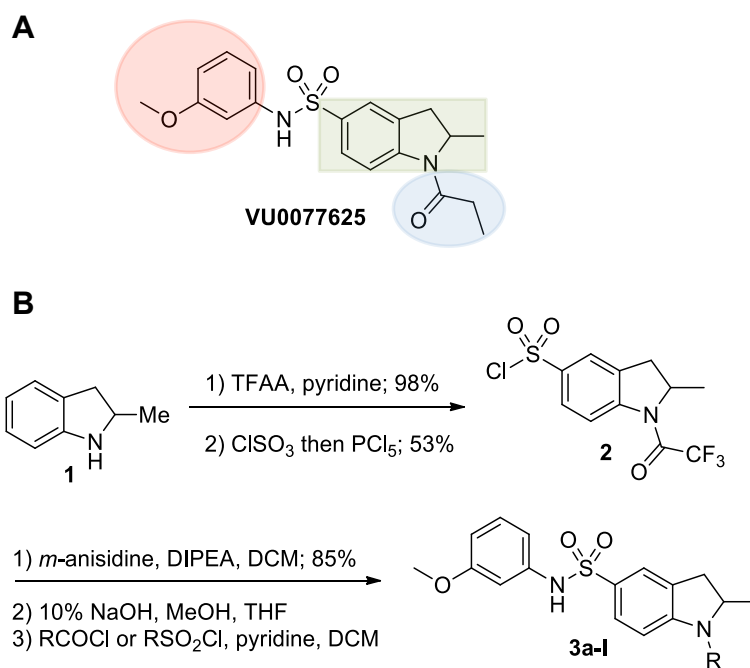
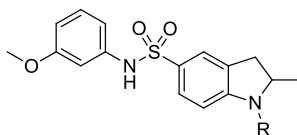


Figure 4. Design and chemical lead optimization strategy for VU625. (A) Modular approach to assess three areas of diversification of VU625: sulfonamide (red shading), central core (green shading), and southern amide (blue shading) portions. (B) General synthetic approach to access VU625 and analogs around the amide and sulfonamide portions.

Design and chemical lead optimization performed by Corey R. Hopkins.

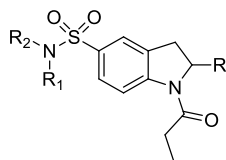
Table 4. Structure-activity relationships and lead optimization summary of VU0077625 scaffold (n=2 independent experiments performed in triplicate)



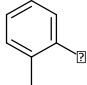
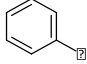
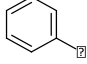
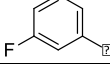
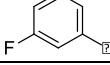
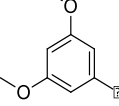
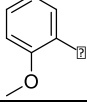
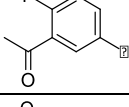
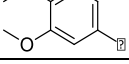
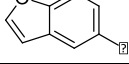
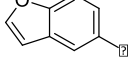
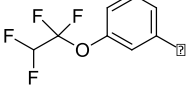
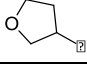
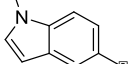
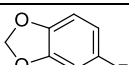
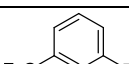
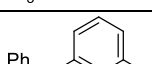
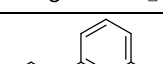
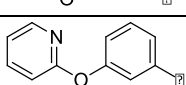
Cmpd	R	VU#	IC₅₀ ± SEM (μM)
3a		VU0077625	0.36 ± 0.02
3b		VU0477197	0.58 ± 0.04
3c		VU0477684	5.20 ± 0.40
3d		VU0477693	4.41 ± 1.11
3e		VU0477694	3.87 ± 1.97
3f		VU0477688	> 30
3g		VU0477685	4.40 ± 0.50
3h		VU0477686	3.29 ± 0.89
3i		VU0477687	2.09 ± 0.49
3j		VU0477690	2.82 ± 0.48
3k		VU0477691	0.76 ± 0.00
3l		VU0477692	0.82 ± 0.48

Next, we evaluated the left-hand sulfonamide portion of the molecule, however, all efforts to change the 3-methoxyaryl moiety led to significant reductions in potency (see **Table 5**). Finally, we explored the central core with the intent of establishing the minimal pharmacophore needed for activity against *AeKir1*. To this end, the indoline core was replaced with simple aryl, heteroaryl or biaryl groups which all led to compounds with much reduced activity (>10-fold loss of potency). However, an interesting SAR was seen with very closely related 6,6- or 6,5-indole or dihydroquinolinone-like structures (**4a-f**, **Table 6**). The simple *N*-methyl indole (VU0481807, **4a**, 0.55 μM , **Table 6**) retained most of the activity as VU625 and addition of a 2-methyl (VU0486620, **4b**, 0.97 μM , **Table 3**) led to a further minor reduction in activity. Expanding the ring system and addition of a lactam (**4c-e**, **Table 6**) was not productive. Lastly, removal of the methyl group in the indoline system of VU625, led to a ~3-fold loss of potency (VU0483404, **4f**, 1.15 μM , **Table 6**).

Table 5. SAR around the left-hand sulfonamide.



Cmpd	VU	R	R ¹	R ²	IC ₅₀ (μ M)
5a	VU0111100	Me	H		3.27
5b	VU0111077	Me	H		3.44
3a	VU0111158	Me	H		0.856
5c	VU0077625	Me	H		0.338
5d	VU0111108	Me	H		1.42
5e	VU0472705	Me	H		1.15
5f	VU0111168	Me	Me		2.16
5g	VU0472699	Me	H		2.36
5h	VU0472694	Me	H		3.49
5i	VU0472696	Me	H		3.25
5j	VU0472695	Me	H		1.36
5k	VU0084675	Me	H		1.12
5l	VU0111098	Me	H		4.94
5m	VU0472698	Me	H		5.24
5n	VU0472697	Me	H		3.54

5o	VU0472702	Me	H		5.25
5p	VU0472700	Me	H		1.55
5q	VU0472703	Me	H		1.87
5r	VU0472701	Me	H		1.97
5s	VU0472704	Me	H		1.62
5t	VU0110817	H	H		>30
5u	VU0110920	H	H		>30
5v	VU0485659	H	H		>30
5w	VU0144119	H	H		>30
5x	VU0485660	H	H		7.50
5y	VU0485652	H	H		>30
5z	VU0485653	H	H		>30
5aa	VU0485654	H	H		>30
5bb	VU0485655	H	H		>30
5cc	VU0077420	H	H		>30
5dd	VU0166512	H	H		>30
5ee	VU0486113	H	H		>30
5ff	VU0486114	H	H		3.47
5gg	VU0486115	H	H		1.40

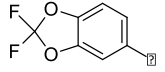
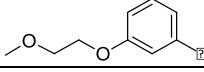
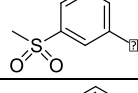
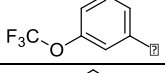
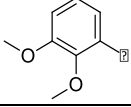
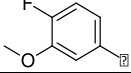
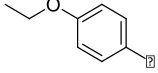
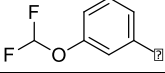
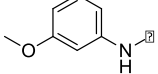
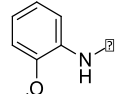
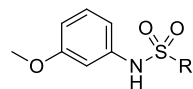
5hh	VU0486121	H	H		>30
5ii	VU0486122	H	H		>30
5jj	VU0486123	H	H		>30
5kk	VU0486124	H	H		>30
5ll	VU0486125	H	H		>30
5mm	VU0486126	H	H		1.93
5nn	VU0486136	H	H		>30
5oo	VU0486137	H	H		>30
5pp	VU0486116	H	Me		>30
5qq	VU0486127	H	Me		>30

Table 6. Structure-activity relationships and lead optimization summary for the central core portion of VU0077625 scaffold (n=2 independent experiments performed in triplicate)



Cmpd	R	VU#	IC₅₀ ± SEM (μM)
4a		VU0481807	0.55 ± 0.08
4b		VU0486620	0.97 ± 0.10
4c		VU0481811	> 30
4d		VU0483082	> 30
4e		VU0483402	> 30
4f		VU0483404	1.15 ± 0.05

Figure 5 summarizes the SAR observed for the VU625 scaffold. The left-hand sulfonamide portion offered the least amount of SAR traction as only the 3-methoxyphenyl (and weaker 2-methoxyphenyl) sulfonamide provided activity. Replacement with an amide, or substituting the 3-methoxyphenyl for other aryl groups all led to less potent compounds. Replacement of the propanamide in the southern fraction was tolerated as long as the substituent was small and aliphatic. Sulfonamides could be exchanged, although there was an observed ~2-3-fold loss of activity. Lastly, the central core was also important for potency. Only very similar compounds such as indole and des-methyl indoline were tolerated.

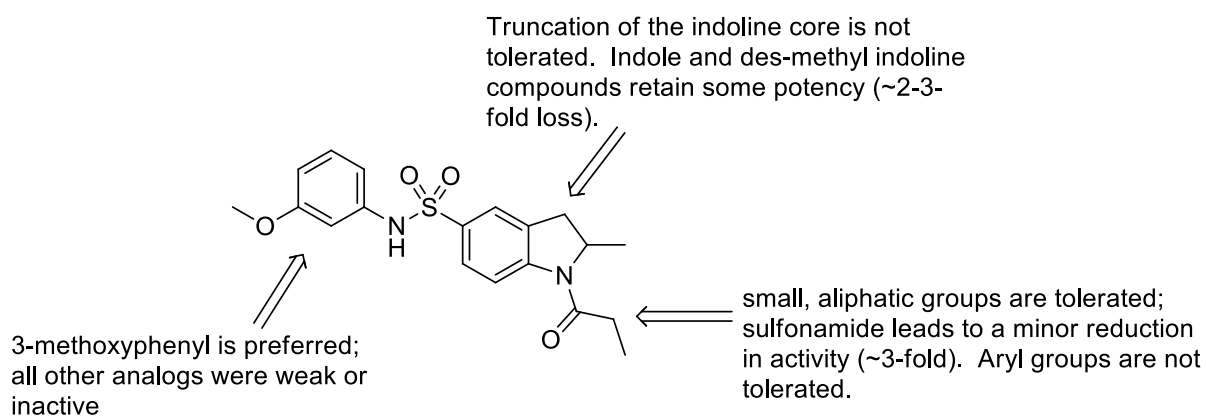


Figure 5. Summary of structure-activity relationship (SAR). Summary of observed SAR of over 100 analogs synthesized exploring all three regions of VU625.

SAR summary provided by Corey R. Hopkins.

VU625-induced toxicity is increased by probenecid

Injection of the *AeKir1* channel inhibitors VU573 or VU590 into the hemolymph of adult female *A. aegypti* mosquitoes leads to their incapacitation and/or death within 24 h (**Appendix A**; [207]). Surprisingly, injection of a high dose of VU625 (690 pmol), which is a more potent inhibitor of *AeKir1* than VU573 and VU590, into the hemolymph of mosquitoes had no significant effects on mosquito behavior or survival within 24 h (**Fig. 6**). Thus, we hypothesized that the lack of in vivo effects could be due to poor bioavailability of VU625 as a result of metabolic detoxification and/or excretion by the mosquito.

We therefore tested probenecid, which is a broad-spectrum inhibitor of organic anion transporters (OATs) and ATP-binding cassette (ABC) transporters [248-250]. Interestingly, both probenecid and VU625 have a sulfonamide moiety in their chemical structure (**Fig. 7**). As shown in **Fig. 6**, injection of probenecid (3.4 nmol per mosquito) along with VU625 (690 pmol) significantly increases the toxicity of VU625 within 24 h compared to injection of VU625 or probenecid alone. The abdomens of these mosquitoes were not severely bloated and obvious sub-lethal effects (e.g., loss of flight) were not apparent. Preliminary experiments in which mosquitoes were treated with piperonyl butoxide (PBO; 100 ng per mosquito), which is a commonly used synergist in insecticide formulations that inhibits the activity of cytochrome P450 enzymes [251-253], did not improve the efficacy of VU625 (data not shown).

We next sought to characterize the dose-response relationship of VU625 in mosquitoes following co-injection with a constant dose of probenecid (3.4 nmol). As shown in **Fig. 8**, co-injection of VU625 with probenecid induces mortality in mosquitoes within 24 h in a biphasic manner with 25% and 75% efficacious doses (ED_{25} and ED_{75}) of 9.9 pmol and 502 pmol, respectively. This biphasic dose-response relationship suggests the inhibition of at least two

distinct molecular targets, for which VU625 has different affinities. This result is consistent with the inhibition of *AeKir1* and *AeKir2B* channels as shown in **Fig. 3C**.

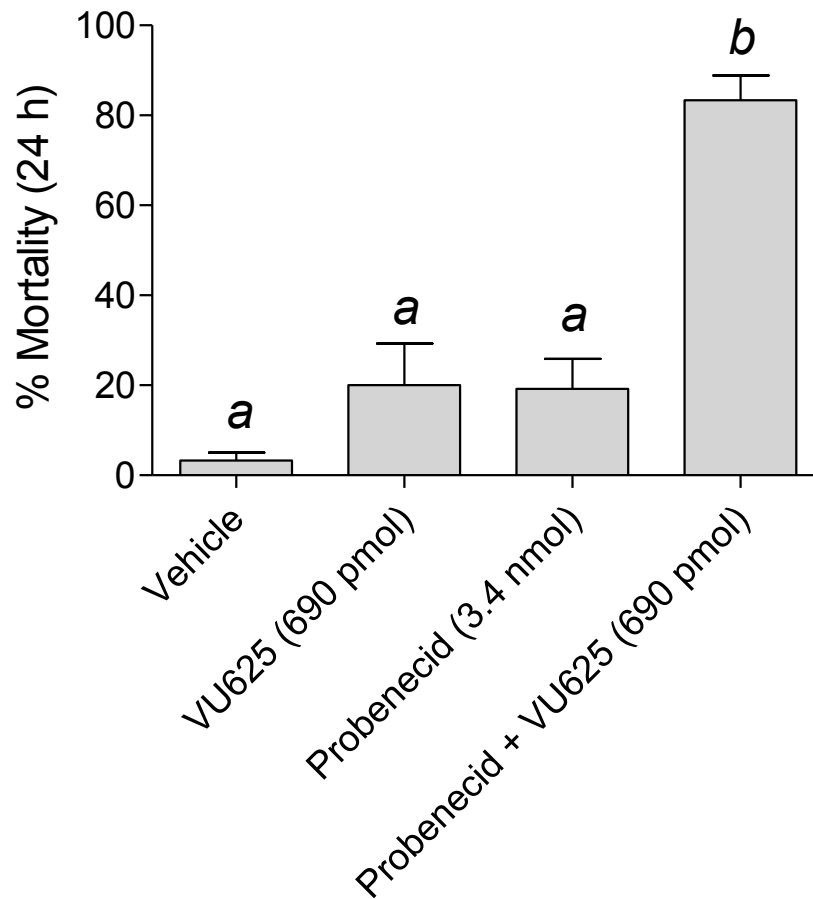
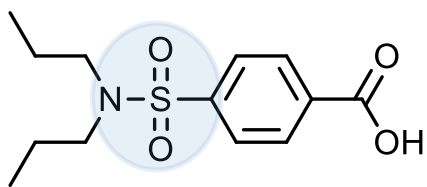
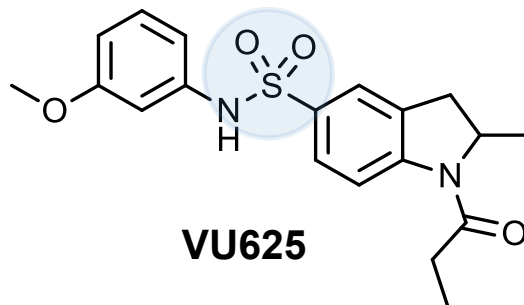


Figure 6. Effects of probenecid and VU625 on survival of adult female mosquitoes (*A. aegypti*). Percent mortality of mosquitoes at 24 h post-injection. Each mosquito was injected with 69 nL of the vehicle containing either VU625 (690 pmol), probenecid (3.4 nmol), or probenecid and VU625. n = 6-7 trials of 10 mosquitoes each per treatment. Lower-case letters indicate statistical categorization of the means as determined by a one-way ANOVA with a Newman-Keuls post-test ($P < 0.05$).

Data collected by Matthew Rouhier and Peter Piermarini.



Probenecid



VU625

Figure 7. VU625 and probenecid share a sulfonamide moiety. The sulfonamide moiety contained in the chemical structure of VU625 and probenecid is shaded in blue.

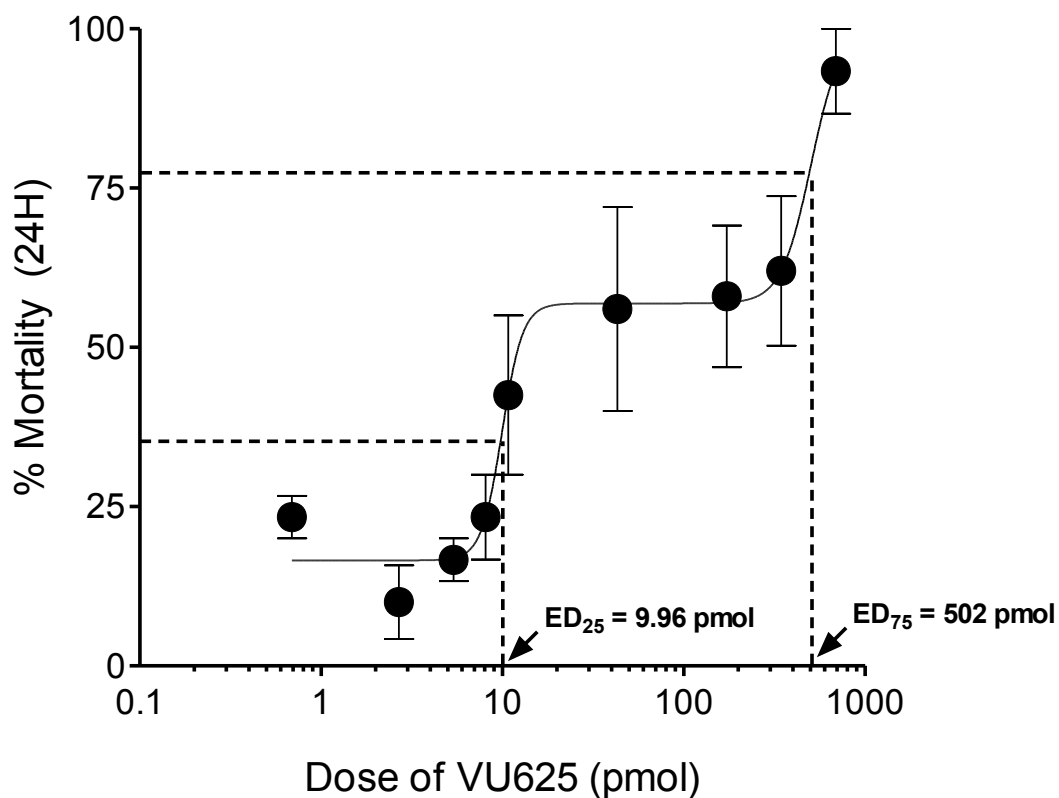


Figure 8. The dose-response curve of the toxic effects of VU625 on adult mosquitoes (*A. aegypti*) is bi-phasic. Percent mortality of mosquitoes at 24 h post-injection. Each mosquito was injected with 69 nL of the vehicle containing probenecid (3.4 nmol) and an appropriate concentration of VU625 to deliver the dose indicated. The ED₂₅ and ED₇₅ were determined by fitting a non-linear curve to the data. n = 3-4 trials of 10 mosquitoes each per dose.

Data collected by Matthew Rouhier and Peter Piermarini.

VU625-induced reduction of urine excretion is enhanced by probenecid

We showed previously [207] and in **Appendix A** that pharmacological inhibition of *AeKir1* with the small molecule inhibitors VU573 and VU590 leads to a decrease in the excretory capacity of *A. aegypti* mosquitoes. Therefore, we sought to determine the effects of VU625 on urine excretion. Consistent with the toxicity studies, we found that VU625 injections alone did not significantly decrease the excretory capacity (583.3 ± 29.52 nL/female) compared to the vehicle controls (644 ± 24.18 nL/female) (**Fig. 9**). Interestingly, injection of probenecid alone significantly reduces the urine output to 467.8 ± 33.53 nL/female, suggesting a potential role of probenecid-sensitive transporters in urine excretion. However, the injection of both VU625 (690 pmol) and probenecid (3.4 nmol) significantly decreases the excretory capacity further to 236.7 ± 24.53 nL/female.

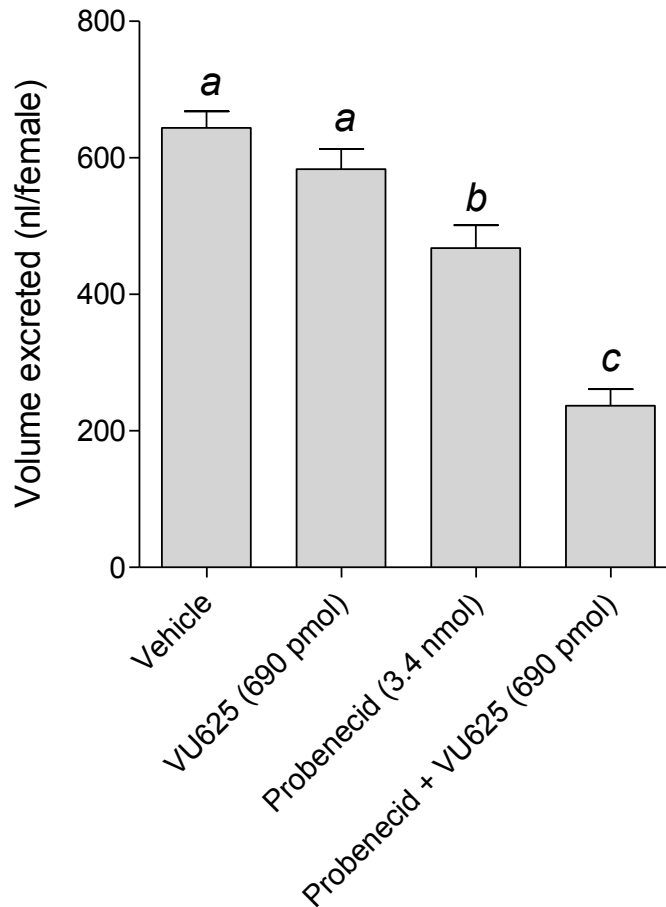


Figure 9. Effects of probenecid and VU625 on the in vivo excretory capacity of adult female mosquitoes (*A. aegypti*). Amount of urine excreted by mosquitoes 1 h after injection with 900 nL of the vehicle (K^+ -PBS₅₀ containing 1.8% DMSO, 0.077% β -cyclodextrin, and 0.008% Solutol), the vehicle containing either VU625 (690 pmol), probenecid (3.4nmol), or probenecid and VU625. Values are means \pm SEM; n = 6-18 trials of 5 mosquitoes per treatment. Lower-case letters indicate statistical categorization of the means as determined by a one-way ANOVA with a Newman-Keuls posttest ($P < 0.05$).

Data collected by Matthew Rouhier and Peter Piermarini.

Discussion

Here, we report the discovery of VU625, the first sub-micromolar inhibitor of a mosquito Kir channel. VU625 is one of 283 confirmed *AeKir1* inhibitors identified in a HTS of approximately 30,000 compounds from the VICB library. It was chosen for lead optimization based on its potency ($IC_{50} = 96.8$ nM), greater than 80-fold selectivity for the *AeKir1* channel over 8 mammalian Kir channels, and clean ancillary pharmacology among a panel of 68 critical mammalian off-targets comprised of voltage-gated ion channels, ion transporters, and receptors (i.e., neurotransmitter, peptide, and G-protein coupled). With the exception of one class of single-nanomolar inhibitors of mammalian Kir1.1 developed by Merck Research Laboratories [22], VU625 is the most potent and selective Kir channel inhibitor reported to date.

This study provides proof-of-concept that conventional drug discovery approaches can be employed successfully to identify small-molecule tools for probing the physiology of insect Kir channels and potential lead compounds for insecticide development. A similar approach has been used recently in insecticide discovery efforts targeting mosquito G-protein coupled receptors [254].

While VU625 is the most potent and selective mosquito Kir channel inhibitor reported to date, it exhibits inhibitory activity against both *AeKir1* and *AeKir2B*, albeit with greater affinity for *AeKir1*. To date, we have reported the activity of two other small-molecule inhibitors of mosquito Kir channels that exhibit differential pharmacology. VU590 is a selective inhibitor of *AeKir1* over *AeKir2B*, whereas VU573 inhibits *AeKir1* and activates *AeKir2B* (companion paper). Thus, VU625 potentially represents a broad-spectrum small-molecule blocker of mosquito Kir channels, pending the characterization of its effects on the other mosquito Kir channels (*AeKir2A*, *AeKir2B'* and *AeKir3* channels), which to date have not yet been expressed

functionally in a heterologous system ([74]; Denton and Piermarini, personal observations). Furthermore, the distinguishing pharmacological properties of each of these Kir channel inhibitors can potentially be employed to determine the relative contributions of Kir channel subtypes in the physiology of various mosquito tissues.

Given the superior in vitro potency of VU625 compared to the *AeKir1* inhibitors VU573 [207] and VU590 (companion paper), we expected VU625 to elicit superior in vivo efficacy. However, we were surprised that high doses of VU625 elicited no observable effects on mosquito survival or excretory capacity when injected directly into the hemolymph. Mosquitoes have evolved robust protective mechanisms for detoxifying and excreting xenobiotics that would harm them otherwise [255,256]. Thus, we investigated whether the molecule may be detoxified and/or excreted.

Preliminary experiments with PBO did not improve the efficacy of VU625, suggesting that detoxification of the compound by cytochrome P450s is unlikely to contribute to its poor in vivo efficacy. However, the co-injection of VU625 with probenecid rescued not only its toxicity, but also its effects on excretory capacity, which suggests that VU625 is likely excreted by OATs and/or ABC transporters in the mosquitoes and thereby rendered ineffective in vivo. The toxicity of VU625 when co-injected with probenecid may be due to the ability of VU625 to inhibit at least two Kir channels, some of which are expressed in the central and peripheral nervous systems, such as Kir1 and Kir2B' [74,75,205,226], and/or a synergistic effect of probenecid that enhances VU625 efficacy to inhibit Kir channels by preventing its renal excretion. Indeed, it is conceivable that the sulfonamide moiety in the structures of VU625 and probenecid causes them to be substrates for OATs and/or ABC transporters. Taken together, these findings highlight efficient xenobiotic transport mechanisms in mosquitoes that render a nanomolar inhibitor of

AeKir1 (VU625) ineffective when introduced directly to the hemolymph. The tissues that contribute to the excretion of VU625 remain to be determined, but presumably involve the Malpighian tubules and/or gut [257,258].

The medicinal chemistry efforts put forth in the present study may be a valuable first step in determining which structural moieties are important for the excretion of VU625 by xenobiotic transporters in mosquitoes. Future studies should assess the *in vivo* efficacy and probenecid-mediated clearance of the VU625 analog series we generated to determine if any of these compounds exhibit potent *in vivo* activity without probenecid.

Perspectives

Here, we show a direct relationship between *in vitro* pharmacology and *in vivo* toxicity of VU625, which is consistent with our previous studies ([207]; **Appendix A**) suggesting that Kir channels inhibitors are promising chemicals for insecticide development. To date, none of the Kir channel inhibitors we have reported (i.e. VU573, VU590, VU625) exhibit toxicity when applied to the cuticle (Piermarini, unpublished observations), which is a waxy, lipophilic structure that creates a physical barrier to insecticide permeation into the hemocoel of mosquitoes. This lack of topical activity severely limits the potential use of the present Kir channel inhibitors as active compounds for incorporation into insecticide-treated bed nets and indoor-residual sprays. The efficacy of common insecticides, such as permethrin, is dependent in part on their lipophilic nature [259,260]. Thus, future chemistry efforts will focus on lipophilic inhibitors of Kir channels. Furthermore, exploring SAR and tolerance of analogs to lipophilic substitutions may reveal more suitable small-molecules compounds for insecticide development.

Chapter IX

SUMMARY AND FUTURE DIRECTIONS

Summary

Inward rectifier potassium (Kir) channels represent an important family of K⁺ channels, which contribute to essential physiological functions in various organisms. While physiological, genetic and pharmacological evidences suggest that Kir channels represent promising drug targets for the development of new therapeutics, there is a need for improved (potent and selective) modulators of this K⁺ ion channel family to assess their integrative physiology and druggability. Indeed, the molecular pharmacology of Kir channels has only seen major expansion in the past five years [261]. In insects, Kir channels are also known to play important physiological functions. In particular, over the past decade, emerging evidence has revealed that Kir channels are involved in physiological functions ranging from osmoregulation, development and immunity [205,206,231,242] as assessed in the fruit fly, *Drosophila melanogaster*. Their roles in mosquitoes have only recently begun to be addressed [72,74], and their potential as insecticidal targets remains largely unexplored. More importantly, the small-molecule pharmacology around mosquito Kir channels was virtually nonexistent, which precluded any efforts to assess their druggability for insecticide development. The projects presented in this dissertation highlight our efforts to fill a major gap in the molecular pharmacology of both mammalian and insect Kir channels, which include the discovery, optimization and characterization of new subtype-specific small molecule modulators.

More specifically, we have 1) implemented fluorescent-based high-throughput (HTS) assays to discover new small-molecule modulators of human and mosquito (*A. aegypti*) Kir

channels, 2) employed medicinal chemistry to optimize and determine the structure-activity relationships of these small molecules to improve on their potency and selectivity, and 3) begun to investigate new roles of Kir channel functions in mosquitoes. In this dissertation, we describe how various new modulators of human (VU573, **Chapter III**; VU717, **Chapter IV**; VU0071063, **Chapter V**) and mosquito (VU625, **Chapter VIII**) Kir channels were discovered from HTS assays. These new pharmacological probes were further characterized in various electrophysiology experiments to confirm their activity and selectivity. In the case of some modulators (i.e. VU573 and VU625), iterative rounds of medicinal chemistry for compound optimization and structure-activity relationships were assayed. Furthermore, the effects of these compounds were determined in native astrocytes (VU717), pancreatic β -cells (VU0071063), and whole-mosquitoes (VU573, VU625).

In summary, the work accomplished in this dissertation supports modern drug discovery efforts to identify new modulators or lead compounds of Kir channels. These new small-molecules modulators can be improved upon to explore the integrative physiology and identify novel functions of Kir channels for new therapeutic and insecticide development.

Future Directions

The results of the projects presented in this dissertation provide us with proof-of-concept studies from targeting various Kir channel subtypes, new lead compounds for modulation of Kir channel activity, and new insights into the physiological roles of Kir channels. All of these findings are critical to expand the small-molecule pharmacology for Kir channels and further explore their biology. Importantly, several new questions have emerged, which warrant further investigations into the mechanisms of action of Kir channels modulators and their in vivo

potential for drug and insecticide development. Moreover, in mosquitoes the diversity of Kir channels and their differential developmental and tissue expression suggest potentially new roles in regulating essential biological processes. The first area of future research that we will focus on is the limitations of the pharmacological tools discussed in this dissertation and potential optimization for in vivo studies. Next, we will address the importance of determining new Kir channel functions in mosquitoes.

One major limitation encountered with these new compounds discovered in this work is their weak potency and relatively poor selectivity in targeting human Kir channels. As discussed in **Chapter III**, VU537 is a low micromolar inhibitor of Kir2.3, Kir3.x and Kir7.1. Although not discussed in that chapter, we have preliminary evidences suggesting that VU573 inhibits other Kir channels albeit with lower potency, which include Kir2.2 and Kir6.2/SUR1. Therefore, determining the contribution of Kir2.3, Kir3.x and Kir7.1 in native tissues where one or more of these subtypes is expressed (e.g. brain, kidney) might prove to be difficult. This issue can be overcome partially by generating through medicinal chemistry, various analogs that will exhibit a decrease in Kir channel activity in a subtype-specific manner. Differently stated, the subtype-specificity of these analogs will help uncover more precisely the contribution of Kir channels in various tissues. Initial lead compounds exhibiting subtype-specific activity against Kir channels can be identified through counterscreens of small molecule libraries (from established focused or primary libraries). Indeed, while employing HTS counterscreening assays against various Kir channel panels to mine a focused library of modulators (as discussed in **Chapter V**), we identified new compounds with subtype-specificity. These initial lead compounds will then be optimized via medicinal chemistry to improve upon their potency and selectivity. The discovery and optimization of such lead compounds will provide useful probes to initially investigate the

contribution of these channels in various biological paradigms, with the goal to develop novel therapeutics.

While we demonstrated in **Chapter V** that VU0071063 is a selective opener for SUR1-containing K_{ATP} channels, its mechanisms of action remain unknown. The importance of determining the mechanism of action of small-molecule modulators is crucial to predict their behaviors *in vivo*. K_{ATP} channel openers represent the largest class of small-molecule modulators of Kir channels [262,263]. However, their mechanisms of action have for the most part been identified to involve SUR subunits [264]. Therefore, it will be interesting to determine whether VU0071063 modulates K_{ATP} activity through its interaction with SUR1 subunits (similarly to diazoxide) and/or interacts directly with Kir6.x subunits. To begin to answer this question, a combination of molecular biology—through mutagenesis of SUR1 subunits—and electrophysiology experiments can be used to test whether the nucleotide binding domains of SUR1 subunits are involved in channel modulation by VU0071063. A similar approach was employed previously to determine the modulatory mechanism of K_{ATP} channels by diazoxide [265]. Next, it will be important to determine whether VU0071063 modulation of K_{ATP} channels is at all depending upon SUR1 subunits. Therefore, we need to test if VU0071063 can open K_{ATP} channels independently of SUR1 subunits. We have already generated a truncated form of the Kir6.2 subunits (Kir6.2 Δ C36, truncation of last 36 amino acid residues), which is known to form functional channels without SUR1 subunits [266]. Using such molecular tools will contribute to identifying the mechanisms by which VU0071063 modulates SUR1-containing K_{ATP} channels. These approaches will ultimately guide efforts to develop optimized analogs of VU0071063 for *in vivo* testing, and thus determine their therapeutic potential for the treatment of hyperinsulinemia.

The discovery of VU625, first potent and selective inhibitor of *Aedes aegypti* Kir1 channels, via HTS is a significant improvement for the development of mosquito specific Kir channel modulators. However, as discussed in **Chapter VIII**, we found that VU625 was ineffective in vivo unless co-administered with probenecid. Therefore, it would be interesting to determine whether the lack of in vivo effect of VU625 is the result of its excretion through efflux mechanisms. Although not discussed in **Chapter VIII**, we have some preliminary data from isolated Malpighian tubule experiments, which suggest that VU625 is indeed effluxed through this epithelial tissue (Klaus Bayenbach, personal communication). To specifically address this question, we can employ in vitro transport assays [267,268] Determining whether VU625 is a substrate for efflux transport mechanisms will inform our medicinal chemistry efforts for the design of small-molecule compounds without structural determinants for efflux liability.

A next line for future research is to determine the role of Kir channels in mosquito development. As discussed in **Chapter VII**, we have shown for the first time that *AgKir1* transcript levels are enriched during the pupal developmental stage. This result suggests a possible role for this gene during mosquito development. One immediate question that could be investigated is to determine the level of expression of the other *Anopheles* Kir genes (i.e. *AgKir2A*, *AgKir2A'*, *AgKir2B*, *AgKir3A* and *AgKir3B*) during development. Furthermore, exploring the roles of these genes during various developmental stages will be critical to identifying novel biological regulatory processes and targets for vector control. To achieve this goal, employing strategies that will disrupt gene/protein functions via genetic or pharmacological approaches during development (i.e. larval stage) should be explored. A major drawback for assessing gene functions in mosquito larval stage through gene silencing remains the delivery method. Current strategies involve dsRNA injections, which are technically difficult when

performed in larvae [269]. The recent development of chitosan nanoparticles-based delivery method for gene silencing via larval feeding has proven successful in knocking-down both *Anopheles* and *Aedes* specific genes [269,270] and could represent a useful tool to address these questions. Hence, by adapting this technique to silence gene expression of Kir channels in vector mosquitoes such as *Anopheles gambiae*, we can begin to identify developmental or behavioral defects that will be associated with one or more of these genes. Furthermore, the various small-molecule compounds (inhibitors and activators) discovered and discussed in this dissertation could be used to further test the functions of these channels during development, by employing this same nanoparticle-feeding method.

In summary, the work discussed in this dissertation has contributed to the discovery of novel small-molecule probes with which to investigate Kir channel functions in humans and mosquitoes. Furthermore, by our efforts to characterize these various compounds, we are expanding on the pharmacology of Kir channel modulators. While these small-molecule probes remain to be optimized for use as therapeutics or insecticides, we hope that they will represent important research tools to map the contribution of Kir channels in various tissues and organ system, and uncover novel physiological roles. In addition, the physiological functions of Kir channels in mosquitoes needs to be further investigated, as they could reveal important and unknown signalling mechanisms for insecticide target and lead to the development of new vector control strategies.

APPENDIX A

PHARMACOLOGICAL VALIDATION OF AN INWARD-RECTIFIER POTASSIUM (KIR) CHANNELS AS AN INSECTICIDE TARGET IN THE YELLOW FEVER MOSQUITO *Aedes Aegypti*

This work is under review and is a collaborative effort between the laboratories of Peter

Piermarini and Jerod S. Denton

My contribution to this work was performing the thallium flux assay on *AeKir1* expressing T-Rex-HEK293 cells to determine the inhibitory effects of VU590 and VU608 compounds on *AeKir1*-mediated fluorescence.

Briefly, we demonstrated in a previous study (see **Chapter VI**) that pharmacological inhibition of mosquito inward rectifier potassium (Kir) channels with VU573 represents a novel mechanism for killing mosquitoes and could represent promising targets for insecticide development. To further validate *Aedes aegypti* Kir 1 (*AeKir1*) channels as insecticidal targets, we sought to determine the effects of another inhibitor, VU590, on mosquito survival and excretory capacity. VU590 is a mammalian Kir1.1 and Kir7.1 inhibitor, which we found to inhibit *AeKir1* activity in thallium flux assays. VU590 is structurally unrelated to VU573. In this study, we report that VU590, but not its inactive analog VU608, decreases urinary excretion when injected in the hemolymph and causes mortality in adults *Aedes aegypti* mosquitoes after 24 h. Furthermore, we determined in electrophysiology experiments that VU590 and VU573 exhibit differential pharmacology against *AeKir1* and *AeKir2B* subtypes expressed in *Xenopus* oocytes. Indeed, while VU590 only inhibits *AeKir1* channel activity, VU573 acts as both an inhibitor of *AeKir1* and potentiator of *AeKir2B*. Importantly, this result suggests that the toxic

effects of VU590 observed in vivo are caused by inhibition of *AeKir1* channel functions. Therefore, we further confirm in this study that targeting *AeKir1* channels is a viable approach for insecticide development, and thus mosquito control.

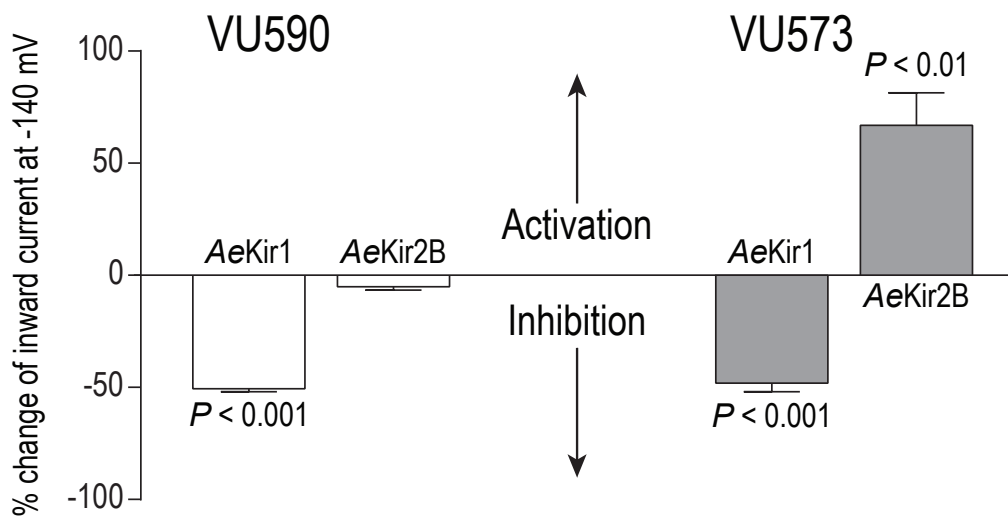


Figure A-1. Effects of VU590 and VU573 on *AeKir1* and *AeKir2B* channels expressed heterologously in *Xenopus* oocytes. Summary of the percent changes of inward currents at -140 mV in *AeKir1* and *AeKir2B* elicited by 50 μ M VU590 and 50 μ M VU573. Positive and negative percent changes indicate activation and inhibition, respectively. *P* values indicate significant inhibition or activation as determined by a one sample t test. Values are means \pm SEM. For VU590 experiments, $n = 3$ oocytes each for *AeKir1* and *AeKir2B*. For VU573 experiments; $n = 5$ and 8 oocytes each for *AeKir1* and *AeKir2B*, respectively. Lower-case letters indicate statistical categorization of the means as determined by a one-way ANOVA with a Newman-Keuls posttest ($P < 0.05$).

Assay performed by Matthew Rouhier and Peter Piermarini.

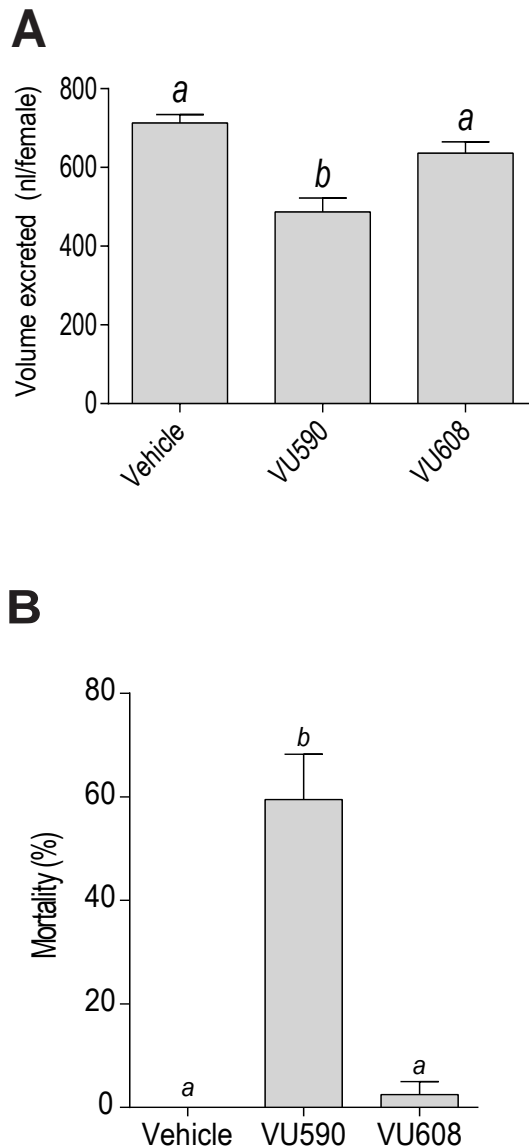


Figure A-2. Effects of VU590 on the urine excretion and survival of adult *A. aegypti* female mosquitoes. (A) Amount of urine excreted by mosquitoes 1 h after injection with 900 nL of the vehicle (K^+ -PBS₅₀ containing 1.8% DMSO, 0.077% β -cyclodextrane, and 0.008% Solutol), the vehicle containing VU590 (0.77 mM), or the vehicle containing VU608 (0.77 mM). Values are means \pm SEM; n = 11 trials of 5 mosquitoes per treatment. (B) Comparison of the toxic effects of the vehicle, VU590, and VU608. Mortality was assessed 24 h after injecting the hemolymph with the vehicle (K^+ -PBS₇₅ with 15% DMSO, 1% β -cyclodextrin, and 0.1% Solutol) or the vehicle containing VU590 or VU608 (2.8 nmol). Values are means \pm SEM; n = 4 trials of 10 mosquitoes. Lower-case letters indicate statistical categorization of the means as determined by a one-way ANOVA with a Newman-Keuls posttest ($P < 0.05$).

Assay performed by Matthew Rouhier and Peter Piermarini.

APPENDIX B

LIST OF PUBLICATIONS

1. **Raphemot R**, Rouhier MF, Swale DR, Days E, Weaver CD, Lovell KM, Konkel LC, Engers DW, Bollinger SF, Hopkins C, Piermarini PM, Denton JS. Discovery and characterization of a potent and selective inhibitor of *Aedes aegypti* inward rectifier potassium channels. *In preparation*.
2. Rouhier MF, **Raphemot R**, Denton JS, Piermarini PM (2014). Pharmacological validation of an inward-rectifying potassium (Kir) channel as an insecticide target in the yellow fever mosquito *Aedes aegypti*. *In revision*.
3. **Raphemot R**, Estévez-Lao TY, Rouhier MF, Piermarini PM, Denton JS, Hillyer JH (2014). Molecular and functional characterization of *Anopheles gambiae* inward rectifier potassium (Kir1) channels: A novel role in egg production. *Insect Biochem Mol Biol*. In press.
4. Rouhier M, Hine R, Park S, **Raphemot R**, Denton J, Piermarini P, Beyenbach K (2014). The excretion of NaCl and KCl loads in mosquitoes: 2. Effects of the small molecule Kir channel inhibitor VU573 and its inactive analog VU342. *In revision*.
5. **Raphemot R**, Swale DR, Dadi PK, Jacobson DA, Cooper P, Wojtovich AP, Banerjee S, Nichols C, Denton JS (2014) Direct activation of β -cell KATP channels with a novel xanthine derivative. *Mol Pharmacol*. doi:10.1124/mol.114.091884.
6. **Raphemot R**, Kadakia R, Olsen ML, Banerjee S, Days E, Smith SS, Weaver CD, and Denton JS (2013) Development and validation of fluorescence- and automated patch clamp-based functional assays for the inward rectifier potassium channel Kir4.1. *Assay Drug Dev Technol*. **11**(9-10): 532-543. doi:10.1089/adt.2013.544. *Journal cover*.
7. **Raphemot R**, Rouhier MF, Hopkins CR, Gogliotti RD, Lovell KM, Hine RM, Ghosalkar D, Longo A, Beyenbach KW, Denton JS, Piermarini PM (2013) Eliciting Renal Failure in Mosquitoes with a Small-Molecule Inhibitor of Inward-Rectifying Potassium Channels. *PLoS ONE* 8(5): e64905. doi:10.1371/journal.pone.0064905.
8. **Raphemot R**, Weaver CD, Denton JS (2013) High-throughput Screening for Small-molecule Modulators of Inward Rectifier Potassium Channels. *J. Vis. Exp.* (71), e4209, doi: 10.3791/4209.
9. **Raphemot R**, Lonergan DF, Nguyen TT, Utley T, Lewis LM, Kadakia R, Weaver CD, Gogliotti R, Hopkins C, Lindsley CW and Denton JS (2011) Discovery, characterization, and structure–activity relationships of an inhibitor of inward rectifier potassium (Kir) channels with preference for Kir2.3, Kir3.X, and Kir7.1. *Front. Pharmacol*. **2**:75. doi: 10.3389/fphar.2011.00075.

REFERENCES

1. Hibino H, Inanobe A, Furutani K, Murakami S, Findlay I, et al. (2010) Inwardly rectifying potassium channels: their structure, function, and physiological roles. *Physiol Rev* 90: 291-366.
2. Denton JS, Jacobson DA (2012) Channeling dysglycemia: ion-channel variations perturbing glucose homeostasis. *Trends Endocrinol Metab* 23: 41-48.
3. Pattnaik BR, Asuma MP, Spott R, Pillers DA (2012) Genetic defects in the hotspot of inwardly rectifying K(+) (Kir) channels and their metabolic consequences: a review. *Mol Genet Metab* 105: 64-72.
4. Hebert SC, Desir G, Giebisch G, Wang W (2005) Molecular diversity and regulation of renal potassium channels. *Physiol Rev* 85: 319-371.
5. Abraham MR, Jahangir A, Alekseev AE, Terzic A (1999) Channelopathies of inwardly rectifying potassium channels. *FASEB J* 13: 1901-1910.
6. Bichet D, Haass FA, Jan LY (2003) Merging functional studies with structures of inward-rectifier K(+) channels. *Nat Rev Neurosci* 4: 957-967.
7. Tao X, Avalos JL, Chen J, MacKinnon R (2009) Crystal structure of the eukaryotic strong inward-rectifier K⁺ channel Kir2.2 at 3.1 Å resolution. *Science* 326: 1668-1674.
8. Nichols CG, Enkvetchakul D and Flagg TP (2006) KATP channels: From structure to disease. *Biological Membranes* 23: 101-110.
9. Lu Z (2004) Mechanism of rectification in inward-rectifier K⁺ channels. *Annu Rev Physiol* 66: 103-129.
10. Dhamoon AS, Jalife J (2005) The inward rectifier current (IK1) controls cardiac excitability and is involved in arrhythmogenesis. *Heart Rhythm* 2: 316-324.
11. Anumonwo JM, Lopatin AN (2010) Cardiac strong inward rectifier potassium channels. *J Mol Cell Cardiol* 48: 45-54.
12. Zobel C, Cho HC, Nguyen TT, Pekhletski R, Diaz RJ, et al. (2003) Molecular dissection of the inward rectifier potassium current (IK1) in rabbit cardiomyocytes: evidence for heteromeric co-assembly of Kir2.1 and Kir2.2. *J Physiol* 550: 365-372.
13. Fleischmann BK, Duan Y, Fan Y, Schoneberg T, Ehlich A, et al. (2004) Differential subunit composition of the G protein-activated inward-rectifier potassium channel during cardiac development. *J Clin Invest* 114: 994-1001.
14. Bingen BO, Neshati Z, Askar SF, Kazbanov IV, Ypey DL, et al. (2013) Atrium-specific Kir3.x determines inducibility, dynamics, and termination of fibrillation by regulating restitution-driven alternans. *Circulation* 128: 2732-2744.
15. Luscher C, Slesinger PA (2010) Emerging roles for G protein-gated inwardly rectifying potassium (GIRK) channels in health and disease. *Nat Rev Neurosci* 11: 301-315.
16. Wakili R, Voigt N, Kaab S, Dobrev D, Nattel S (2011) Recent advances in the molecular pathophysiology of atrial fibrillation. *J Clin Invest* 121: 2955-2968.
17. Ehrlich JR, Biliczki P, Hohnloser SH, Nattel S (2008) Atrial-selective approaches for the treatment of atrial fibrillation. *J Am Coll Cardiol* 51: 787-792.
18. Kenna S, Roper J, Ho K, Hebert S, Ashcroft SJ, et al. (1994) Differential expression of the inwardly-rectifying K-channel ROMK1 in rat brain. *Brain Res Mol Brain Res* 24: 353-356.

19. Simon DB, Karet FE, Rodriguez-Soriano J, Hamdan JH, DiPietro A, et al. (1996) Genetic heterogeneity of Bartter's syndrome revealed by mutations in the K⁺ channel, ROMK. *Nat Genet* 14: 152-156.
20. Lewis LM, Bhawe G, Chauder BA, Banerjee S, Lornsen KA, et al. (2009) High-throughput screening reveals a small-molecule inhibitor of the renal outer medullary potassium channel and Kir7.1. *Mol Pharmacol* 76: 1094-1103.
21. Bhawe G, Chauder BA, Liu W, Dawson ES, Kadakia R, et al. (2011) Development of a selective small-molecule inhibitor of Kir1.1, the renal outer medullary potassium channel. *Mol Pharmacol* 79: 42-50.
22. Pasternak A, Shahripour A, Tang H, Teumelsan NH, Yang L, et al. (2010) Inhibitors of the renal outer medullary potassium channel. Google Patents.
23. Kofuji P, Ceelen P, Zahs KR, Surbeck LW, Lester HA, et al. (2000) Genetic inactivation of an inwardly rectifying potassium channel (Kir4.1 subunit) in mice: phenotypic impact in retina. *J Neurosci* 20: 5733-5740.
24. Neusch C, Rozengurt N, Jacobs RE, Lester HA, Kofuji P (2001) Kir4.1 potassium channel subunit is crucial for oligodendrocyte development and in vivo myelination. *J Neurosci* 21: 5429-5438.
25. Rozengurt N, Lopez I, Chiu CS, Kofuji P, Lester HA, et al. (2003) Time course of inner ear degeneration and deafness in mice lacking the Kir4.1 potassium channel subunit. *Hear Res* 177: 71-80.
26. Olsen ML, Higashimori H, Campbell SL, Hablitz JJ, Sontheimer H (2006) Functional expression of Kir4.1 channels in spinal cord astrocytes. *Glia* 53: 516-528.
27. Djukic B, Casper KB, Philpot BD, Chin LS, McCarthy KD (2007) Conditional knock-out of Kir4.1 leads to glial membrane depolarization, inhibition of potassium and glutamate uptake, and enhanced short-term synaptic potentiation. *J Neurosci* 27: 11354-11365.
28. Bockenbauer D, Feather S, Stanescu HC, Bandulik S, Zdebik AA, et al. (2009) Epilepsy, ataxia, sensorineural deafness, tubulopathy, and KCNJ10 mutations. *N Engl J Med* 360: 1960-1970.
29. Scholl UI, Choi M, Liu T, Ramaekers VT, Hausler MG, et al. (2009) Seizures, sensorineural deafness, ataxia, mental retardation, and electrolyte imbalance (SeSAME syndrome) caused by mutations in KCNJ10. *Proc Natl Acad Sci U S A* 106: 5842-5847.
30. Ashcroft FM (1988) Adenosine 5'-triphosphate-sensitive potassium channels. *Annu Rev Neurosci* 11: 97-118.
31. Flagg TP, Enkvetchakul D, Koster JC, Nichols CG (2010) Muscle KATP channels: recent insights to energy sensing and myoprotection. *Physiol Rev* 90: 799-829.
32. Nichols CG, Singh GK, Grange DK (2013) KATP channels and cardiovascular disease: suddenly a syndrome. *Circ Res* 112: 1059-1072.
33. Matsuda T, Ito M, Ishimaru S, Tsuruoka N, Saito T, et al. (2006) Blockade by NIP-142, an antiarrhythmic agent, of carbachol-induced atrial action potential shortening and GIRK1/4 channel. *J Pharmacol Sci* 101: 303-310.
34. Tang H, Walsh SP, Yan Y, de Jesus RK, Shahripour A, et al. (2012) Discovery of Selective Small Molecule ROMK Inhibitors as Potential New Mechanism Diuretics. *ACS Medicinal Chemistry Letters* 3: 367-372.
35. Watanabe Y, Hara Y, Tamagawa M, Nakaya H (1996) Inhibitory effect of amiodarone on the muscarinic acetylcholine receptor-operated potassium current in guinea pig atrial cells. *J Pharmacol Exp Ther* 279: 617-624.

36. Gogelein H, Brendel J, Steinmeyer K, Strubing C, Picard N, et al. (2004) Effects of the atrial antiarrhythmic drug AVE0118 on cardiac ion channels. *Naunyn Schmiedebergs Arch Pharmacol* 370: 183-192.
37. Zhou W, Arrabit C, Choe S, Slesinger PA (2001) Mechanism underlying bupivacaine inhibition of G protein-gated inwardly rectifying K⁺ channels. *Proc Natl Acad Sci U S A* 98: 6482-6487.
38. Barrett-Jolley R, Dart C, Standen NB (1999) Direct block of native and cloned (Kir2.1) inward rectifier K⁺ channels by chloroethylclonidine. *Br J Pharmacol* 128: 760-766.
39. Rodriguez-Menchaca AA, Navarro-Polanco RA, Ferrer-Villada T, Rupp J, Sachse FB, et al. (2008) The molecular basis of chloroquine block of the inward rectifier Kir2.1 channel. *Proc Natl Acad Sci U S A* 105: 1364-1368.
40. Dabrowski M, Larsen T, Ashcroft FM, Bondo Hansen J, Wahl P (2003) Potent and selective activation of the pancreatic beta-cell type K(ATP) channel by two novel diazoxide analogues. *Diabetologia* 46: 1375-1382.
41. Liu B, Jia Z, Geng X, Bei J, Zhao Z, et al. (2007) Selective inhibition of Kir currents by antihistamines. *Eur J Pharmacol* 558: 21-26.
42. Ehrlich JR, Nattel S (2009) Novel approaches for pharmacological management of atrial fibrillation. *Drugs* 69: 757-774.
43. Kobayashi T, Washiyama K, Ikeda K (2009) Pregnenolone sulfate potentiates the inwardly rectifying K channel Kir2.3. *PLoS One* 4: e6311.
44. Caballero R, Dolz-Gaiton P, Gomez R, Amoros I, Barana A, et al. (2010) Flecainide increases Kir2.1 currents by interacting with cysteine 311, decreasing the polyamine-induced rectification. *Proc Natl Acad Sci U S A* 107: 15631-15636.
45. Kobayashi T, Washiyama K, Ikeda K (2003) Inhibition of G protein-activated inwardly rectifying K⁺ channels by fluoxetine (Prozac). *Br J Pharmacol* 138: 1119-1128.
46. Ohno Y, Hibino H, Lossin C, Inanobe A, Kurachi Y (2007) Inhibition of astroglial Kir4.1 channels by selective serotonin reuptake inhibitors. *Brain Res* 1178: 44-51.
47. Weigl LG, Schreibmayer W (2001) G protein-gated inwardly rectifying potassium channels are targets for volatile anesthetics. *Mol Pharmacol* 60: 282-289.
48. Kaneko N, Matsuda R, Hata Y, Shimamoto K (2009) Pharmacological characteristics and clinical applications of K201. *Curr Clin Pharmacol* 4: 126-131.
49. Kaufmann K, Romaine I, Days E, Pascual C, Malik A, et al. (2013) ML297 (VU0456810), the first potent and selective activator of the GIRK potassium channel, displays antiepileptic properties in mice. *ACS Chem Neurosci* 4: 1278-1286.
50. Wang HR, Wu M, Yu H, Long S, Stevens A, et al. (2011) Selective inhibition of the K(ir)2 family of inward rectifier potassium channels by a small molecule probe: the discovery, SAR, and pharmacological characterization of ML133. *ACS Chem Biol* 6: 845-856.
51. Shindo T, Yamada M, Isomoto S, Horio Y, Kurachi Y (1998) SUR2 subtype (A and B)-dependent differential activation of the cloned ATP-sensitive K⁺ channels by pinacidil and nicorandil. *Br J Pharmacol* 124: 985-991.
52. Hashimoto N, Yamashita T, Tsuruzoe N (2008) Characterization of in vivo and in vitro electrophysiological and antiarrhythmic effects of a novel IKACH blocker, NIP-151: a comparison with an IKr-blocker dofetilide. *J Cardiovasc Pharmacol* 51: 162-169.
53. Su S, Ohno Y, Lossin C, Hibino H, Inanobe A, et al. (2007) Inhibition of astroglial inwardly rectifying Kir4.1 channels by a tricyclic antidepressant, nortriptyline. *J Pharmacol Exp Ther* 320: 573-580.

54. Liu Y, Ren G, O'Rourke B, Marban E, Seharaseyon J (2001) Pharmacological comparison of native mitochondrial K(ATP) channels with molecularly defined surface K(ATP) channels. *Mol Pharmacol* 59: 225-230.
55. Cui Y, Tinker A, Clapp LH (2003) Different molecular sites of action for the KATP channel inhibitors, PNU-99963 and PNU-37883A. *Br J Pharmacol* 139: 122-128.
56. de Boer TP, Nalos L, Stary A, Kok B, Houtman MJ, et al. (2010) The anti-protozoal drug pentamidine blocks KIR2.x-mediated inward rectifier current by entering the cytoplasmic pore region of the channel. *Br J Pharmacol* 159: 1532-1541.
57. Kuzhikandathil EV, Oxford GS (2002) Classic D1 dopamine receptor antagonist R-(+)-7-chloro-8-hydroxy-3-methyl-1-phenyl-2,3,4,5-tetrahydro-1H-3-benzazepine hydrochloride (SCH23390) directly inhibits G protein-coupled inwardly rectifying potassium channels. *Mol Pharmacol* 62: 119-126.
58. Ponce-Balbuena D, Lopez-Izquierdo A, Ferrer T, Rodriguez-Menchaca AA, Arechiga-Figueroa IA, et al. (2009) Tamoxifen inhibits inward rectifier K⁺ 2.x family of inward rectifier channels by interfering with phosphatidylinositol 4,5-bisphosphate-channel interactions. *J Pharmacol Exp Ther* 331: 563-573.
59. Liu Y, Liu D, Printzenhoff D, Coghlan MJ, Harris R, et al. (2002) Tenidap, a novel anti-inflammatory agent, is an opener of the inwardly rectifying K⁺ channel hKir2.3. *Eur J Pharmacol* 435: 153-160.
60. Kobayashi T, Ikeda K, Kumanishi T (2000) Inhibition by various antipsychotic drugs of the G-protein-activated inwardly rectifying K(+) (GIRK) channels expressed in xenopus oocytes. *Br J Pharmacol* 129: 1716-1722.
61. Kobayashi T, Washiyama K, Ikeda K (2004) Inhibition of G protein-activated inwardly rectifying K⁺ channels by various antidepressant drugs. *Neuropsychopharmacology* 29: 1841-1851.
62. Ulens C, Daenens P, Tytgat J (1999) The dual modulation of GIRK1/GIRK2 channels by opioid receptor ligands. *Eur J Pharmacol* 385: 239-245.
63. Raphemot R, Swale DR, Dadi PK, Jacobson DA, Cooper P, et al. (2014) Direct Activation of beta-cell KATP Channels with a Novel Xanthine Derivative. *Mol Pharmacol*.
64. Raphemot R, Lonergan DF, Nguyen TT, Utley T, Lewis LM, et al. (2011) Discovery, characterization, and structure-activity relationships of an inhibitor of inward rectifier potassium (Kir) channels with preference for Kir2.3, Kir3.x, and Kir7.1. *Front Pharmacol* 2: 75.
65. Raphemot R, Kadakia RJ, Olsen ML, Banerjee S, Days E, et al. (2013) Development and validation of fluorescence-based and automated patch clamp-based functional assays for the inward rectifier potassium channel Kir4.1. *Assay Drug Dev Technol* 11: 532-543.
66. van den Berg H, Zaim M, Yadav RS, Soares A, Ameneshewa B, et al. (2012) Global trends in the use of insecticides to control vector-borne diseases. *Environ Health Perspect* 120: 577-582.
67. Hemingway J, Hawkes NJ, McCarroll L, Ranson H (2004) The molecular basis of insecticide resistance in mosquitoes. *Insect Biochem Mol Biol* 34: 653-665.
68. Hemingway J, Beaty BJ, Rowland M, Scott TW, Sharp BL (2006) The Innovative Vector Control Consortium: improved control of mosquito-borne diseases. *Trends Parasitol* 22: 308-312.

69. Williams JC, Jr., Hagedorn HH, Beyenbach KW (1983) Dynamic changes in flow rate and composition of urine during the post-bloodmeal diuresis in *Aedes aegypti* (L.). *J Comp Physiol* 153: 257-265.
70. Beyenbach KW (2003) Transport mechanisms of diuresis in Malpighian tubules of insects. *J Exp Biol* 206: 3845-3856.
71. Benoit JB, Denlinger DL (2010) Meeting the challenges of on-host and off-host water balance in blood-feeding arthropods. *J Insect Physiol* 56: 1366-1376.
72. Scott BN, Yu MJ, Lee LW, Beyenbach KW (2004) Mechanisms of K⁺ transport across basolateral membranes of principal cells in Malpighian tubules of the yellow fever mosquito, *Aedes aegypti*. *J Exp Biol* 207: 1655-1663.
73. Masia R, Aneshansley D, Nagel W, Nachman RJ, Beyenbach KW (2000) Voltage clamping single cells in intact malpighian tubules of mosquitoes. *Am J Physiol Renal Physiol* 279: F747-754.
74. Piermarini PM, Rouhier MF, Schepel M, Kosse C, Beyenbach KW (2013) Cloning and functional characterization of inward-rectifying potassium (Kir) channels from Malpighian tubules of the mosquito *Aedes aegypti*. *Insect Biochem Mol Biol* 43: 75-90.
75. Rouhier MF, Piermarini PM (2014) Identification of life-stage and tissue-specific splice variants of an inward rectifying potassium (Kir) channel in the yellow fever mosquito *Aedes aegypti*. *Insect Biochem Mol Biol* 48C: 91-99.
76. Ehrlich JR (2008) Inward Rectifier Potassium Currents as a Target for Atrial Fibrillation Therapy. *J Cardiovasc Pharmacol* 52: 129-135.
77. Bhawe G, Lonergan D, Chauder BA, Denton JS (2010) Small-molecule modulators of inward rectifier K⁺ channels: recent advances and future possibilities. *Future Med Chem* 2: 757-774.
78. Swartz KJ (2007) Tarantula toxins interacting with voltage sensors in potassium channels. *Toxicon* 49: 213-230.
79. Jin W, Lu Z (1998) A novel high-affinity inhibitor for inward-rectifier K⁺ channels. *Biochemistry* 37: 13291-13299.
80. Jin W, Lu Z (1999) Synthesis of a stable form of tertiapin: a high-affinity inhibitor for inward-rectifier K⁺ channels. *Biochemistry* 38: 14286-14293.
81. Roy A, McDonald PR, Sittampalam S, Chaguturu R (2010) Open access high throughput drug discovery in the public domain: a Mount Everest in the making. *Curr Pharm Biotechnol* 11: 764-778.
82. Weaver CD, Harden D, Dworetzky SI, Robertson B, Knox RJ (2004) A thallium-sensitive, fluorescence-based assay for detecting and characterizing potassium channel modulators in mammalian cells. *J Biomol Screen* 9: 671-677.
83. Niswender CM, Johnson KA, Luo Q, Ayala JE, Kim C, et al. (2008) A novel assay of Gi/o-linked G protein-coupled receptor coupling to potassium channels provides new insights into the pharmacology of the group III metabotropic glutamate receptors. *Mol Pharmacol* 73: 1213-1224.
84. Ho K, Nichols CG, Lederer WJ, Lytton J, Vassilev PM, et al. (1993) Cloning and expression of an inwardly rectifying ATP-regulated potassium channel. *Nature* 362: 31-38.
85. Zou B, Yu H, Babcock JJ, Chanda P, Bader JS, et al. (2010) Profiling diverse compounds by flux- and electrophysiology-based primary screens for inhibition of human Ether-a-go-go related gene potassium channels. *Assay Drug Dev Technol* 8: 743-754.

86. Welling PA, Ho K (2009) A comprehensive guide to the ROMK potassium channel: form and function in health and disease. *Am J Physiol Renal Physiol* 297: F849-863.
87. Ji W, Foo JN, O'Roak BJ, Zhao H, Larson MG, et al. (2008) Rare independent mutations in renal salt handling genes contribute to blood pressure variation. *Nat Genet* 40: 592-599.
88. Dobrev D, Friedrich A, Voigt N, Jost N, Wettwer E, et al. (2005) The G protein-gated potassium current I(K,ACh) is constitutively active in patients with chronic atrial fibrillation. *Circulation* 112: 3697-3706.
89. Voigt N, Friedrich A, Bock M, Wettwer E, Christ T, et al. (2007) Differential phosphorylation-dependent regulation of constitutively active and muscarinic receptor-activated IK,ACh channels in patients with chronic atrial fibrillation. *Cardiovasc Res* 74: 426-437.
90. Makary S, Voigt N, Maguy A, Wakili R, Nishida K, et al. (2011) Differential protein kinase C isoform regulation and increased constitutive activity of acetylcholine-regulated potassium channels in atrial remodeling. *Circ Res* 109: 1031-1043.
91. Walsh KB (2010) A real-time screening assay for GIRK1/4 channel blockers. *J Biomol Screen* 15: 1229-1237.
92. Kitamura H, Yokoyama M, Akita H, Matsushita K, Kurachi Y, et al. (2000) Tertiapin potently and selectively blocks muscarinic K(+) channels in rabbit cardiac myocytes. *J Pharmacol Exp Ther* 293: 196-205.
93. Hashimoto N, Yamashita T, Tsuruzoe N (2006) Tertiapin, a selective IKACH blocker, terminates atrial fibrillation with selective atrial effective refractory period prolongation. *Pharmacol Res* 54: 136-141.
94. Tanaka H, Hashimoto N (2007) A multiple ion channel blocker, NIP-142, for the treatment of atrial fibrillation. *Cardiovasc Drug Rev* 25: 342-356.
95. Machida T, Hashimoto N, Kuwahara I, Ogino Y, Matsuura J, et al. (2011) Effects of a highly selective acetylcholine-activated K⁺ channel blocker on experimental atrial fibrillation. *Circ Arrhythm Electrophysiol* 4: 94-102.
96. Katherine Fallen SB, Jonathan Sheehan, Daniel Addison, L. Michelle Lewis, Jens Meiler and Jerod S. Denton (2009) The Kir channel immunoglobulin domain is essential for Kir1.1 (ROMK) thermodynamic stability, trafficking and gating. *Channels* 3: 57-68.
97. Chuang H, Jan YN, Jan LY (1997) Regulation of IRK3 inward rectifier K⁺ channel by m1 acetylcholine receptor and intracellular magnesium. *Cell* 89: 1121-1132.
98. Caroti P, Ceccotti, C., Da Settimo, A., Palla, F., Primofiore, G. (1986) A facile synthesis of 5,7-dihydro-5-oxopyrido[3',2':5,6]pyrimido[1,2-a]benzimidazoles. A new heterocyclic ring system. *Journal of heterocyclic chemistry* 82: 1833-1836.
99. Zhou H, Tate SS, Palmer LG (1994) Primary structure and functional properties of an epithelial K channel. *Am J Physiol* 266: C809-824.
100. Pasternak AP, Shahipour, A., Tang, H., Teumelsan, N. H., Yang, L., Zhu, Y., Walsh, S. P. (2010) Inhibitors of the renal outer medullary potassium channel. In: Merck, editor.
101. Krapivinsky G, Medina I, Eng L, Krapivinsky L, Yang Y, et al. (1998) A novel inward rectifier K⁺ channel with unique pore properties. *Neuron* 20: 995-1005.
102. Wang HR, Wu M, Yu H, Long S, Stevens A, et al. Selective inhibition of the K(ir)2 family of inward rectifier potassium channels by a small molecule probe: the discovery, SAR, and pharmacological characterization of ML133. *ACS Chem Biol* 6: 845-856.

103. Li Q, Rottlander M, Xu M, Christoffersen CT, Frederiksen K, et al. Identification of novel KCNQ4 openers by a high-throughput fluorescence-based thallium flux assay. *Anal Biochem* 418: 66-72.
104. Zou B, Yu H, Babcock JJ, Chanda P, Bader JS, et al. Profiling diverse compounds by flux- and electrophysiology-based primary screens for inhibition of human Ether-a-go-go related gene potassium channels. *Assay Drug Dev Technol* 8: 743-754.
105. Huang XP, Mangano T, Hufeisen S, Setola V, Roth BL Identification of human Ether-a-go-go related gene modulators by three screening platforms in an academic drug-discovery setting. *Assay Drug Dev Technol* 8: 727-742.
106. Schmalhofer WA, Swensen AM, Thomas BS, Felix JP, Haedo RJ, et al. A pharmacologically validated, high-capacity, functional thallium flux assay for the human Ether-a-go-go related gene potassium channel. *Assay Drug Dev Technol* 8: 714-726.
107. Bridal TR, Margulis M, Wang X, Donio M, Sorota S Comparison of human Ether-a-go-go related gene screening assays based on IonWorks Quattro and thallium flux. *Assay Drug Dev Technol* 8: 755-765.
108. Delpire E, Days E, Lewis LM, Mi D, Kim K, et al. (2009) Small-molecule screen identifies inhibitors of the neuronal K-Cl cotransporter KCC2. *Proc Natl Acad Sci U S A* 106: 5383-5388.
109. Nishida M, MacKinnon R (2002) Structural basis of inward rectification: cytoplasmic pore of the G protein-gated inward rectifier GIRK1 at 1.8 Å resolution. *Cell* 111: 957-965.
110. Nishida M, Cadene M, Chait BT, MacKinnon R (2007) Crystal structure of a Kir3.1-prokaryotic Kir channel chimera. *Embo J* 26: 4005-4015.
111. de Boer TP, Houtman MJ, Compier M, van der Heyden MA (2010) The mammalian K(IR)2.x inward rectifier ion channel family: expression pattern and pathophysiology. *Acta Physiol (Oxf)* 199: 243-256.
112. Plaster NM, Tawil R, Tristani-Firouzi M, Canun S, Bendahhou S, et al. (2001) Mutations in Kir2.1 cause the developmental and episodic electrical phenotypes of Andersen's syndrome. *Cell* 105: 511-519.
113. Ryan DP, da Silva MR, Soong TW, Fontaine B, Donaldson MR, et al. (2010) Mutations in potassium channel Kir2.6 cause susceptibility to thyrotoxic hypokalemic periodic paralysis. *Cell* 140: 88-98.
114. Zaritsky JJ, Redell JB, Tempel BL, Schwarz TL (2001) The consequences of disrupting cardiac inwardly rectifying K(+) current (I(K1)) as revealed by the targeted deletion of the murine Kir2.1 and Kir2.2 genes. *J Physiol* 533: 697-710.
115. Lopez-Izquierdo A, Ponce-Balbuena D, Moreno-Galindo EG, Arechiga-Figueroa IA, Rodriguez-Martinez M, et al. (2011) The antimalarial drug mefloquine inhibits cardiac inward rectifier K⁺ channels: evidence for interference in PIP₂-channel interaction. *J Cardiovasc Pharmacol* 57: 407-415.
116. Lopez-Izquierdo A, Arechiga-Figueroa IA, Moreno-Galindo EG, Ponce-Balbuena D, Rodriguez-Martinez M, et al. (2011) Mechanisms for Kir channel inhibition by quinacrine: acute pore block of Kir2.x channels and interference in PIP₂ interaction with Kir2.x and Kir6.2 channels. *Pflugers Arch* 462: 505-517.
117. Ferrer T, Ponce-Balbuena D, Lopez-Izquierdo A, Arechiga-Figueroa IA, de Boer TP, et al. (2011) Carvedilol inhibits Kir2.3 channels by interference with PIP₂-channel interaction. *Eur J Pharmacol* 668: 72-77.

118. Ookata K, Tojo A, Suzuki Y, Nakamura N, Kimura K, et al. (2000) Localization of inward rectifier potassium channel Kir7.1 in the basolateral membrane of distal nephron and collecting duct. *J Am Soc Nephrol* 11: 1987-1994.
119. Nakamura N, Suzuki Y, Sakuta H, Ookata K, Kawahara K, et al. (1999) Inwardly rectifying K⁺ channel Kir7.1 is highly expressed in thyroid follicular cells, intestinal epithelial cells and choroid plexus epithelial cells: implication for a functional coupling with Na⁺,K⁺-ATPase. *Biochem J* 342 (Pt 2): 329-336.
120. Yang D, Zhang X, Hughes BA (2008) Expression of inwardly rectifying potassium channel subunits in native human retinal pigment epithelium. *Exp Eye Res* 87: 176-183.
121. Pondugula SR, Raveendran NN, Ergonul Z, Deng Y, Chen J, et al. (2006) Glucocorticoid regulation of genes in the amiloride-sensitive sodium transport pathway by semicircular canal duct epithelium of neonatal rat. *Physiol Genomics* 24: 114-123.
122. Hejtmancik JF, Jiao X, Li A, Sergeev YV, Ding X, et al. (2008) Mutations in KCNJ13 cause autosomal-dominant snowflake vitreoretinal degeneration. *Am J Hum Genet* 82: 174-180.
123. Sergouniotis PI, Davidson AE, Mackay DS, Li Z, Yang X, et al. (2011) Recessive mutations in KCNJ13, encoding an inwardly rectifying potassium channel subunit, cause leber congenital amaurosis. *Am J Hum Genet* 89: 183-190.
124. Paulais M, Bloch-Faure M, Picard N, Jacques T, Ramakrishnan SK, et al. (2011) Renal phenotype in mice lacking the Kir5.1 (Kcnj16) K⁺ channel subunit contrasts with that observed in SeSAME/EAST syndrome. *Proc Natl Acad Sci U S A* 108: 10361-10366.
125. Lourdel S, Paulais M, Cluzeaud F, Bens M, Tanemoto M, et al. (2002) An inward rectifier K⁽⁺⁾ channel at the basolateral membrane of the mouse distal convoluted tubule: similarities with Kir4-Kir5.1 heteromeric channels. *J Physiol* 538: 391-404.
126. Huang C, Sindic A, Hill CE, Hujer KM, Chan KW, et al. (2007) Interaction of the Ca²⁺-sensing receptor with the inwardly rectifying potassium channels Kir4.1 and Kir4.2 results in inhibition of channel function. *Am J Physiol Renal Physiol* 292: F1073-1081.
127. Lachheb S, Cluzeaud F, Bens M, Genete M, Hibino H, et al. (2008) Kir4.1/Kir5.1 channel forms the major K⁺ channel in the basolateral membrane of mouse renal collecting duct principal cells. *Am J Physiol Renal Physiol* 294: F1398-1407.
128. Uwai Y, Saito H, Hashimoto Y, Inui KI (2000) Interaction and transport of thiazide diuretics, loop diuretics, and acetazolamide via rat renal organic anion transporter rOAT1. *J Pharmacol Exp Ther* 295: 261-265.
129. Hasegawa M, Kusuhara H, Adachi M, Schuetz JD, Takeuchi K, et al. (2007) Multidrug resistance-associated protein 4 is involved in the urinary excretion of hydrochlorothiazide and furosemide. *J Am Soc Nephrol* 18: 37-45.
130. Hasannejad H, Takeda M, Taki K, Shin HJ, Babu E, et al. (2004) Interactions of human organic anion transporters with diuretics. *J Pharmacol Exp Ther* 308: 1021-1029.
131. Vallon V, Rieg T, Ahn SY, Wu W, Eraly SA, et al. (2008) Overlapping in vitro and in vivo specificities of the organic anion transporters OAT1 and OAT3 for loop and thiazide diuretics. *Am J Physiol Renal Physiol* 294: F867-873.
132. Zaika O, Mamenko M, Palygin O, Boukelmoune N, Staruschenko A, et al. (2013) Direct inhibition of basolateral Kir4.1/5.1 and Kir4.1 channels in the cortical collecting duct by dopamine. *Am J Physiol Renal Physiol*.

133. Zhang X, Su J, Cui N, Gai H, Wu Z, et al. (2011) The disruption of central CO₂ chemosensitivity in a mouse model of Rett syndrome. *Am J Physiol Cell Physiol* 301: C729-738.
134. Katz DM, Dutschmann M, Ramirez JM, Hilaire G (2009) Breathing disorders in Rett syndrome: progressive neurochemical dysfunction in the respiratory network after birth. *Respir Physiol Neurobiol* 168: 101-108.
135. Kerr AM (1992) A review of the respiratory disorder in the Rett syndrome. *Brain Dev* 14 Suppl: S43-45.
136. Fallen K, Banerjee S, Sheehan J, Addison D, Lewis LM, et al. (2009) The Kir channel immunoglobulin domain is essential for Kir1.1 (ROMK) thermodynamic stability, trafficking and gating. *Channels (Austin)* 3: 57-68.
137. Raphemot R, Weaver CD, Denton JS (2013) High-throughput screening for small-molecule modulators of inward rectifier potassium channels. *J Vis Exp*.
138. Golden AP, Li N, Chen Q, Lee T, Nevill T, et al. (2011) IonFlux: a microfluidic patch clamp system evaluated with human Ether-a-go-go related gene channel physiology and pharmacology. *Assay Drug Dev Technol* 9: 608-619.
139. Spencer CI, Li N, Chen Q, Johnson J, Nevill T, et al. (2012) Ion channel pharmacology under flow: automation via well-plate microfluidics. *Assay Drug Dev Technol* 10: 313-324.
140. Yu SP, Kerchner GA (1998) Endogenous voltage-gated potassium channels in human embryonic kidney (HEK293) cells. *Journal of Neuroscience Research* 52: 612-617.
141. Zhu G, Zhang Y, Xu H, Jiang C (1998) Identification of endogenous outward currents in the human embryonic kidney (HEK 293) cell line. *J Neurosci Methods* 81: 73-83.
142. Furutani K, Ohno Y, Inanobe A, Hibino H, Kurachi Y (2009) Mutational and in silico analyses for antidepressant block of astroglial inward-rectifier Kir4.1 channel. *Mol Pharmacol* 75: 1287-1295.
143. Yeung SY, Millar JA, Mathie A (1999) Inhibition of neuronal KV potassium currents by the antidepressant drug, fluoxetine. *Br J Pharmacol* 128: 1609-1615.
144. Thomas D, Gut B, Wendt-Nordahl G, Kiehn J (2002) The antidepressant drug fluoxetine is an inhibitor of human ether-a-go-go-related gene (HERG) potassium channels. *J Pharmacol Exp Ther* 300: 543-548.
145. Maertens C, Wei L, Voets T, Droogmans G, Nilius B (1999) Block by fluoxetine of volume-regulated anion channels. *Br J Pharmacol* 126: 508-514.
146. Katchman AN, Koerner J, Tosaka T, Woosley RL, Ebert SN (2006) Comparative evaluation of HERG currents and QT intervals following challenge with suspected torsadogenic and nontorsadogenic drugs. *J Pharmacol Exp Ther* 316: 1098-1106.
147. Ransom CB, Sontheimer H (1995) Biophysical and pharmacological characterization of inwardly rectifying K⁺ currents in rat spinal cord astrocytes. *J Neurophysiol* 73: 333-346.
148. Bridal TR, Margulis M, Wang X, Donio M, Sorota S (2010) Comparison of human Ether-a-go-go related gene screening assays based on IonWorks Quattro and thallium flux. *Assay Drug Dev Technol* 8: 755-765.
149. Li Q, Rottlander M, Xu M, Christoffersen CT, Frederiksen K, et al. (2011) Identification of novel KCNQ4 openers by a high-throughput fluorescence-based thallium flux assay. *Anal Biochem* 418: 66-72.

150. Titus SA, Beacham D, Shahane SA, Southall N, Xia M, et al. (2009) A new homogeneous high-throughput screening assay for profiling compound activity on the human ether-a-go-go-related gene channel. *Anal Biochem* 394: 30-38.
151. Ashcroft FM (2007) The Walter B. Cannon Physiology in Perspective Lecture, 2007. ATP-sensitive K⁺ channels and disease: from molecule to malady. *Am J Physiol Endocrinol Metab* 293: E880-889.
152. Nichols CG, Koster JC, Remedi MS (2007) beta-cell hyperexcitability: from hyperinsulinism to diabetes. *Diabetes Obes Metab* 9 Suppl 2: 81-88.
153. Grover GJ, Garlid KD (2000) ATP-Sensitive potassium channels: a review of their cardioprotective pharmacology. *J Mol Cell Cardiol* 32: 677-695.
154. Hansen JB (2006) Towards selective Kir6.2/SUR1 potassium channel openers, medicinal chemistry and therapeutic perspectives. *Curr Med Chem* 13: 361-376.
155. Jacobson DA, Weber CR, Bao S, Turk J, Philipson LH (2007) Modulation of the pancreatic islet beta-cell-delayed rectifier potassium channel Kv2.1 by the polyunsaturated fatty acid arachidonate. *J Biol Chem* 282: 7442-7449.
156. Wojtovich AP, Brookes PS (2008) The endogenous mitochondrial complex II inhibitor malonate regulates mitochondrial ATP-sensitive potassium channels: implications for ischemic preconditioning. *Biochim Biophys Acta* 1777: 882-889.
157. Wojtovich AP, Sherman TA, Nadtochiy SM, Urciuoli WR, Brookes PS, et al. (2011) SLO-2 is cytoprotective and contributes to mitochondrial potassium transport. *PLoS One* 6: e28287.
158. Wojtovich AP, Brookes PS (2009) The complex II inhibitor atpenin A5 protects against cardiac ischemia-reperfusion injury via activation of mitochondrial KATP channels. *Basic Res Cardiol* 104: 121-129.
159. Roe MW, Worley JF, 3rd, Mittal AA, Kuznetsov A, DasGupta S, et al. (1996) Expression and function of pancreatic beta-cell delayed rectifier K⁺ channels. Role in stimulus-secretion coupling. *J Biol Chem* 271: 32241-32246.
160. Philipson LH, Rosenberg MP, Kuznetsov A, Lancaster ME, Worley JF, 3rd, et al. (1994) Delayed rectifier K⁺ channel overexpression in transgenic islets and beta-cells associated with impaired glucose responsiveness. *J Biol Chem* 269: 27787-27790.
161. de Tullio P, Servais AC, Fillet M, Gillotin F, Somers F, et al. (2011) Hydroxylated analogues of ATP-sensitive potassium channel openers belonging to the group of 6- and/or 7-substituted 3-isopropylamino-4H-1,2,4-benzothiadiazine 1,1-dioxides: toward an improvement in sulfonylurea receptor 1 selectivity and metabolism stability. *J Med Chem* 54: 8353-8361.
162. Pirotte B, de Tullio P, Nguyen QA, Somers F, Fraikin P, et al. (2010) Chloro-substituted 3-alkylamino-4H-1,2,4-benzothiadiazine 1,1-dioxides as ATP-sensitive potassium channel activators: impact of the position of the chlorine atom on the aromatic ring on activity and tissue selectivity. *J Med Chem* 53: 147-154.
163. Coetzee WA (2013) Multiplicity of effectors of the cardioprotective agent, diazoxide. *Pharmacol Ther* 140: 167-175.
164. Carr RD, Brand CL, Bodvarsdottir TB, Hansen JB, Sturis J (2003) NN414, a SUR1/Kir6.2-selective potassium channel opener, reduces blood glucose and improves glucose tolerance in the VDF Zucker rat. *Diabetes* 52: 2513-2518.
165. Alemzadeh R, Fledelius C, Bodvarsdottir T, Sturis J (2004) Attenuation of hyperinsulinemia by NN414, a SUR1/Kir6.2 selective K-adenosine triphosphate channel

- opener, improves glucose tolerance and lipid profile in obese Zucker rats. *Metabolism* 53: 441-447.
166. Zdravkovic M, Kruse M, Rost KL, Moss J, Kecskes A, et al. (2005) The effects of NN414, a SUR1/Kir6.2 selective potassium channel opener, in healthy male subjects. *J Clin Pharmacol* 45: 763-772.
 167. Zdravkovic M, Kruse M, Rost KL, Moss J, Kecskes A (2007) The effects of NN414, a SUR1/Kir6.2 selective potassium channel opener in subjects with type 2 diabetes. *Exp Clin Endocrinol Diabetes* 115: 405-406.
 168. Khelili S, Lebrun P, de Tullio P, Pirotte B (2006) Synthesis and pharmacological evaluation of some N-arylsulfonyl-N-methyl-N'-(2,2-dimethyl-2H-1-benzopyran-4-yl)ureas structurally related to cromakalim. *Bioorg Med Chem* 14: 3530-3534.
 169. Sebille S, Gall D, de Tullio P, Florence X, Lebrun P, et al. (2006) Design, synthesis, and pharmacological evaluation of R/S-3,4-dihydro-2,2-dimethyl-6-halo-4-(phenylaminocarbonylamino)-2H-1-benzopyrans: toward tissue-selective pancreatic beta-cell KATP channel openers structurally related to (+/-)-cromakalim. *J Med Chem* 49: 4690-4697.
 170. Sebille S, de Tullio P, Florence X, Becker B, Antoine MH, et al. (2008) New R/S-3,4-dihydro-2,2-dimethyl-6-halo-4-(phenylaminothiocarbonylamino)-2H-1-benzopyrans structurally related to (+/-)-cromakalim as tissue-selective pancreatic beta-cell K(ATP) channel openers. *Bioorg Med Chem* 16: 5704-5719.
 171. Khelili S, Florence X, Bouhadja M, Abdelaziz S, Mechouch N, et al. (2008) Synthesis and activity on rat aorta rings and rat pancreatic beta-cells of ring-opened analogues of benzopyran-type potassium channel activators. *Bioorg Med Chem* 16: 6124-6130.
 172. Florence X, Sebille S, Tullio P, Lebrun P, Pirotte B (2009) New R/S-3,4-dihydro-2,2-dimethyl-2H-1-benzopyrans as K(ATP) channel openers: modulation of the 4-position. *Bioorg Med Chem* 17: 7723-7731.
 173. Florence X, Dilly S, de Tullio P, Pirotte B, Lebrun P (2011) Modulation of the 6-position of benzopyran derivatives and inhibitory effects on the insulin releasing process. *Bioorg Med Chem* 19: 3919-3928.
 174. Nielsen FE, Jacobsen P, Worsaae A, Arkhammar PO, Wahl P, et al. (2004) 2-(4-Methoxyphenoxy)-5-nitro-N-(4-sulfamoylphenyl)benzamide activates Kir6.2/SUR1 K(ATP) channels. *Bioorg Med Chem Lett* 14: 5727-5730.
 175. Peat AJ, Townsend C, Craig McKay M, Garrido D, Terry CM, et al. (2004) 3-trifluoromethyl-4-nitro-5-arylpyrazoles are novel K(ATP) channel agonists. *Bioorg Med Chem Lett* 14: 813-816.
 176. Sheppard DN, Welsh MJ (1992) Effect of ATP-sensitive K⁺ channel regulators on cystic fibrosis transmembrane conductance regulator chloride currents. *J Gen Physiol* 100: 573-591.
 177. Dai ZK, Cheng YJ, Chung HH, Wu JR, Chen IJ, et al. (2010) KMUP-1 ameliorates monocrotaline-induced pulmonary arterial hypertension through the modulation of Ca²⁺ sensitization and K⁺-channel. *Life Sci* 86: 747-755.
 178. Lin RJ, Wu BN, Lo YC, Shen KP, Lin YT, et al. (2002) KMUP-1 relaxes rabbit corpus cavernosum smooth muscle in vitro and in vivo: involvement of cyclic GMP and K(+) channels. *Br J Pharmacol* 135: 1159-1166.

179. Wu BN, Lin RJ, Lin CY, Shen KP, Chiang LC, et al. (2001) A xanthine-based KMUP-1 with cyclic GMP enhancing and K(+) channels opening activities in rat aortic smooth muscle. *Br J Pharmacol* 134: 265-274.
180. Wu BN, Lin RJ, Lo YC, Shen KP, Wang CC, et al. (2004) KMUP-1, a xanthine derivative, induces relaxation of guinea-pig isolated trachea: the role of the epithelium, cyclic nucleotides and K⁺ channels. *Br J Pharmacol* 142: 1105-1114.
181. Kubo M, Nakaya Y, Matsuoka S, Saito K, Kuroda Y (1994) Atrial natriuretic factor and isosorbide dinitrate modulate the gating of ATP-sensitive K⁺ channels in cultured vascular smooth muscle cells. *Circ Res* 74: 471-476.
182. Larsson O, Ammala C, Bokvist K, Fredholm B, Rorsman P (1993) Stimulation of the KATP channel by ADP and diazoxide requires nucleotide hydrolysis in mouse pancreatic beta-cells. *J Physiol* 463: 349-365.
183. Adebisi A, McNally EM, Jaggar JH (2008) Sulfonylurea receptor-dependent and -independent pathways mediate vasodilation induced by ATP-sensitive K⁺ channel openers. *Mol Pharmacol* 74: 736-743.
184. Grimmsmann T, Rustenbeck I (1998) Direct effects of diazoxide on mitochondria in pancreatic B-cells and on isolated liver mitochondria. *Br J Pharmacol* 123: 781-788.
185. Wojtovich AP, Urciuoli WR, Chatterjee S, Fisher AB, Nehrke K, et al. (2013) Kir6.2 is not the mitochondrial KATP channel but is required for cardioprotection by ischemic preconditioning. *Am J Physiol Heart Circ Physiol* 304: H1439-1445.
186. Sato T, Sasaki N, Seharaseyon J, O'Rourke B, Marban E (2000) Selective pharmacological agents implicate mitochondrial but not sarcolemmal K(ATP) channels in ischemic cardioprotection. *Circulation* 101: 2418-2423.
187. Suzuki M, Sasaki N, Miki T, Sakamoto N, Ohmoto-Sekine Y, et al. (2002) Role of sarcolemmal K(ATP) channels in cardioprotection against ischemia/reperfusion injury in mice. *J Clin Invest* 109: 509-516.
188. WHO (2011) World Malaria Report 2011. WHO; World Health Organization. pp. 248.
189. WHO (2012) Global strategy for dengue prevention and control. Geneva: WHO; World Health Organization. pp. 43.
190. Asidi A, N'Guessan R, Akogbeto M, Curtis C, Rowland M (2012) Loss of household protection from use of insecticide-treated nets against pyrethroid-resistant mosquitoes, benin. *Emerg Infect Dis* 18: 1101-1106.
191. Maharaj R (2011) Global trends in insecticide resistance and impact on disease vector control measures *Open Access Insect Physiol* 3: 27-33.
192. Greenwood B, Owusu-Agyei S (2012) Epidemiology. *Malaria in the post-genome era. Science* 338: 49-50.
193. Beyenbach KW, Piermarini PM (2009) Osmotic and ionic regulation in insects. In: Evans DH, editor. *Osmotic and ionic regulation: cells and animals*. Boca Raton: CRC press. pp. 231-293.
194. Beyenbach KW, Piermarini PM (2011) Transcellular and paracellular pathways of transepithelial fluid secretion in Malpighian (renal) tubules of the yellow fever mosquito *Aedes aegypti*. *Acta Physiol* 202: 387-407.
195. Williams JC, Hagedorn HH, Beyenbach KW (1983) Dynamic changes in flow rate and composition of urine during the post blood meal diuresis in *Aedes aegypti*. *J Comp Physiol [B]* 153: 257-266.

196. Beyenbach KW (2003) Transport mechanisms of diuresis in Malpighian tubules of insects. *J Exp Biol* 206: 3845-3856.
197. Coast GM (2009) Neuroendocrine control of ionic homeostasis in blood-sucking insects. *J Exp Biol* 212: 378-386.
198. Scott BN, Yu MJ, Lee LW, Beyenbach KW (2004) Mechanisms of K⁺ transport across basolateral membranes of principal cells in Malpighian tubules of the yellow fever mosquito, *Aedes aegypti*. *J Exp Biol* 207: 1655-1663.
199. Piermarini PM, Hine RM, Schepel M, Miyauchi JT, Beyenbach KW (2011) Role of an apical K,Cl cotransporter in urine formation by renal tubules of the yellow fever mosquito (*Aedes aegypti*). *Am J Physiol Regul Integr Comp Physiol* 301: R1318-1337.
200. Schepel SA, Fox AJ, Miyauchi JT, Sou T, Yang JD, et al. (2010) The single kinin receptor signals to separate and independent physiological pathways in Malpighian tubules of the yellow fever mosquito. *Am J Physiol Regul Integr Comp Physiol* 299: R612-622.
201. Ramsay JA (1954) Active Transport of Water by the Malpighian Tubules of the Stick Insect, *Dixippus Morosus* (Orthoptera, Phasmidae). *J Exp Biol* 31: 104-113.
202. Masia R, Aneshansley D, Nagel W, Nachman RJ, Beyenbach KW (2000) Voltage clamping single cells in intact Malpighian tubules of mosquitoes. *Am J Physiol Renal Physiol* 279: F747-F754.
203. Drake LL, Boudko DY, Marinotti O, Carpenter VK, Dawe AL, et al. (2010) The Aquaporin gene family of the yellow fever mosquito, *Aedes aegypti*. *PLoS one* 5: e15578.
204. Bhave G, Lonergan D, Chauder BA, Denton JS (2010) Small-molecule modulators of inward rectifier K channels: recent advances and future possibilities. *Future Med Chem* 2: 757-774.
205. Döring F, Wischmeyer E, Kühnlein RP, Jäckle H, Karschin A (2002) Inwardly Rectifying K (Kir) Channels in *Drosophila*. *J Biol Chem* 277: 25554–25561.
206. Evans JM, Allan AK, Davies SA, Dow JA (2005) Sulphonylurea sensitivity and enriched expression implicate inward rectifier K⁺ channels in *Drosophila melanogaster* renal function. *J Exp Biol* 208: 3771-3783.
207. Raphemot R, Rouhier MF, Hopkins CR, Gogliotti RD, Lovell KM, et al. (2013) Eliciting renal failure in mosquitoes with a small-molecule inhibitor of inward-rectifying potassium channels. *PLoS One* 8: e64905.
208. Estevez-Lao TY, Hillyer JF (2014) Involvement of the *Anopheles gambiae* Nimrod gene family in mosquito immune responses. *Insect Biochem Mol Biol* 44: 12-22.
209. Piermarini PM, Grogan LF, Lau K, Wang L, Beyenbach KW (2010) A SLC4-like anion exchanger from renal tubules of the mosquito (*Aedes aegypti*): evidence for a novel role of stellate cells in diuretic fluid secretion. *American Journal of Physiology - Regulatory, Integrative and Comparative Physiology* 298: R642–R660.
210. Piermarini PM, Hine RM, Schepel M, Miyauchi J, Beyenbach KW (2011) Role of an apical K,Cl cotransporter in urine formation by renal tubules of the yellow fever mosquito (*Aedes aegypti*). *Am J Physiol Regul Integr Comp Physiol* 301: R1318–R1337.
211. Petersen TN, Brunak S, von Heijne G, Nielsen H (2011) SignalP 4.0: discriminating signal peptides from transmembrane regions. *Nat Meth* 8: 785-786.
212. Mohana Rao JK, Argos P (1986) A conformational preference parameter to predict helices in integral membrane proteins. *Biochim Biophys Acta* 869: 197-214.
213. Nishida M, Cadene M, Chait BT, MacKinnon R (2007) Crystal structure of a Kir3.1-prokaryotic Kir channel chimera. *EMBO* 26: 4005-4015.

214. Abascal F, Zardoya R, Posada D (2005) ProtTest: selection of best-fit models of protein evolution. *Bioinformatics* 21: 2104-2105.
215. Guindon S, Dufayard JF, Lefort V, Anisimova M, Hordijk W, et al. (2010) New algorithms and methods to estimate maximum-likelihood phylogenies: assessing the performance of PhyML 3.0. *Syst Biol* 59: 307-321.
216. Boc A, Diallo AB, Makarenkov V (2012) T-REX: a web server for inferring, validating and visualizing phylogenetic trees and networks. *Nucleic Acids Res* 40: W573-579.
217. Piermarini PM, Weihrauch D, Meyer H, Huss M, Beyenbach KW (2009) NHE8 is an intracellular cation/H exchanger in renal tubules of the yellow fever mosquito *Aedes aegypti*. *Am J Physiol Renal Physiol* 296: F730-F750.
218. Newman EA (1993) Inward-rectifying potassium channels in retinal glial (Müller) cells. *J Neurosci* 13: 3333-3345.
219. Kubo Y, Baldwin TJ, Jan YN, Jan LY (1993) Primary structure and functional expression of a mouse inward rectifier potassium channel. *Nature* 362: 127-133.
220. Hillyer JF, Estevez-Lao TY (2010) Nitric oxide is an essential component of the hemocyte-mediated mosquito immune response against bacteria. *Dev Comp Immunol* 34: 141-149.
221. Livak KJ, Schmittgen TD (2001) Analysis of relative gene expression data using real-time quantitative PCR and the 2(-Delta Delta C(T)) Method. *Methods* 25: 402-408.
222. Estevez-Lao TY, Boyce DS, Honegger HW, Hillyer JF (2013) Cardioacceleratory function of the neurohormone CCAP in the mosquito *Anopheles gambiae*. *J Exp Biol* 216: 601-613.
223. Coggins SA, Estevez-Lao TY, Hillyer JF (2012) Increased survivorship following bacterial infection by the mosquito *Aedes aegypti* as compared to *Anopheles gambiae* correlates with increased transcriptional induction of antimicrobial peptides. *Dev Comp Immunol* 37: 390-401.
224. King JG, Hillyer JF (2013) Spatial and temporal in vivo analysis of circulating and sessile immune cells in mosquitoes: hemocyte mitosis following infection. *BMC Biol* 11.
225. Andereck JW, King JG, Hillyer JF (2010) Contraction of the ventral abdomen potentiates extracardiac retrograde hemolymph propulsion in the mosquito hemocoel. *PLoS One* 5: e12943.
226. Baker DA, Nolan T, Fischer B, Pinder A, Crisanti A, et al. (2011) A comprehensive gene expression atlas of sex- and tissue-specificity in the malaria vector, *Anopheles gambiae*. *BMC Genomics* 12: 296.
227. Reidenbach KR, Cook S, Bertone MA, Harbach RE, Wiegmann BM, et al. (2009) Phylogenetic analysis and temporal diversification of mosquitoes (Diptera: Culicidae) based on nuclear genes and morphology. *BMC Evol Biol* 9: 298.
228. Beaty BJ, Marquardt WC (1996) *The biology of disease vectors*; Beaty BJ, Marquardt WC, editors. Niwot, CO: University Press of Colorado. 632 p.
229. Becker N, Petric D, Zgomba M, Boase C, Dahl C, et al. (2010) *Mosquitoes and Their Control*. New York: Springer-Verlag; 2nd ed.
230. Bartholomay LC, Waterhouse RM, Mayhew GF, Campbell CL, Michel K, et al. (2010) Pathogenomics of *Culex quinquefasciatus* and meta-analysis of infection responses to diverse pathogens. *Science* 330: 88-90.
231. Dahal GR, Rawson J, Gassaway B, Kwok B, Tong Y, et al. (2012) An inwardly rectifying K⁺ channel is required for patterning. *Development* 139: 3653-3664.

232. Rouhier MF, Piermarini PM (2014) Identification of life-stage and tissue-specific splice variants of an inward rectifying potassium (Kir) channel in the yellow fever mosquito *Aedes aegypti*. *Insect Biochem Mol Biol*: In press.
233. Duch C, Vonhoff F, Ryglewski S (2008) Dendrite elongation and dendritic branching are affected separately by different forms of intrinsic motoneuron excitability. *J Neurophysiol* 100: 2525-2536.
234. Hayashi JH, Levine RB (1992) Calcium and potassium currents in leg motoneurons during postembryonic development in the hawkmoth *Manduca sexta*. *J Exp Biol* 171: 15-42.
235. Duch C, Levine RB (2000) Remodeling of Membrane Properties and Dendritic Architecture Accompanies the Postembryonic Conversion of a Slow into a Fast Motoneuron. *J Neurosci* 20: 6950-6961.
236. Moody WJ, Lansman JB (1983) Developmental regulation of Ca²⁺ and K⁺ currents during hormone-induced maturation of starfish oocytes. *Proc Natl Acad Sci* 80: 3096-3100.
237. Tosti E, Boni R (2004) Electrical events during gamete maturation and fertilization in animals and humans. *Hum Reprod Update* 10: 53-65.
238. Tosti E (2006) Calcium ion currents mediating oocyte maturation events. *Reprod Biol Endocrinol* 4: 26.
239. Von Stetina JR, Orr-Weaver TL (2011) Developmental control of oocyte maturation and egg activation in metazoan models. *Cold Spring Harb Perspect Biol* 3: a005553.
240. Yamamoto DS, Hatakeyama M, Matsuoka H (2013) Artificial activation of mature unfertilized eggs in the malaria vector mosquito, *Anopheles stephensi* (Diptera, Culicidae). *J Exp Biol* 216: 2960-2966.
241. Boisson B, Jacques JC, Choumet V, Martin E, Xu J, et al. (2006) Gene silencing in mosquito salivary glands by RNAi. *FEBS Lett* 580: 1988-1992.
242. Eleftherianos I, Won S, Chtarbanova S, Squiban B, Ocorr K, et al. (2011) ATP-sensitive potassium channel (KATP)-dependent regulation of cardiotropic viral infections. *Proc Natl Acad Sci* 108: 12024-12029.
243. WHO (2013) World Malaria Report WHO; World Health Organization.
244. Maharaj R (2011) Global trends in insecticide resistance and impact on disease vector control measures. *Open Access Insect Physiology*: 27.
245. Denton JS, Pao AC, Maduke M (2013) Novel diuretic targets. *Am J Physiol Renal Physiol* 305: F931-942.
246. Rene Raphemot DFL, Thuy T. Nguyen, Thomas Utley, L. Michelle Lewis, Rishin Kadakia, C. David Weaver, Rocco Gogliotti, Corey Hopkins, Craig W. Lindsley and Jerod S. Denton (2011) Discovery, characterization and structure-activity relationships of an inhibitor of inward rectifier potassium (Kir) channels with preference for Kir2.3, Kir3.X and Kir7.1. *Front Pharmacol* 2.
247. L. Michelle Lewis GB, Brian A. Chauder, Sreedatta Banerjee, Katharina A. Lornsen, Rey Redha, Katherine Fallen, Craig W. Lindsley, C. David Weaver, and Jerod S. Denton (2009) High-throughput screening reveals a small-molecule inhibitor of the renal outer medullary potassium channel and Kir7.1. *Mol Pharmacol* 76: 1094-1103.
248. Feller N, Broxterman HJ, Währer DC, Pinedo HM (1995) ATP-dependent efflux of calcein by the multidrug resistance protein (MRP): no inhibition by intracellular glutathione depletion. *FEBS Lett* 368: 385-388.

249. Jaehde U, Sörgel F, Reiter A, Sigl G, Naber KG, et al. (1995) Effect of probenecid on the distribution and elimination of ciprofloxacin in humans. *Clin Pharmacol Ther* 58: 532-541.
250. Hill G, Cihlar T, Oo C, Ho ES, Prior K, et al. (2002) The anti-influenza drug oseltamivir exhibits low potential to induce pharmacokinetic drug interactions via renal secretion-correlation of in vivo and in vitro studies. *Drug Metab Dispos* 30: 13-19.
251. Metcalf RL (1967) Mode of action of insecticide synergists. *Annu Rev Entomol* 12: 229-256.
252. Wilkinson CF (1968) Detoxification of pesticides and the mechanism of synergism; Hodgson E, editor. Raleigh, NC.: North Carolina State University Press.
253. Shono T, Kasai S, Kamiya E, Kono Y, Scott JG (2002) Genetics and mechanisms of permethrin resistance in the YPER strain of house fly. *Pestic Biochem Physiol* 73: 27–36.
254. Meyer JM, Ejendal KF, Avramova LV, Garland-Kuntz EE, Giraldo-Calderon GI, et al. (2012) A "genome-to-lead" approach for insecticide discovery: pharmacological characterization and screening of *Aedes aegypti* D(1)-like dopamine receptors. *PLoS Negl Trop Dis* 6: e1478.
255. Li X, Schuler MA, Berenbaum MR (2007) Molecular mechanisms of metabolic resistance to synthetic and natural xenobiotics. *Annu Rev Entomol* 52: 231-253.
256. Dermauw W, Van Leeuwen T (2014) The ABC gene family in arthropods: Comparative genomics and role in insecticide transport and resistance. *Insect Biochem Mol Biol* 45C: 89-110.
257. O'Donnell MJ (2009) Too much of a good thing: how insects cope with excess ions or toxins in the diet. *J Exp Biol* 212: 363-372.
258. O'Donnell MJ (2008) Insect Excretory Mechanisms. In: Simpson SJ, editor. *Advances in Insect Physiology*. London: Academic Press. pp. 1-122.
259. Tice CM (2001) Selecting the right compounds for screening- does Lipinski's Rule of 5 for pharmaceuticals apply to agrochemicals? *Pest Manag Sci* 57: 3-16.
260. Akamatsu M (2011) Importance of physicochemical properties for the design of new pesticides. *J Agric Food Chem* 59: 2909-2917.
261. Swale DR, Kharade SV, Denton JS (2014) Cardiac and renal inward rectifier potassium channel pharmacology: emerging tools for integrative physiology and therapeutics. *Curr Opin Pharmacol* 15C: 7-15.
262. Jahangir A, Terzic A (2005) K(ATP) channel therapeutics at the bedside. *J Mol Cell Cardiol* 39: 99-112.
263. Lawson K (2000) Is there a role for potassium channel openers in neuronal ion channel disorders? *Expert Opin Investig Drugs* 9: 2269-2280.
264. Uhde I, Toman A, Gross I, Schwanstecher C, Schwanstecher M (1999) Identification of the potassium channel opener site on sulfonylurea receptors. *J Biol Chem* 274: 28079-28082.
265. Shyng S, Ferrigni T, Nichols CG (1997) Regulation of KATP channel activity by diazoxide and MgADP. Distinct functions of the two nucleotide binding folds of the sulfonylurea receptor. *J Gen Physiol* 110: 643-654.
266. Tucker SJ, Gribble FM, Zhao C, Trapp S, Ashcroft FM (1997) Truncation of Kir6.2 produces ATP-sensitive K⁺ channels in the absence of the sulphonylurea receptor. *NATURE* 387: 179-183.
267. Balimane PV, Chong S (2005) A combined cell based approach to identify P-glycoprotein substrates and inhibitors in a single assay. *Int J Pharm* 301: 80-88.

268. Takeuchi A, Masuda S, Saito H, Doi T, Inui K (2001) Role of kidney-specific organic anion transporters in the urinary excretion of methotrexate. *Kidney Int* 60: 1058-1068.
269. Zhang X, Zhang J, Zhu KY (2010) Chitosan/double-stranded RNA nanoparticle-mediated RNA interference to silence chitin synthase genes through larval feeding in the African malaria mosquito (*Anopheles gambiae*). *Insect Mol Biol* 19: 683-693.
270. Mysore K, Flannery EM, Tomchaney M, Severson DW, Duman-Scheel M (2013) Disruption of *Aedes aegypti* olfactory system development through chitosan/siRNA nanoparticle targeting of semaphorin-1a. *PLoS Negl Trop Dis* 7: e2215.